Aeromechanical Stability Augmentation Using Semi-Active Friction-Based Lead-Lag Damper

A Thesis
Presented to
The Academic Faculty

by

Sandeep Agarwal

In Partial Fulfillment
of the Requirements for the Degree
Doctor of Philosophy

School of Aerospace Engineering
Georgia Institute of Technology
December 2005

Aeromechanical Stability Augmentation Using Semi-Active Friction-Based Lead-Lag Damper

Approved by:

Dr. Olivier A. Bauchau,
School of Aerospace Engineering,
Committee Chair

Dr. Robert G. Loewy,
School of Aerospace Engineering

Dr. Massimo Ruzzene,
School of Aerospace Engineering

Dr. Dewey H. Hodges,
School of Aerospace Engineering

Dr. Aldo A. Ferri,
School of Mechanical Engineering

Date Approved: November 18, 2005

In the memory of my father...

ACKNOWLEDGEMENTS

First and foremost, I would like to express my sincere thanks to my dissertation advisor, Dr. Olivier Bauchau, for his continuous support and guidance throughout my doctoral study. This work would not have been possible without all the insightful discussions with him.

I thank my committee members, Dr. Robert Loewy, Dr. Dewey Hodges, Dr. Massimo Ruzzene and Dr. Aldo Ferri for their time, effort and enlightening suggestions which were essential in improving the quality of this work.

I would like to thank Dr. Jeff Jagoda, Associate Chair for Graduate Studies and Research in the School of Aerospace Engineering, for providing financial support throughout my stay at Georgia Tech.

My acknowledgements would never be complete without recognizing Dr. Armanios and Dr. Holmes for their help on my career decisions. They have been a good mentor and I would always be thankful to them for their valuable suggestions.

My lab mates deserve special mention for their constant help and stimulating discussions. I would like to thank Dr. Roxana Vasilescu, Samer Tawfik, Serkan Ozbay, and Kwangtae Ha for their help when I need it. Special thanks to Yuan Tan and Richard Cross for proof reading my thesis and suggesting improvements.

Finally, I would like to thank my family for their love, support and encouragement without which this endeavor would not have been possible.

TABLE OF CONTENTS

LIST OF TABLES

LIST OF FIGURES

SUMMARY

Lead-lag dampers are present in most rotors to provide the required level of damping in all flight conditions. These dampers are a critical component of the rotor system, but they also represent a major source of maintenance cost. In present rotor systems, both hydraulic and elastomeric lead-lag dampers have been used. Hydraulic dampers are complex mechanical components that require hydraulic fluids and have high associated maintenance costs. Elastomeric dampers are conceptually simpler and provide a "dry" rotor, but are rather costly. Furthermore, their damping characteristics can degrade with time without showing external signs of failure. Hence, the dampers must be replaced on a regular basis. A semi-active friction based lead-lag damper is proposed as a replacement for hydraulic and elastomeric dampers. Damping is provided by optimized energy dissipation due to frictional forces in semi-active joints. An actuator in the joint modulates the normal force that controls energy dissipation at the frictional interfaces, resulting in large hysteretic loops.

Various selective damping strategies are developed and tested for a simple system containing two different frequency modes in its response, one of which needs to be damped out. The system reflects the situation encountered in rotor response where 1P excitation is present along with the potentially unstable regressive lag motion. Simulation of the system response is obtained to compare their effectiveness. Next, a control law governing the actuation in the lag damper is designed to generate the desired level of damping for performing adaptive selective damping of individual blade lag motion. Further, conceptual design of a piezoelectric friction based lag damper for a full-scale rotor is presented and various factors affecting size, design and maintenance cost, damping capacity, and power requirements of the damper are discussed. The selective semi-active damping strategy is then studied in the context of classical ground resonance problem. In view of the inherent nonlinearity in the system due to friction phenomena, multiblade transformation from rotating frame to

nonrotating frame is not useful. Stability analysis of the system is performed in the rotating frame to gain an understanding of the dynamic characteristics of rotor system with attached semi-active friction based lag dampers. This investigation is extended to the ground resonance stability analysis of a comprehensive UH-60 model within the framework of finite element based multibody dynamics formulations. Simulations are conducted to study the performance of several integrated lag dampers ranging from passive to semi-active ones with varying levels of selectivity. Stability analysis is performed for a nominal range of rotor speeds using Prony's method.

CHAPTER I

INTRODUCTION

Although it would be most desirable to completely eliminate lead-lag dampers from helicopter rotor systems, this ideal goal remains elusive despite significant research in this area. Designs have been proposed that eliminate the need for lead-lag dampers in ground resonance or air resonance cases, but designs that manage to achieve both goals simultaneously have not been fully satisfactory. Furthermore, lead-lag damping is also required during maneuvering flight, such as descent flight conditions. Consequently, lead-lag dampers are found on most rotor systems despite the added mechanical complexity and cost. Hydraulic dampers are complex mechanical components that require the use of hydraulic fluids in the rotating system. This results in high maintenance costs to prevent oil leaks and subsequent failure. Elastomeric dampers are conceptually simpler and provide a "dry" rotor, but are rather costly. Furthermore, their damping characteristics can degrade due to temperature and stress cycling, thus resulting in high maintenance cost. More often than not, this degradation occurs without external signs of failure and hence the dampers must be replaced on a regular basis, further contributing to the high cost of the device. Figure 1.1 shows the respective costs per flight hour for the AH-64 helicopter; main rotor lead-lag dampers are the most expensive item to maintain.

1.1 Semi-Active Friction Lead-Lag Damper

Effective vibration reduction in structural systems can be obtained by means of adaptive joints. Figure 1.2 depicts an adaptive joint as developed by Gaul [47]. The piezoelectric element is used to modulate the normal force at the frictional interface, thereby controlling the resulting frictional force. For low values of the normal force, sliding takes place at the interface, but according to Coulomb's law the frictional force remains small, as does the resulting energy dissipation. For high values of the normal force, high static frictional forces

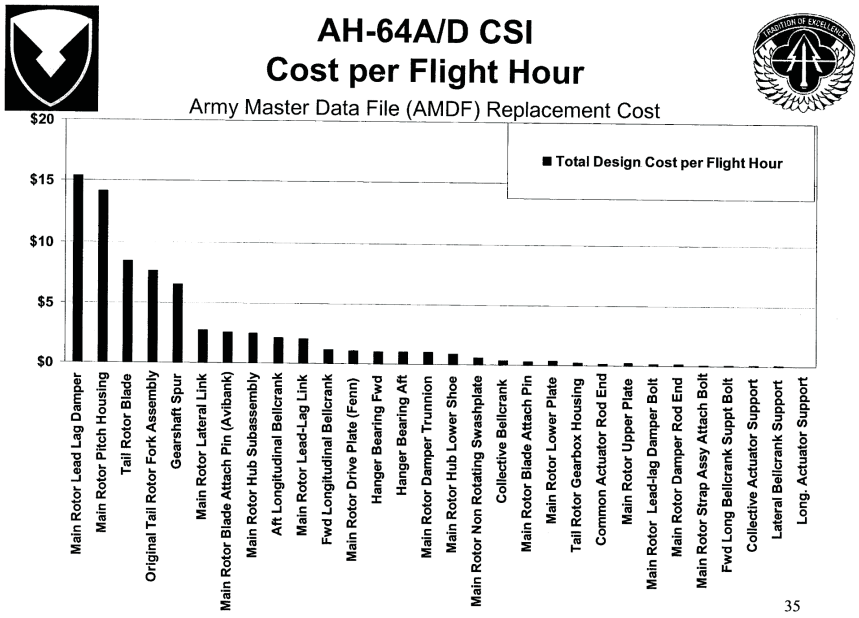

Figure 1.1: Respective costs of various critical rotor components

are obtained and the joint remains locked; no energy is dissipated since no relative motion is taking place. An instrumented damper provides the optimal normal force which will maximize energy dissipation by using a real-time control system that modulates the normal force at the joint interface.

Figure 1.3 illustrates the hysteresis loops obtained in instrumented and non-instrumented joints. A non-instrumented joint, i.e. one providing a constant normal force, produces the inner curve, that has only a modest hysteretic area and consequently dissipates only a small amount of energy. On the other hand, the controlled version of the joint, corresponding to the outer curves, is characterized by a significant increase in the hysteretic area, therefore greatly increasing the damping effectiveness of the system.

The proposed device is semi-active, in the sense that the characteristics of a passive element, the frictional interface, is dynamically modified by means of a piezoelectric actuator. This approach was shown to be very effective for damping structural vibrations in space

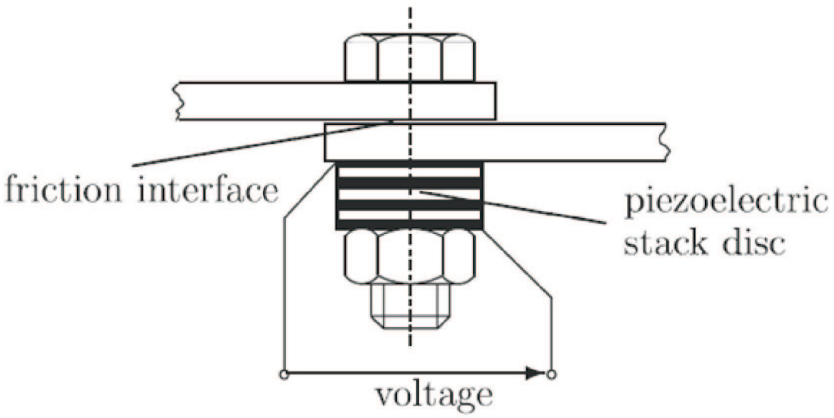

Figure 1.2: A semi-active joint

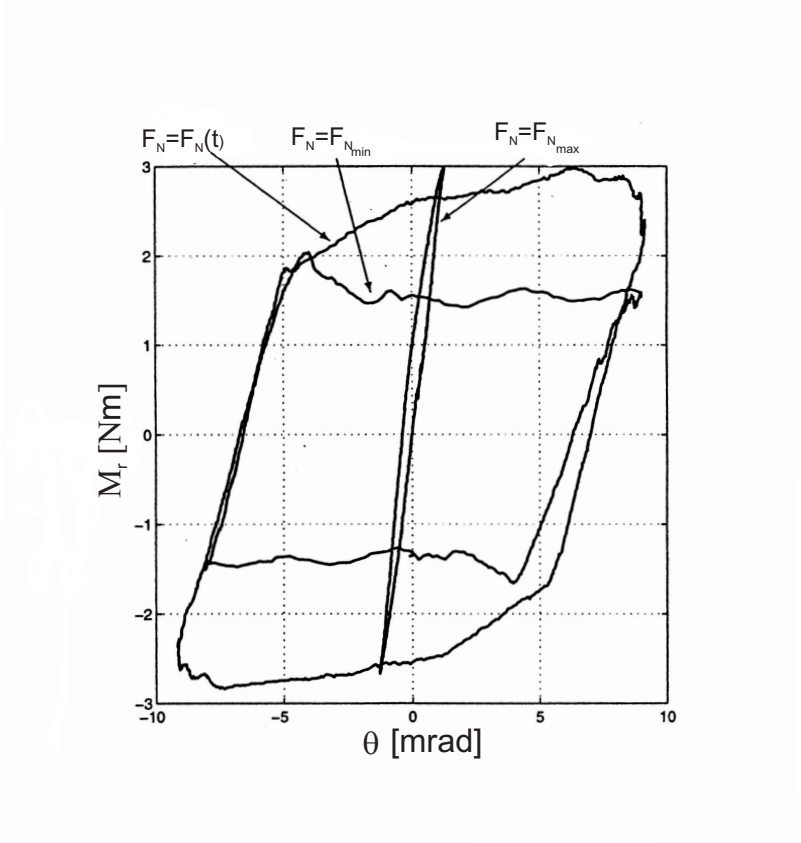

Figure 1.3: Hysteresis loops for joints with various normal forces, ref. [47]

structures [45].

The proposed semi-active friction dampers rely on a control system to modulate the normal force at the frictional interface, in an effort to maximize energy dissipation. Linking together the control systems of the blades opens up new avenues for system level optimization, by providing Adaptive Selective Individual (ASI) lead-lag damping capabilities.

"Adaptive" means that the damping provided by the system can be tuned to various flight conditions; this can be achieved in a simple way with the semi-active dampers proposed here since the damping level is tunable by design. This is contrast with conventional designs that rely on a pre-determined damping level, which must be a compromise between the optimal damping levels that would be required for the various flight conditions.

"Selective" refers to the fact that the proposed device can target specific lag frequencies for damping, while conventional design are typically unable to distinguish among the various frequencies contained in the blade response. To be more precise, consider for instance the problem of ground resonance. In this case, damping is required for the rotor "regressive" mode, but not for the collective modes, since these do not affect the center of gravity position of the rotor. In forward flight, hydraulic or elastomeric dampers will provide damping of the 1/rev motions of the blade that, in fact, might not be required. In turn, this increases loads in the blade as well as wear and fatigue of the damper and lead-lag link. In all these situations, the control system that actuates the piezoelectric elements could be designed to target the specific frequencies at which damping is actually needed, while providing little or no damping for the others.

Finally, the word "individual" refers to the fact that the proposed control system can provide damping to each individual blade in a locally optimized manner, hence achieving individual blade lead-lag damping. Indeed, the semi-active dampers provide tunable damping to each blade, and the centralized control system has the flexibility to operate the various

dampers in a locally optimal manner. This option is not available with conventional, passive designs that lack a centralized control system which could take local selective actions based on the global behavior of the system.

One important aspect of the proposed semi-active dampers is the very modest amount of power required for operation. This contrasts with many proposed active rotor concepts that require unrealistic power levels. In the event of an engine-out emergency, the small amount of required power could be drawn from the system APU, or could be generated by a small electric generator that takes advantage of the relative motion of the rotating shaft and fixed shaft housing. Indeed, if the engine is out, the shaft will be rotating, and sufficient power would be generated to operate the damping system until safe landing.

1.2 Objective and Scope of the Current Work

The present research effort investigates the suitability of semi-active dampers for rotorcraft lead-lag damper applications. The enhanced energy dissipation associated with the controlled frictional behavior of the proposed devices has been proven to be effective in damping structural vibrations of large space structures. The semi-active dampers could be low-cost alternatives to hydraulic and elastomeric dampers. Furthermore, this design solution opens the door to adaptive, selective and individual damping control of the rotor. These concepts promise to be very effective and do not seem to have been explored so far, probably for the lack of a viable solution for providing the required tunable damping.

The research effort focuses on a conceptual design of the proposed device. A model of the semi-active friction damper is developed and several issues affecting its practical application in commercial rotors are discussed. The second objective of the research is to design a semi-active control strategy governing damper operation that adjusts the magnitude and operational interval of frictional resistance to achieve selective damping of unstable modes, thereby reducing excessive burden on the power plant and extending the service life of

the damper. The realistic model of the complex rotorcraft system is developed within the framework of finite element based multibody dynamics formulation [5], including an adaptive controller to perform adaptive selective damping of regressive lag modes of individual blades. The damping capacity of semi-active friction dampers is assessed in comparison to that of hydraulic damper. This dissertation is organized into six chapters.

In Chapter 2, a survey of relevant work published in the literature is presented. The significant studies related to analytical and experimental study of aeromechanical stability of helicopters are reviewed. Various control approaches are studied and tested to augment aeromechanical stability in rotorcraft applications ranging from passive techniques to more robust active techniques. The various elements of the two control approaches are summarized, and several control approaches developed to stabilize helicopters against ground and air resonance are reviewed. Semi-active control methods imbibe best features of both approaches. Various semi-active lag damping techniques attempted by various researchers are summarized. Semi-active friction based damping, being the focus of current investigation, is discussed in detail, and various control laws developed along the lines are presented.

In Chapter 3, the concept of semi-active damping using friction modulation is presented. The control laws based on Lyapunov's stability theory are formulated. Further, to investigate the concept of selective damping, several strategies, with heuristically chosen damper operational timing schedule, are considered to perform selective damping of component mode of a system motion resembling rotor lag motion.

In Chapter 4, the classical ground resonance analysis of a coupled rotor-fuselage system integrated with semi-active friction damping mechanism is presented. A four-bladed isotropic rotor model connected to the fuselage is modeled as a spring-mass-damper system and further analyzed. A semi-active lag damper employing friction modulation is modeled as a feedback control law, and rotor stability with respect to unstable modes is investigated. The objective of this analysis is to validate the semi-active friction damping concept and

ascertain the actuating capacity desired to perform the task. This would further assist in damper design for realistic helicopter rotor systems.

In Chapter 5, the proposed concept is applied to the case of UH-60 rotorcraft. A comprehensive model of UH-60 is developed using the flexible multibody finite element code DYMORE. To assess the ground resonance stability of the system, rotor simulations are performed in a range of nominal rotor speeds. Prony method is used to analyze system stability with respect to several damping strategies.

In Chapter 6, the conceptual design of a piezoelectric, friction-based lag damper for a full-scale rotor is presented. Various aspects of the design, such as damper size, design and maintenance cost, damping capacity, and power requirements of the damper are discussed.

The significant conclusions obtained from the present study are presented in Chapter 7. Some suggestions for further research are also included.

CHAPTER II

LITERATURE SURVEY

Over the last two decades, increasing effort has been devoted to simplify rotor hub designs. The desire to build a rotor with lower parts count, reduced weight, drag and maintenance requirements has encouraged the design and development of bearingless main rotors (BMR) for helicopters. The BMR achieves the objectives of reduced life-cycle costs, improved hub designs and superior handling qualities by replacing flap and lag hinges and the pitch bearing with a flexbeam/torque tube assembly. The out-of-plane rotor flap mode is typically well damped due to aerodynamic forces, as are the pitching and/or torsional rotor modes. The in-plane rotor mode, or lag mode, has relatively little aerodynamic damping. The rotors are typically classified into soft-inplane rotors and stiff-inplane rotors depending on the magnitude of lag natural frequency in relation to rotor speed. Soft-inplane rotors have fundamental in-plane or lag mode natural frequency lower than the rotor speed, while it is the opposite for stiff-inplane rotors.

Soft-inplane hingeless rotor systems have several advantages over their stiff-inplane counterparts ranging from reduced weight and maintenance to reduced vibration and loads. The hubs with lower loads need less structural weight to support those loads. Consequently, a soft-inplane hub results in potentially less weight and improved reliability. A soft-inplane hingeless rotor can use more blades than a stiff-inplane, articulated or rigid hub. As the number of blades increases, the noise and vibration levels decrease, increasing passenger comfort. In spite of benefiting from these advantages, soft-inplane rotor systems are inherently vulnerable to the aeromechanical instabilities of ground and air resonance. Ground resonance is a coalescence of the rotor lag mode with the landing gear modes while the helicopter is on the ground. Air resonance is a coalescence of the rotor lag mode with the fuselage modes while the helicopter is in high-speed forward flight. At least in part

because of the potential for air and ground resonance in a soft-inplane hub, the Bell XV-15, the Bell-Boeing V-22 Osprey, and the new Bell Augusta 609 have stiff-inplane, gimbaled rotors which do not experience these instabilities. The traditional approach to alleviate aeromechanical instability is by providing blade lead-lag damping mechanism. Hence, helicopters have traditionally been equipped with passive elastomeric or hydraulic lag dampers at the rotor hub. These passive dampers have certain drawbacks. Hydraulic dampers are prone to leakage problems and can result in high damping forces when amplitude increases. Elastomeric dampers are sensitive to temperature, exhibiting significant loss of damping at extreme temperatures and have been found to cause limit cycle oscillations in rotor blades. Other than passive dampers, the passive damping concept utilizing aeroelastic couplings to augment rotor-body aeromechanical stability has also been investigated. Aeroelastic couplings, being continuous variables, make the task of determining an optimum combination of aeroelastic couplings that result in satisfactory rotor-body aeromechanical stability characteristics over a broad range of variations in configuration and operating conditions a challenging task. Further, implementation methods for the aeroelastic couplings have not been successfully answered so far. In addition to passive techniques, active control techniques have been investigated to improve helicopter aeromechanical stability. Active vibration reduction strategies including individual blade control (IBC) and active pitch control using the swash-plate require additional hardware and thus have high power requirements, additional weight and higher complexity.

Recently, there has been growing interest in the use of semi-active techniques to suppress helicopter vibrations. The semi-active techniques have already been successfully tested for engineering applications such as automobile suspensions, space structures and implemented in others such as seismic structures. Semi-active devices combine the positive aspects of passive and active control devices in that they are controllable (like the active devices) but require little power to operate. The closed loop semi-active systems are inherently stable owing to the 'passive' nature of the control and are insensitive with respect to the spillover problem. The helicopter rotor equipped with semi-active damper will have reduced hub

Figure 2.1: Bell 412 with soft-inplane rotor

Figure 2.2: Bell Boeing V-22 Osprey with stiff-inplane rotor

complexity and weight in addition to adaptive compensation in response to variations in operating environment.

In this research, lead-lag damping by semi-active friction modulation is studied and further, an innovative design for a lead-lag damper employing the technique is presented. The literature survey performed failed to identify any published work similar to the concept proposed in this work suggesting the uniqueness of this approach. Relevant background work published in the open literature is presented in this chapter. The literature review is separated into two sections corresponding to the two main aspects of this research, namely: the aeromechanical stability of helicopters and the control techniques in the context of aeromechanical stability augmentation. The semi-active friction based damping technique, being the source of inspiration behind this work, has been discussed in detail and several relevant control laws developed have been reviewed.

2.1 Aeromechanical Stability Augmentation

Aeromechanical stability of helicopters is a nonlinear phenomenon involving interactions between aerodynamic, inertial and elastic forces. The striking advantages of hingeless and bearingless rotor systems over articulated rotors such as reduced weight, maintenance, vibration, and loads, is countered by their susceptibility to instabilities such as air resonance and ground resonance due to the interaction of the poorly damped cyclic lag mode with the coupled low frequency flap modes and rigid or elastic airframe modes. A comprehensive review of bearingless rotor programs is given by Huber [58]. The phenomenon of ground resonance has been investigated extensively ever since this problem was identified in the autogyros of the 1930's and early 1940's. The characterization of air and ground resonance is recognized as one of the top twenty advances in vertical flight history by the American Helicopter Society (Carlson [18]). During ground resonance, the cyclic lag modes produce a wobble of the rotor center of gravity (see figures 2.3 and 2.4) causing shifting fore and aft and laterally of the effective mass of the rotor which couples with the vibration of the fuselage to produce large displacements. Air resonance is a similar aeromechanical instability,

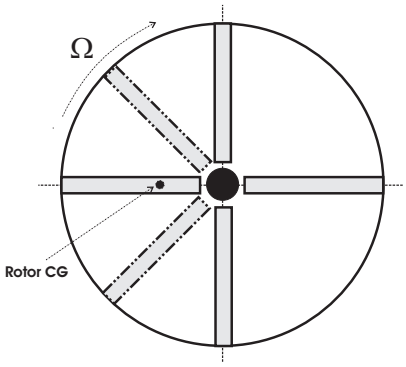

Figure 2.3: Rotor CG movement due to ζ_c lag mode

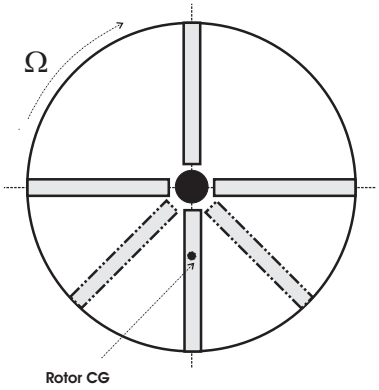

Figure 2.4: Rotor CG movement due to ζ_s lag mode

differing from ground resonance in the source of the fuselage stiffness and damping. While in ground resonance, the sole source of both stiffness and damping is typically the landing gear assembly; in air resonance, gravity (or, alternatively, rotor thrust) and aerodynamic damping are sources of stiffness and damping. Air resonance results in large vibrations, leading to passenger discomfort and material fatigue, and poorer handling qualities (Ormiston [87]).

Coleman [21] was first to study the phenomenon of ground resonance and provide a mathematical explanation for it. The analysis was based on a simple four-degree-of-freedom model which included body pitch and roll and high and low frequency lag modes for the blade (in the non-rotating frame), neglecting the aerodynamic effect. The instability was found to occur when the low frequency lag mode coalesces with the body mode. In 1958, Coleman and Feingold [22] published an analysis of ground resonance for articulated rotors considering four degrees of freedom. The rotor aerodynamic force was neglected as before.

Other early analysis of ground and air resonance are conducted by Hooper [56] and Gabel [40]. Donham, Cardinale, and Sachs [24] added aerodynamic effects to their analytical formulation and tested the Lockheed XH-51A to show ground and air resonance instabilities. Lytwyn, Miao, and Woitsch [72] extended the basic Coleman analysis for hingeless rotors, which have more severe air resonance problems. Their analysis added quasi-steady aerodynamics to show that the BO-105 hingeless helicopter was inherently stable due to the aerodynamic damping. The works showed the importance of aerodynamic forces for accurate modeling of ground and air resonance for hingeless rotors. In the 1980s, Johnson [60], Bousman [12], Ormiston [86], Friedmann and Venkatesan [39], and other researchers studied mathematical models for aeromechanical stability analysis. Bousman compared theory with experimental data and concluded that the absence of dynamic inflow in the theoretical model is the cause for the discrepancy between the predicted damping and experimental results and that predicted by theoretical model. Johnson added dynamic inflow to the theoretical model with dynamic inflow and obtained better agreement with the experimental data than the results based on a model without dynamic inflow. Friedmann, using a theoretical model based on a quasi-steady aerodynamic model, also compared his prediction with Bousman's results. His theoretical model based on a quasi-steady aerodynamic model gave better agreement with the experimental data than the agreement noted by Bousman. Nagabhushanam and Gaonkar [80], using the finite-state wake model, studied aeromechanical stability of hingeless-rotor helicopters in ground-contact, hover, and trimmed flight. The correlations from the finite state wake, dynamic inflow and vortex models were generally satisfactory. Recently, Sela and Rosen [93] analyzed the effect of alternate inter-blade connection for ground resonance. They also showed that the rotor anisotropy (damping and stiffness of connectors) had some added benefits. Many aspects of aeromechanical stability such as causes of instability, analytical and empirical modeling of the phenomena and means to improve, have been studied over the last fifty years (Hohenemser [55], Ormiston [85], Miao [79], Friedmann [37], Chopra [20], Smith [101]).

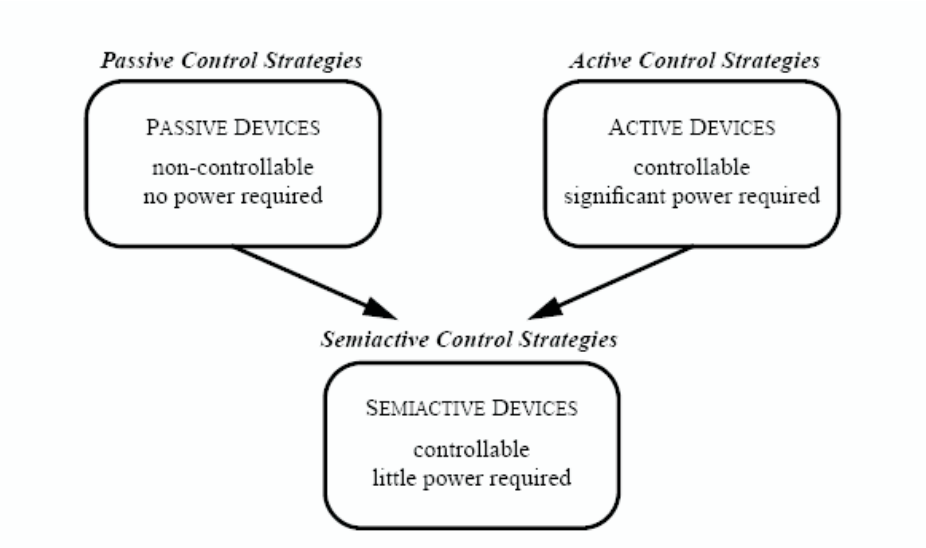

Figure 2.5: Control strategies

2.2 Control Strategies

Vibration and noise in a dynamic system can be reduced by a number of means. These can be broadly classified into active, passive, and semi-active strategies. Selecting a particular strategy involves a number of decisions. Figure 2.5 shows graphically how these control devices and their control strategies are related. Passive control provides energy storage and energy dissipation mechanisms to resist the energy demand of the system whereas stable active control reduces the energy demand of the system by applying control forces or displacements, and adjusting their magnitude over time in such a manner that the resulting motion is constrained within the desired limits. If the control is passive, the percentage of the energy storage (elastic) versus energy dissipation (damping) required has to be taken into consideration, and the type and properties of passive energy dissipation devices need to be specified. If active control is used to supplement passive control, the type and capacity of the force actuator needs to be established. A variety of control approaches to augment aeromechanical stability of BMR's is summarized in Table 1 and have been investigated.

Table 2.1: Aeromechanical Stability Augmentation Techniques

Passive	Active	Semi-Active
Hydraulic Dampers	Blade Pitch Control	ER & MR Fluids
Elastomeric Dampers	Individual Blade Control	Variable Friction Dampers
Fluid Based Dampers	Active Constrained Layer Damping	
Aeroelastic Coupling		
Rotor Anisotropy		

2.2.1 Passive Approaches

Passive strategies have been employed extensively for augmenting aeromechanical stability in soft-inplane rotors. Passive control resources are characterized by the dissipative nature of their control forces and the fixed characteristics of the devices (e.g., damping coefficient). Once installed, a passive system cannot be modified easily. Thus, passive devices are often optimally tuned to protect the structure from a particular dynamic loading, and thus the performance of these devices is suboptimal for other loading scenarios and configurations. The inability to change a passive control system dynamically to compensate for an unexpected loading tends to result in an overly conservative design. When self-weight is an important design constraint such as in aircraft structures, one must avoid being overly conservative. Additionally, studies show that the passive control is not very effective in fine-tuning the response in a local region. Notwithstanding these limitations, the potential for improving the performance by dynamically modifying the loading and system properties exists.

Common techniques for passive lag damping include the use of hydraulic, elastomeric or fluid-based dampers in addition to structural and aerodynamic design optimization of blades, each of which is further discussed in detail below.

2.2.1.1 Hydraulic Dampers

Hydraulic dampers rely upon throttled flow of fluids that generate damping forces proportional to the square of velocity. This can result in extremely high damping forces when amplitudes increase. Hydraulic dampers are prone to leakage problems and have a short life due to a large number of moving components and seal wear resulting in higher maintenance cost. The weight and size of these dampers result in another penalty due to high parasitic load and aerodynamic drag (McGuire, D. P. [76], Panda, *et al.* [90], Wereley and Kamath [118]).

The modeling of nonlinear hydraulic dampers for rotorcraft applications is very well explored (Tarzanin and Panda [108]). The focus of recent research in hydraulic dampers has been associated with the implementation of nonlinear behavior in the aeroelastic code and the improvement of materials to reduce the damper size and weight and extend its life.

2.2.1.2 Elastomeric Dampers

Elastomeric dampers employing bonded elastomeric material exhibit viscoelastic behavior under dynamic conditions, dissipating energy through hysteresis. These materials respond nonlinearly to the amplitude of motion, frequency of motion, and temperature. Compared with conventional hydraulic dampers, elastomeric dampers are lighter in weight and have fewer parts. They do not have the sliding seals of hydraulic dampers and are not affected by sand and dust. Elastomeric dampers exhibit gradual deterioration, detectable by visual inspection (Panda *et al.* [90]). These elastomers are rapidly gaining popularity as a solution for designing lag dampers with high damping capability, and have been utilized for both articulated and BMR rotor systems; examples include the Boeing AH-64 Apache, the Boeing CH-47F Chinook, the Bell model 412, the Sikorsky RAH-66 Comanche, and the McDonnell Douglas Explorer.

Many researchers have focused on the analytical and empirical modeling of the nonlinear behavior of elastomeric dampers. Friedmann [38] provided a comprehensive review of

the elastomeric models developed in the last decade. Recent developments in the area of material science have led to the development of very high loss factor elastomers. Nevertheless, the design of elastomeric dampers is hindered by its complex behavior (McGuire [76]). An elastomeric damper is nonlinear and highly dependent on frequency, temperature and loading conditions such as preload and excitation amplitudes. The damping of an elastomer has been shown to degrade substantially at low amplitudes, causing undesirable limit cycle oscillations. Consequently, alternative methods for augmenting aeromechanical stability are explored.

2.2.1.3 Fluid Filled Dampers

Fluid filled dampers combine benefits of bonded elastomeric dampers such as simplicity, lightweight, reliability, energy storage capacity, multi-axis spring rate capability and maintenance free operation with the broader range of dynamic capability provided by non-toxic, non-corrosive fluids. These dampers are exclusively manufactured by the Lord Corporation under the trade name of Fluidlastic. Fluidlastic dampers (McGuire [76]) enjoy several advantages over hydraulic dampers in the sense that they do not require dynamic seals, extremely close tolerances, plated surfaces and polished finishes on the components. As they are hermetically sealed, they are not affected by sand and dust, are not prone to leakage, and are thus designed to be maintenance-free. Recent application of Fluidlastic includes the Bell 430 (BMR), the NH90 (articulated) and the RAH-66 Comanche. McGuire tested Fluidlastic and elastomeric dampers at Lord to assess their feasibility for helicopter lead-lag dampers. The dynamic test results showed less dependency of elastic stiffness of Fluidlastic damper on the dynamic amplitude of the input and higher loss factor in comparison to elastomeric damper. Panda *et al.* [90] discussed the efforts of Boeing Helicopters in the development and implementation of the fluid filled polymer based dampers. The study showed that these dampers have a more consistent hysteresis loop (less dependent on strain and temperature) compared to elastomeric dampers and can provide higher damping due to higher loss factor. In addition, the frequency dependence of the loss factor was found to be much lower than that of elastomeric dampers.

Panda and Mychalowycz [89] tested 1/6-Froude-scale RAH-66 Comanche helicopter BMR in the wind and compared the experimental results with those obtained from analytical simulation using the mathematical model developed by Boeing. The performance comparison of elastomeric and Fluidlastic dampers showed that the elastomeric snubbers/dampers resulted in limit cycle instability due to their nonlinear stiffness, which was eliminated by Fluidlastic dampers. The Fluidlastic dampers provide more uniform stiffness and hence have superior performance.

2.2.1.4 Aeroelastic Coupling

Certain drawbacks associated with the use of passive lag dampers such as hub complexity, weight, aerodynamic drag, and maintenance requirements have led researchers to explore the concept of a damperless rotor. Out of the several concepts proposed (Ormiston [88]) for the design of a damperless, yet aeromechanically stable configuration, the use of aeroelastic couplings to augment rotor-body aeromechanical stability has shown some promise. A number of mechanisms such as skewed flexures, hub and control system geometry, elastically tailored composites, and distribution of flap and lag stiffness relative to the effective location of the pitch bearing have been observed to create kinematic couplings, such as pitch-lag coupling, pitch-flap coupling, and structural flap-lag coupling (Ormiston [84], Bousman, *et al.* [15], Bousman [14]). Ormiston [84] analytically showed the effect of different couplings on the aeromechanical stability of a helicopter. The results presented applied to isolated rotor blade condition and did not reflect the effects of rotor-body coupling. Bousman *et al.* [13, 14] experimentally observed that for air resonance, negative pitch-lag coupling individually or in combination with flap-lag coupling substantially increases the lead-lag damping of the experimental rotor compared to the baseline. While pitch-lag coupling alone was not able to stabilize the unstable region, combined effect of both negative pitch-lag coupling and flap-lag coupling provided some damping in the unstable region. King [66] and Nagabhushanam and Gaonkar [80] once again concluded negative pitch-lag coupling to be an important parameter in improving air resonance stability compared to pitch-flap and

flap-lag couplings. Sharpe [94] experimentally investigated the importance of including torsional flexibility in addition to the coupling between flap and lag bending on a stiff in-plane hingeless rotor in hover. Yeager *et al.* [123] obtained aeromechanical stability data for a soft in-plane hingless rotor in hover and forward flight. The investigation examined the influence of blade sweep, droop, and precone, as well as blade pitch-flap coupling. Zotto and Loewy [125] observed that pitch-lag coupling increases the landing gear damping requirements for ground resonance stability despite reducing the required lag damping in hover. Venkatesan [111] analytically studied the combined effects of pitch-lag, pitch-flap and structural flap-lag coupling on ground resonance. It was showed that pitch-lag and flap-lag couplings, although they do not have much influence on the lag regressive mode damping at rotor angular speeds where regressive mode frequency coalesces with body pitch and roll motion frequencies (observed by Bousman), positive pitch-flap coupling increased the damping at these critical rotor speeds. Maier *et al.* [73] investigated a soft in-plane isolated rotor in hover and forward flight. The stability data was collected for a variety of flight conditions and showed the influence of collective pitch in hover and shaft angle, and collective pitch in forward flight. Tracy and Chopra [109] conducted an experimental study of an elastically tailored composite blade with coupling due to the orientation of the plies. The experiment was conducted on a 6-ft diameter Froude-scale model and the experimental results were compared with the analytical results. The study showed good improvement in damping due to the elastically tailored composite flexure. The negative bending-torsion (pitch-lag) coupling was found to be a stabilizing factor, while the positive bending-torsion coupling could destabilize the system.

Gandhi and Hathaway [42] addressed the need for utilizing optimization techniques to design the coupling for a broad range of operating conditions such as rotor speeds, thrust levels, and changes in body inertia. This is necessary since a good coupling design for one operating condition is often bad for some other operating condition. The authors demonstrated that by considering a range of operating conditions simultaneously, an overall feasible configuration could be developed.

2.2.1.5 Rotor Anisotropy

Rotor anisotropy results from dissimilarity between the blades in a rotor. Studies on the influence of variations in the blade properties revealed its effectiveness in enhancing aeromechanical stability if used properly, as imbalanced rotor anisotropy is a source of high 1/rev hub vibrations. Thus, an even number of blades in a rotor system in conjunction with identical opposite blades is required. The dissimilarity in the blades can be introduced by varying certain properties such as stiffness, damping, inertia and aerodynamic properties from one set of blades to another. Weller and Peterson [117] experimentally examined the influence of lag dampers with dissimilar stiffness on the rotor-body aeromechanical stability characteristics using a 4-bladed BMR model. Wang and Chopra [112, 113, 114] studied an unbalanced rotor with a single dissimilar blade. An improvement in the aeromechanical stability was observed for dissimilarity in mass and lag stiffness of the blade. However, dissimilarities in elastic, inertial and aerodynamic properties resulted in a drastic increase in vibratory hub loads. Gandhi [41] and Gandhi and Malovrh [43] analytically investigated balanced rotor anisotropy for aeromechanical stability augmentation. The results of the study showed that dissimilarity in the lag stiffness, blade mass and blade length are beneficial for aeromechanical stability while dissimilarity in flap stiffness, lag damping and aerodynamic properties has virtually no influence.

2.2.2 Active Control

An active structural control is one which has the ability to determine the present state of the structure, decide on a set of actions that will change this state to a more desirable one, and carry out these actions in a controlled manner in a short period. Such control systems can theoretically accommodate unpredictable environmental changes, meet exacting performance requirements over a wide range of operating conditions, and possibly compensate for the failure of a limited number of structural components. The use of active control for aeromechanical stability augmentation has been explored by many researchers and has shown some promise. However, safety and stabilization of such an approach require in-depth study before it can be safely integrated into the system.

2.2.2.1 Active Blade Pitch Control

Most of the studies on active aeromechanical stability augmentation have dealt with active control of the blade pitch using the swash-plate or the pitch link to increase the lag damping, and moments on the hub to mitigate the coupled rotor-body vibrations. Straub and Warmbrodt [105] analytically studied two mechanisms to stabilize ground resonance by controlling the swash-plate based on the fuselage position, velocity and acceleration feedback. The first mechanism dealt with controlling body pitch and roll through flapping moments, and second one involved augmenting the lead-lag damping through Coriolis coupling with blade flapping. The scheduling of feedback parameters led to increase in damping augmentation. Straub [104] later used a linear optimal controller (LQG) for a four-bladed articulated rotor helicopter and showed that choice of appropriate feedback signals from these full-state compensators resulted in sufficient lead-lag damping of the closed loop system throughout the range of rotor speed under consideration. Takahashi and Friedmann [106] again used active control through cyclic inputs to the swash-plate to control air resonance of a hingeless rotor. The feedback of body states in this study resulted in poor lead-lag damping and destabilization of the progressive lead-lag mode.

Weller [116] experimentally studied the aeromechanical stability of a BMR by controlling the cyclic inputs though the swash-plate, which were proportional to fuselage pitch and roll position and velocity. Results showed that the fuselage position feedback had a stabilizing influence on the minimum damping at resonance. Following this work, Gandhi and Weller [44] conducted analytical study of the same BMR configuration and investigated the use of acceleration feedback.

2.2.2.2 Individual Blade Control

Apart from studies involving swash-plate control to augment aeromechanical stability, few researchers have attempted to use the concept of individual blade control (IBC). The technique involves implementation of actuators for each blade in the rotating system. Ham *et al.*

[51] showed that feeding back lag velocity to the individual blade pitch control can generate blade-flap velocity which results in an in-plane moment due to Coriolis force, opposing lag motion. Kessler and Reichert [65] studied the concept of IBC on an articulated rotor analytically. The study conducted on a single blade model, neglecting fuselage coupling, resulted in significant active damping by position and rate feedback without significantly altering the rotor dynamics. Scheduling of the feedback gain was not necessary and a simple controller gain was sufficient for a whole range of advance ratios. Hathaway and Gandhi [52] analytically studied IBC for alleviation of ground resonance problems in hingeless as well as a bearingless main rotor using fuselage interaction. The results showed the effectiveness of this technique over both aeroelastic coupling and active control through the swash-plate to introduce the cyclic pitch inputs.

2.2.2.3 Constrained Layer Damping

In the Constrained Layer Damping treatment, a viscoelastic material (VEM) layer is sandwiched between the base structure and a constraining layer. The configuration is termed as passive constrained layer (PCL) treatment (Fasana *et al.* [29], Cai *et al.* [16], Zheng *et al.* [124]) if the constraining layer is used as a passive element. Such system has effectiveness limited to narrow range of operating conditions due to the degradation of the damping characteristics of the viscoelastic layers with temperature and frequency. In the active control systems (Baz and Ro [10], Derham and Hagood [23], Chen and Chopra [19]), constraining layers consist of piezoelectric layers with the structural system having built-in sensing and actuation capabilities. The shear deformation of viscoelastic damping layer can be controlled and actively tuned to enhance the damping characteristics. The constrained layer damping treatment has been used extensively for structural vibration reduction by numerous researchers (Shen [95, 96, 97], Azvine *et al.* [2], Veley and Rao [110], Lesieutre and Lee [68], Liao and Wang [69, 70, 71], however, the implementation of this treatment in a helicopter rotor system for lag damping enhancement has not received much attention. Recently, Smith and Wereley [99, 100] studied the feasibility of passive constrained layer damping on helicopter flex beams for rotorcraft stability augmentation. The results

obtained for a cantilever beam in both rotating and non-rotating environment showed that the passive constrained layer damping treatment could significantly increase the structural damping.

2.2.3 Semi-Active Control

Semi-active control devices, also called "smart" control devices, assume the positive aspects of both passive and active control devices. A semi-active control strategy is similar to the active control strategy. However, the control actuator does not directly apply force to the structure, but instead it is used to control the properties of a passive energy device, e.g., a controllable passive damper. Semi-active control strategies are dissipative in nature, inherently stable, and require a little energy to operate. Semi-active control strategies appear to be particularly promising in addressing a number of the challenges facing active control strategies, in that the devices are low power, fail-safe, and reliable. The semi-active nature of the damper allow it to be in service when desired. In flight configuration when high damping is not required (usually forward flight), the damping can be reduced using an active signal. The reduced damping would reduce the damper loads and thus increase the damper life. In addition, this type of damper could actively compensate for the loss of damping due to environmental changes.

2.2.3.1 ER & MR Dampers

Electrorheological (ER) and magnetorheological (MR) fluids are able to change between free flowing Newtonian fluid and a semi-solid with controllable yield strength within milliseconds when exposed to electric or magnetic fields, respectively. These fluids date back to the late 1940's (Winslow [121, 122], and Rainbow [92]). MR fluids have been recognized as having a number of attractive characteristics for use in vibration control applications, over the last several years (Kamath and Wereley [62, 64], Gordaninejad *et al.* [50], Weiss *et al.* [115], Ginder *et al.* [48], Spencer *et al.* [102], Spencer and Sain [103], Dyke and Spencer [27], Dyke *et al.* [28]). Some examples of literature proposing ER fluids for application to structural control include Sims *et al.* [98], Taniwangsa and Kelly [107], and Ohta *et al.* [83].

MR fluids has been found to be a potential material for developing adaptive dampers due to their high damping capability and smaller size as compared to conventional elastomeric or hydraulic damper systems. Hurt and Wereley [59] did a comprehensive study of various designs for MR and ER fluid dampers for stability augmentation of hingeless and bearingless rotors. There are numerous studies examining the MR dampers for helicopter lag damping applications. Kamath *et al.* [63] tested an MR damper and a Fulidlastic damper. The results showed degradation in damping and stiffness of MR dampers due to inherent nonlinearities in the ON condition. Marathe *et al.* [75] explored the feasibility of using MR fluid-based dampers for lag damping augmentation in helicopters. A rotor aeromechanical model integrated with a MR damper model was analyzed with two different control schemes - namely the On-Off scheme and the Feedback Linearization scheme. The results showed that an MR damper of a size comparable to an elastomeric damper can provide sufficient damping for ground resonance stabilization and can significantly reduce periodic damper loads with a judicious choice of operation scheme. For a given uncertainty bound, Marathe *et al.* [74] derived a worst case scenario and developed a robust controller for MR dampers.

Wereley *et al.* [119] tested a scaled MR damper for helicopter lag damping. The test results showed the reduced stiffness of the MR damper when in the OFF condition than in the ON condition and thus enhanced possibility to reduce damper loads in forward flight by operating it in the OFF condition. Kamath and Werely [61] investigated distributed damping of the rotorcraft flexbeam using ER fluids. A non-linear model was developed that accurately simulates the dynamic characteristics of the ER fluid. Model parameters were estimated for different values of electric fields using the least squares technique.

2.2.3.2 Variable Friction Dampers

It is well known that dry friction is an effective means of energy dissipation in many mechanical systems. Previously, friction dampers were used only in passive contexts (Ferri [30]). Because the slip force is constant in a passive Coulomb friction damper, this damper

sticks for relatively low slip velocity without any energy dissipation. A semi-active friction damper controls the slip force by increasing or decreasing the contact force through feedback of desired damping. Variable friction dampers have been proposed as cost-efficient vibration control systems for flexible structures. Semi-active friction dampers have been utilized in suspension system of automobiles (Ferri and Heck [36]) and proposed for building structures or bridges subjected to earthquake excitation (Dowdell and Cherry [25], Hayen and Iwan [53], Akbay and Aktan [1]). Gaul *et al.* [46] designed two types of semi-active joints for a large truss structure and used global as well as local controllers to study the effectiveness of semi-active controls in large space structures. Semi-active friction damping has also been studied in the context of turbomachinery blades with shrouded interfaces properly designed to provide displacement dependent dry friction damping (Menq *et al.* [78]).

While many studies use a discontinuous Coulomb model (Ferri and Heck [35], Whiteman and Ferri [120]), references (Menq *et al.* [78, 77]) utilize a series spring-friction model that resulted in a "hysteretic spring" characteristic. Gaul and Nitsche [47] and Nitsche and Gaul [82] used the dynamic friction model proposed by Canudas de Wit *et al.* [17]. The friction model was designed to reproduce all observed friction phenomena such as presliding displacement, stick-slip motion with Stribeck effect, and other rate-dependent phenomena.

To improve the energy dissipation process of a friction damper, various control strategies have been suggested. Ferri and Heck [36] compared control laws based on pure linear viscous damping with the similar ones including saturation and filtering effects. The saturation reduced the peak acceleration level, and filtering provided the lower bandwidth in the actuator. Although the peak acceleration was found comparable, displacement was found to be much smaller for the one with filtering and saturation effects. Dupont *et al.* [26] and Gaul and Nitsche [47] used control laws based on minimization of the Lyapunov function representing the total energy of the system. Lane and Ferri [67] compared the viscous joint control with that of clipped LQR design. LQR based control was found to be far more effective in dissipating energy at the cost of being the most complex controller of the

linear, constant gain design. The semi-active friction damping concept has further inspired researchers to develop smart joints since friction in joints is the major source of damping in structures having jointed connections. If controlled, friction in these joints can increase the inherent damping of the structures and thereby control the vibration response.

2.2.3.3 Semi-Active Joints

Joints provide significant amount of passive damping for flexible structures by means of dry friction. Hertz and Crawley [54] and Ferri [31, 32, 33] investigated ways to improve the damping properties of joints. A considerable amount of damping enhancement was found when normal load was allowed to vary with displacement. The need for active damping in deployable space structures, where vibration damping by passive joints is not sufficient and other sources of damping are not realizable, was recognized (Ferri and Heck [34], Namba, Akoi and Natori [81], Gaul, Albrecht and Wirnitzer [45]). Ferri and Heck [34] considered passive joint and active joint configurations. The passive joint was created by implementing curved contact surfaces that allowed the normal force to vary with the change of rotation angle. Semi-active joints allowed the normal force to vary to optimize the energy dissipation based on the feedback from the distributed sensors. The passive joint required the initial tension and the curvatures of the contact surfaces to be chosen a priori which limited the amount of damping that could be possibly achieved in real time. Ferri and Heck [35], studied various control schemes to vary the normal force in the joint which has already been described above. Pun and Semercigil [91] used the Variable Stiffness Control (VSC) method to actively change the stiffness of the joint using an active torsional spring. The unclamping and reclamping action of the active spring at the instance of maximum displacement dissipated energy quickly. A semi-active joint designed and patented (German Patent under DE 19702518 C2) by Gaul utilized a piezoelectric stack actuator to vary the normal force.

Although semi-active friction dampers have been studied and successfully implemented in several engineering applications, literature available lacked any record of its study/application

for aeromechanical stability augmentation and hence the motivation behind the present work.

CHAPTER III

SEMI-ACTIVE FRICTION CONTROLLED DAMPING

Semi-active damping techniques improve upon the performance of active and passive devices by ensuring the stability of closed loop systems with minimal power input and avoiding the often required tuning of devices at the natural frequency of the system. The stability of semi-active devices, based on the fact that they can only absorb or store energy in a structure, has made it quite attractive, particularly in the field of vibration damping. Out of several ways to accomplish semi-active damping as mentioned in the literature survey, dry-friction based damping has gained recent attention owing to its simple modeling and easy implementation.

Friction based damping is often referred as braking, similar to that in automobiles. The constant damping rate provided by passive friction dampers is independent of the frequency of the motion. The constant normal force on the friction interface, often subjected to a variable environment dependent friction coefficient, makes it unreliable in extreme conditions. The passive friction dampers are not asymptotically stable i.e., the friction interface can stick away from the equilibrium position. The undesirable characteristics of traditional friction damper can be eliminated by actively controlling the schedule of normal force magnitude, thus transforming it from passive to semi-active. In fact, lag damping is required for certain flight conditions only at the initiation of instability and damper can be switched off upon feedback of stable operation of the system. In this chapter, control laws are derived to maximize energy dissipation in the friction element. The control technique is further supplemented to perform selective type damping of specific mode/modes in the dynamic response of the system.

3.1 Control of Semi-Active Friction Dampers

Several approaches have been taken to derive semi-active control laws which maximize damper energy dissipation in an instantaneous sense by modulating the normal force at the friction interface. A brief review of which is given in the previous chapter. The control algorithms have been compared for piezoelectric friction dampers on the basis of several criteria such as maximum applied control load, resulting peak displacement and peak acceleration. Although clipped-optimal and bang-bang control are found to significantly reduce the peak displacement, they often amplify the peak acceleration of the structure when the structural responses are relatively small or the capacity of the friction damper is sufficiently high, resulting in acceleration jumps. In the following section, a semi-active control law based on maximum energy dissipation is derived based on Lyapunov's stability criterion. The control law developed is further modified to provide selective damping of unstable modes in the dynamic response.

3.1.1 Controller Design

Assume that the system dynamics can be described by a linear model with n degrees of freedom, while friction in m dampers is nonlinear. In general, $m < n$. The system forcing can be denoted generically as $\underline{F_{ext}}$. Here an underline is used to emphasize the vector interpretation.

$$M\underline{\ddot{x}} + C\underline{\dot{x}} + K\underline{x} + \sum_{i=1}^{m} f_i \underline{b_i} = \underline{F_{ext}} \tag{3.1}$$

Where $\underline{b_i}$ is defined such that $\underline{b_i}^T \underline{x}$ is the relative displacement of the i^{th} friction damper and f_i is the friction force in the i^{th} damper.

A variety of approaches have been proposed in the literature for the control of semi-active devices. In developing the control laws, it is to be noted that it is possible to directly command the i^{th} friction damper to generate a specified force f_i which is not possible with other semi-active dampers such as MR and ER dampers because their damper response is dependent on the local motion of the structure where damper is attached. In some cases it is possible to employ Lyapunov's direct approach to stability analysis in the design of

a feedback controller. The approach requires the use of a Lyapunov function, denoted by $V(\underline{x}, \underline{\dot{x}})$, which must be a positive definite function of the states of the system, $\underline{x}$ and $\underline{\dot{x}}$. Assuming that the origin is a stable equilibrium point, according to Lyapunov's stability theory, if the rate of change of the Lyapunov function, $\dot{V}$ is negative semi-definite , the origin is stable in the sense of Lyapunov. Thus in developing the control law, the goal is to choose control inputs for each device that will result in making $\dot{V}$as negative as possible. An infinite number of Lyapunov functions may be selected, that may result in a variety of control laws. In this approach, the Lyapunov function is chosen to represent the total mechanical energy in the structure, as in

$$V = \frac{1}{2}\underline{x}^T K \underline{x} + \frac{1}{2}\dot{\underline{x}}^T M \underline{\dot{x}} \tag{3.2}$$

The rate of change of energy of the system is given by time derivative of this Lyapunov function, given as

$$\dot{V} = \underline{\dot{x}}^T \left(K\underline{x} + M\underline{\ddot{x}}\right) \tag{3.3}$$

Substituting from Eq. (3.1), one obtains

$$\dot{V} = \underline{\dot{x}}^T \left(\underline{F_{ext}} - C\underline{\dot{x}} - \sum_{i=1}^{m} f_i \underline{b_i}\right) \tag{3.4}$$

Only the last term containing the normal force can be controlled and is the term of interest for optimized energy dissipation control. Thus

$$\dot{V}_d = -\underline{\dot{x}}^T \sum_{i=1}^{m} f_i \underline{b_i} \tag{3.5}$$

In terms of Coulomb's law, friction force can be expressed as

$$f_i = \begin{cases} \mu N_i \operatorname{sgn}(v_i) & \text{if } v_i \neq 0 \\ f_{i_a} & \text{if } v_i = 0 \text{ and } \ |f_{i_a}| < \mu N_i \\ \mu N_i \operatorname{sgn}(f_{i_a}) & \text{otherwise} \end{cases} \tag{3.6}$$

where f_{i_a} is the applied force on the frictional interface and the sliding velocity v_i at i^{th} damper is given by $\underline{b_i}^T \underline{\dot{x}}$.

Substituting Eq. 3.6 into Eq. 3.5

$$\dot{V}_d = -\mu \underline{N}^T \, |\underline{v}| \tag{3.7}$$

The dissipative nature of frictional forces can be observed from the above equation. To maximize this function with respect to normal load $\underline{N}$, one arrive at the control law

$$\underline{N} = \begin{cases} \underline{N}_{\max} & \text{if } \underline{v} \neq \underline{0} \\ \underline{0} & \text{if } \underline{v} = \underline{0} \end{cases} \tag{3.8}$$

The resulting control law will command the maximum voltage when relative velocity is such that energy is being dissipated (producing large dissipative forces), and command the minimum voltage when energy is not being dissipated. This algorithm is classified as the bang-bang controller and is dependent on the states of the system.

3.1.2 Selective Damping

For cases where stability of the system is of concern and affected by certain modes of the system that tend to go unstable, an intelligent approach is to identify the contributing modes in the system response and subsequently damp out the unstable ones. The mode selection can be done by studying the frequency response of the system. The advantages of selective damping are two-fold. Firstly, the amount of power consumption is less since fewer and required-only modes are damped out. Secondly, in the absence of unstable modes, unwanted loading on parts of the system by the damper, often a cause of fatigue, is removed. In particular, wear and tear of the parts and heat generation due to unnecessary frictional resistance could be avoided.

3.1.3 Viscous Damping

It has been observed that for high contact pressure and slow sliding speed at the frictional interface, classic Coulomb friction is unable to predict the stick-slip behavior. The bang-bang controller developed above thus, would cause damper to stick without dissipating energy in the case of low-level excitation. To improve the energy dissipation of a friction

damper it seems natural to decrease the slip force with decreasing slip velocity and vice-versa. The velocity proportional controller $N = k\,|v|$ prevent the damper from sticking and produces response resembling a linear viscous damper.

3.1.4 Results

As seen from above relations, a semi-active control law based on the Coulomb friction law is quite straightforward. To further augment the damping law with selective damping characteristics, the response of the system is studied with respect to different damping techniques and compared in this section.

The motion of a system consisting of two modes with different frequencies, one of which has to be suppressed, is considered. The frequency of the lower frequency mode is assumed to be of 0.33 magnitude while its amplitude is taken to be of unit magnitude. The amplitude and frequency of the higher frequency mode are assigned to be 10 times and 3 times larger than the respective quantities of the lower frequency mode. The friction damper characteristics consist of friction coefficient of magnitude 0.3 and normal load of unit magnitude. The case is quite similar to the observed lag motion of rotor blades which contains regressive lag mode, the primary cause of instability and modes with integer multiple of the rotor speed (n P). In order to distinguish between different modes, naming convention of 'l' mode and 'p' mode is used to refer to lower and higher frequency mode, respectively. The objective is to damp out the lower frequency mode. The system response is assumed to remain unchanged throughout the time of consideration, and the effectiveness of each damping strategy is evaluated based on amount of work performed.

The time rate of response denoted by v can be separated for the two modes as

$$v = v_l + v_p \tag{3.9}$$

The velocity of the total response and that of individual modes is shown in Figure 3.1. Assuming system response remains unchanged, total instantaneous power as well as work performed by the damper can be evaluated as

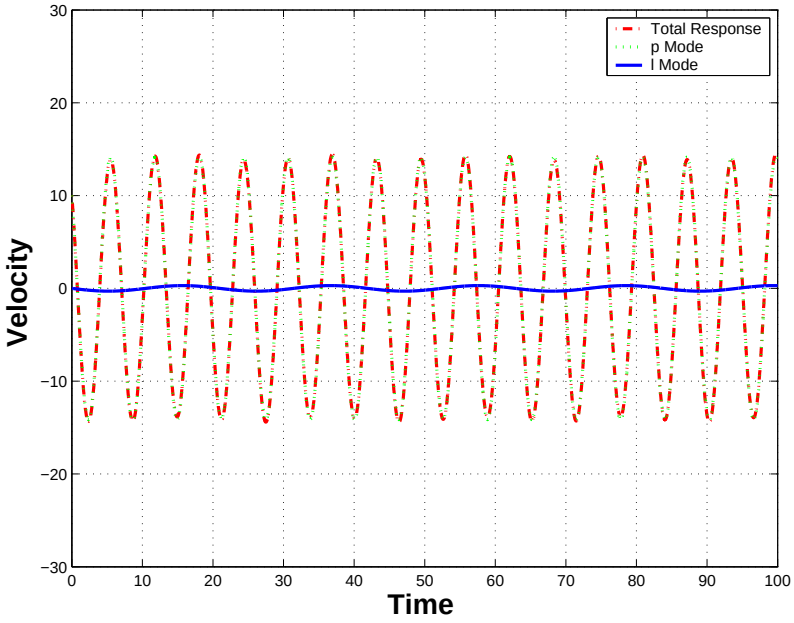

Figure 3.1: Response velocity variation

$$P = -\mu N \left| v \right| \tag{3.10}$$

$$W = \int_0^t P dt \tag{3.11}$$

The instantaneous power spent and work done by damper on each mode separately can be obtained as

$$\begin{aligned} P_l &= -\mu N v_l, \quad P_p = -\mu N v_p \qquad \text{if } v > 0 \\ P_l &= \quad \mu N v_l, \quad P_p = \quad \mu N v_p \qquad \text{if } v < 0 \end{aligned} \tag{3.12}$$

$$\begin{aligned} W_l &= \int_0^t P_l dt \\ W_p &= \int_0^t P_p dt \end{aligned} \tag{3.13}$$

3.1.4.1 Case 1: Friction force acts all the time

In this case, friction damper is active throughout the time for which system response is obtained. As quite expected, the damper behaves indiscriminately to any particular modal

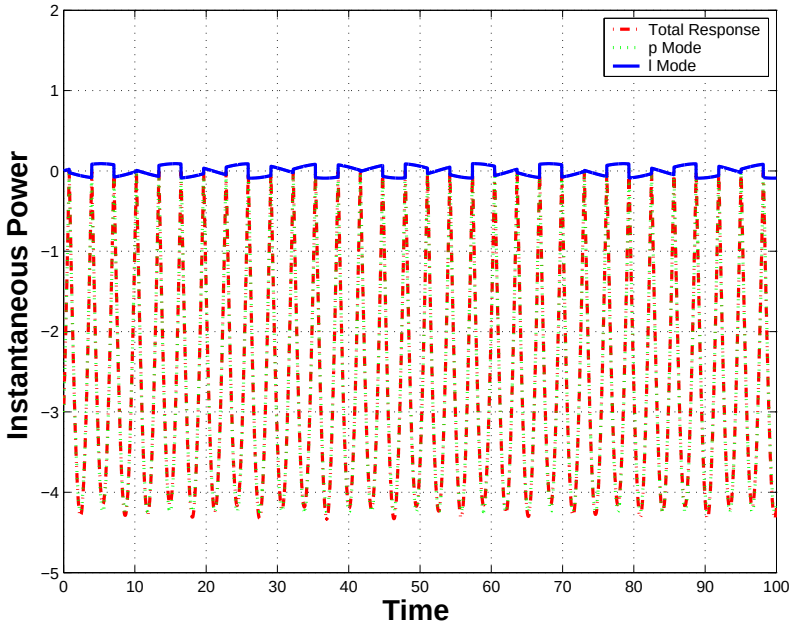

Figure 3.2: Instantaneous power variation for Case 1

component. Figure 3.2 depicts the instantaneous power supplied for the total response and the same for each mode separately. The work done by the damper in dissipating 'l' and 'p' mode is compared in Figure 3.3. The contribution of the damper in damping out the 'l' mode is negligible. A magnified plot for work done on 'l' mode is shown in 3.4. Friction, although dissipative overall, can be seen to actually return some of the stored energy to this mode at certain instants of time. The friction force variation is shown in Figure 3.5. The change in the direction of friction force with the change of sign of the total response velocity can be noticed.

3.1.4.2 Case 2: Friction force acts when velocity of 'l' mode is maximum

Friction damper acts whenever 'l' mode has maximum velocity. In order to specify a definite time range, a bandwidth of 20% of the half of time period about the maximum velocity amplitude point is chosen. The damper, thus, discriminates against the 'p' mode by operating only during the time when maximum energy in the 'l' mode will be dissipated. Figure 3.6 depicts total instantaneous power supplied and the same for each mode separately. The work done by the damper in dissipating 'l' and 'p' modes is compared in Figure 3.7. A magnified plot for work done on 'l' mode, shown in Figure 3.8, exhibits the inefficiency of

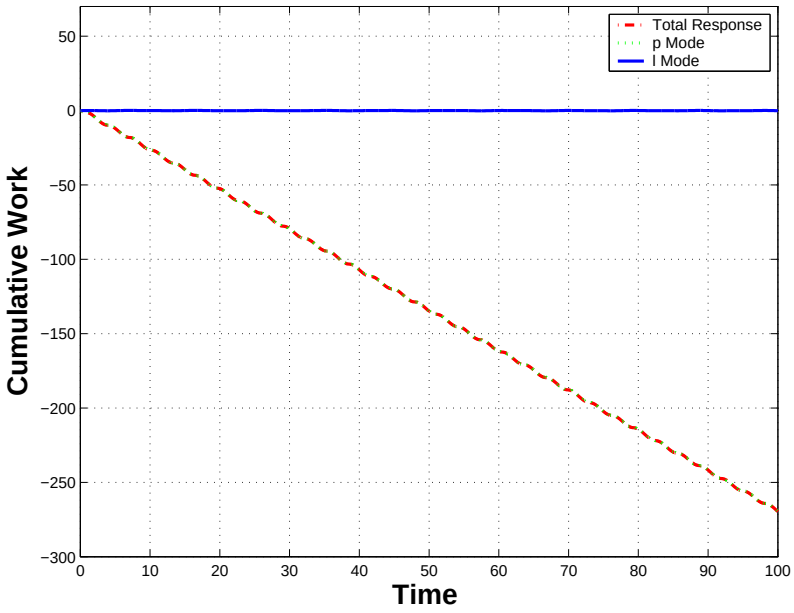

Figure 3.3: Work done for Case 1

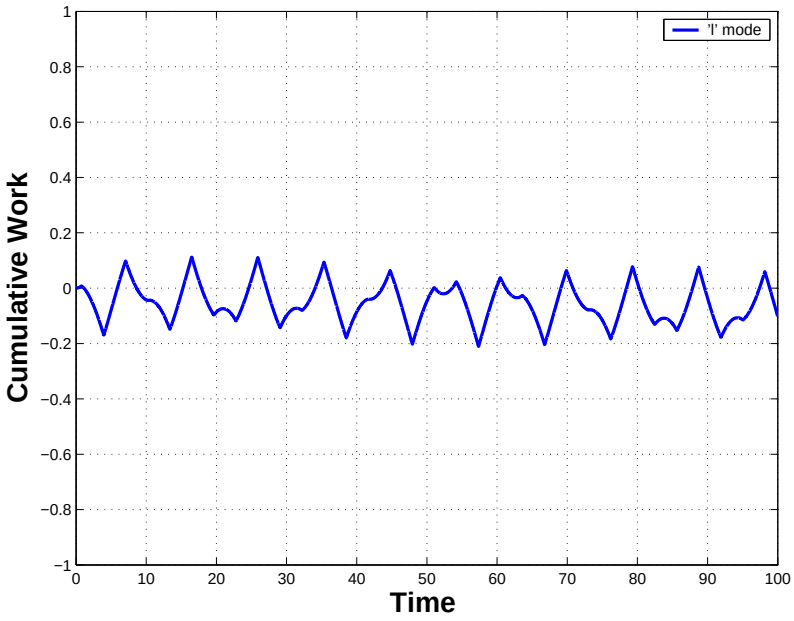

Figure 3.4: Work done on 'l' mode for Case 1

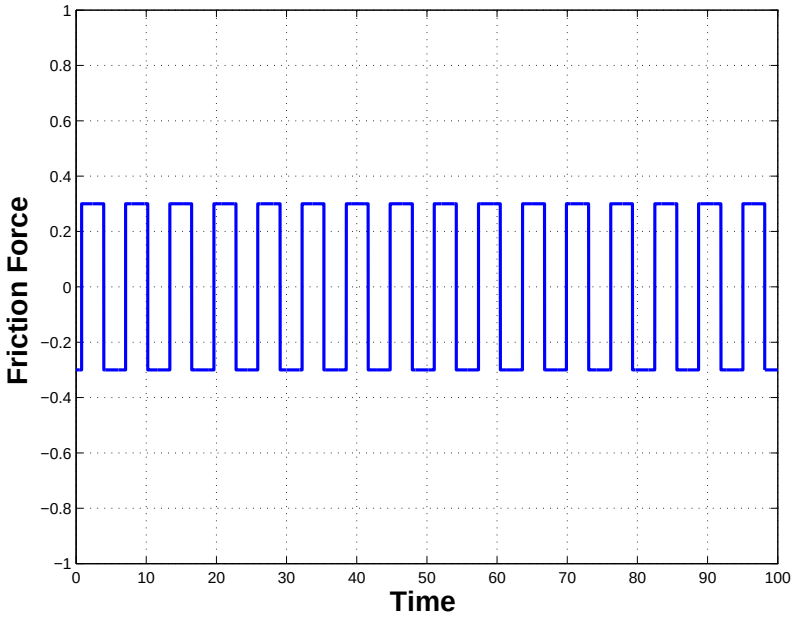

Figure 3.5: Friction force variation for Case 1

this control approach since the operation of the damper in fact returns some of the stored energy to the 'l' mode during some of its selected operation intervals. The response is attributed to the fact that at certain instants, although maximum, 'l' mode velocity direction is opposite to that of the total response velocity. The damper operation can be observed from the friction force variation plot in Figure 3.9.

3.1.4.3 Case 3: Friction force acts when velocity of the response is in same direction as 'l' mode

In this case, the friction damper acts whenever the total response velocity is in the same direction as that of 'l' mode alone. Figure 3.10 shows instantaneous power supplied for dissipation of each mode separately. The comparison of the plot with Figure 3.13 reveals that the damper is active only during the time when the 'l' mode velocity is in the same direction as total response velocity. The work done by the damper in dissipating 'l' and 'p' mode is shown in Figure 3.11. Although negligible compared to the total dissipation, the damping of 'l' mode can be observed from plot in Figure 3.12 to be significant as compared to previous case. A comparison with the plot in Case 1 reveals that selective damping can be achieved by using the present control law.

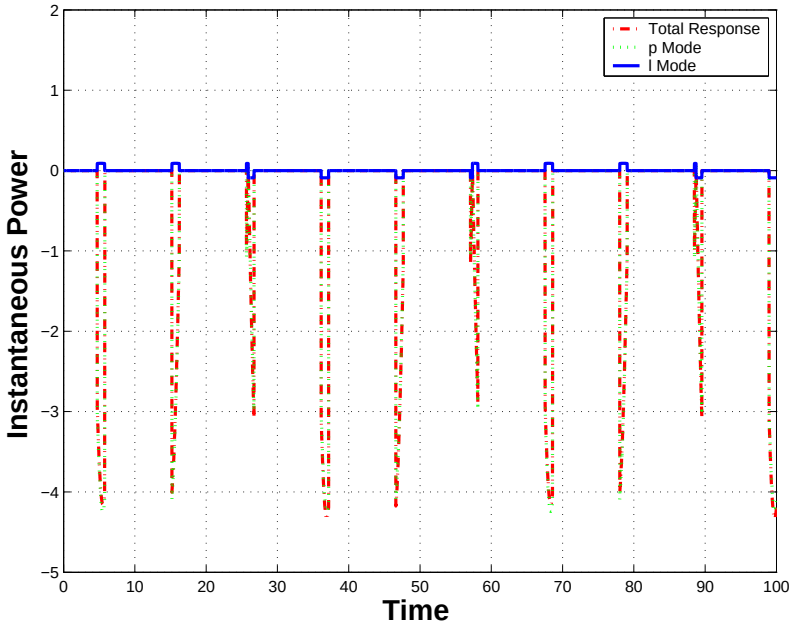

Figure 3.6: Instantaneous power variation for Case 2

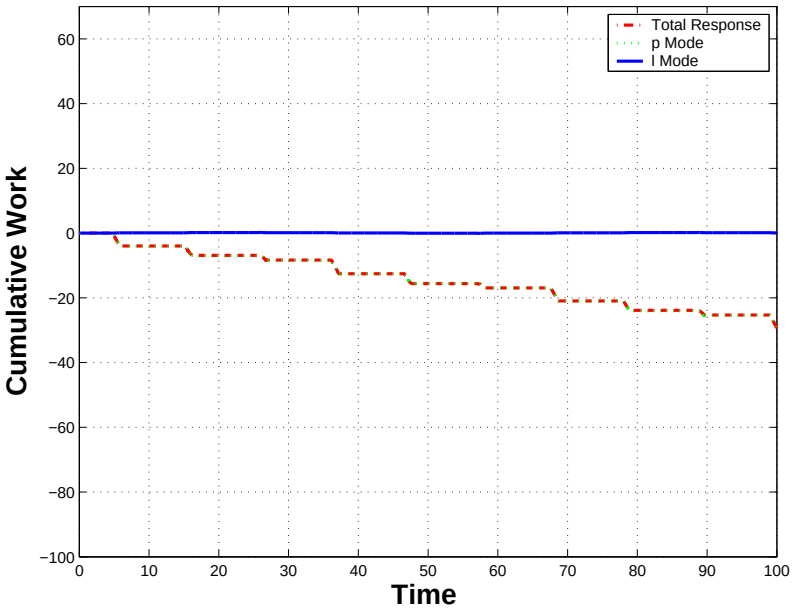

Figure 3.7: Work done for Case 2

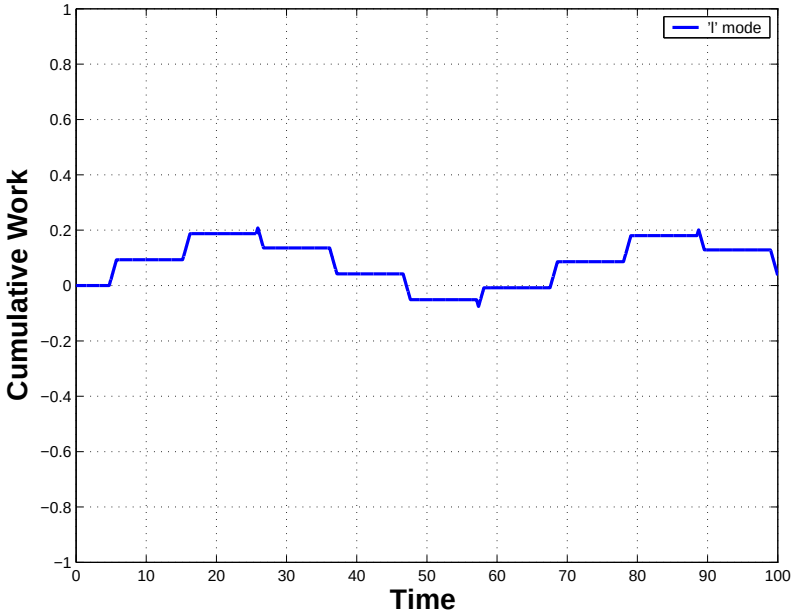

Figure 3.8: Work done on 'l' mode for Case 2

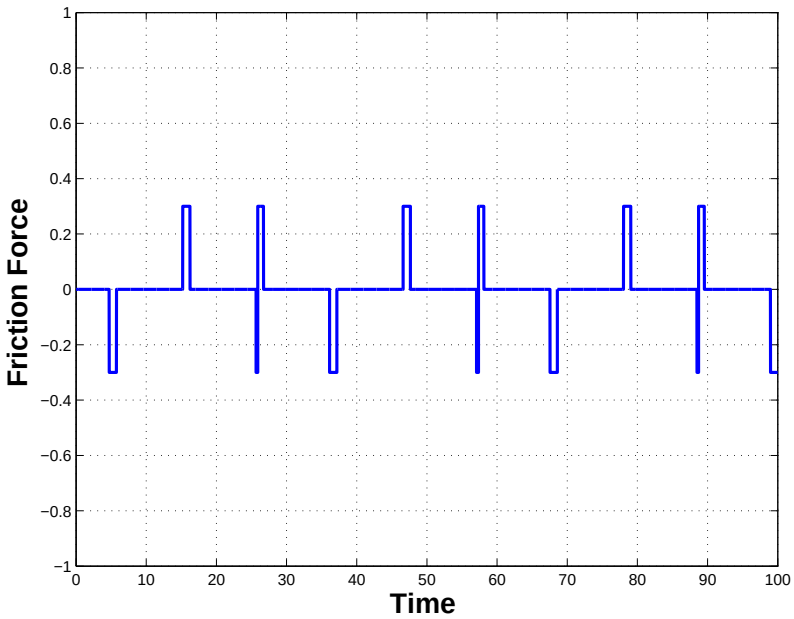

Figure 3.9: Friction force variation for Case 2

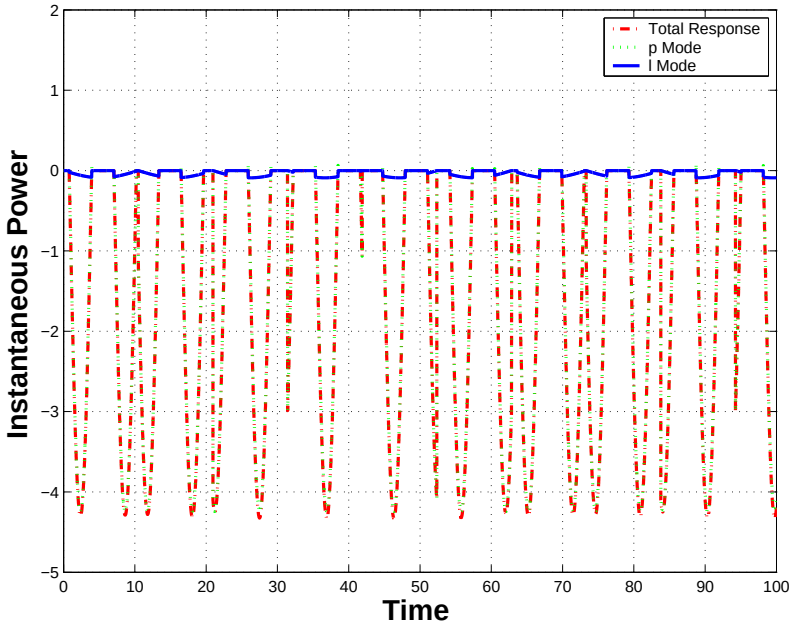

Figure 3.10: Instantaneous power variation for Case 3

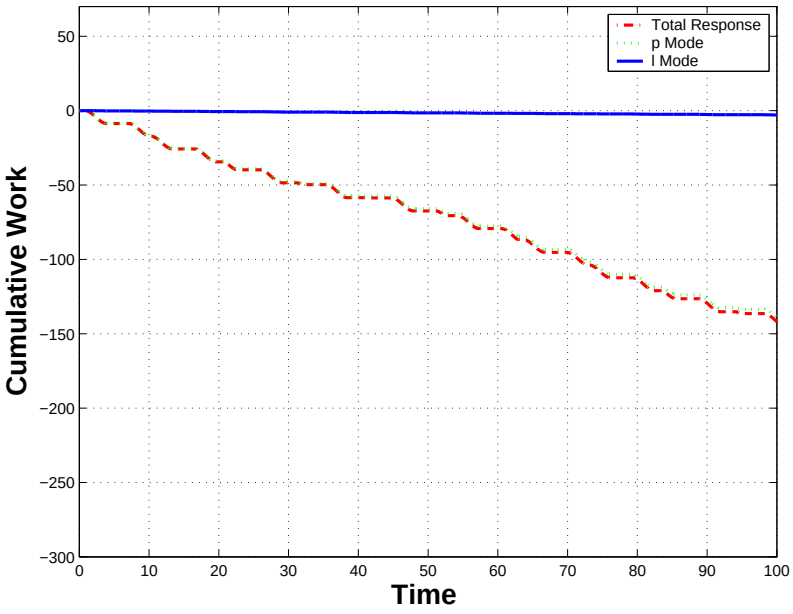

Figure 3.11: Work done for Case 3

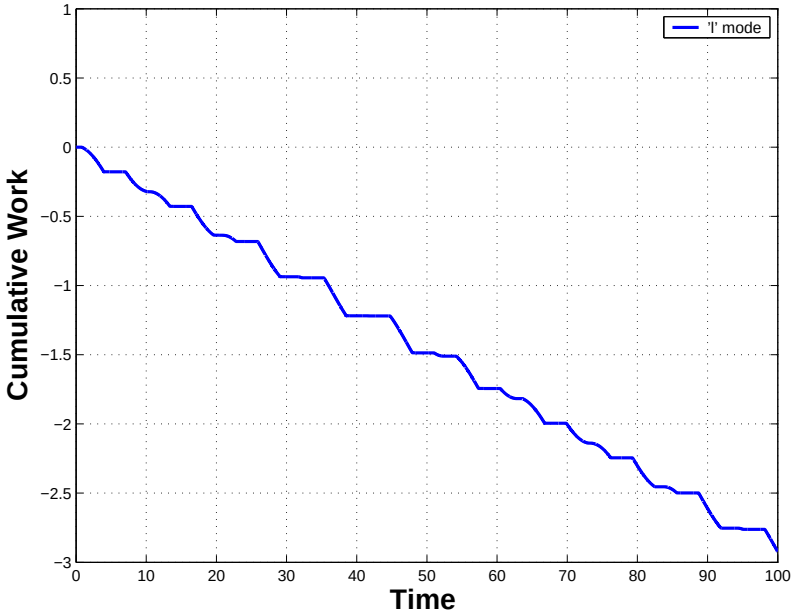

Figure 3.12: Work done on 'l' mode for Case 3

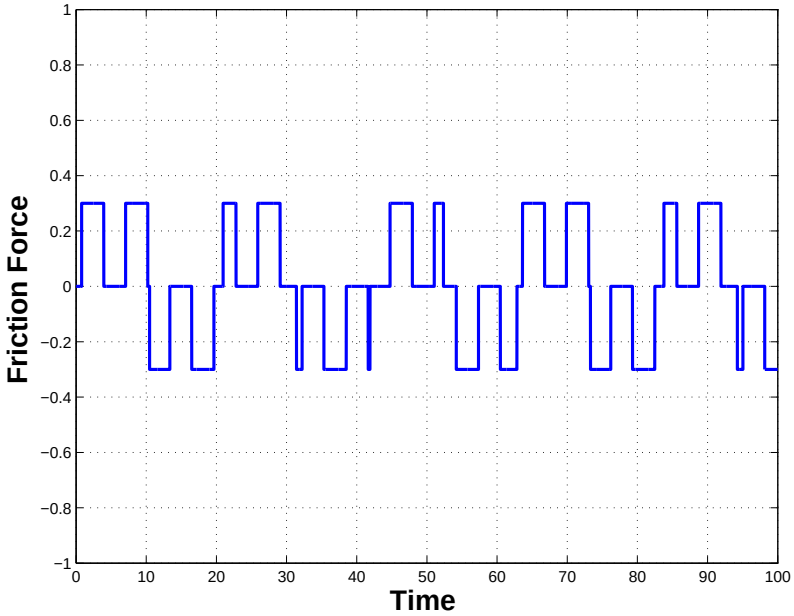

Figure 3.13: Friction force variation for Case 3

3.1.4.4 *Case 4: Friction force acts when velocity of 'l' mode is maximum and has same direction as total velocity of response*

Based on the performance of the control approach in Case 3, Cases 2 and 3 are combined together in the present approach. The algorithm is highly selective in the sense that damper operation intervals are chosen from those of Case 3 with 'l' mode velocity high (in a certain time range around the maximum) as well. The outcome is less damping for the 'p' mode as can be observed from instantaneous power supplied and work done plots (Figure 3.14, 3.15, 3.16). The two conditions, velocity of the 'l' mode being maximum and having same sign as that of total velocity, may not occur together. Their frequency of occurring together is dependent on the frequency of 'l' mode and its contribution in the response of the system represented by the amplitude. As a result, absolute damping of the 'l' mode is significantly less as compared to previous case.

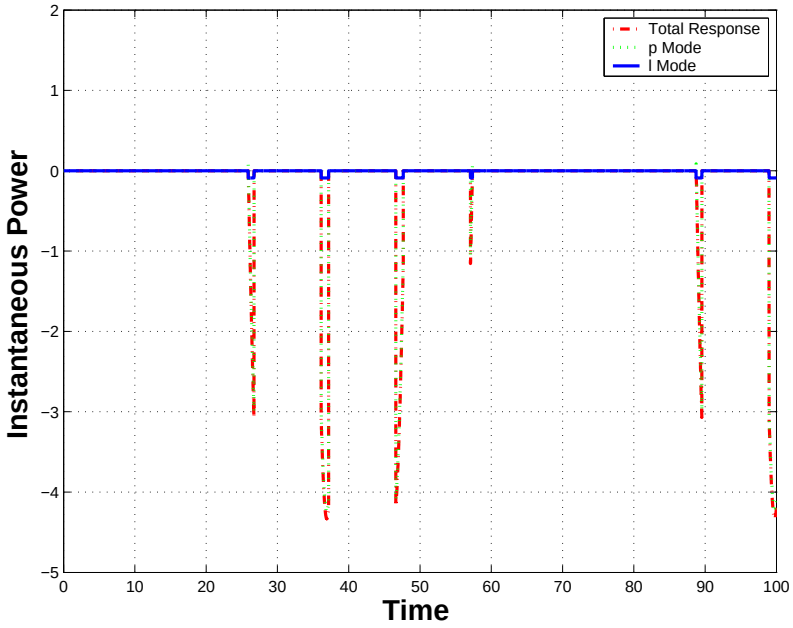

Figure 3.14: Instantaneous power variation for Case 4

3.1.4.5 *Case 5: Friction force acts when velocity of 'l' mode has same direction as total velocity of response and normal force is proportional to 'l' mode velocity*

In this mode, viscous type damping is introduced by making friction force proportional to the velocity of the response. In addition, damper acts only when total velocity and 'l'

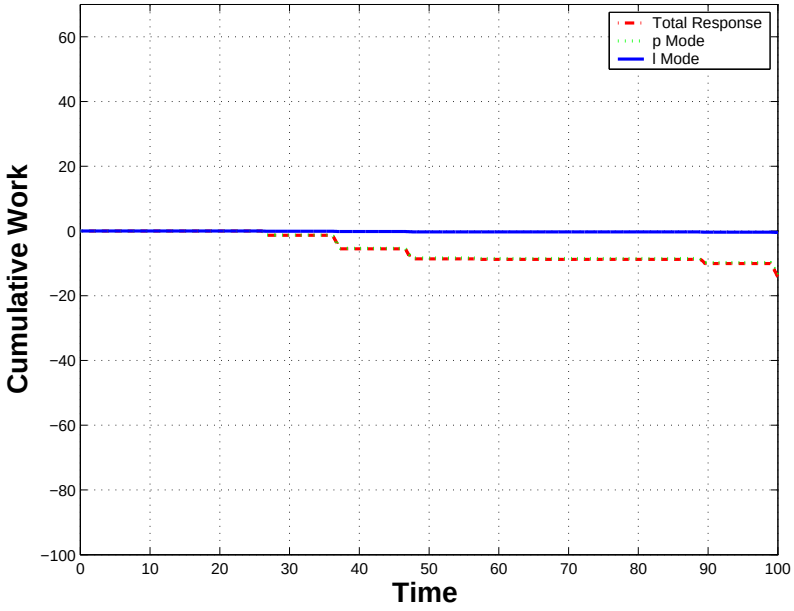

Figure 3.15: Work done for Case 4

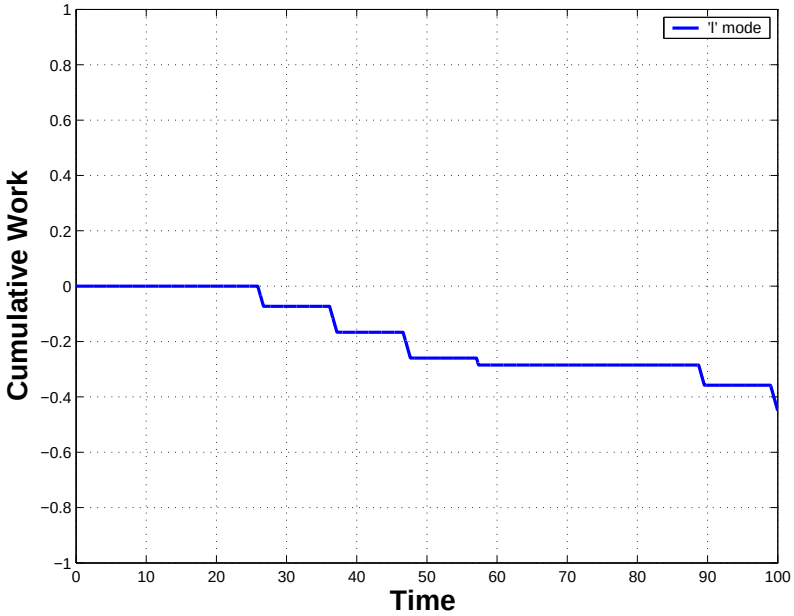

Figure 3.16: Work done on 'l' mode for Case 4

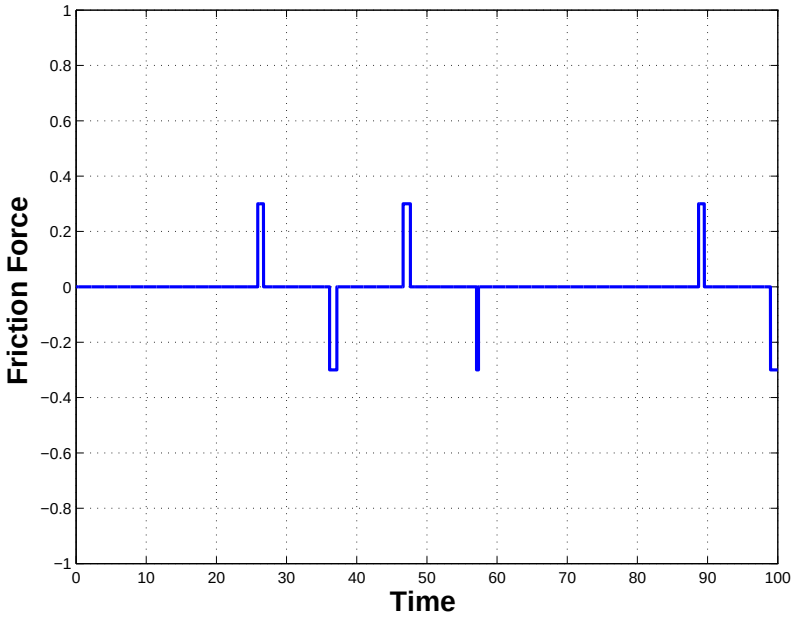

Figure 3.17: Friction force variation for Case 4

mode velocity have the same direction. The control law in Case 3 is modified by specifying the normal force as $N = \left(\frac{N_{\max}}{v_{\max}}\right) v_l$ where N_{max} is set to unity. The instantaneous power supplied for the 'l' mode damping as shown in Figure 3.18 is almost of the same pattern as in Case 3. As a result, the amount of work done to damp out 'l' mode as shown in Figure 3.20 is similar to the corresponding plot in Case 3. The work done by the damper in dissipating energy of the 'p' mode shown in Figure 3.19 can be seen to be relatively lower than the one in Case 3. The viscous type behavior of friction force can be observed from Figure 3.21

The last three cases are compared for their efficiency in implementing selective damping. The comparison is shown in Table 3.1. From the standpoint of selective damping, Case 4 gives the best performance since it results in the largest percentage of work performed on the 'l' mode. However, absolute amount of work done on the same mode is significantly less compared to other cases. Case 3 results in maximum amount of work performed on the 'l' mode. Case 5 gives a compromise performance between Case 3 and Case 4 in the sense that work done on dissipating energies of other modes is less while comparable amount of work is done on the 'l' mode.

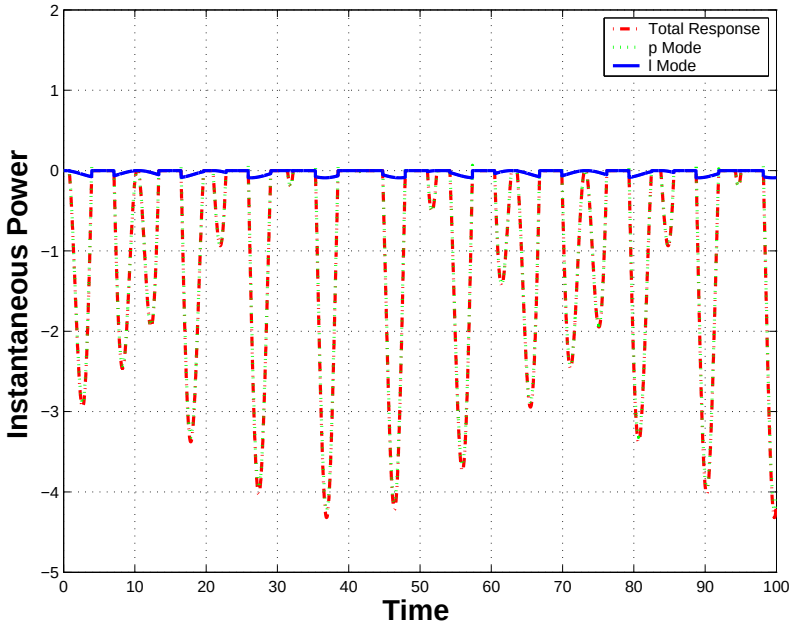

Figure 3.18: Instantaneous power variation for Case 5

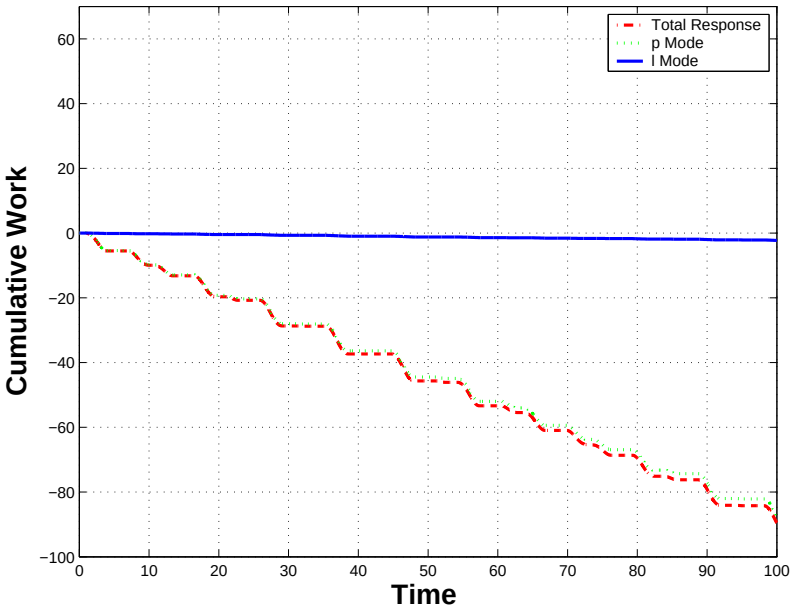

Figure 3.19: Work done for Case 5

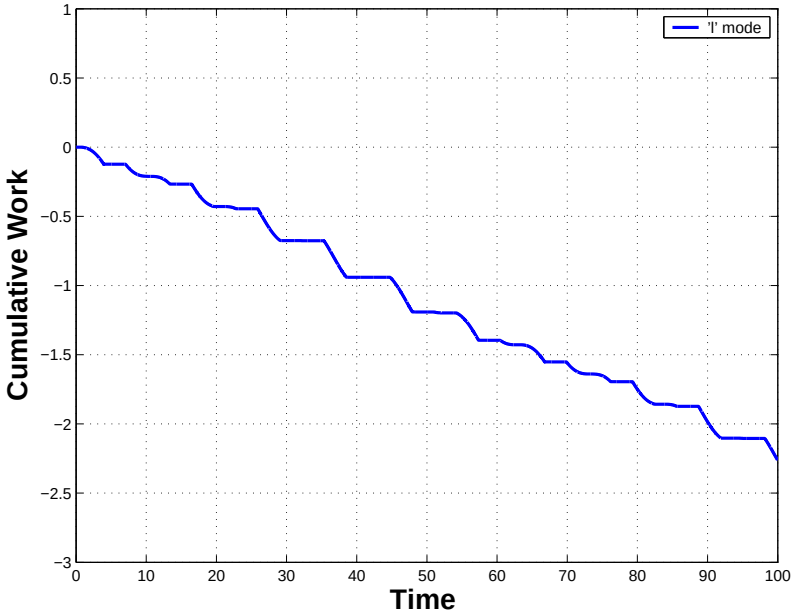

Figure 3.20: Work done on 'l' mode for Case 5

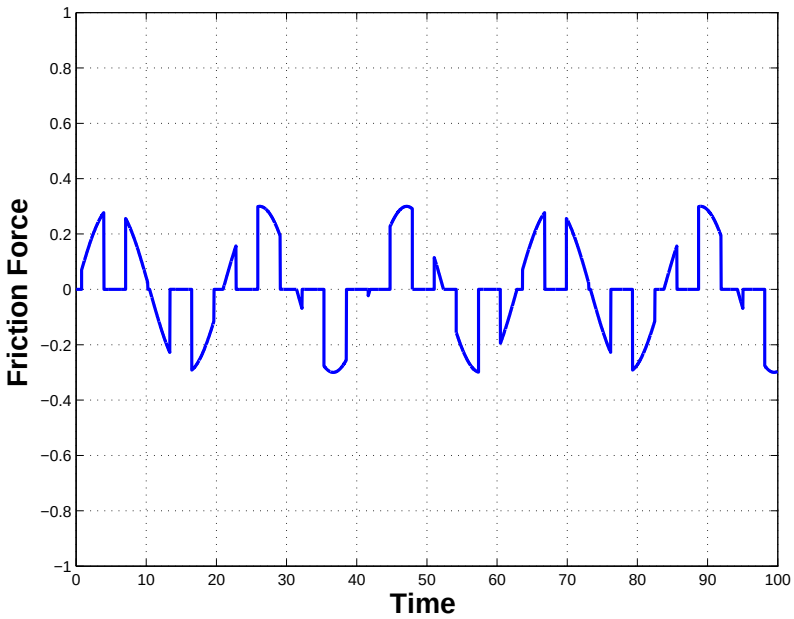

Figure 3.21: Friction force variation for Case 5

Table 3.1: Comparison of selective damping control techniques

	Work done on 'l' mode	**Work done on 'p' mode**	**% of Work done on 'l'mode**
Case 3	2.923	138.994	2.060
Case 4	0.450	13.762	3.169
Case 5	2.264	87.354	2.526

CHAPTER IV

GROUND RESONANCE ANALYSIS

Ground resonance is a dynamic instability involving the coupling of blade lag motion with the in-plane motion of the rotor hub. This instability is characterized by resonance of the frequency of the rotor lag motion (specifically the low frequency lag mode in the nonrotating frame) with the natural frequency of the structure supporting the rotor. Since the lag frequency depends on the rotor rotational speed, such resonances define certain critical speed ranges for the rotor. An instability is possible at a resonance if the rotating lag frequency v_ζ is below 1/rev, as seen in the articulated and soft in-plane hingeless rotors. The critical mode is usually an oscillation of the helicopter on the landing gear when in contact with the ground, hence the name ground resonance.

The hub in-plane motions are coupled with the cyclic lag modes ζ_c and ζ_s, which correspond to the lateral and longitudinal shifts of the net rotor center of gravity from the center of rotation. Since the low frequency lag mode involves whirling of the rotor center of gravity about the shaft, ground resonance is potentially very destructive; hence avoiding this instability is an important consideration in helicopter design.

The classic ground resonance analysis considers four degrees of freedom: longitudinal and lateral in-plane motion of the rotor hub, and the two cyclic lag degrees of freedom. The actual vibration modes of the rotor support, such as motion of the helicopter on its landing gear, involves the tilt of the shaft as well, but it is the in-plane motion of the hub that is the dominant factor in ground resonance. The rotor aerodynamic forces have little influence on ground resonance, compared to the structural and inertial forces.

In this chapter, ground resonance analysis is performed based on the classical model.

An equivalent spring-mass-damper model of rotor-fuselage is described in Section 4.1. Generally, the model in the nonrotating frame of reference is sufficient to assess the stability of the system. The proposed work involves a friction damper, and as a result, there is high nonlinearity associated with the damping terms. It is not possible to transform the system dynamics to the nonrotating frame without involving terms from the rotating frame. The system equations are derived in the nonrotating frame for the rotor with no lag damper and later in the blade reference system in Section 4.2 for the same system with friction based lag damper. Different control algorithms are applied to study the effectiveness of the selective damping in Section 4.3

4.1 Ground Resonance Model

It is always desirable to select a simplified model in a study that can impart reasonable understanding of the phenomenon. The classical ground resonance model considers four degrees of freedom: longitudinal and lateral in-plane motion of the rotor hub and two cyclic lag degrees of freedom of the rotor blade. The rotor aerodynamic force is neglected in the analysis because it has little influence on ground resonance compared to structural and inertial forces. A simplified schematic model of the helicopter considered for numerical studies is shown in Figure 4.1. The analysis examines a rotor having four identical rigid blades attached to the fuselage which itself is modeled as an equivalent spring-mass-damper system located at the hub center. A single blade with the lag damper attachment is shown in Figure 4.2. Each blade has a lag hinge offset by a distance e from the center of rotation. A lead lag damper attachment is assumed to exists across the blade and lag hinge, whenever considered for analysis. The lateral and longitudinal equivalent mass (M_x, M_y), stiffness, (k_x, k_y) and damping (c_x, c_y) represent the in-plane lateral and longitudinal fuselage mode characteristics. The rigid blades undergo lag motions, represented by the lead-lag displacement variable ϕ_k for k^{th} blade. The mathematical model for the analysis is derived in Appendix A under the assumptions of small lag motion.

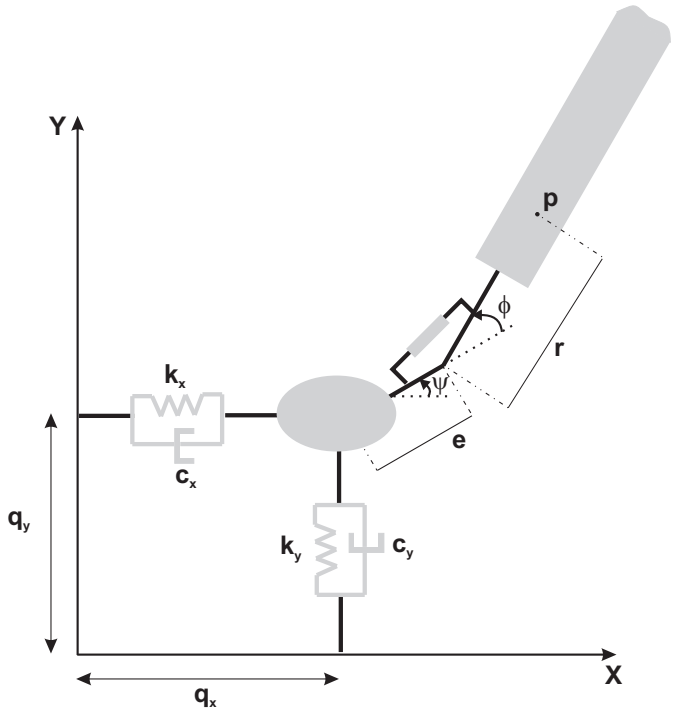

Figure 4.1: Ground resonance spring-mass-damper model

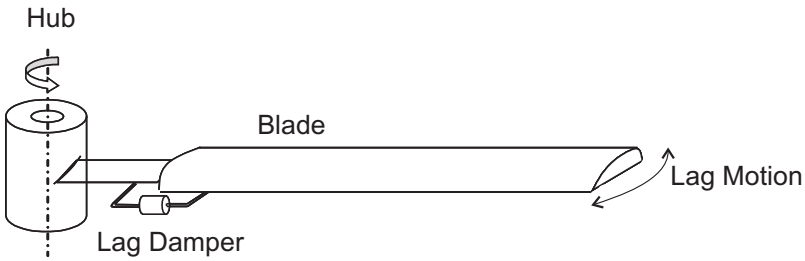

Figure 4.2: Rotor blade with lag damper attached

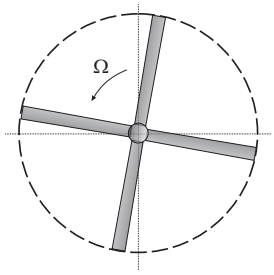

Figure 4.3: Rotor collective lag mode

4.2 Non-Rotating Reference Frame

The rotor equations in the rotating frame describe the motion of each blade separately, while those in the nonrotating frame describe the motion of the rotor as a whole. For the stability analysis of the coupled rotor/body motion, the blade equations are generally analyzed in the nonrotating frame. This can be achieved using multiblade coordinate transformations, which move the differential equations from the rotating to the nonrotating frame. A N bladed rotor has N modes in the fixed frame. For the four bladed rotor, the modes correspond to a collective mode, a differential mode and two cyclic modes which are depicted in Figures 4.3-4.6. All the blades oscillate in phase and with equal amplitude in the collective mode. While alternate blades move out of phase, though with the same amplitude in differential mode, also referred as scissors mode, the last two modes of rotor involve the motion of one set of diametrically opposite blades either leading or lagging that of the other set of diametrically opposite blades by a phase of 90 degrees. The low and high frequency cyclic rotor modes are also termed as rotor regressive and progressive modes respectively since the speed of center of gravity rotation is always lower and higher than the rotor speed in the respective modes. The equations of motion of a four bladed rotor for the coupled fuselage and rotor motion are derived in section A.1 of Appendix A. In the absence of damping of any sort for the fuselage and lag motion, equations can be rewritten as

$$\frac{d^2\bar{q}_x}{d\tau^2} - \frac{\bar{S}_\zeta}{2\bar{M}_x}\frac{d^2\zeta_s}{d\tau^2} + \frac{\omega_x^2}{\Omega^2}\bar{q}_x = 0 \tag{4.1}$$

$$\frac{d^2\bar{q}_y}{d\tau^2} + \frac{\bar{S}_\zeta}{2\bar{M}_y}\frac{d^2\zeta_c}{d\tau^2} + \frac{\omega_y^2}{\Omega^2}\bar{q}_y = 0 \tag{4.2}$$

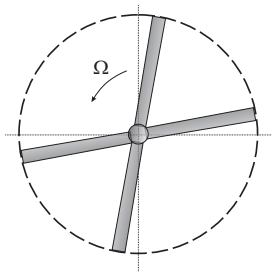

Figure 4.4: Rotor differential lag mode

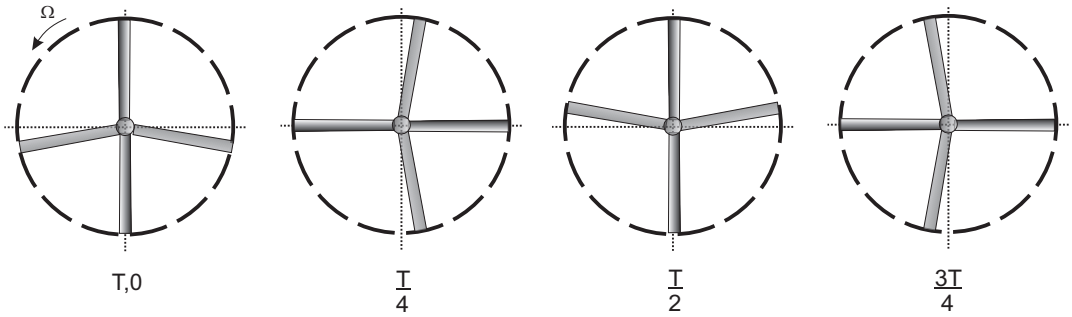

Figure 4.5: Rotor progressive lag mode

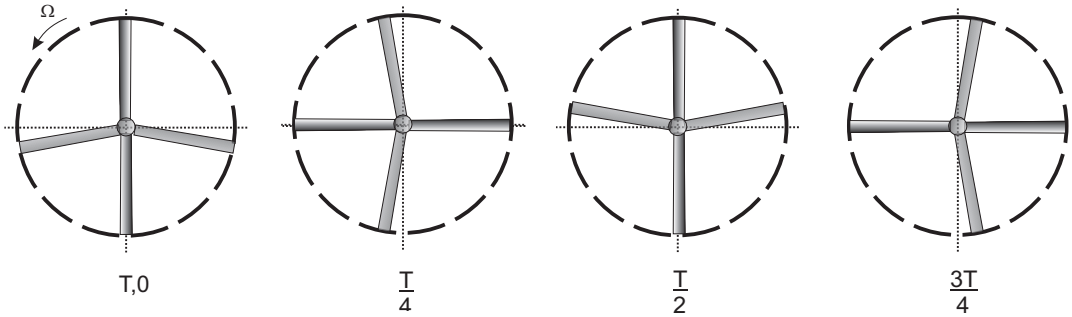

Figure 4.6: Rotor regressive lag mode

$$\frac{d^2\zeta_0}{d\tau^2} + v_\zeta^2\zeta_0 = 0 \tag{4.3}$$

$$\frac{d^2\zeta_E}{d\tau^2} + v_\zeta^2\zeta_E = 0 \tag{4.4}$$

$$\frac{d^2\zeta_s}{d\tau^2} - 2\frac{d\zeta_c}{d\tau} - \bar{S}_\zeta\frac{d^2\bar{q}_x}{d\tau^2} + \left(v_\zeta^2 - 1\right)\zeta_s = 0 \tag{4.5}$$

$$\frac{d^2\zeta_c}{d\tau^2} + 2\frac{d\zeta_s}{d\tau} + \bar{S}_\zeta\frac{d^2\bar{q}_y}{d\tau^2} + \left(v_\zeta^2 - 1\right)\zeta_c = 0 \tag{4.6}$$

The uncoupled dynamics of rotor and hub is studied by setting $\bar{S}_\zeta$ equal to zero. The uncoupled hub motion consists of pure harmonic oscillations with natural frequencies ω_x and ω_y as noticeable from Equations 4.1 and 4.2. The collective and differential lag modes, dynamics of which are given by Equations 4.3 and 4.4, are non-reactive modes and their frequency is independent of fuselage effects. The uncoupled (i.e., shaft-fixed) cyclic lag motion, without any sort of structural, aerodynamic, or mechanical damping, is a pure oscillation as well with frequencies $|1 \pm v_\zeta|$. The cyclic lag motion is represented by components ζ_s and ζ_c whose dynamics are given by Equations 4.5 and 4.6. The high frequency lag mode corresponds to a progressive whirling motion of the center of gravity at frequency $1 + v_\zeta$. For a stiff in-plane hingeless rotor ($v_\zeta > 1/rev$), the low frequency lag mode is a regressive whirling motion of the center of gravity at frequency $v_\zeta - 1$, while for an articulated rotor, $v_\zeta < 1/rev$, and the low frequency lag mode is a progressive whirling mode of the center of gravity at frequency $1 - v_\zeta$. The uncoupled rotor and support motion is stable and a ground resonance instability can only be due to the inertial coupling when $\bar{S}_\zeta \neq 0$.

The coupling of rotor and support exhibits an interesting variation of frequencies with rotor angular speed. At some rotor speed, the frequency of the rotor lag motion (specifically the low frequency lag mode) coalesces with the natural frequency of the supporting structure resulting in instability due to resonance of the modes. The ground resonance solution is generally presented graphically in a form known as a Coleman diagram, which is a plot

Table 4.1: Rotor and Fuselage characteristics

Dimensionalized Form	**Value**
Number of blades, N	4
Rotor radius, R	18.5 ft
Operational rotor speed, Ω_0	300 RPM
Blade mass, m	6.5 slugs
Blade mass moment, S	65.0 slug-ft
Blade mass moment of inertia, I	800.0 slug-ft^2
Lag hinge offset, e	1.0 ft
Lag spring, k_q	0.0 ft-lb/rad
Hub mass, M_x	550.0 slugs
Hub mass, M_y	225.0 slugs
Hub spring, k_x	85000.0 lb/ft
Hub spring, k_y	85000.0 lb/ft
Fuselage support frequency, ω_x	12.148 rad/s
Fuselage support frequency, ω_y	18.402 rad/s

of the full system modal frequencies referred to a fixed (inertial) system as a function of the rotor speed Ω. The Coleman diagram and the modal damping diagram together are used to characterize stability of a rotor/fuselage system. The system characteristics used for analysis is given in Table 4.1. The analysis assumes no damping associated with rotor or fuselage. The Coleman plot in Figure 4.7 presents the frequency variation of two fuselage modes and cyclic rotor modes with rotor speed. It is quite clear from the figure that while the progressive lag frequency is higher than those of fuselage modes, the regressive lag frequency becomes locked with the longitudinal fuselage mode first and, subsequently, with the lateral fuselage mode over a specific rotor speed range. The stability characteristics of the system is shown in Figure 4.8. The system becomes unstable whenever there is coalescence of the rotor low frequency mode with the fuselage modes and is identified from the negative value of the relative damping of the unstable modes, which indeed are the two fuselage modes. The amount of instability given by the magnitude of relative damping reaches a maximum at 0.8 relative rotor speed.

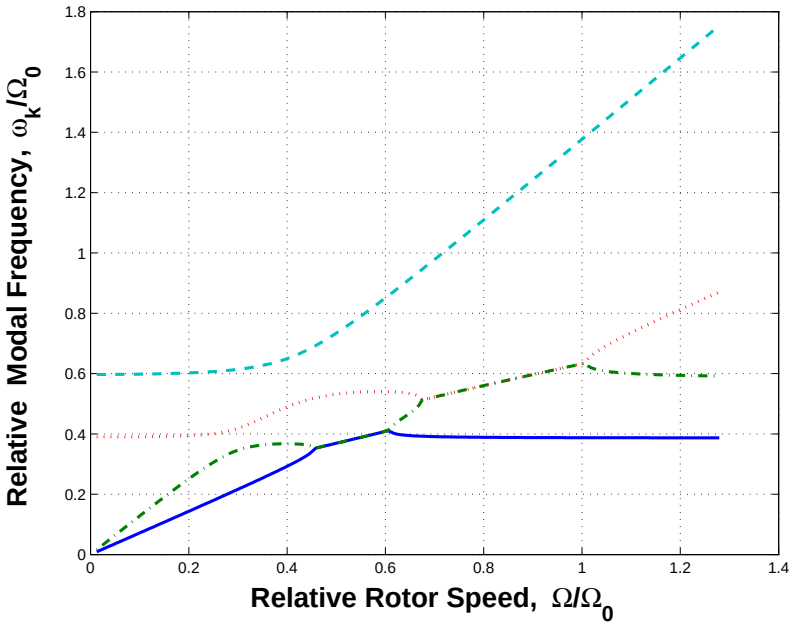

Figure 4.7: Coleman diagram for coupled motion - No damper

It is clear that dynamic instabilities occur as a result of coupling of the lag regressive mode and the fuselage motion. To alleviate these instabilities, most rotors are equipped with lag dampers. The landing gear components of fuselage have dampers as well for shock absorption. The system with linear viscous damping can be analyzed in a similar manner as above. The case with the presence of linear viscous dampers for support motion is considered next. The nondimensional damping coefficients are $\bar{c}_x = 0.1450$ and $\bar{c}_y = 0.1664$. The damping coefficients are nondimensionalized as follows:

$$\bar{c}_x = \frac{c_x}{(M_x + Nm)\,\Omega} \tag{4.7}$$

$$\bar{c}_y = \frac{c_y}{(M_y + Nm)\,\Omega} \tag{4.8}$$

The Coleman diagram is presented in Figure 4.9. A little increase in minimum damping of the regressive mode is obtained as shown in Figure 4.10. Although enhancing the stability of such a system, fuselage dampers are unable to stabilize ground resonance. The time response of rotor and fuselage modes, at the point of maximum instability, i.e., 0.8 relative

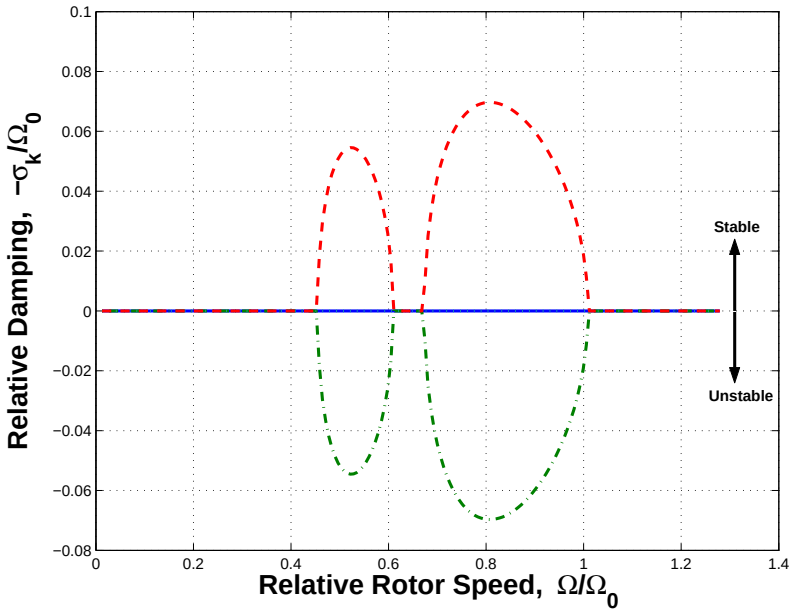

Figure 4.8: Stability characteristic diagram for coupled motion - No damper

rotor speed, is obtained in response to an initial perturbation. The longitudinal and lateral fuselage modes along with response of blade 1 are depicted in Figures 4.11-4.15. The collective and differential modes are non-reactive modes and do not grow with time, while the cyclic modes and fuselage modes go unbounded. The locus of the rotor center of mass is plotted in Figure 4.16. The x and y coordinates of the center of mass location are non-dimensionalized with respect to rotor radius.

In order to perform selective damping of the unstable modes, frequency analysis of the response leading to identification of unstable modes is necessary. The power spectral density (PSD) for rotor modes, normalized by its maximum amplitude, is obtained in the stable and unstable range . The relative rotor speed 0.2, corresponding to a stable point in the stability characteristics plot, is chosen. The frequency spectrum plots for the rotor modes in stable region are shown in Figures 4.17-4.20. The frequency analysis of the collective and the differential mode shows the presence of a single frequency close to v_ζ while that of the cyclic mode components a_1 and b_1 indicates the presence of two distinct frequencies which are close to $1 - v_\zeta$ and $1 + v_\zeta$, referred as the regressive and the progressive lag frequency respectively. Had there been no damping in the system, the frequency of each

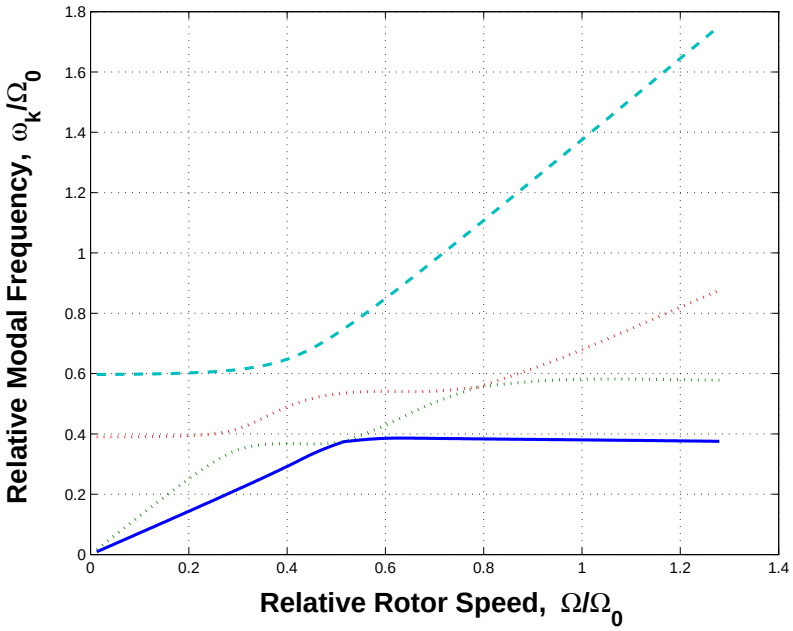

Figure 4.9: Coleman diagram for coupled motion - With fuselage damper

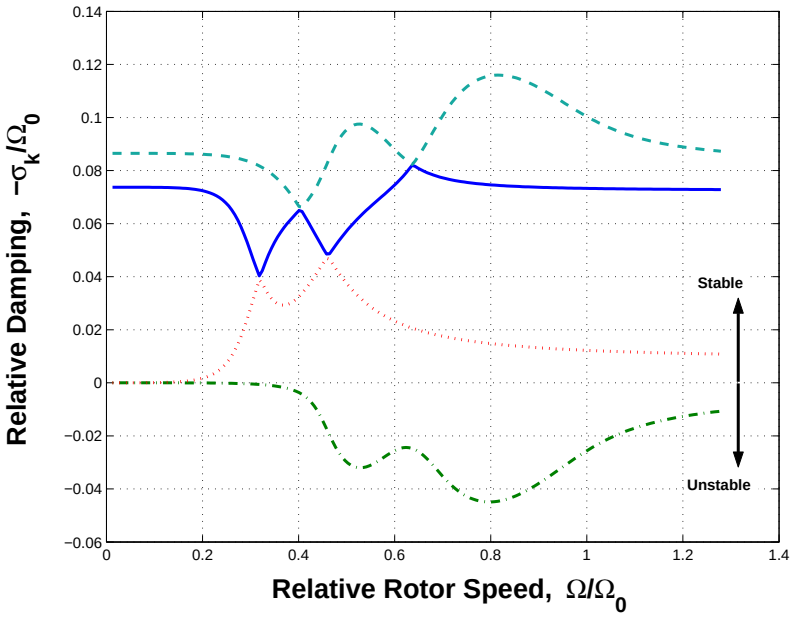

Figure 4.10: Stability characteristic diagram for coupled motion - With fuselage damper

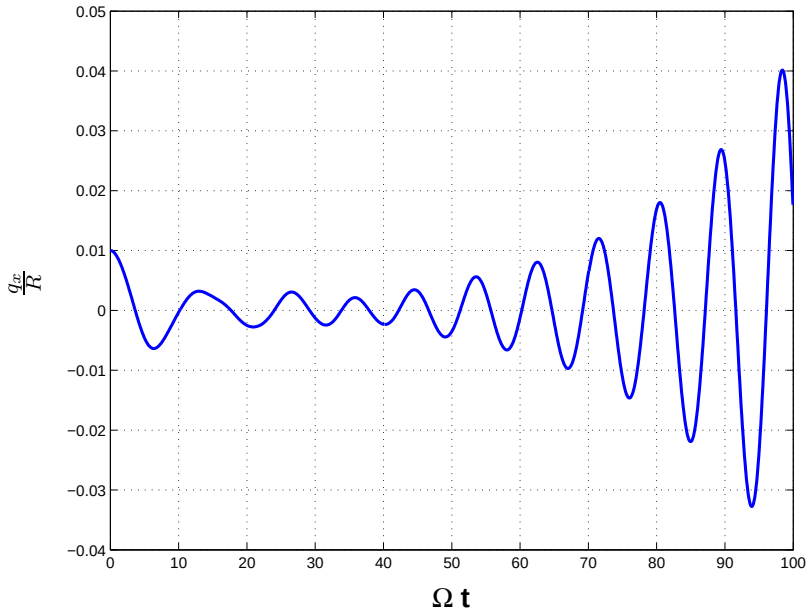

Figure 4.11: Fuselage motion in longitudinal direction at $\Omega/\Omega_0 = 0.8$

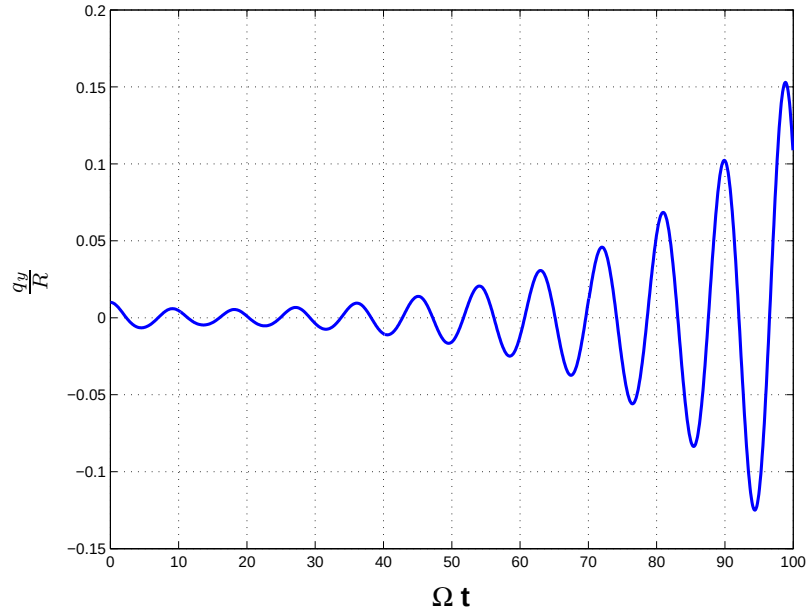

Figure 4.12: Fuselage motion in lateral direction at $\Omega/\Omega_0 = 0.8$

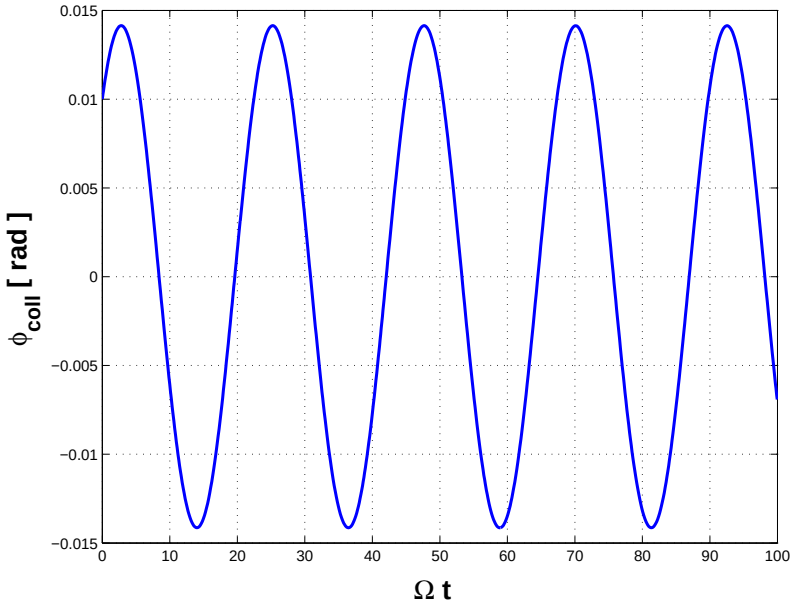

Figure 4.13: Rotor collective mode at $\Omega/\Omega_0 = 0.8$

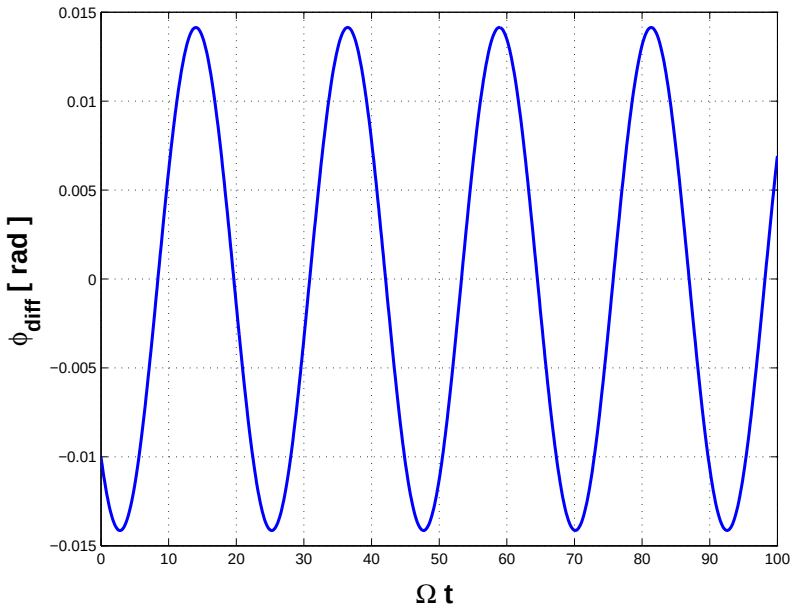

Figure 4.14: Blade 1 differential mode at $\Omega/\Omega_0 = 0.8$

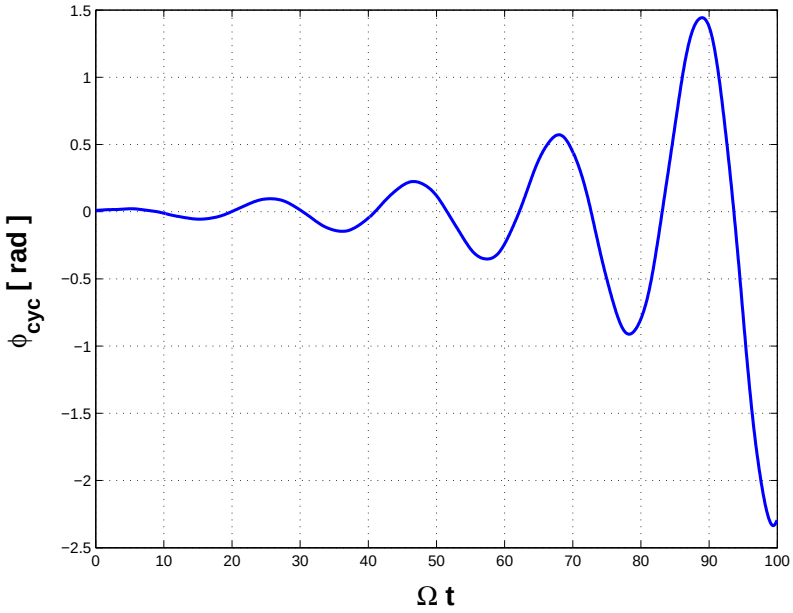

Figure 4.15: Blade 1 cyclic mode at $\Omega/\Omega_0 = 0.8$

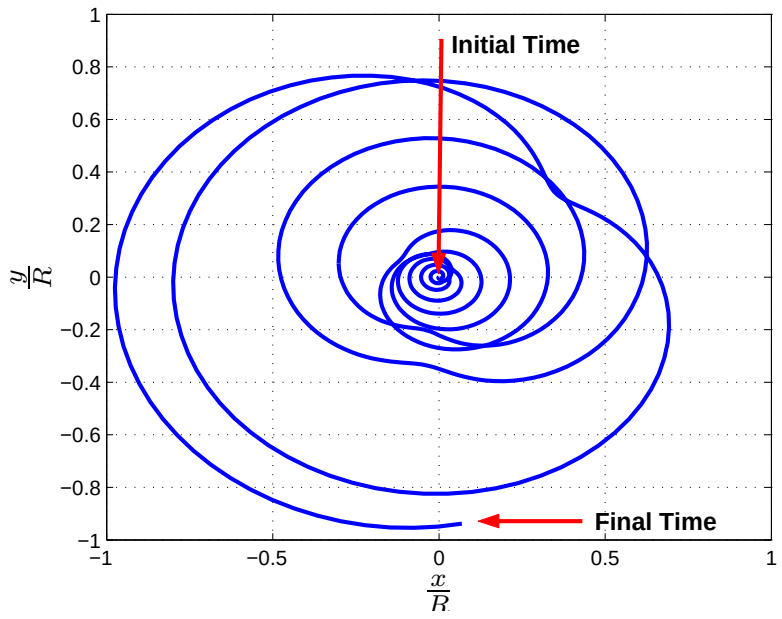

Figure 4.16: Motion of rotor center of mass at $\Omega/\Omega_0 = 0.8$

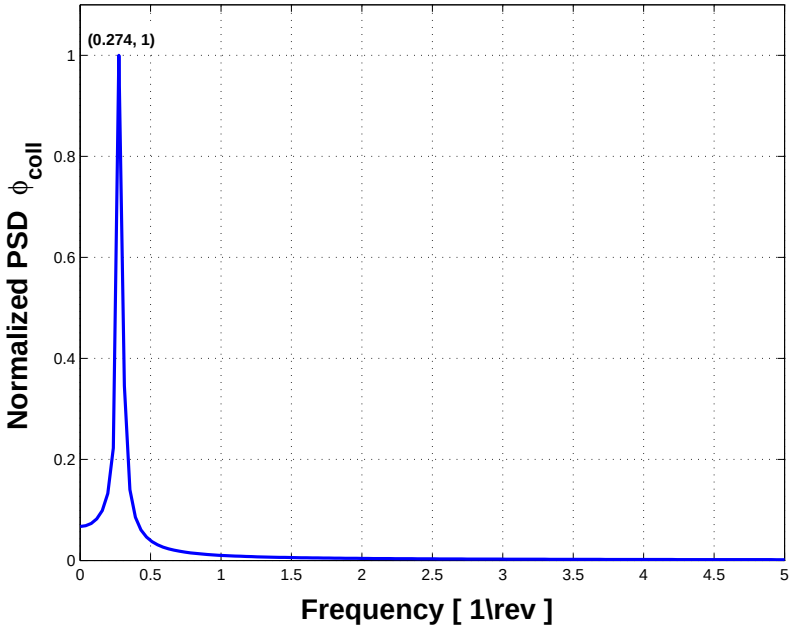

Figure 4.17: Power spectral density of collective mode at $\Omega/\Omega_0 = 0.2$

mode would have matched exactly to their corresponding frequency. The cyclic mode itself shows the presence of a single frequency close to v_ζ. Next, frequency analysis is done at relative rotor speed 0.8, which is the point corresponding to maximum instability. The collective and differential modes, shows the presence of a single frequency as before. The cyclic mode components, however, shows dominance of the regressive lag frequency this time. Again, referring to the cyclic mode as a whole, only a single frequency is identifiable. The frequency plots for the unstable region are shown in Figures 4.21-4.24. The dominance of regressive mode leads to conclusion that during instability, the mode interacts with the fuselage modes and is solely responsible for instability and therefore, needs to be suppressed. In the next section, friction based lag damper performing selective damping of regressive mode is developed and later system response is analyzed.

4.3 Semi-Active Selective Lag Damping

The dynamic model of the rotor, with added friction dampers for the lag motion, is developed in the section A.2 of Appendix A. Coulomb's law is chosen to characterize friction in the damper model. Under the presence of nonlinear dampers such as friction-based damper,

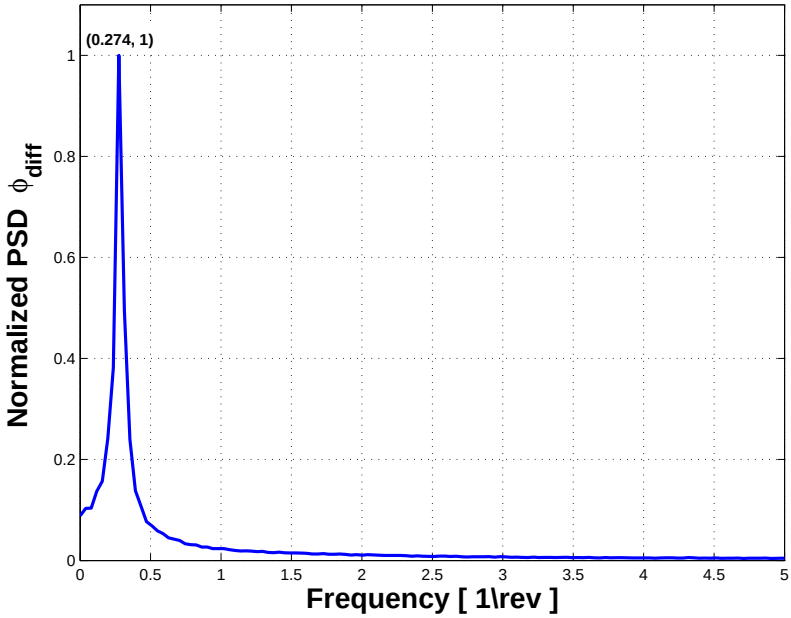

Figure 4.18: Power spectral density of differential mode at $\Omega/\Omega_0 = 0.2$

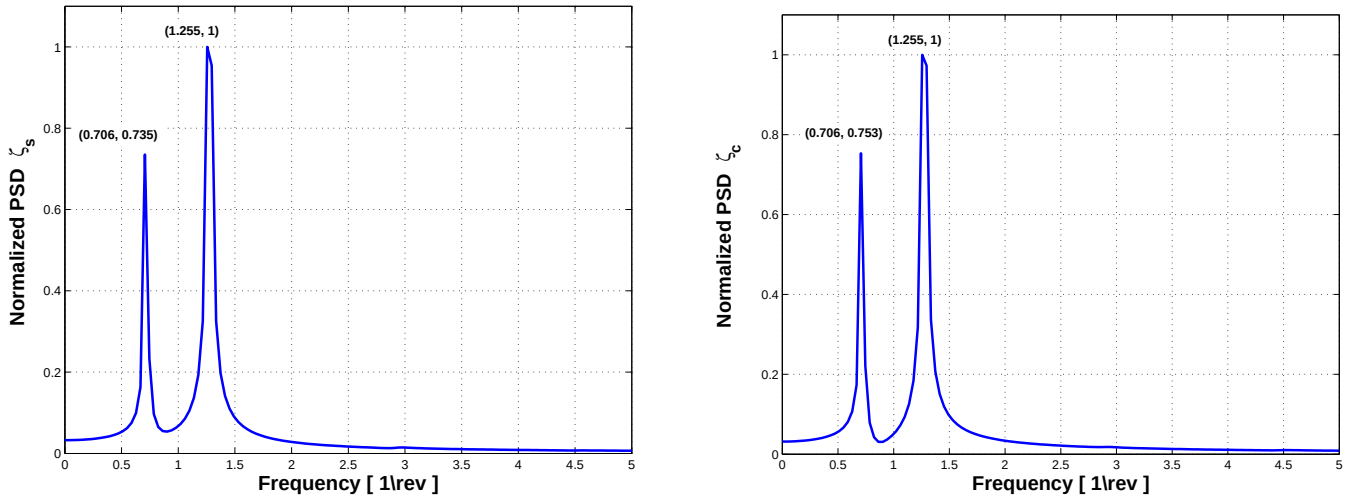

(a) ζ_s (b) ζ_c

Figure 4.19: Power spectral density of cyclic mode components at $\Omega/\Omega = 0.2$

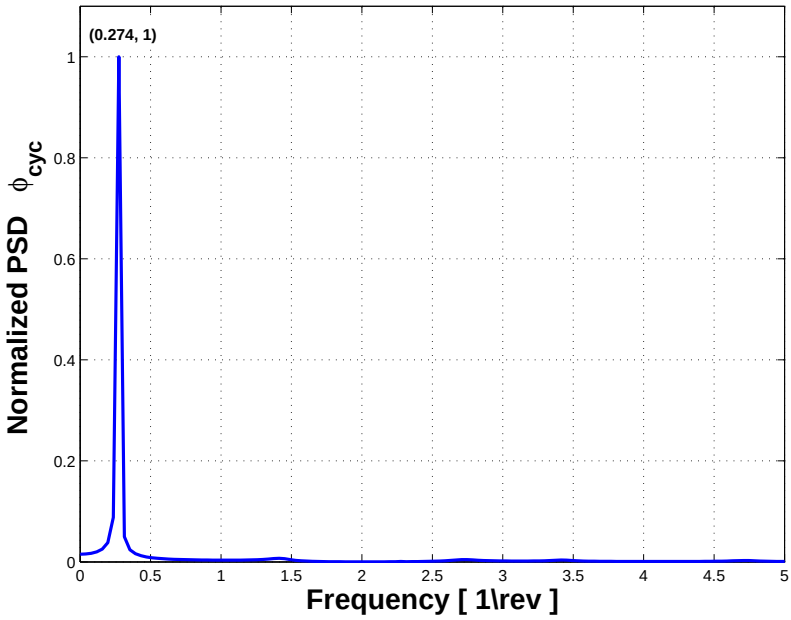

Figure 4.20: Power spectral density of cyclic mode at $\Omega/\Omega_0 = 0.2$

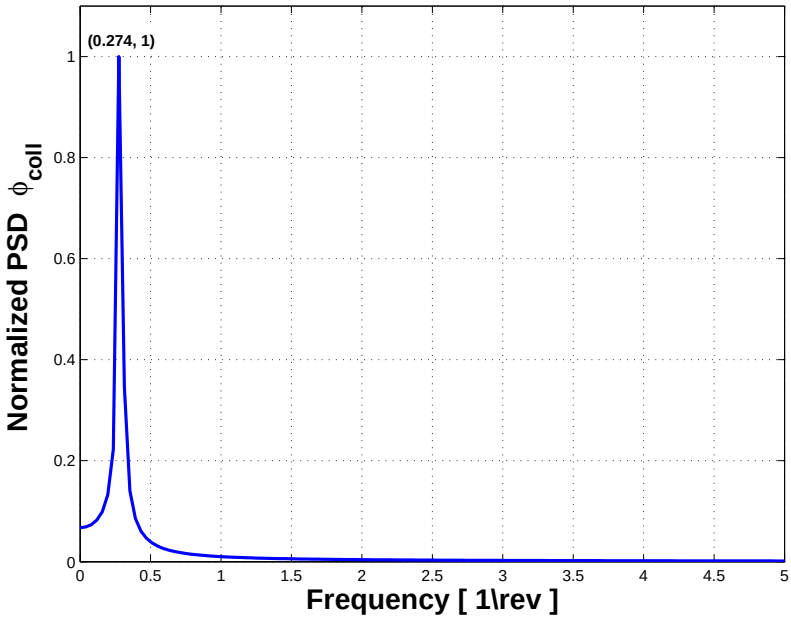

Figure 4.21: Power spectral density of collective mode at $\Omega/\Omega_0 = 0.8$

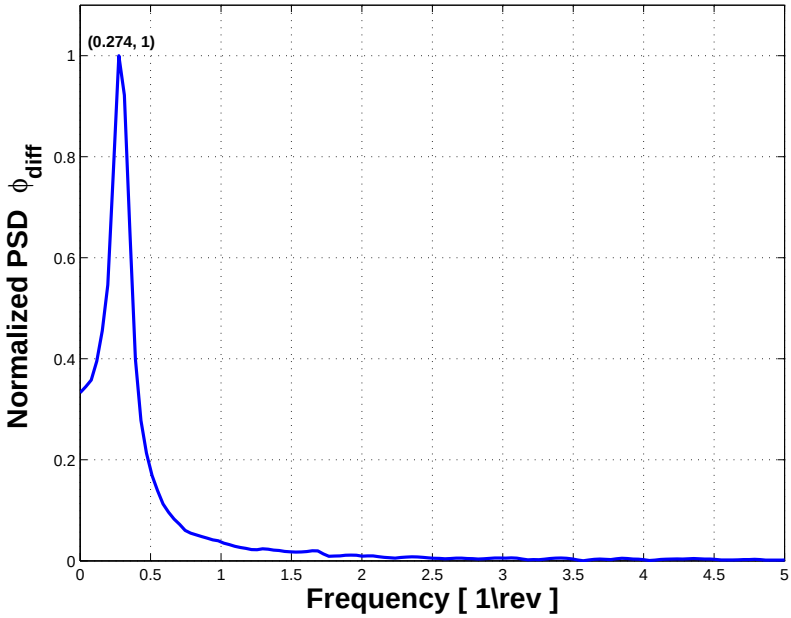

Figure 4.22: Power spectral density of differential mode at $\Omega/\Omega_0 = 0.8$

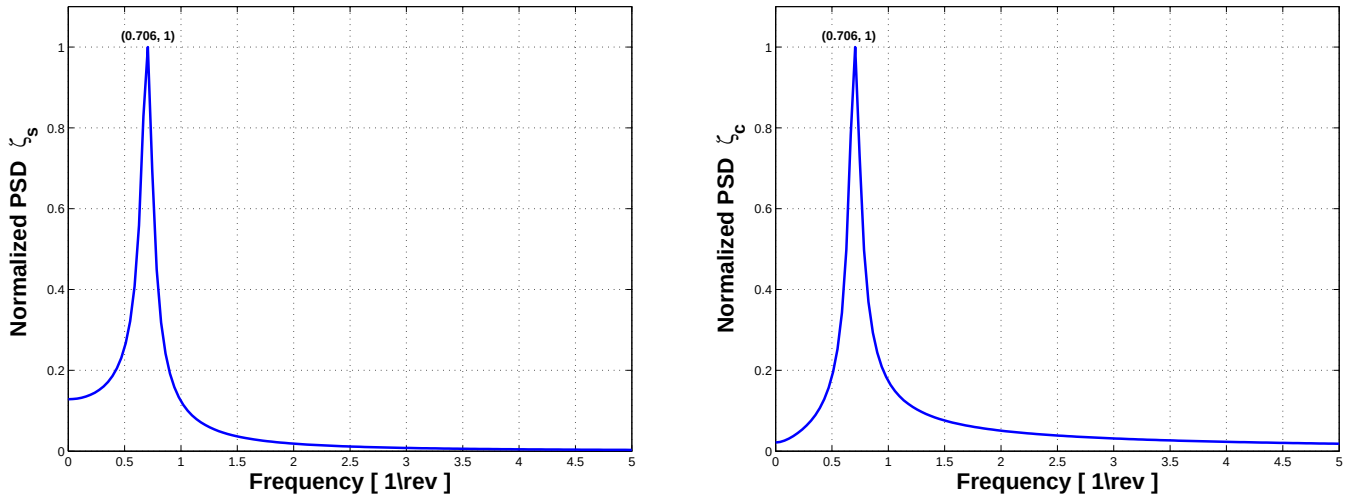

(a) ζ_s (b) ζ_c

Figure 4.23: Power spectral density of cyclic mode components at $\Omega/\Omega = 0.8$

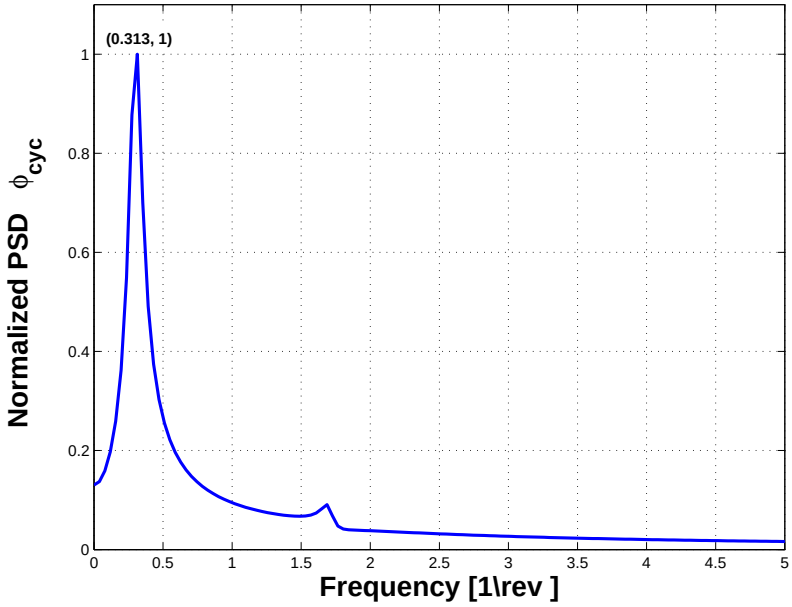

Figure 4.24: Power spectral density of cyclic mode at $\Omega/\Omega_0 = 0.8$

multiblade coordinate transformation does not eliminate the periodic coefficients of the rotor modal terms in the nonrotating system. Hence, transformation from the rotating to the nonrotating frame is not useful and there is a need for stability assessment of the system in the rotating frame itself. Again, due to the nonlinear time-dependent damping term, eigenvalue analysis cannot be done to yield modal frequencies and modal damping of the system. Hence, time response of blades motion is studied for rotor operation at a particular rotor speed. The rotor-fuselage parameters for analysis are taken to be the same as used before and are given in Table 4.1. Although direct transformation to the nonrotating frame is not possible, cyclic mode, collective and differential modes can be extracted from the time response of blades as shown in section A.3 of Appendix A.

The selective damping control strategy was proposed and analyzed in the previous chapter. A targeted damping of a mode component distinctly recognized by its amplitude and frequency in a response consisting of two distinct modes was achieved. The control law aptly maximized damping of the targeted mode while keeping energy spent on other mode under control. By setting normal load proportional to the relative velocity, stick-slip behavior of friction was taken care of. Under extreme conditions resulting in large slip rate, the control

law would command the actuator to generate force of proportional magnitude which might cause mechanical damage to the actuator. Hence, the control law needs to be modified to limit the voltage applied or in turn the force generated by actuator.

The control law governing actuator load output is defined as

$$N = N_{max} \tanh\left(\left|\frac{\dot{\phi}}{\dot{\phi}_0}\right|\right) \tag{4.9}$$

where $\dot{\phi}$ is the lag velocity, N_{max} is the maximum load capability of actuator, and $\dot{\phi}_0$ is the damping rate control parameter and is further explained below.

The purpose of introducing trigonometric function tanh in the control law governing actuator response is justified by the fact that the function is a useful and tractable approximation for the saturation behavior of many devices. The piezoelectric actuators used to vary the normal load are designed for sound functioning within specified operation voltage range. It is common practice to saturate the control voltage input at a level just below the maximum threshold of the actuator in order to prevent potential mechanical/thermal damage. The other parameter $\dot{\phi}_0$ decides the steepness of load profile or damping rate for damper employing this control law. For better understanding by visualization, the above control law is plotted in Figure 4.25. The term $\dot{\phi}$ has been allowed to vary linearly from 0 to 0.5. As observed from the plot, steepness of the plot can be increased by lowering the magnitude of the parameter $\dot{\phi}_0$. In other words, a higher damping rate can be achieved with a lower value of $\dot{\phi}_0$. The damping rate can be mathematically evaluated as

$$\frac{dN}{d\dot{\phi}} = \frac{1}{\dot{\phi}_0} N_{max} \operatorname{sech}^2\left(\left|\frac{\dot{\phi}}{\dot{\phi}_0}\right|\right) \tag{4.10}$$

As opposed to constant damping rate given by viscous damper, the damping provided by semi-active damper is adaptive in the sense that damping is dependent on the magnitude of the lag mode as well. The damping rate can be chosen by setting the parameter $\dot{\phi}_0$.

The cyclic lag mode given by Equation A.19, has a single dominant frequency, the

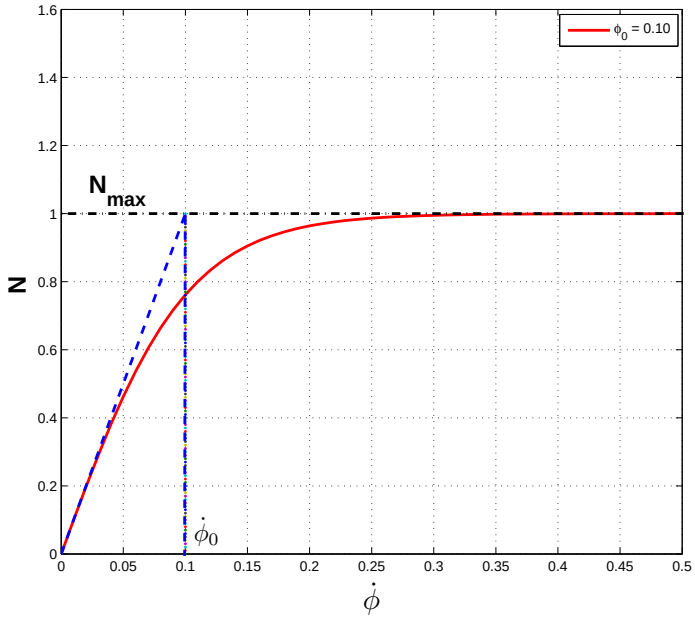

Figure 4.25: Control law governing actuator response

regressive lag frequency during instability and is the one that needs to be suppressed. The mode is termed as regressive lag mode and represented by ϕ_r. The remaining content of lag mode is represented by ϕ_o such that $\phi = \phi_r + \phi_o$. Depending on the level of selective nature, two damping strategies are proposed and compared in the following section.

4.3.1 Selective Damping Law 1

In this control law, normal load over frictional interface is made proportional to instantaneous regressive lag velocity.

$$N = N_{max} \tanh\left(\left|\frac{\dot{\phi}_r}{\dot{\phi}_0}\right|\right) \tag{4.11}$$

4.3.2 Selective Damping Law 2

This control law goes one step further than previous law by modulating the operation interval of the damper as well. The control law is based on selective damping strategy tested in the previous chapter.

$$N = \begin{cases} N & \text{if } \operatorname{sgn}\left(\dot{\phi}\dot{\phi}_r\right) = 1 \\ 0 & \text{else} \end{cases} \tag{4.12}$$

where N on the right hand side of the equation is same as given by Equation 4.11.

4.4 Results

To investigate the efficiency of semi-active friction damper based on two selective control strategies, the response of the system is evaluated for a small perturbation at relative rotor speed of magnitude 0.8 which corresponds to the point of maximum instability. The damper arm length given by d_i for i^{th} damper in Equation A.37 and damping parameter $\dot{\phi}_0$ are set to 1.0 *ft* and 0.01, respectively.

4.4.1 Selective Damping Law 1

The time histories of the fuselage and lag motion are plotted in Figures 4.26 and 4.27 respectively. It can be seen that the friction damper is able to suppress the instability within a couple of seconds. However, a similar investigation of the system response with the same maximum normal load level but $\dot{\phi}_0 = 0.05$ demonstrated insufficiency of the damper to suppress instability. This suggests that a study on significance of damping parameter for ground resonance stability needs to be conducted. The time history of applied damper moment is plotted in Figure 4.28. The tendency of the damper to apply load proportional to lag velocity is established. As seen from the plot, when the instability is completely suppressed, the damper is rendered almost redundant and can be turned off. Figures 4.29-4.31 show the total work done by the damper to dissipate lag mode as well its modal components individually i.e., the regressive mode and remaining modes termed as 'other' modes. While friction damping ensures that the system energy is always dissipated, the selective law guarantees regressive mode energy is always dissipated irrespective of that of other modes. As can be seen from the figure, work done on regressive mode is always dissipative while work done on other modes can be positive depending on their phase in reference to regressive mode.

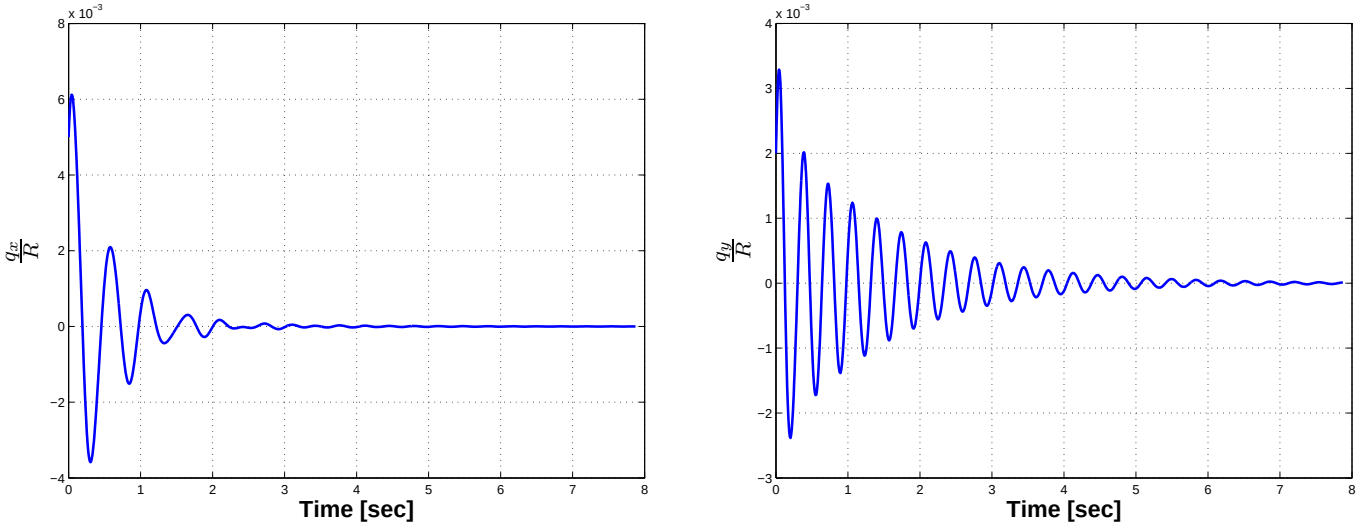

(a) Longitudinal direction (b) Lateral direction

Figure 4.26: Fuselage motion - Selective damping law 1

4.4.2 Selective Damping Law 2

Keeping all the modeling parameters same except the friction damping control law, response of the system is evaluated again. The time response of the fuselage motion as well as the blade lag motion is plotted in Figures 4.33 and 4.34 respectively. The response is similar to that obtained with Damping Law 1. The sufficiency of the friction based damping technique in stabilizing ground resonance, irrespective of level of selectiveness, is emphasized. Next, rotor mode components in the nonrotating frame are obtained and plotted in Figure 4.35. The regressive lag mode is shown in Figure 4.36. The damper moment is plotted in Figure 4.37. On comparison with same plots from previous results, only a slight difference is seen. While damper remained continuously active in the previous case, it goes 'on' and 'off' for small instants in present case. The damper switching is suggestive of the nature of the selective damping law 2. The total work done by the dampers as well as work done by dampers exclusively on the regressive mode is shown in Figures 4.38 and 4.39 respectively. The work done by the damper on remaining modes of the lag response is plotted in Figure 4.40. While the work done on regressive modes is always negative causing the damping of that mode, cumulative work done on other modes is positive for some blades and negative

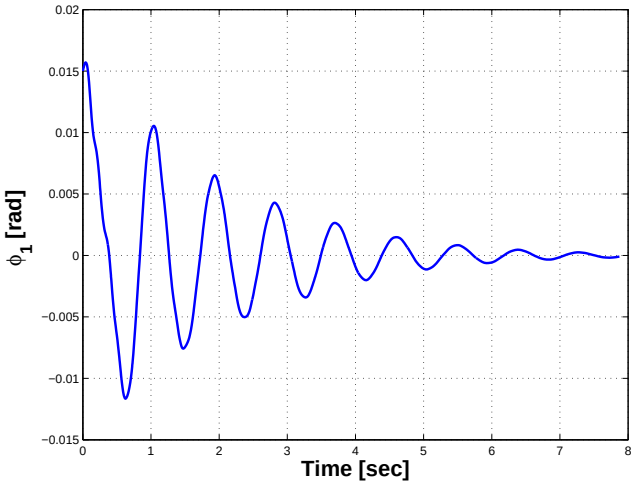

(a) Blade 1

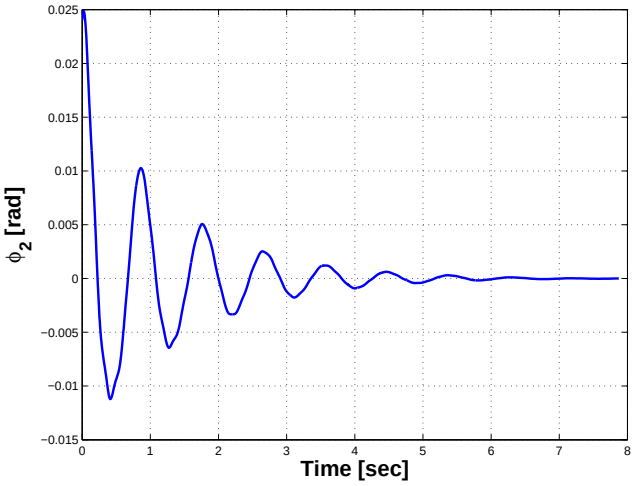

(b) Blade 2

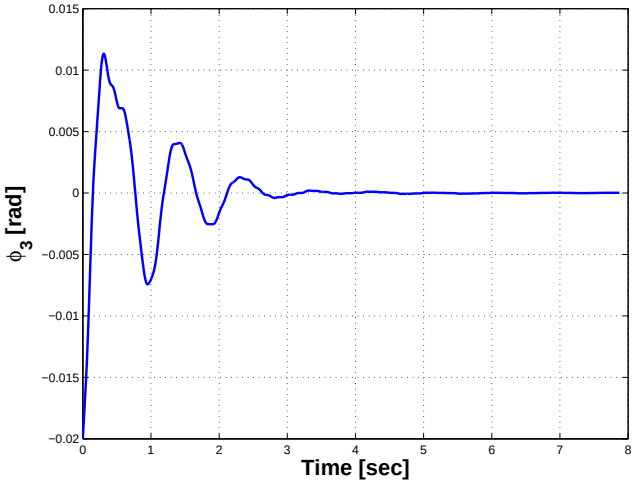

(c) Blade 3

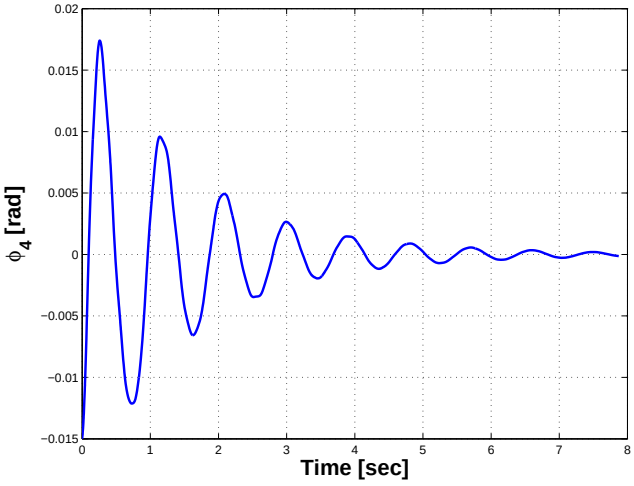

(d) Blade 4

Figure 4.27: Blade lag motion - Selective damping law 1

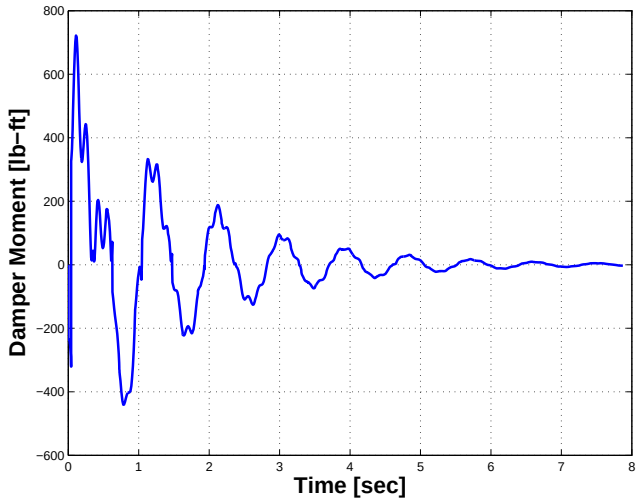

(a) Blade 1

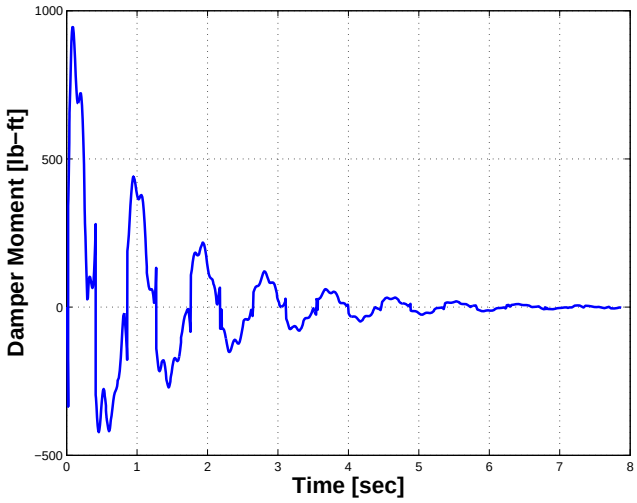

(b) Blade 2

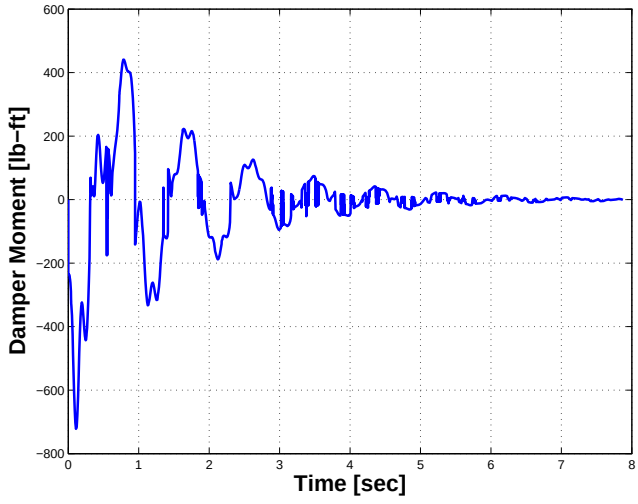

(c) Blade 3

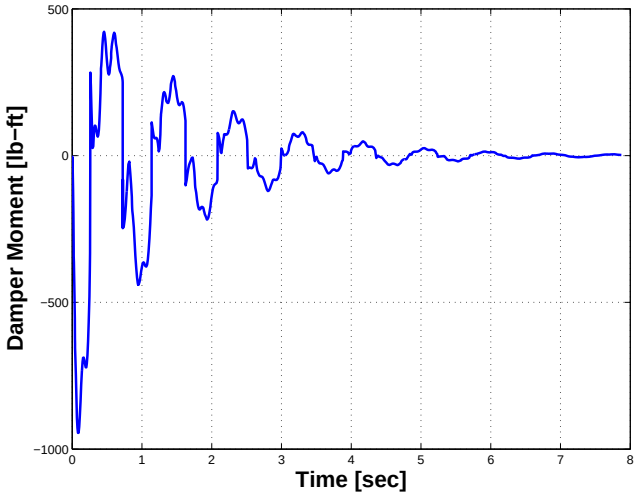

(d) Blade 4

Figure 4.28: Friction moment variation - Selective damping law 1

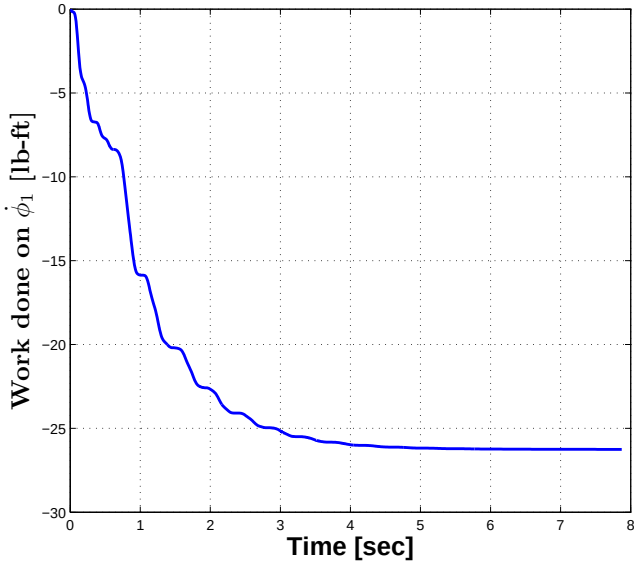

(a) Blade 1

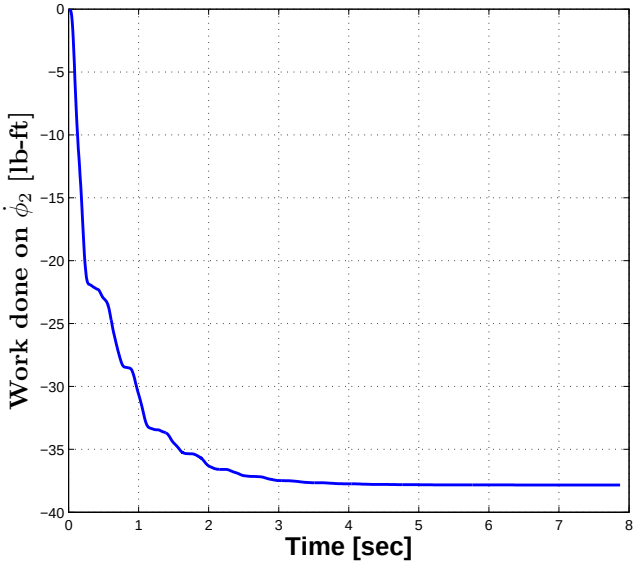

(b) Blade 2

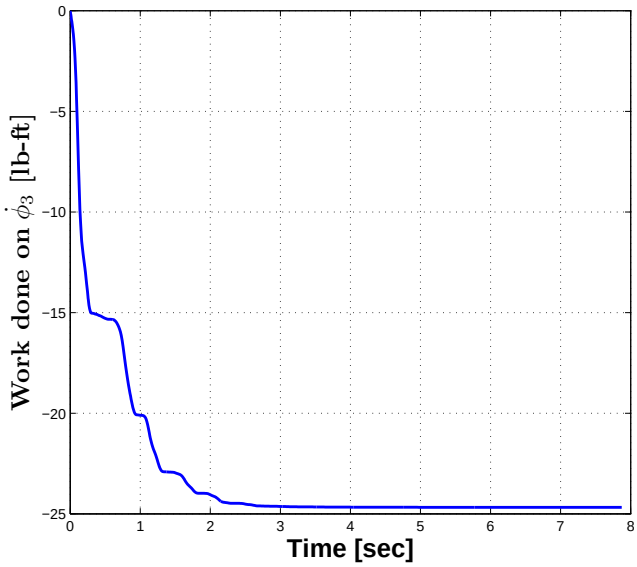

(c) Blade 3

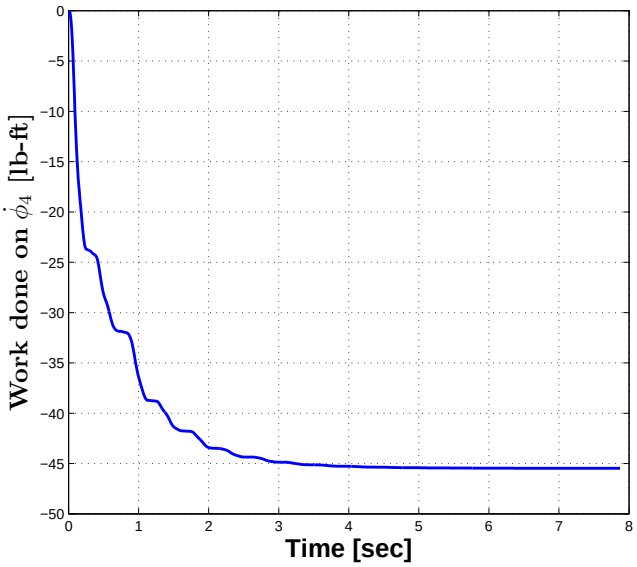

(d) Blade 4

Figure 4.29: Work done by the damper - Selective damping law 1

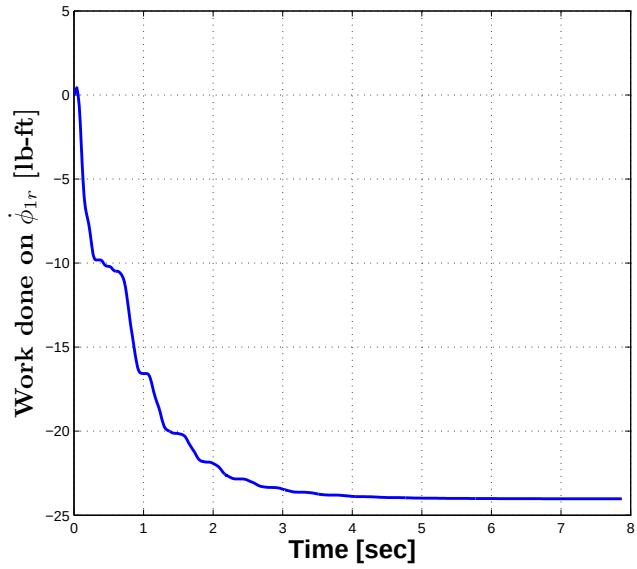

(a) Blade 1

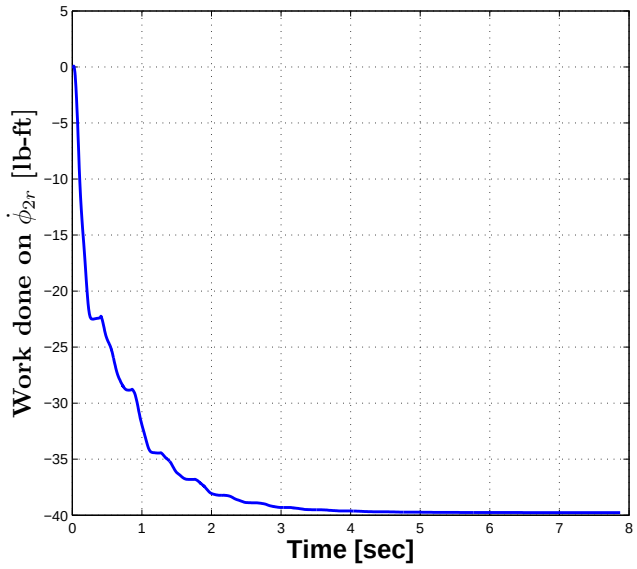

(b) Blade 2

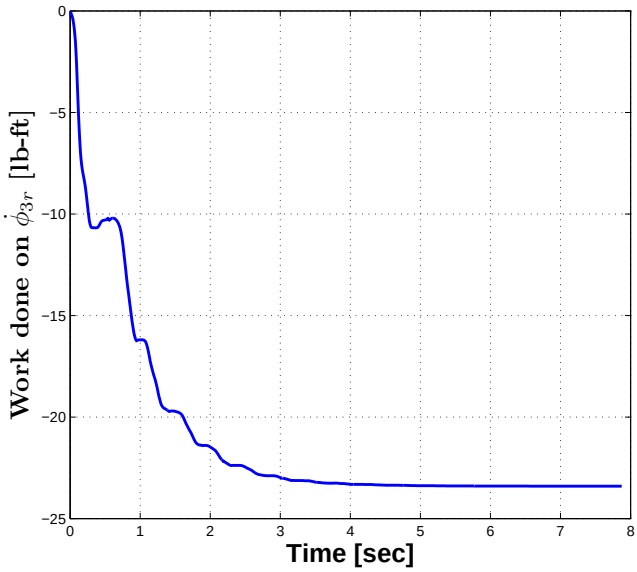

(c) Blade 3

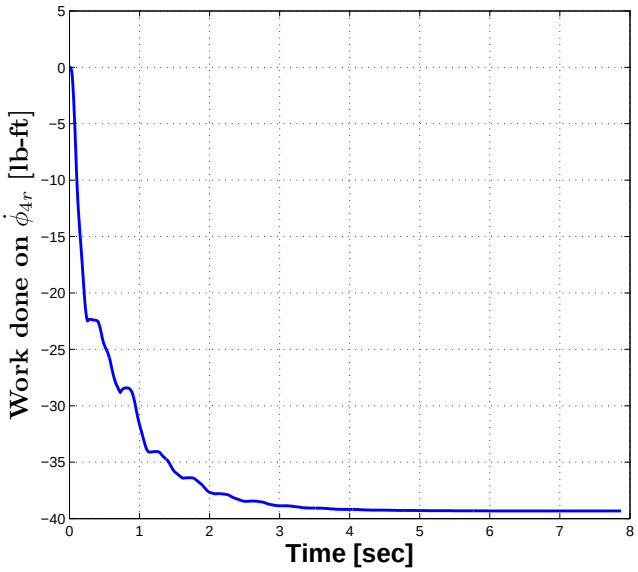

(d) Blade 4

Figure 4.30: Work done on regressive mode - Selective damping law 1

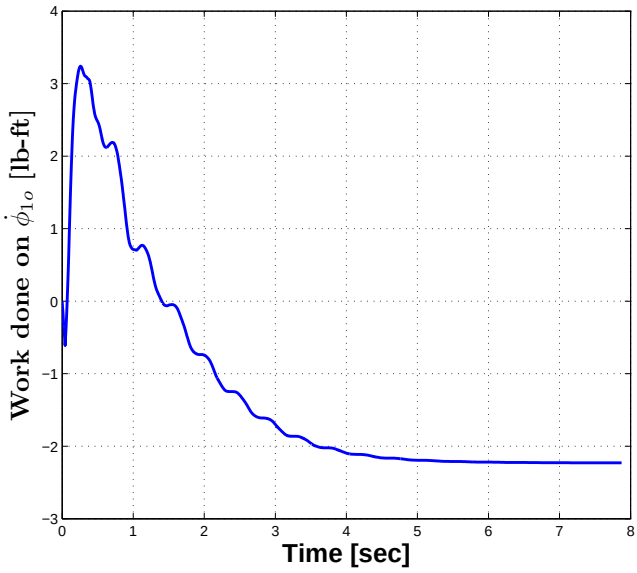

(a) Blade 1

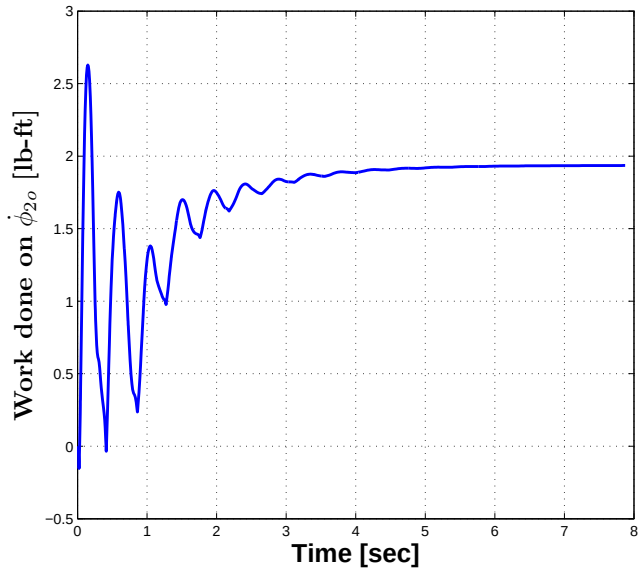

(b) Blade 2

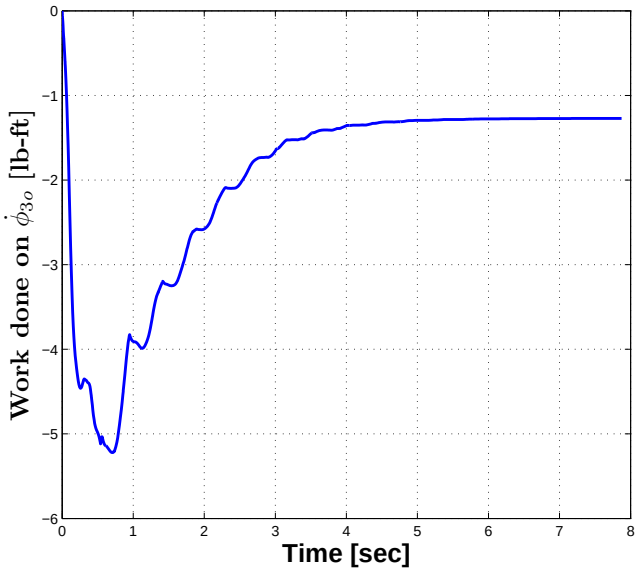

(c) Blade 3

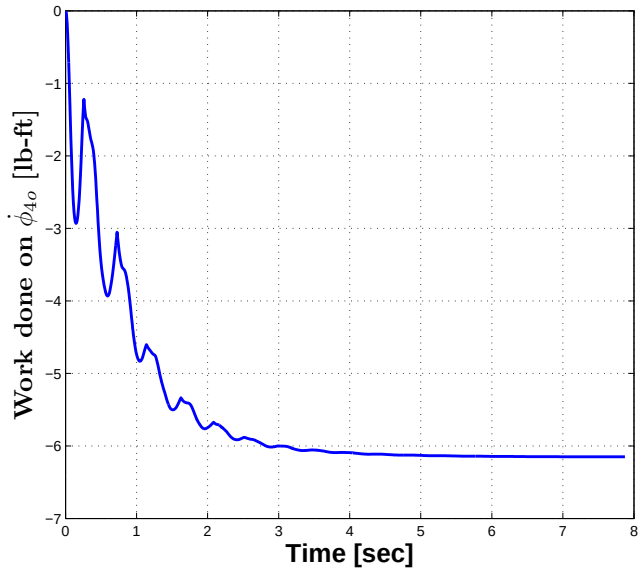

(d) Blade 4

Figure 4.31: Work done on rest of the modes - Selective damping law 1

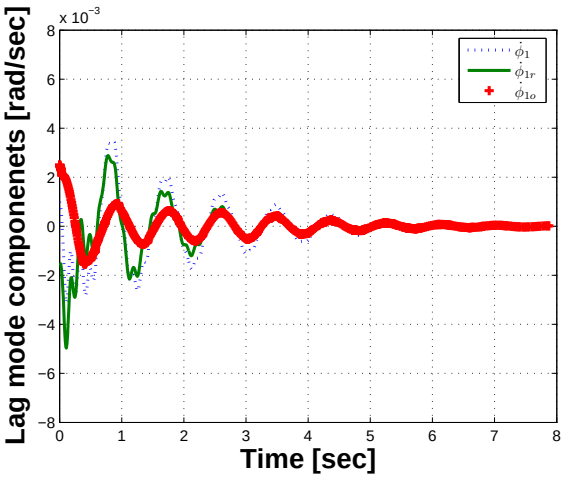

(a) Blade 1

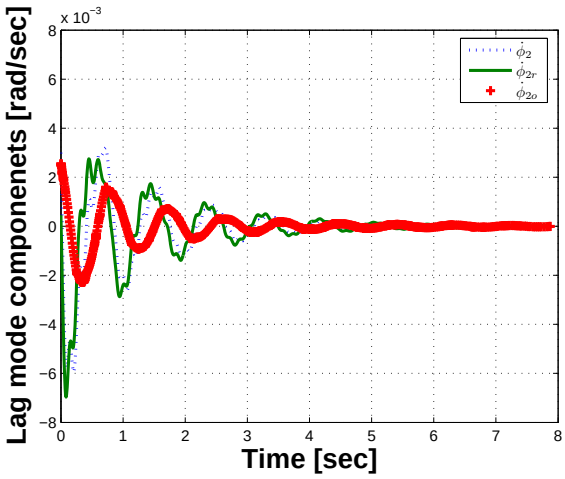

(b) Blade 2

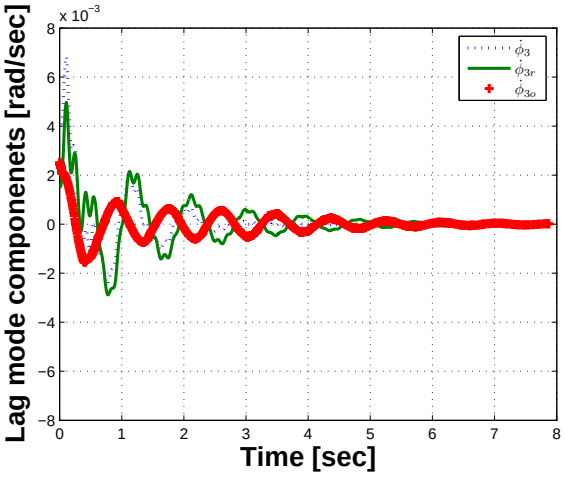

(c) Blade 3

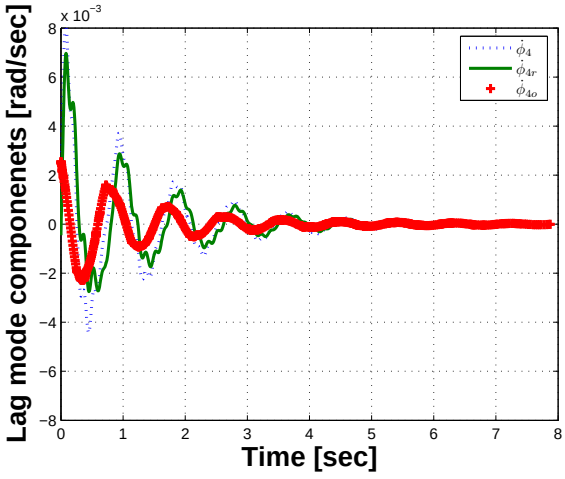

(d) Blade 4

Figure 4.32: Regressive mode as compared to rest of the modes - Selective damping law 1

for others. The components of the lag mode are compared in Figure 4.41. The control law turning damper 'off' whenever sign of regressive mode is opposite to the total lag mode can be observed. The motion of center of mass of the rotor is plotted in Figure 4.42. The time histories of the normal load applied by the dampers in all the four blades are shown in Figure 4.43. As seen from the plot, maximum load applied by the actuator on frictional interface is of the order of 2700 *lbs* and is gradually found to decrease until no load is applied when instability is completely suppressed.

On comparing it with the same plots for the selective damping law 1, only a little difference is observed. The damper does not seem to save much energy by employing selective law 2. The reason becomes quite clear after looking at the modal components of the lag response plotted in Figures 4.32 and 4.41 for the two cases respectively . The amplitude of the regressive mode is of the same order as that of the rest of the modal content in the response and the most important of all is the frequency difference between the modal components, which seems to be very small as seen from frequency spectrum plots in Figures 4.21-4.24. The selective damping law 2, investigated in depth in chapter 3, utilized the phase lag difference between the modal components to perform selective damping. Due to negligible difference in the initial phase of modal components as well as negligible difference in frequency of the regressive mode and rest of modal components, selective damping law 2 performed no better than law 1.

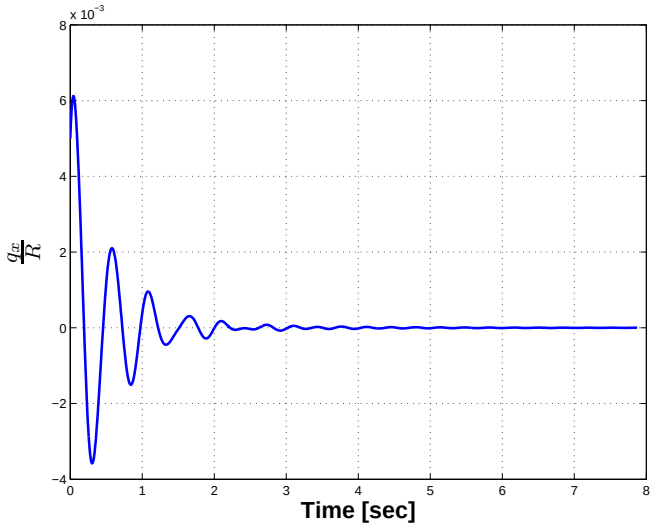

(a) Longitudinal direction

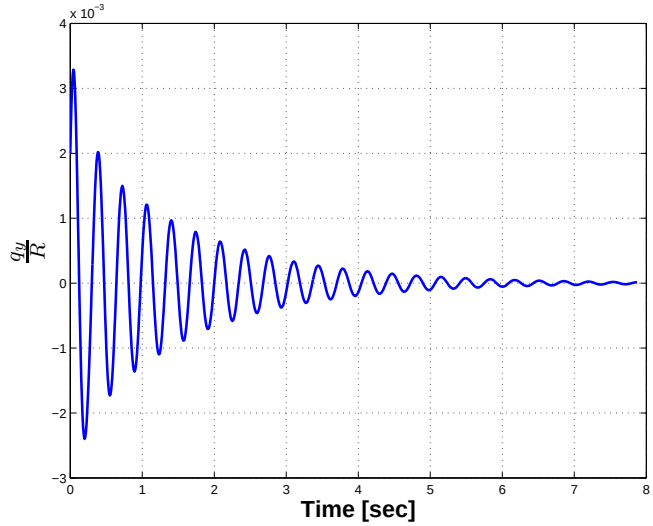

(b) Lateral direction

Figure 4.33: Fuselage motion - Selective damping law 2

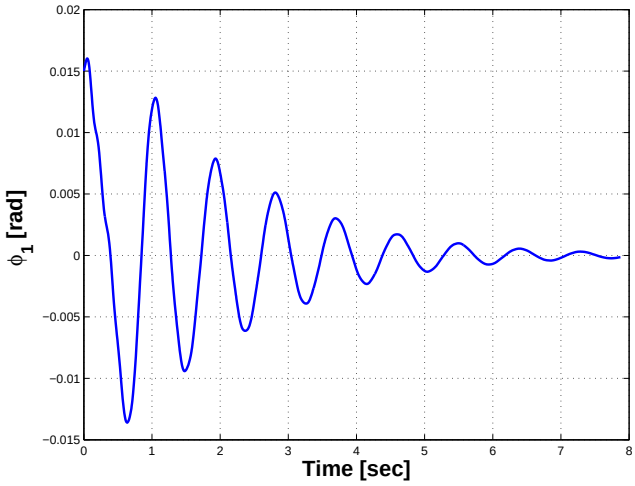

(a) Blade 1

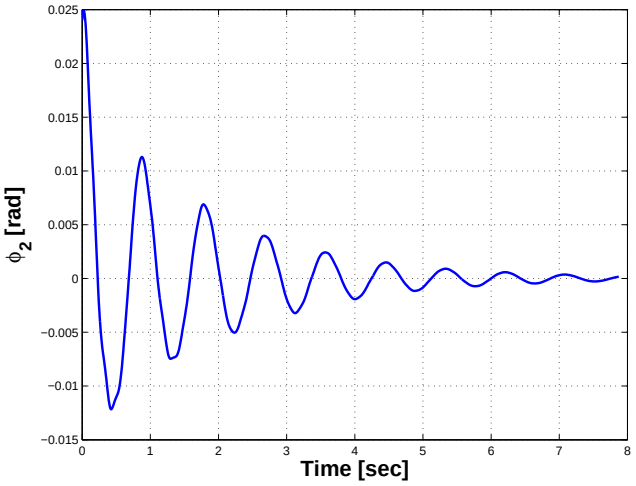

(b) Blade 2

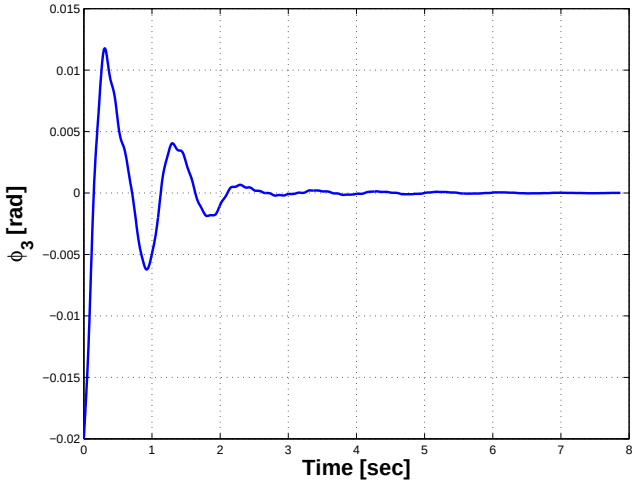

(c) Blade 3

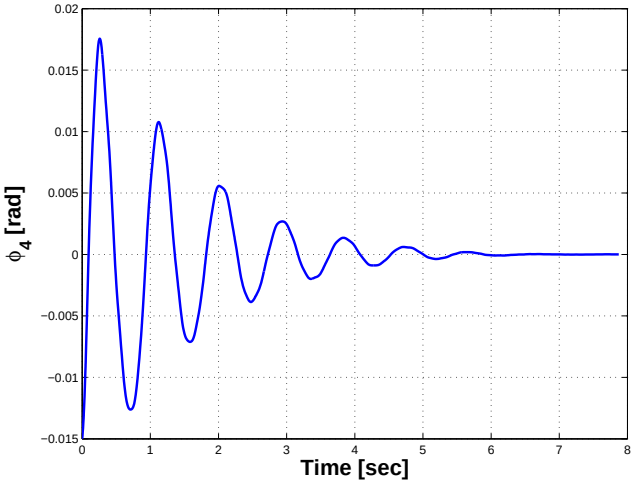

(d) Blade 4

Figure 4.34: Blade lag motion - Selective damping law 2

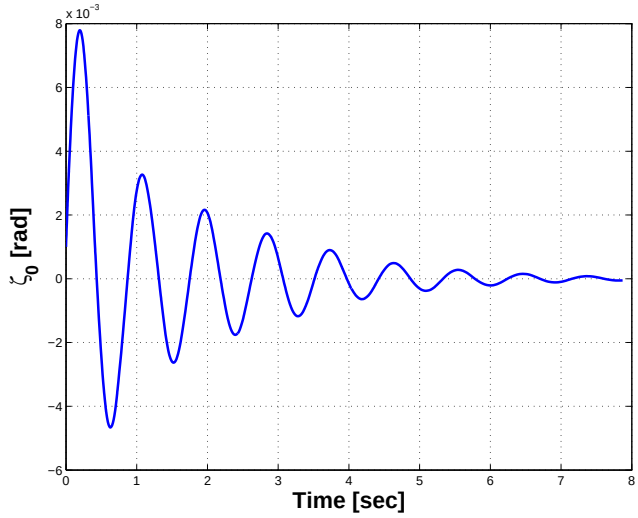

(a) Collective

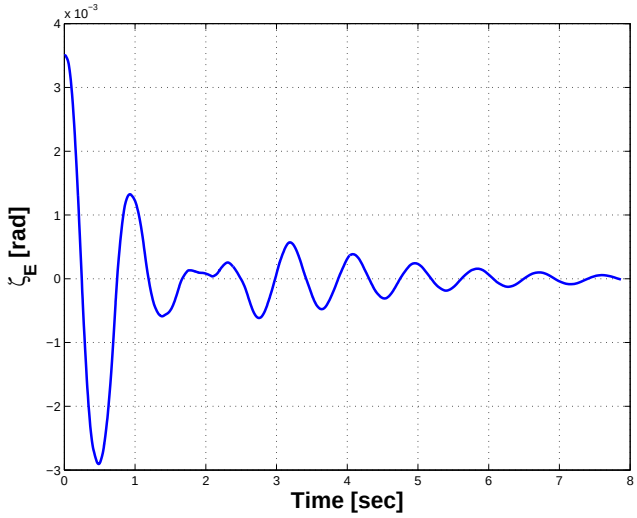

(b) Differential

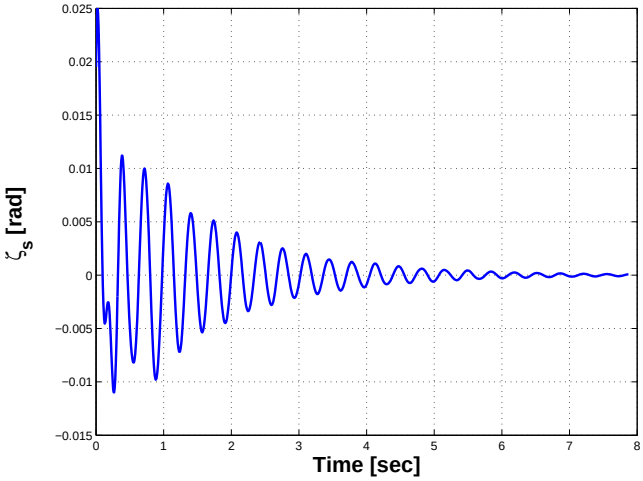

(c) Cyclic

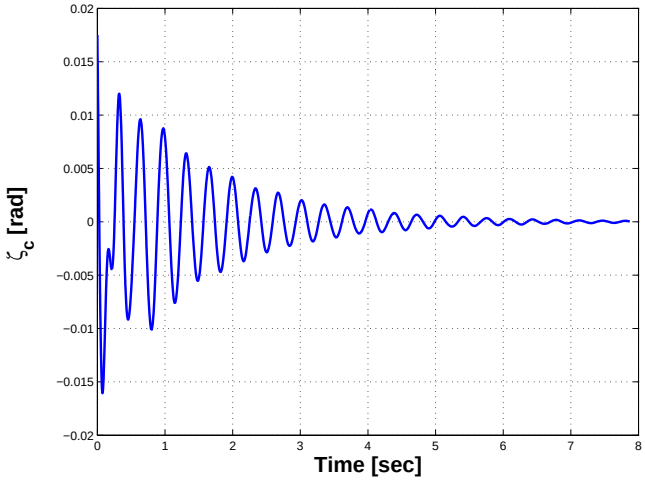

(d) Cyclic

Figure 4.35: Components of rotor modes in nonrotating frame - Selective damping law 2

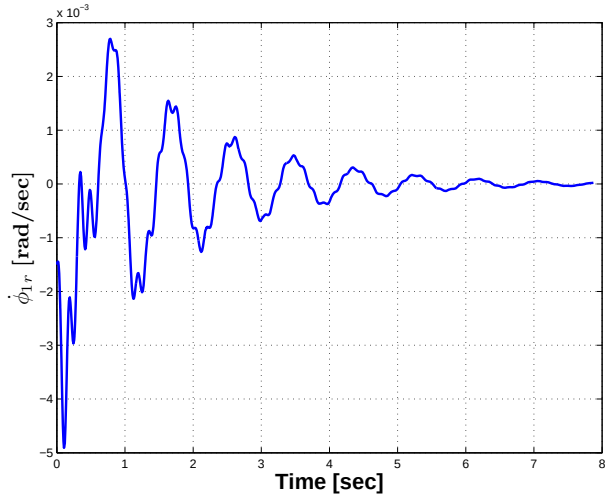

(a) Blade 1

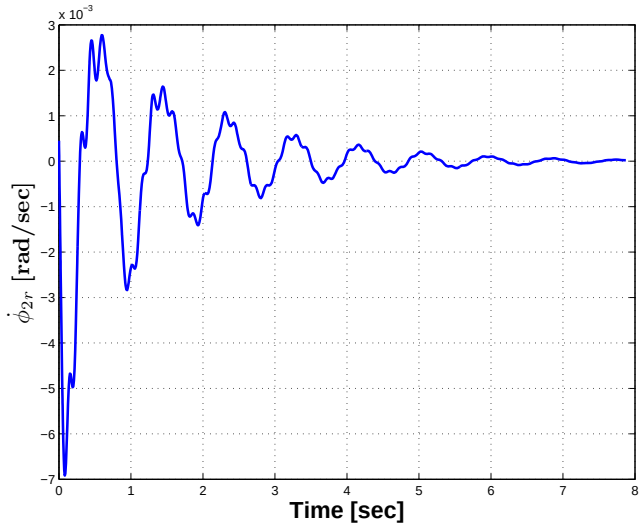

(b) Blade 2

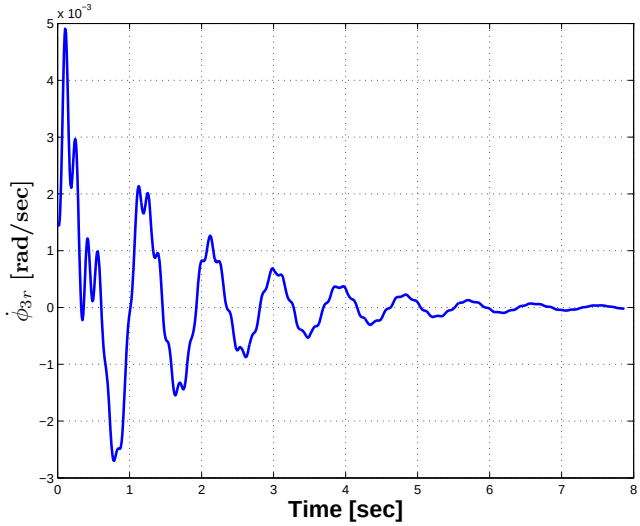

(c) Blade 3

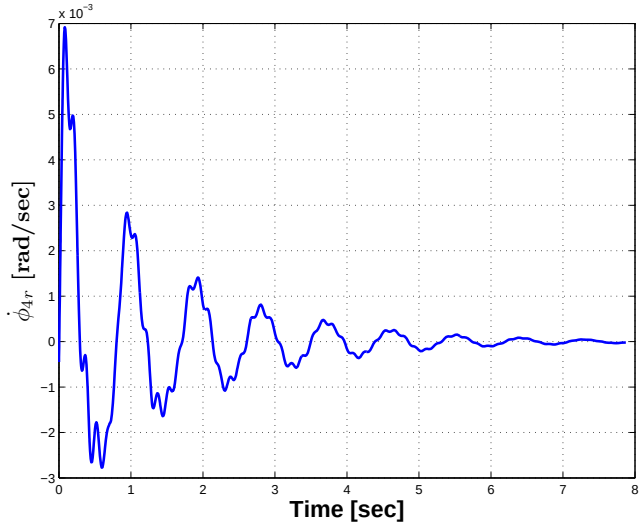

(d) Blade 4

Figure 4.36: Regressive lag mode variation - Selective damping law 2

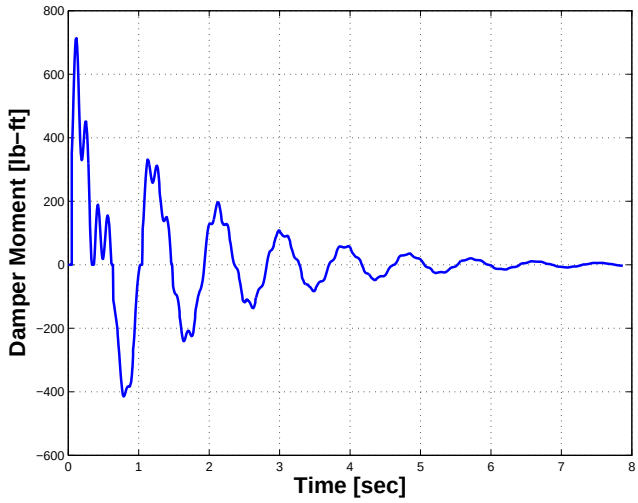

(a) Blade 1

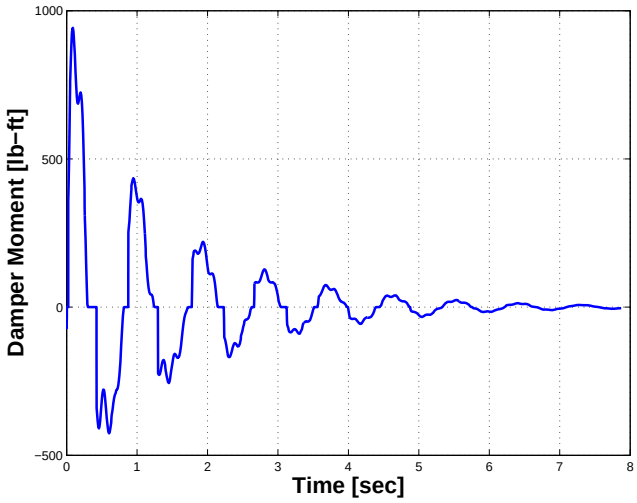

(b) Blade 2

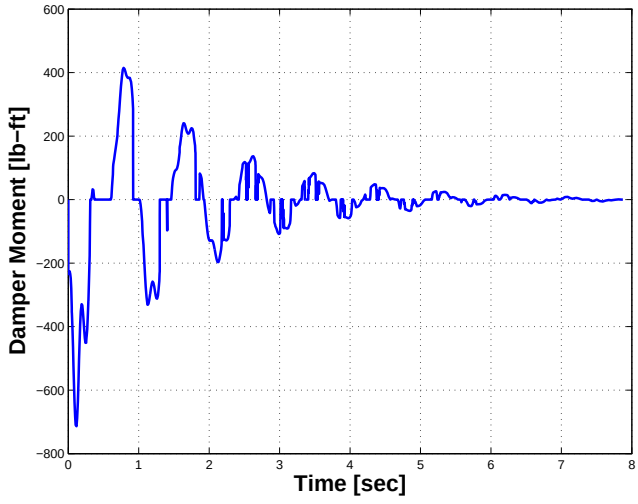

(c) Blade 3

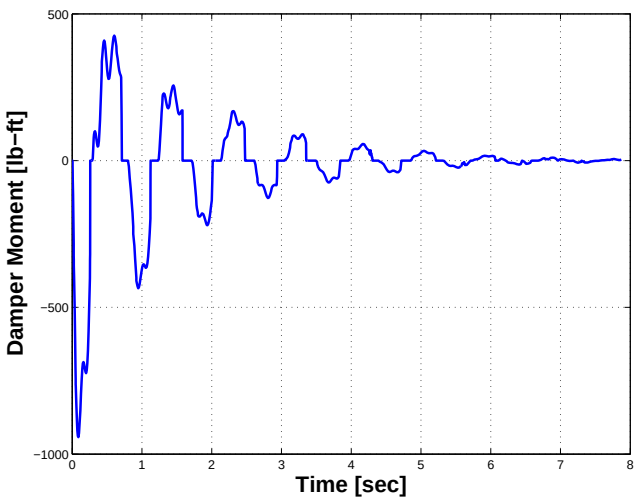

(d) Blade 4

Figure 4.37: Friction moment variation - Selective damping law 2

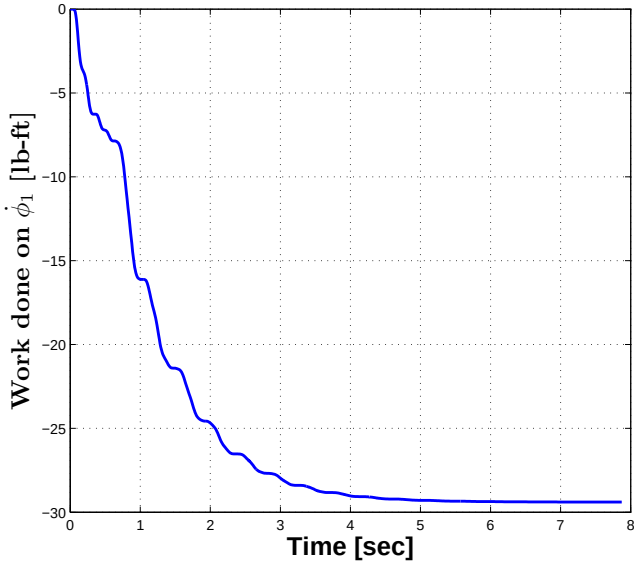

(a) Blade 1

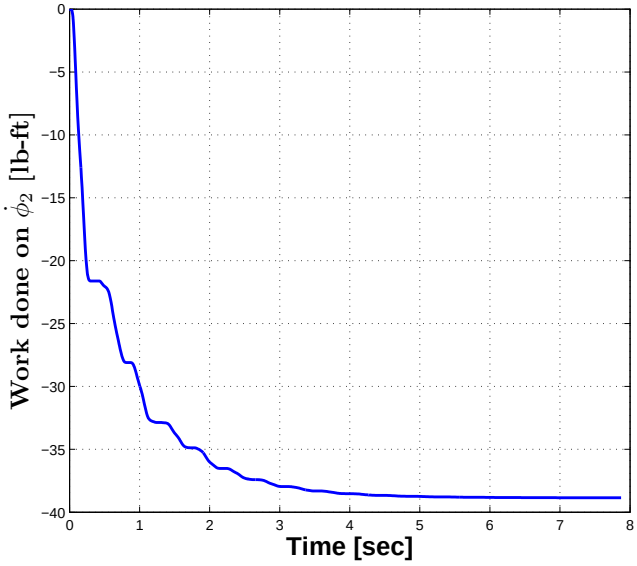

(b) Blade 2

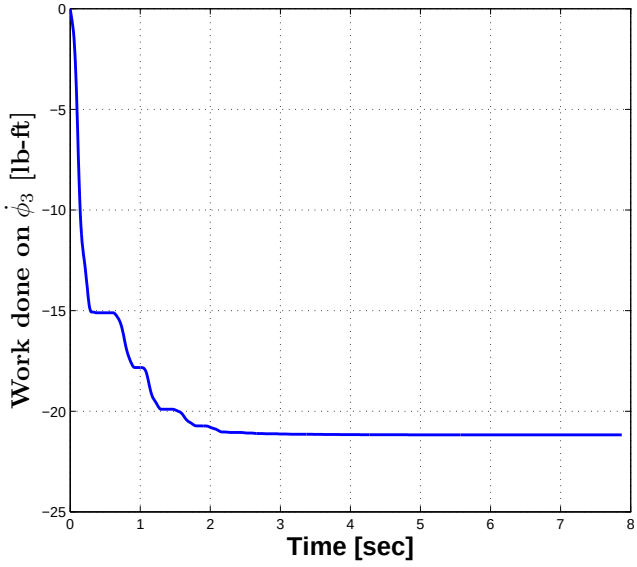

(c) Blade 3

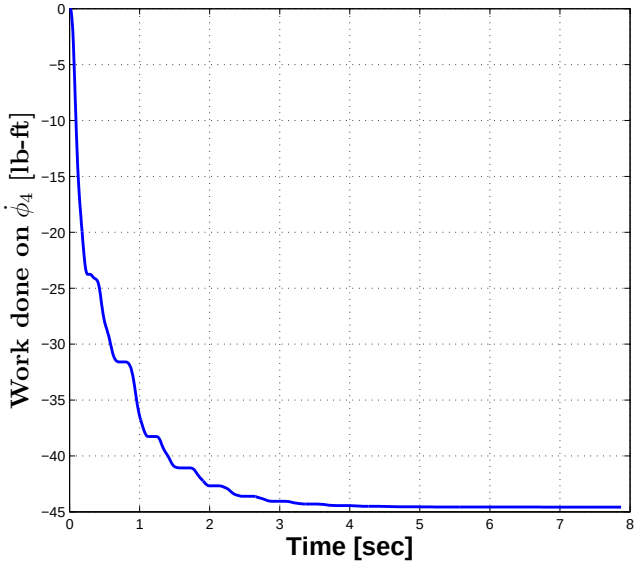

(d) Blade 4

Figure 4.38: Work done by the dampers - Selective damping law 2

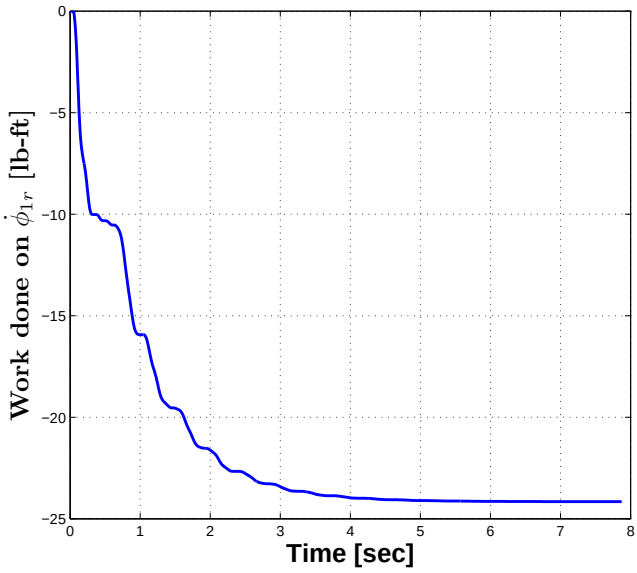

(a) Blade 1

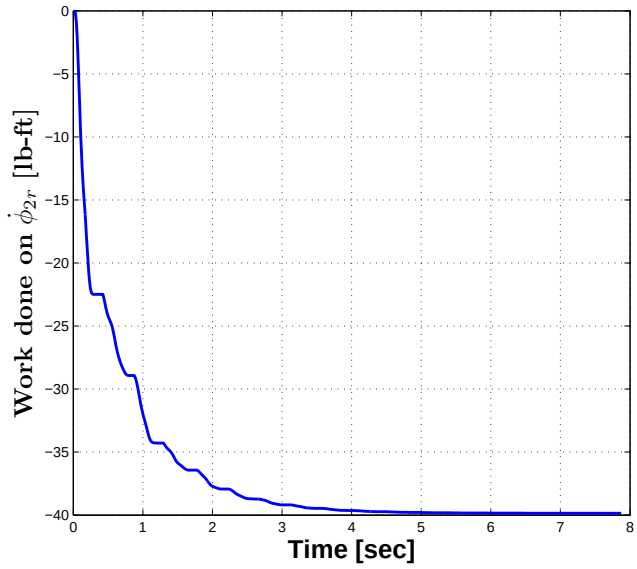

(b) Blade 2

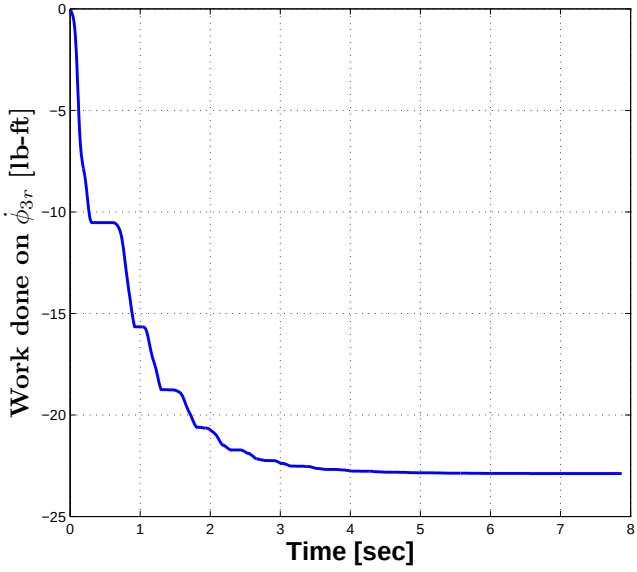

(c) Blade 3

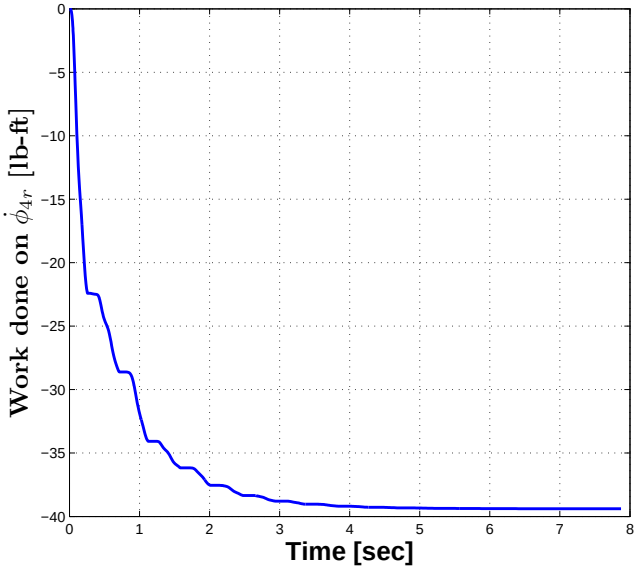

(d) Blade 4

Figure 4.39: Work done on the regressive mode - Selective damping law 2

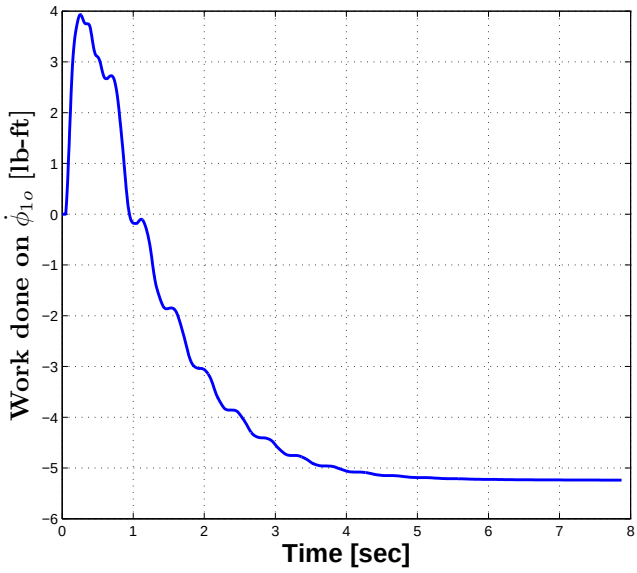

(a) Blade 1

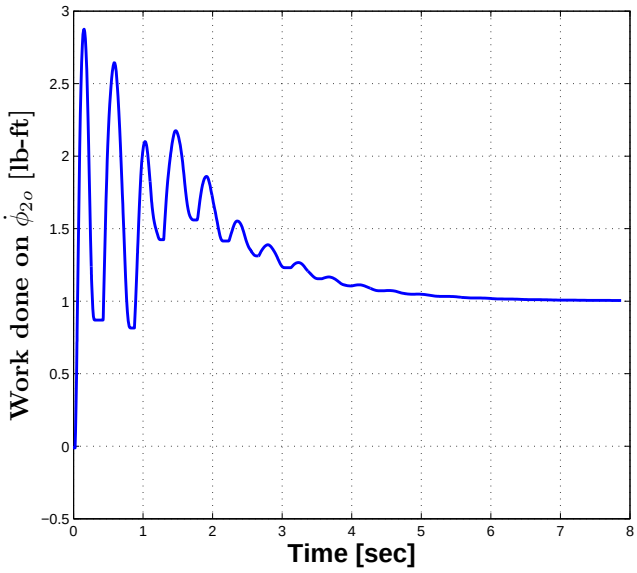

(b) Blade 2

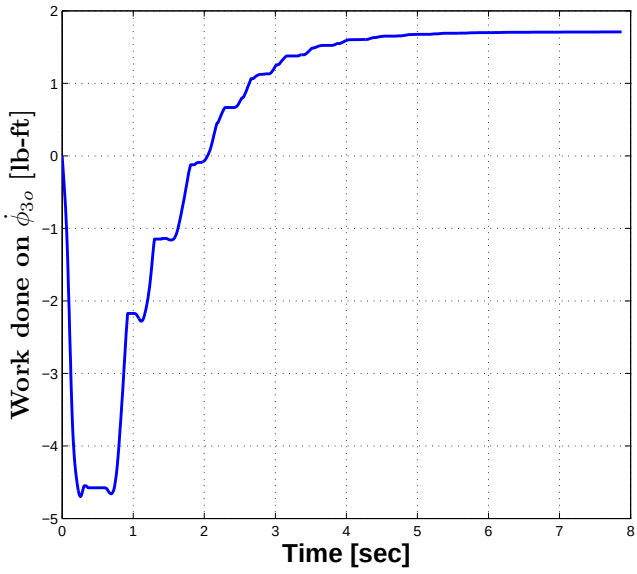

(c) Blade 3

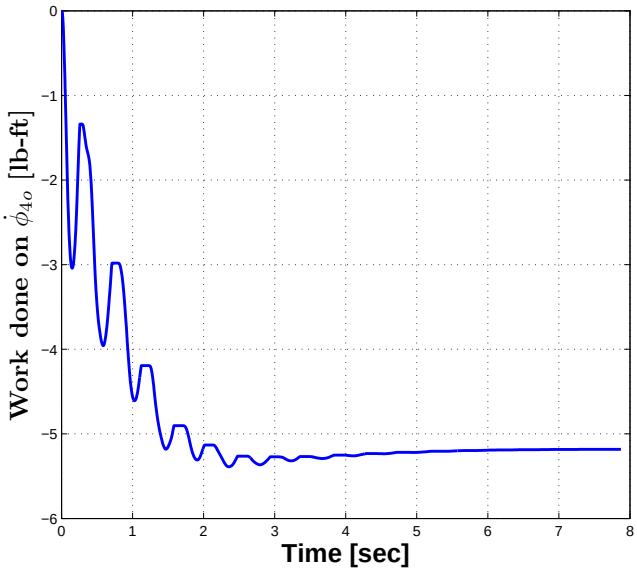

(d) Blade 4

Figure 4.40: Work done on rest of the modes - Selective damping law 2

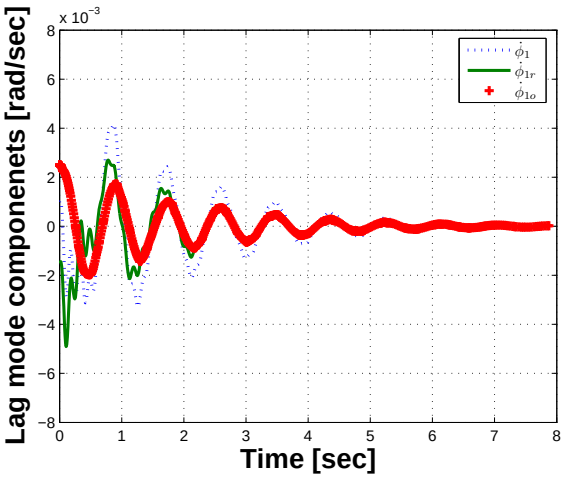

(a) Blade 1

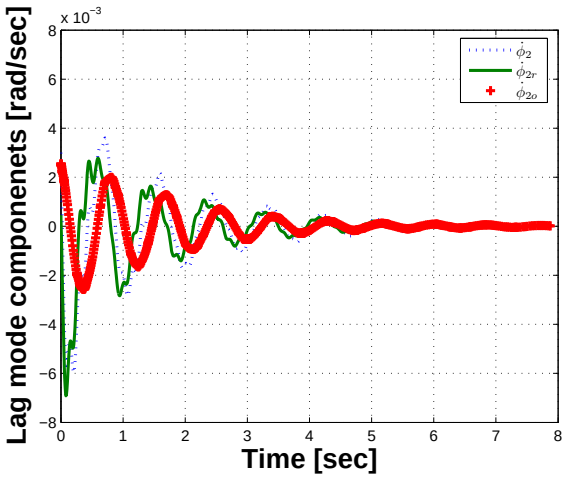

(b) Blade 2

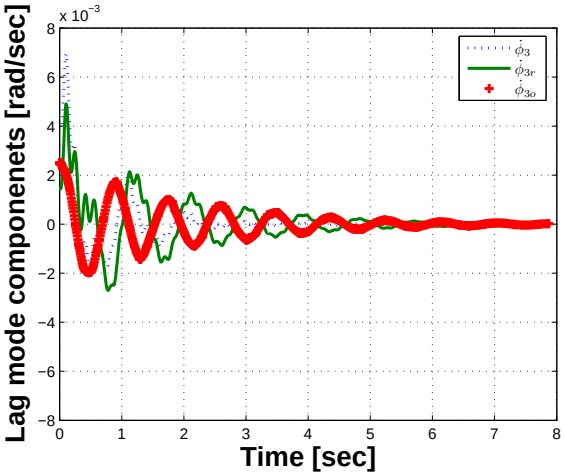

(c) Blade 3

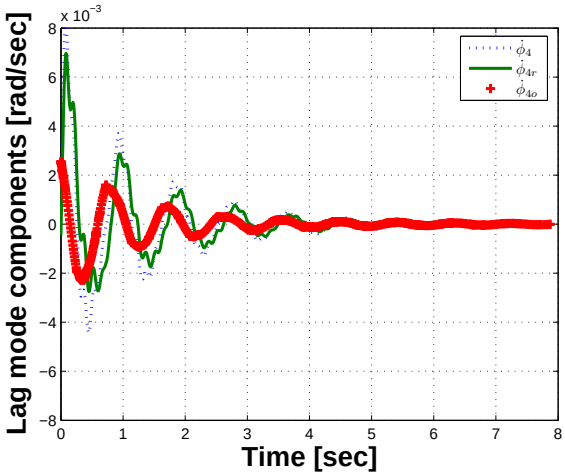

(d) Blade 4

Figure 4.41: Regressive mode as compared to rest of the modes - Selective damping law 2

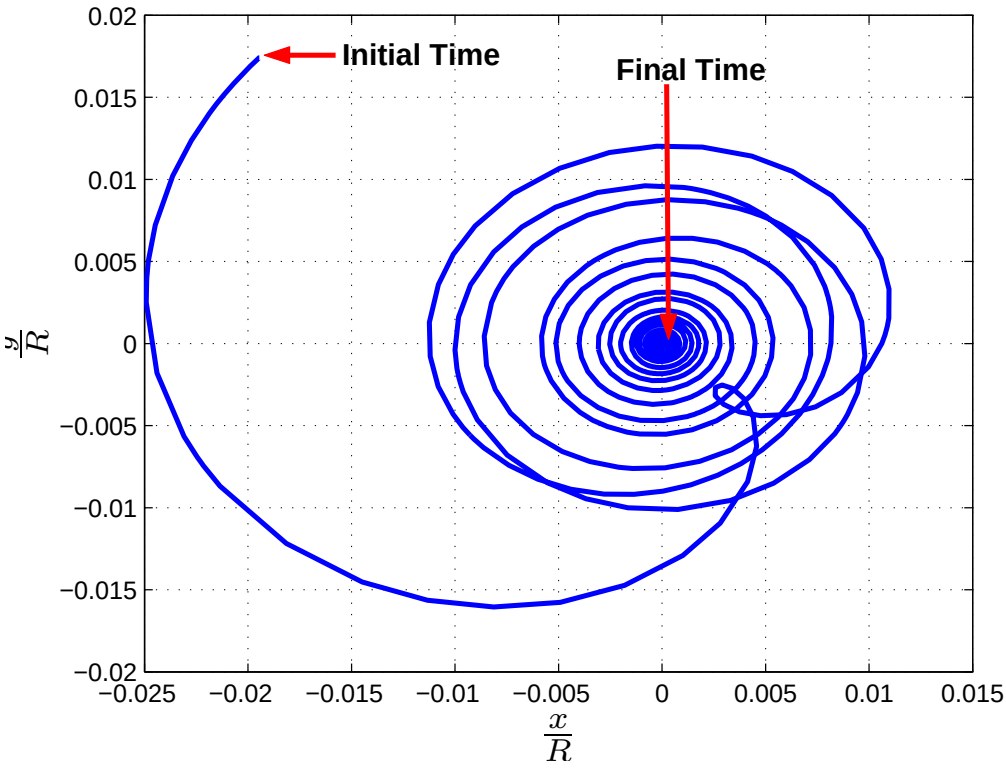

Figure 4.42: Rotor centre of mass motion - Selective damping law 2

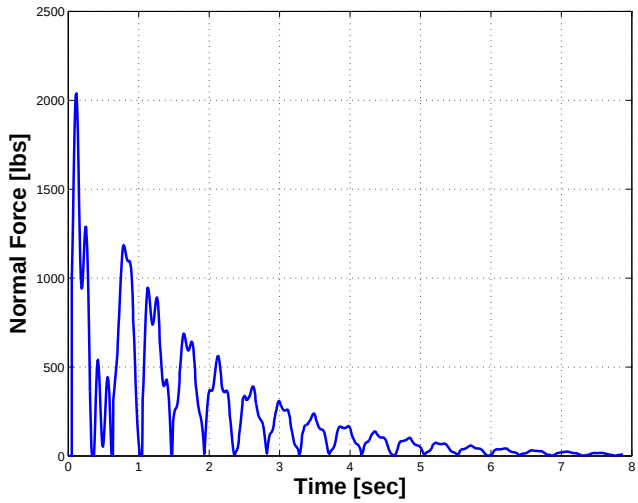

(a) Blade 1

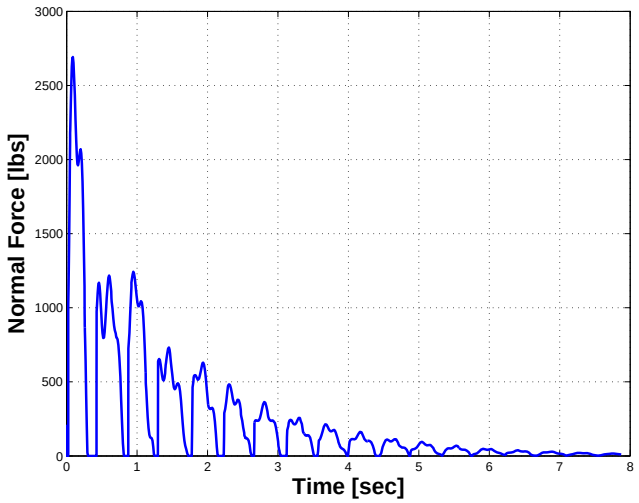

(b) Blade 2

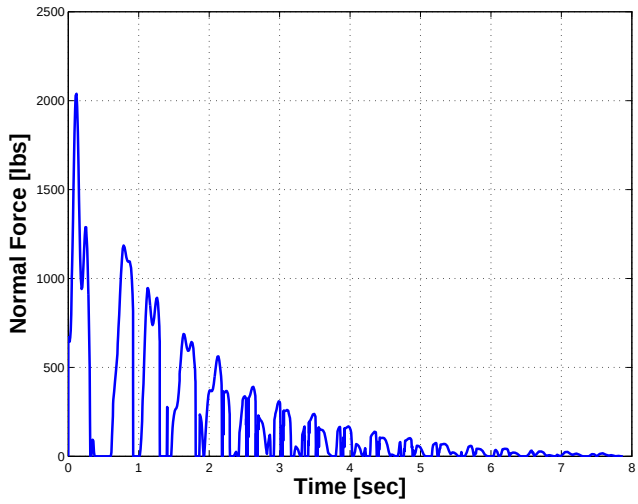

(c) Blade 3

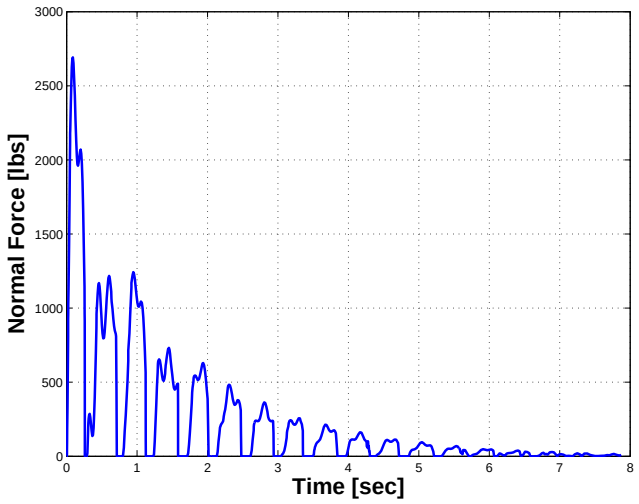

(d) Blade 4

Figure 4.43: Actuator applied normal load in blade-attached damper - Selective damping law 2

CHAPTER V

UH-60 ANALYSIS

The semi-active lag damping concept presented in previous chapter is applied to the UH-60 helicopter model in this chapter. A multibody based comprehensive model of the helicopter is developed using DYMORE, a finite element based tool for the analysis of nonlinear elastic multibody systems developed at Rotorcraft Center of Excellence at Georgia Tech. The semi-active lag damping concept is implemented as feedback control law modulating the frictional resistance in the lag joint attached to the blade and hub. The stability of the system with reference to ground resonance motion is studied and the effectiveness of the concept is analyzed.

In the next section, a brief overview of finite element based multibody dynamics formulations is presented.

5.1 Multibody Dynamics Formulations

Multibody formulations allow the modeling of novel rotorcraft configurations of arbitrary topology through the assembly of basic components chosen from an extensive library of elements. The element library includes the basic structural elements such as rigid bodies, composite capable beams and shells, and joint models. Although a large number of joint configurations are possible, most applications can be treated using the simple lower pairs. More advanced joints, such as contact and backlash elements are also available in many commercial codes. All elements are referred to a single inertial frame, and hence, arbitrarily large displacements and finite rotations must be treated exactly. No modal reduction is performed, i.e. the full finite element equations are used at all times. In fact, with today's advances in computer hardware, inexpensive PCs provide enough computational power to

run complex rotor systems. Hence, resorting to modal reduction in order to save CPU time might no longer be an overwhelming argument, especially when considering the possible loss of accuracy associated with this reduction [6].

Rigid bodies can be used for modeling components whose flexibility can be neglected or for introducing localized masses. For example, in certain applications, the flexibility of the swash-plate may be negligible and hence, a rigid body representation of this component is acceptable. Beams are typically used for modeling rotor blades, but can also be useful for representing transmission shafts, pitch-links, or wings of a tilt rotor aircraft. In view of the increasing use of composite materials in rotorcraft, the ability to model components made of laminated composite materials is of importance. Specifically, it must be possible to represent shearing deformation effects, the offset of the center of mass and the shear center from the beam reference line, and all the elastic couplings that can arise from the use of tailored composite materials. Ref. [7] gives details and examples of application of the integration of a cross-sectional analysis procedure with the multibody dynamic simulation.

A distinguishing feature of multibody systems is the presence of a number of joints that impose constraints on the relative motion of the various bodies of the system. Articulated rotors and their kinematic chains are easily modeled with the help of lower pair joints, i.e. the revolute, prismatic, screw, cylindrical, planar and spherical joints. For example, a conventional blade articulation can be modeled with the help of three revolute joints representing pitch, lag and flap hinges. Another example is provided by the pitch-link, which is connected to the pitch-horn by means of a spherical joint, and to the upper swash-plate by a universal joint to eliminate rotation about its own axis.

All joints are formulated with the explicit definition of the relative displacements and rotations as additional unknown variables. This allows the introduction of generic spring and/or damper elements in the joints, as usually required for the modeling of realistic configurations. Furthermore, the time histories of joint relative motions can be driven

according to suitably specified time functions. For example, in a helicopter rotor, collective and cyclic pitch settings can be obtained by prescribing the time history of the relative rotation at the corresponding joints.

5.1.1 Robust Integration of Multibody Dynamics Equations

Special implicit integration procedures for non-linear finite element multibody dynamics have been developed in Refs. [8, 4]. These algorithms are designed so that a number of precise requirements are exactly met at the discrete solution level. This guarantees robust numerical performance of the simulation processes. In particular, the following requirements are met by the schemes: nonlinear unconditional stability, a rigorous treatment of all nonlinearities, the exact satisfaction of the constraints, and the presence of high frequency numerical dissipation. The proof of nonlinear unconditional stability stems from two physical characteristics of multibody systems that are reflected in the numerical scheme: the preservation of the total mechanical energy and the vanishing of the work performed by constraint forces. Numerical dissipation is obtained by letting the solution drift from the constant energy manifold in a controlled manner in such a way that at each time step, energy can be dissipated but not created. The use of these unconditionally stable schemes is particularly important in intermittent contact problems whose dynamic response is very complex due to the large, rapidly varying contact forces applied to the system and to the dramatic change in stiffness when a contact condition is activated. More details on these non-linearly stable schemes can be found in Ref. [4] and references cited therein.

5.1.2 Solution Procedures

Once a multibody representation of a rotorcraft system has been defined, several types of analysis can be performed on the virtual prototype. A static analysis solves the static equations of the problem, i.e. the equations resulting from setting all time derivatives equal to zero. The deformed configuration of the system under the applied static loads is then computed. The static loads can be of various types such as prescribed static loads, steady aerodynamic loads, or the inertial loads associated with prescribed rigid body motions.

Once the static solution has been found, the dynamic behavior of small amplitude perturbations about this equilibrium configuration can be studied. This is done by first linearizing the dynamic equations of motion, then extracting the eigenvalues and eigenvectors of the resulting linear system. Due to the presence of gyroscopic effects, the eigenpairs are, in general, complex. Finally, static analysis is also useful for providing the initial conditions to a subsequent dynamic analysis. For instance, a rotor run-down simulation would be started with initial conditions corresponding to the static solution for the rotor rotating at nominal speed under gravity and aerodynamic loads.

A dynamic analysis solves the nonlinear equations of motion for the complete multibody system. The initial conditions are taken to be at rest, or those corresponding to a previously determined static or dynamic equilibrium configuration. Complex multibody systems often involve rapidly varying responses. In such event, the use of a constant time step is computationally inefficient, and crucial phenomena could be overlooked due to insufficient time resolution. Automated time step size adaptivity is therefore an important part of the dynamic analysis solution procedure. A simple but effective time adaptive procedure is developed for the integrators used in this effort, as detailed in Ref. [3]. This automated procedure is crucial for the analysis of contact problems. Indeed, very small time steps must be used during the short period when impact occurs, whereas much larger time steps can be used when the stops are not in contact. Using the small time step for the entire duration of the simulation would needlessly increase the required computational resources.

The finite element based, multibody dynamic analysis of rotorcraft generates massive amounts of data that can be processed in a variety of ways. Apart from standard time history plots of positions, velocities and stresses in any point of the model, objects of the multibody system can be viewed in a symbolic manner to help model validation, or with associated predefined geometrical shapes to improve the realism of the visualization. For static analysis, step-by-step visualization is provided together with eigenmode animation. For dynamic analysis, the time dependent system configuration is displayed, and different vector-type attributes, such as linear or angular velocities, internal forces or moments, curvatures or strains, and aerodynamic forces or moments can be added.

5.2 UH-60 Multibody Model

A brief description of comprehensive UH-60 helicopter model as implemented in DYMORE is presented in this section. The two parts of the helicopter model, namely rotor and fuselage-landing gear are developed separately and then coupled together.

5.2.1 Rotor Model

Figure 5.1 depicts the conceptual representation of a rotor system as a flexible multibody system that is used for this study. The picture shows a classical configuration for the control chain, consisting of a swash-plate with rotating and non-rotating components. The lower swash-plate motion is controlled by actuators that provide the vertical and angular control inputs. The upper swash-plate is connected to the rotor shaft through a scissors-like mechanism, and controls the blade pitching motions through pitch-links. This familiar control linkage configuration can be modeled using the following elements: rigid bodies, used to model the lower and upper swash-plate components and scissors links, and beams for modeling the flexible shaft and pitch-link. These bodies are connected through standard mechanical joints: a hinge, called a revolute joint in the terminology of multibody dynamics, connects the upper and lower swash-plates, allowing the former to rotate at the shaft angular velocity while the latter is non-rotating. Revolute joints also connect the scissors links to each other and to the upper swash-plate, thereby synchronizing the shaft and upper swash-plate. Other types of joints are required for the model. For instance, the lower swash-plate is allowed to tilt with respect to an element that slides along the shaft, but does not rotate about the shaft direction. The universal joint, a sequence of two revolute joints whose mutually orthogonal axes of rotation lie in a common plane, serves this purpose. Similarly, the pitch-link is connected to the pitch-horn by means of a spherical joint that allows the connected components to be at an arbitrary orientation with respect to each other.

The Sikorsky's UH-60 is a four-bladed helicopter whose physical properties are described in Ref. [11] and references therein. Figure 5.2 shows the configuration of the rotor system

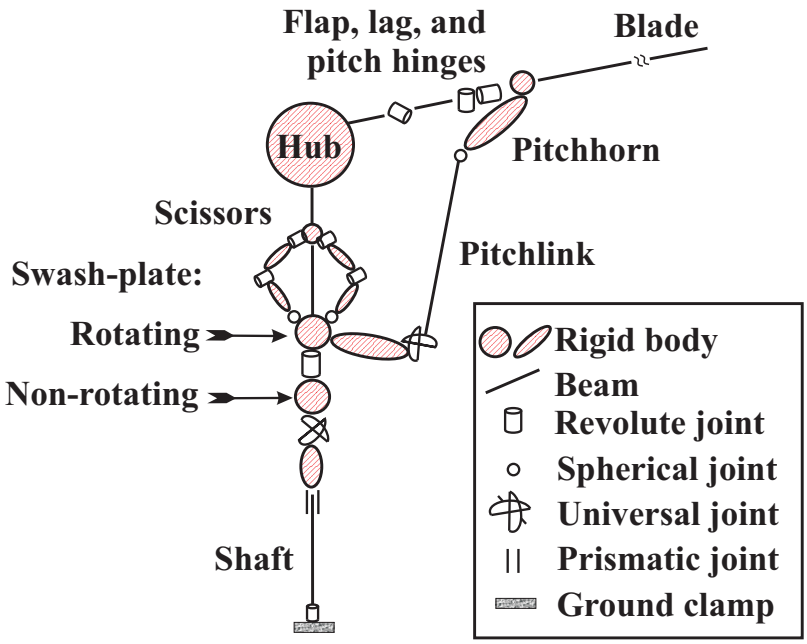

Figure 5.1: Multibody of the rotor

featuring the blade root retention structure, pitch link and pith horn, swash-plate, and lead-lag damper. The blade is modeled using thirteen cubic beam elements. The root retention structure is split into three separate segments modeled, from hub to blade, with three, two, and two cubic beam elements, respectively. The first segment is attached to the hub. The first two segments are connected to each other by an elastomeric bearing modeled by three co-located revolute joints. The physical characteristics of the bearing are simulated by springs and dampers in the joints. The last two segments are rigidly connected to each other and to the pitch horn. Finally, the last segment is rigidly connected to the blade and damper horn. The pitch angle of the blade is set by the following control linkages: the swash-plate, pitch link, and pitch horn. The pitch link, modeled by three cubic beam elements, is attached to the rigid swash-plate by means of a universal joint and to the rigid pitch horn by a spherical joint. The damper arm and damper horn are modeled with rigid bodies. The lead-lag damper is modeled as a prismatic joint damper with pressure relief valves, as described in earlier sections; its end points are connected to the damper arm and horn; the physical properties of the device can be found in Ref. [57].

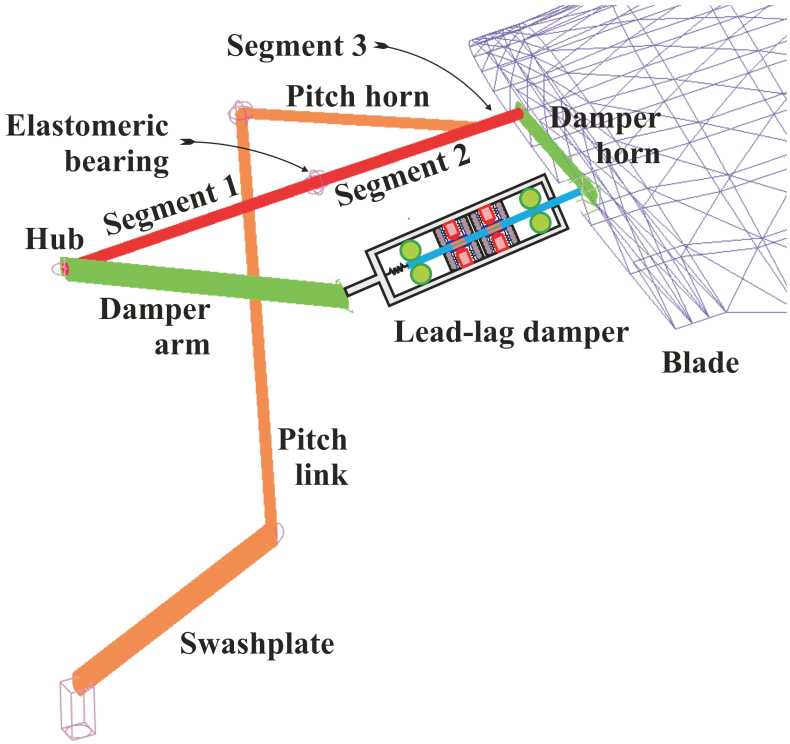

Figure 5.2: Sikorsky's rotor system with integrated semi-active lag damper

5.2.2 Fuselage-Landing Gear Model

The rotor-fuselage-landing gear model of the Sikorsky's UH-60 helicopter is shown in Figure 5.3. The landing gear and rotor assembly are attached to the fuselage at its two end attachment points. The center of gravity of the fuselage-landing gear model lies at the attachment of the gear with the fuselage. The landing gear consists of three supporting structures, left, right and tail gear respectively. The structure is transformed to a simplified spring-mass-damper model as shown in the Figure 5.5. The fuselage is represented by a rigid body with appropriate mass and inertia characteristics. Each gear consists of a oleo strut and tires represented by springs and damper. The multibody representation as implemented in DYMORE is derived from the spring-mass-damper model as shown in the Figure 5.4. The representation is built from the basic structural elements such as rigid bodies, constraint elements and joint models such as prismatic and flexible ones. The oleo struts are modeled as prismatic joints which are connected to the tires. The tires have three linear degrees of freedom and are modeled as flexible joints. Tail oleo has an additional flexible joint in the

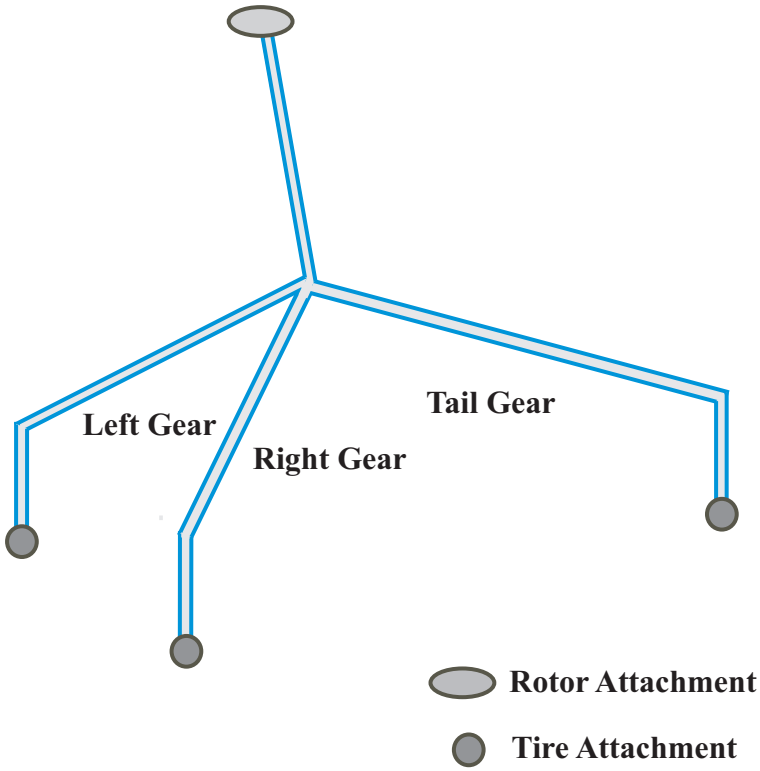

Figure 5.3: UH-60 fuselage-landing gear model

oleo strut.

5.3 Semi-Active Damper Model

The lead-lag damper is modeled as a prismatic joint installed across the lead-lag hinge by attaching one end to the damper arm and the other to the damper horn. The lag motion of the blade causes relative axial deflection of the joint resulting in generation of resistive force through in-built damping mechanism.

In the computational model of UH-60 rotor, the semi-active damping mechanism is realized by designing a feedback controller enforcing frictional resistance variation in the joint as guided by the control law. The semi-active and selective damping control laws as derived in previous chapter need feedback of the lag mode and the regressive component of the lag mode respectively. For the lag damper, the damper stroke q is proportional to the lag motion. A similar quantity proportional to regressive component of lag motion,

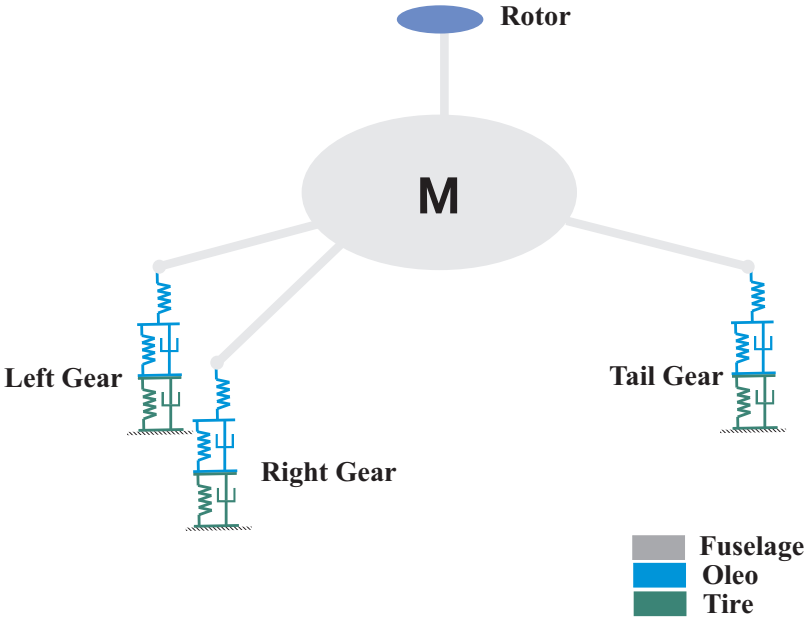

Figure 5.4: UH-60 fuselage-landing gear spring-mass-damper model

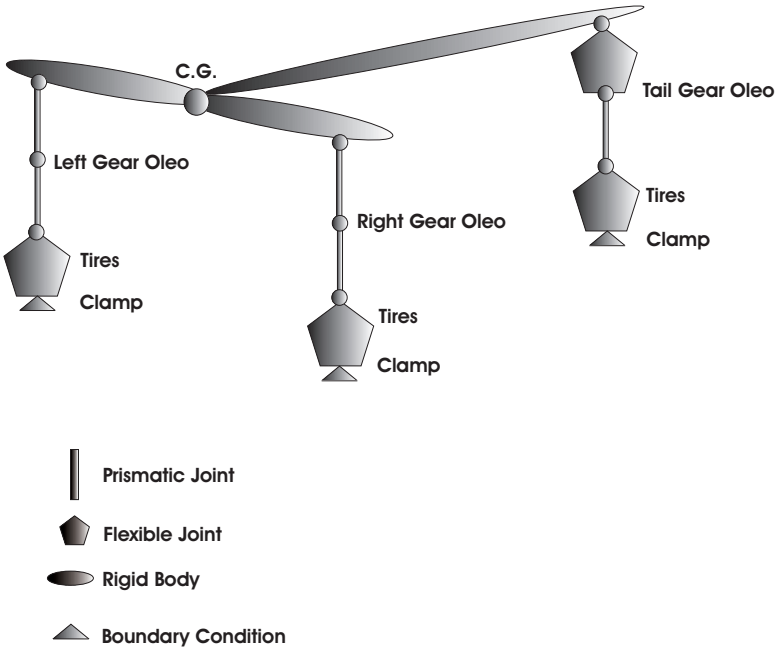

Figure 5.5: UH-60 landing gear multibody model

represented by q_r is obtained using the multiblade coordinate transformation. Using this transformation technique, the time rate of regressive lag component given by $\dot{\phi}_r$ can be obtained as shown in Appendix B. In the present scenario, regressive component of damper stroke rate, $\dot{q}_r$ is of interest. The computational code DYMORE has in-built sensors for mechanical measurements. Sensors working in conjunction with controllers are designed to compute quantities at each time step of the simulation. Velocity sensors sense the relative motion of the prismatic lag joint. The multibody coordinate transformation is then utilized to obtain time rate regressive lag component $\dot{q}_r$ in a similar manner.

$$\dot{q}_{ir} = \frac{1}{2}\sin(\psi_i)\sum_{j=1}^{4}\dot{q}_j\sin(\psi_j) + \frac{1}{2}\cos(\psi_i)\sum_{j=1}^{4}\dot{q}_j\cos(\psi_j) \tag{5.1}$$

5.4 Friction Modeling

The number of friction models proposed in literature is immense and can be subdivided with respect to their detail in describing surface contact properties occurring on a microscopic and macroscopic level. In the past decade, major effort and contributions have been made in the development of friction models, suitable for analysis and controller synthesis, which have limited complexity but a rich similarity to practically observed friction properties. The following qualities of a friction model are considered to be important for controller design, which are encountered when a mechanical system with friction accelerates from zero velocity:

- Presliding displacement (stiction), which is a spring-like behavior in the stick phase due to limited stiffness of contact asperities.
- Static friction, that is assumed to be independent of the velocity, but varies as a function of the dwell-time when sticking and the rate of increase of the applied force.
- Stribeck curve, i.e., a continuous drop in the friction force for small velocities, which originates from the transition of boundary lubrication to full fluid lubrication through partial fluid lubrication.

- Frictional lag, which is a dynamic behavior that results in a larger friction force for increasing velocities than for decreasing velocities and becomes more apparent for large acceleration and/or deceleration.

The LuGre model is a dynamic friction model presented by Canudas de Wit *et al.* [17]. The model visualizes the friction phenomenon at microscopic level where even the visibly smooth surfaces are irregular and the contact between two such surfaces occurs at number of bristle-like asperities. These bristles have certain stiffness and deflect like elastic springs when a tangential force is applied. Friction is modeled as an average deflection force of elastic springs. If the deflection is sufficiently large, the bristles start to slip. The average bristle deflection for a steady state motion is determined by the velocity. It is lower at low velocities, which implies that the steady state deflection decreases with increasing velocity. This models the phenomenon that the surfaces are pushed apart by the lubricant, and models the Stribeck effect. The model also includes rate dependent friction phenomena such as varying break-away force and frictional lag. The model has the form

$$\frac{dz}{dt} = v - \sigma_0 \frac{|v|}{g(v)} z \tag{5.2}$$

$$\mu = \sigma_0 z + \sigma_1(v)\frac{dz}{dt} + \sigma_2 v \tag{5.3}$$

$$g(v) = \mu_k + (\mu_s - \mu_k)e^{-(v/v_0)^2} \tag{5.4}$$

where μ is the instantaneous friction coefficient, z the average bristle deflection, v the relative velocity between the two surfaces, $g(v)$ the Stribeck curve for steady-state velocities, σ_0 the bristle stiffness, and σ_1 and σ_2 control parameters for dynamic dependence of friction on velocity. The symbols μ_s and μ_k represent the standard coefficients of static and dynamic friction respectively. The model qualitatively describes presliding behavior as observed from experimental investigation conducted by researchers.

5.5 Ground Resonance Analysis

The ground resonance analysis of the UH-60 model is performed in the absence of aerodynamic forces and pitch variation. A constant time step size of 256 steps per revolution is used for the structural equations. Helicopter simulations are obtained for discrete rotor speeds in the nominal range 0-300 RPM for at least 50 rotor revolutions to allow all the transients to die out and obtain a periodic solution. The stability of the system is analyzed for several lag damper configurations as discussed further. For friction based dampers, the saturation normal load N_{max} and damping parameter $\dot{\phi}_0$ are kept at constant value of 2000 *lbs* and 0.2 respectively, for simulations at all rotor speeds. Effect of variation of the saturation normal load and damping parameter will be considered later in the chapter.

The presence of friction dampers adds nonlinearity to the system which is reflected as small noise in the system response. The Prony's method is used for the stability analysis where the tolerably high order of the fit can sufficiently produce an effective partitioning of the signal and noise.

5.5.1 No Lag Damper

In this configuration, damping associated with the lag damper is assumed to be absent. Figures 5.6 and 5.7 show damping rate and regressive lag frequency variation with respect to rotor speed for the present system configuration. The results correspond to that for a single blade. Results for other three blades are found to be similar. It can be seen that instability begins at around 75 RPM and reaches maximum around 150 RPM. The regressive lag frequency variation is found to be proportional to the rotor speed as expected. The instability at 150 RPM can be observed from time history of damper stroke plot as shown in Figure 5.8. The roll motion of the fuselage during instability can be observed from the out-of-phase motion of left and right gear as shown in Figure 5.9.

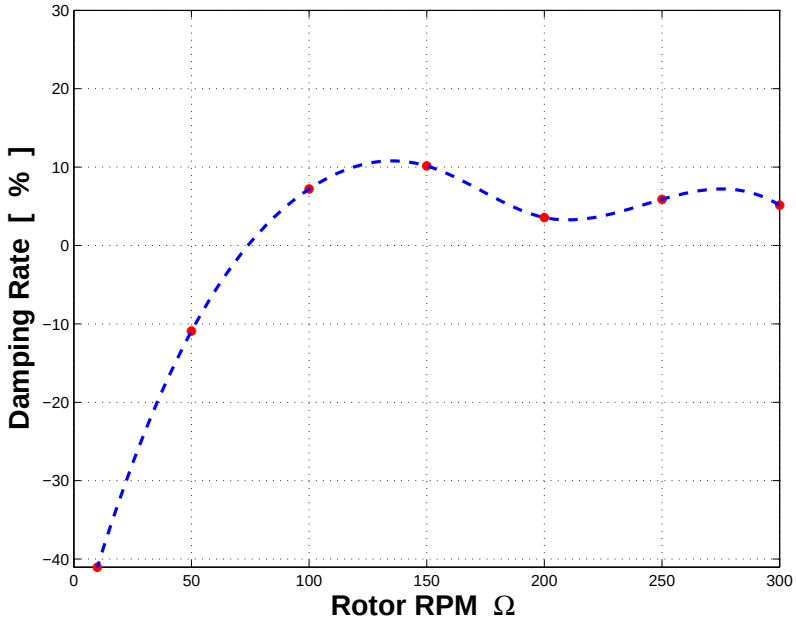

Figure 5.6: Damping as a function of rotor speed - No lag damper

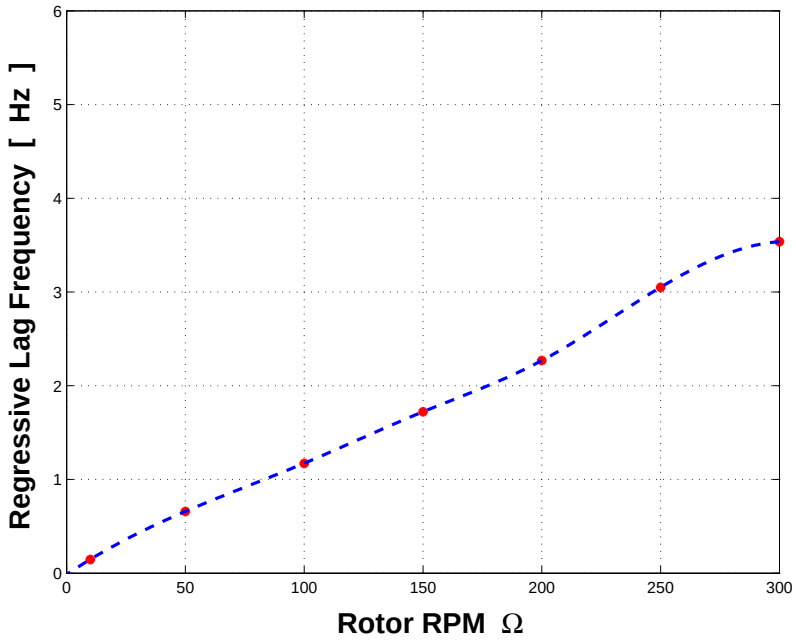

Figure 5.7: Lag regressive frequency as a function of rotor speed - No lag damper

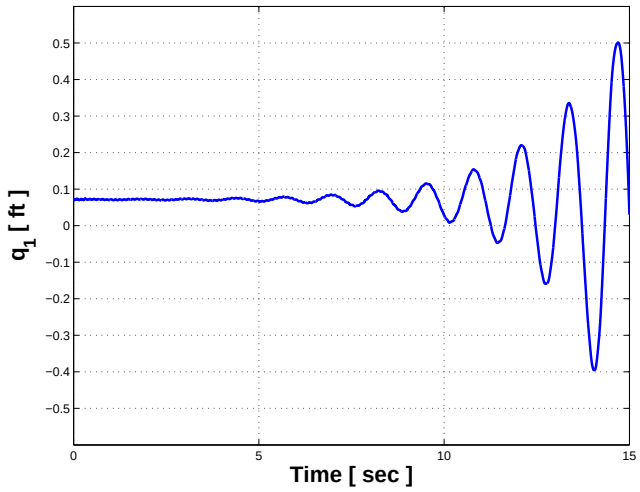

(a) Blade 1

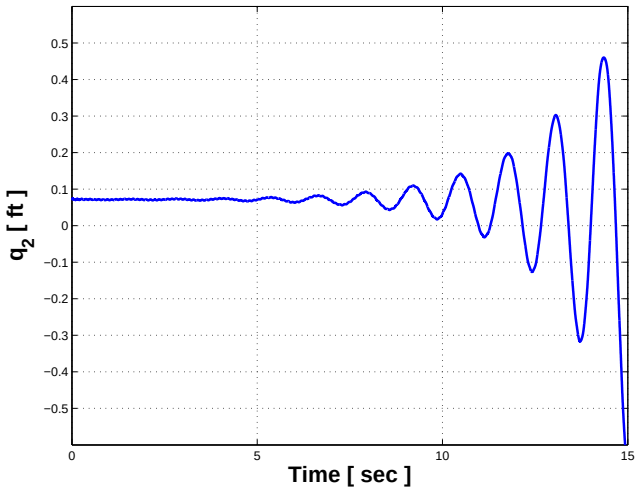

(b) Blade 2

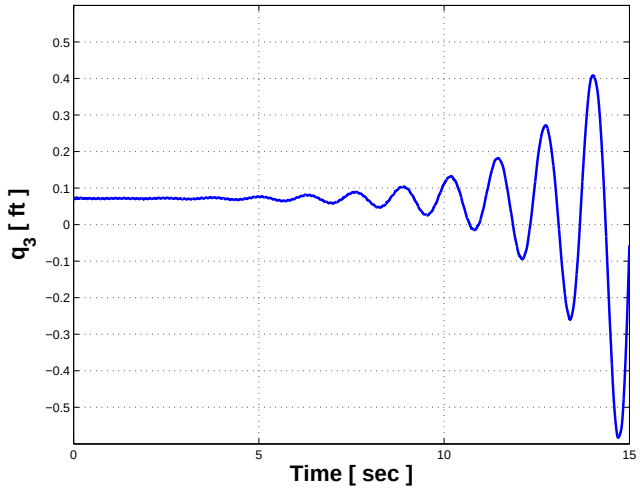

(c) Blade 3

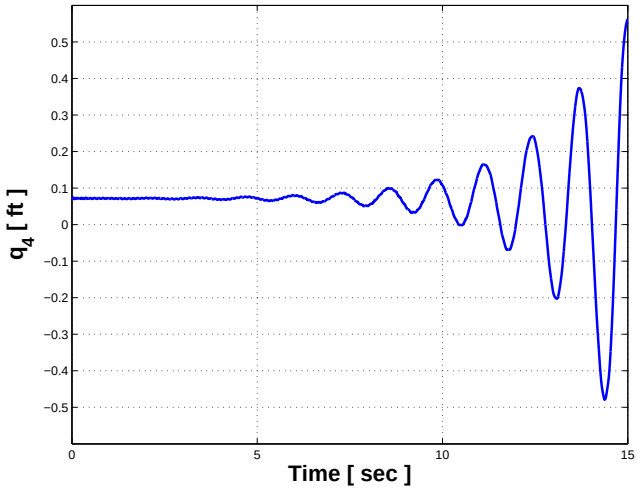

(d) Blade 4

Figure 5.8: Damper stroke - No damper

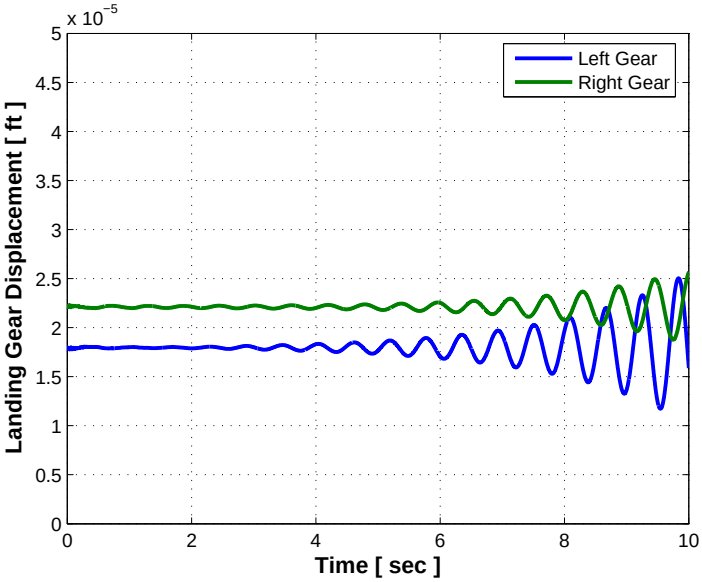

Figure 5.9: Landing gear motion - No lag damper

5.5.2 Hydraulic Damper

The prismatic joint model of the lag damper is replaced by the hydraulic model of the damper as developed by authors of reference [9]. Figures 5.10 and 5.15 show damping rate and lag frequency variation with respect to rotor speed. A stable operation at nominal rotor speed in the presence of damper is observed. The time histories of the damper stroke, damper force and work done by the damper at 150 RPM are shown in Figures 5.12, 5.13 and 5.14 respectively.

5.5.3 Semi-Active Damper

The semi-active damper where normal load is a function of lag velocity as given by Equation 4.9 in the previous chapter with lag velocity $\dot{\phi}_i$ replaced by damper stroke rate $\dot{q}_i$ is chosen. Figures 5.16 and 5.17 show damping rate and lag frequency variation with respect to rotor speed respectively. Next, simulations are performed at 150 RPM. The time history of the damper stroke and its time rate is shown in Figures 5.18 and 5.19 respectively. The damper stroke, representative of lag displacement motion, is stabilized to an equilibrium position within a few seconds. The normal load clearly follows the pattern of relative velocity as shown in Figure 5.20. The friction force variation is plotted in Figure 5.21. On comparing it

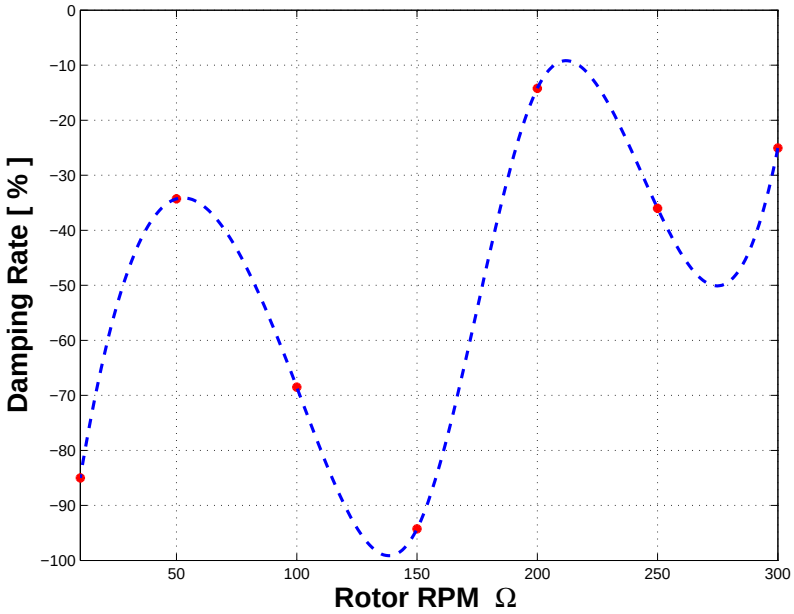

Figure 5.10: Damping as a function of rotor speed - Hydraulic damper

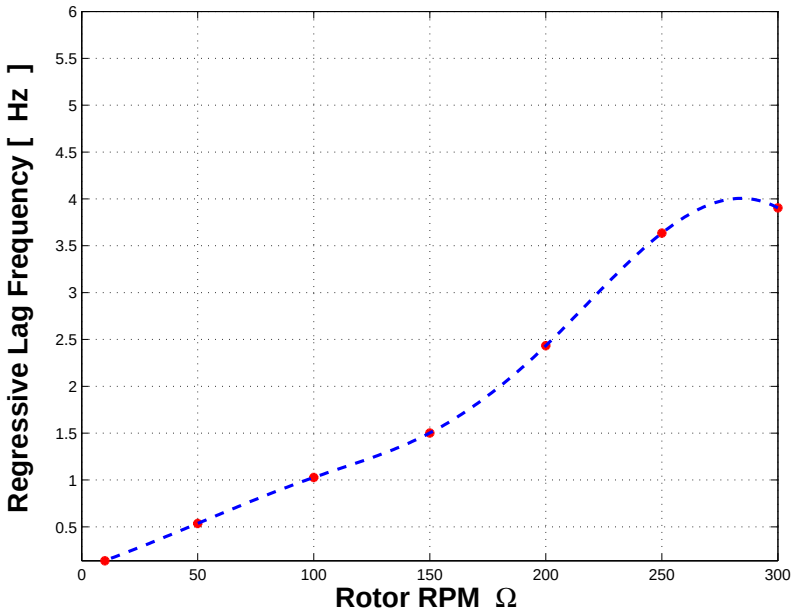

Figure 5.11: Lag regressive frequency as a function of rotor speed - Hydraulic damper

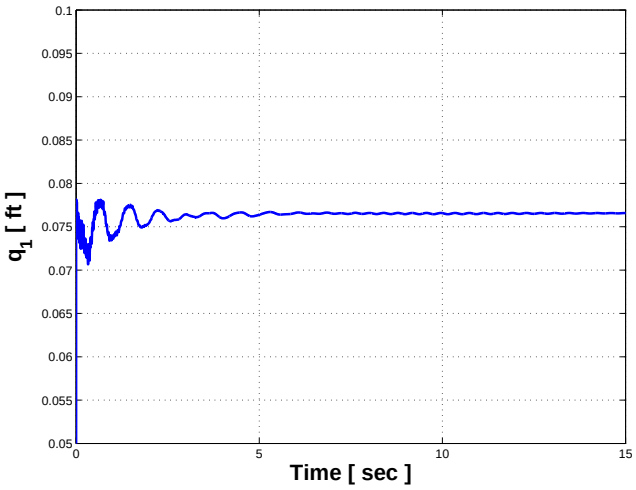

(a) Blade 1

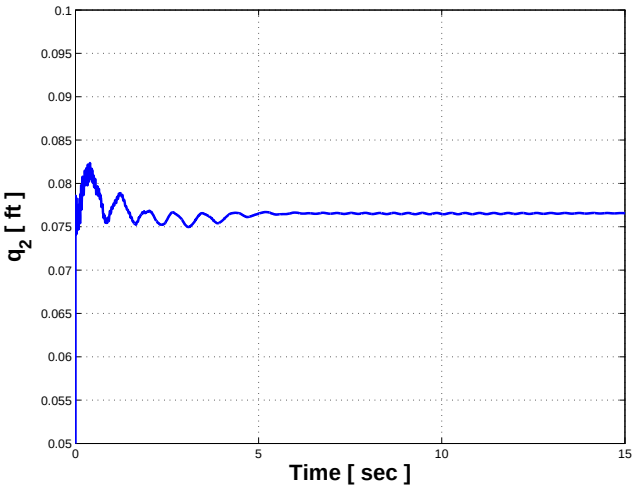

(b) Blade 2

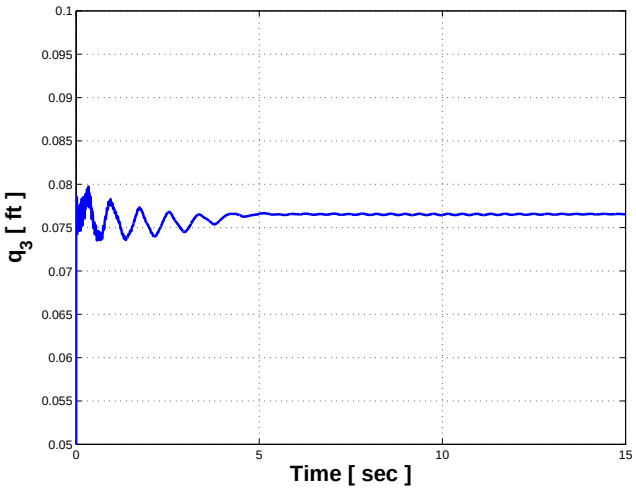

(c) Blade 3

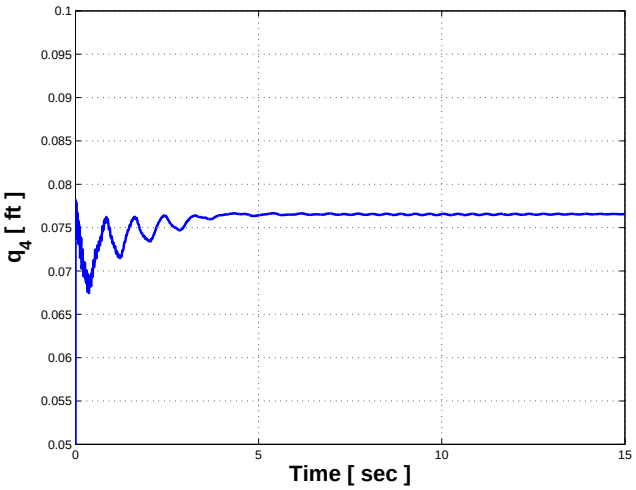

(d) Blade 4

Figure 5.12: Damper stroke - Hydraulic damper

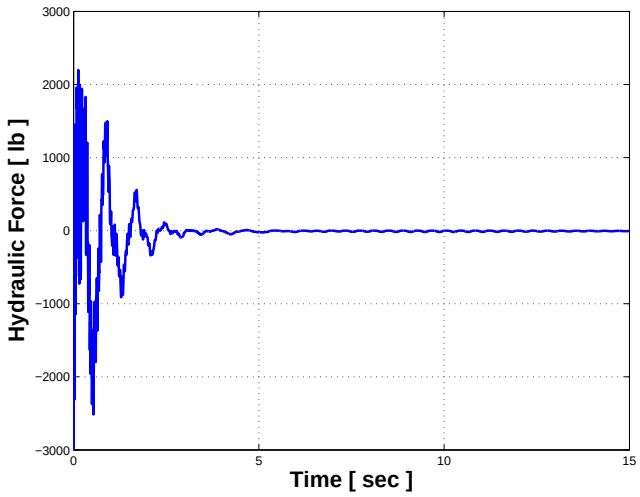

(a) Blade 1

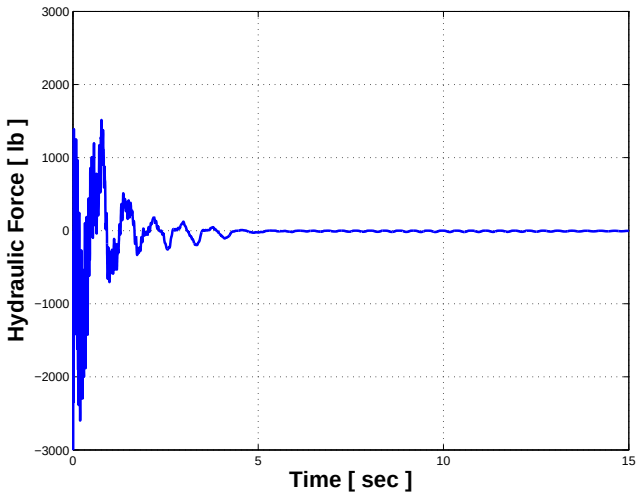

(b) Blade 2

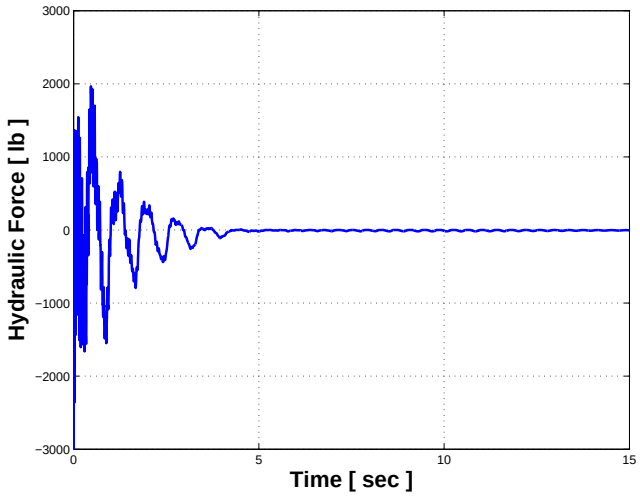

(c) Blade 3

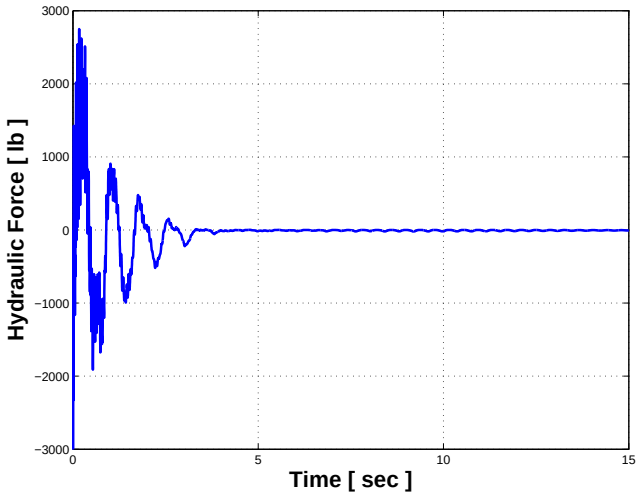

(d) Blade 4

Figure 5.13: Hydraulic damper force variation

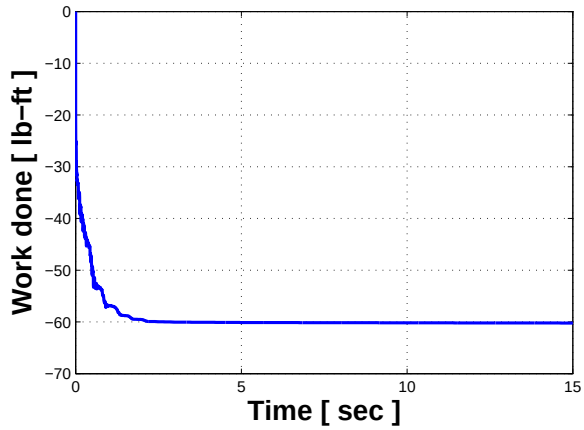

(a) Blade 1

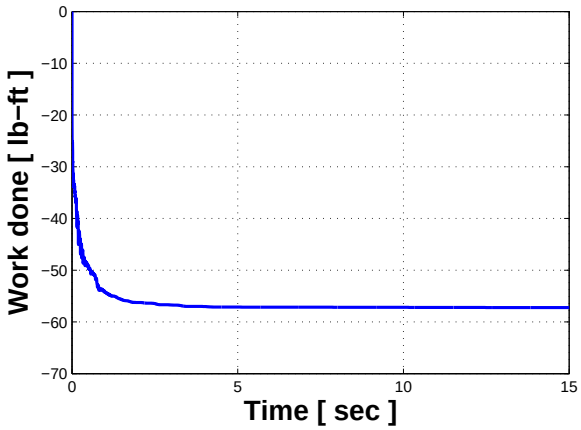

(b) Blade 2

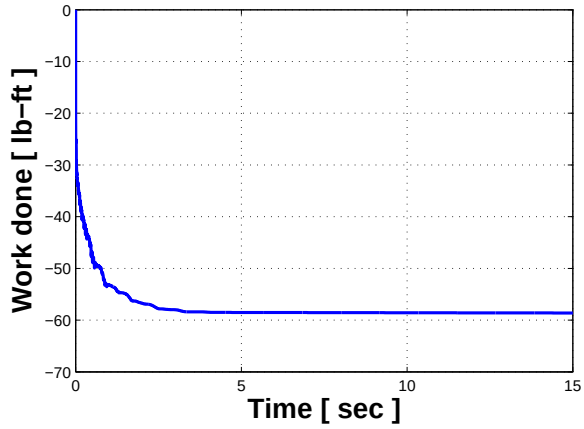

(c) Blade 3

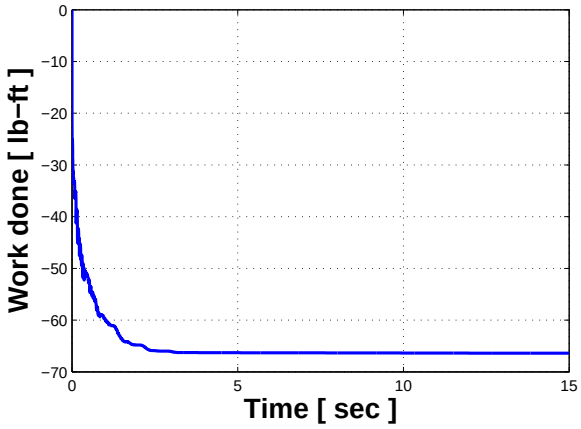

(d) Blade 4

Figure 5.14: Work done by the Hydraulic damper

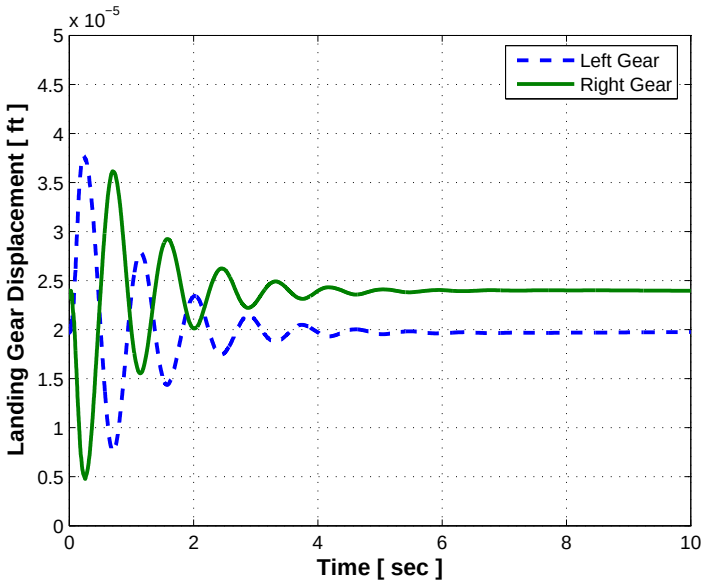

Figure 5.15: Landing gear displacement - Hydraulic damper

with hydraulic force variation plots in Figure 5.13, it is seen that hydraulic damper applied 10 times larger load and hence faster damping. A higher damping rate can be achieved with semi-active damper also by increasing the saturation normal load level. Effect of higher normal loads will be considered later in the chapter. Finally, work done by the damper is shown in Figure 5.22. It is seen that work done to damp the lag motion is of the same order as observed in the case of hydraulic damper. The landing gear motion is shown in Figure 5.23. A damping in the rolling motion of the fuselage followed by in-phase motion of left and right gear is observed.

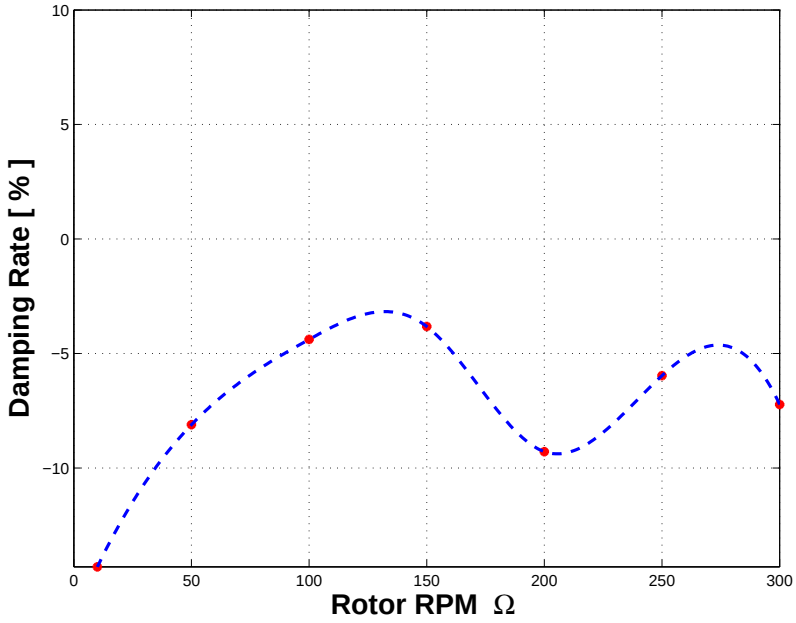

Figure 5.16: Damping as a function of rotor speed - Semi-active damping law

5.5.4 Selective Damping law 1

The control law for Selective damping law 1 is given by Equation 4.11 in the previous chapter with the regressive lag velocity $\dot{\phi}_{\mathrm{r}}$ replaced by the damper regressive stroke rate $\dot{q}_{\mathrm{r}}$. Figures 5.24 and 5.25 show the damping rate and the lag frequency variation with respect to rotor speed. The damper stroke motion is shown in Figure 5.26. The damper stroke rate and its regressive component are shown in Figure 5.27. Again, the simulations are performed at the same rotor speed, 150 RPM. The normal load variation and friction force variation in each damper attached to the blade are shown in Figures 5.28 and 5.29 respectively. Finally, work done by the damper is shown in Figure 5.30. On comparing similar plots for semi-active damper, it is seen that the time taken to damp out the lag motion is much less using semi-active strategy than selective damping strategy even when the magnitude of maximum applied normal load is of comparable magnitude. For better understanding, the normal force variation for semi-active and selective damping strategies is visualized in the smaller time range in Figure 5.31. It is clear that the semi-active damper applies higher load in the beginning while the selective damper, for which damper force is proportional to the regressive motion, applies lower load until regressive mode becomes a dominant modal

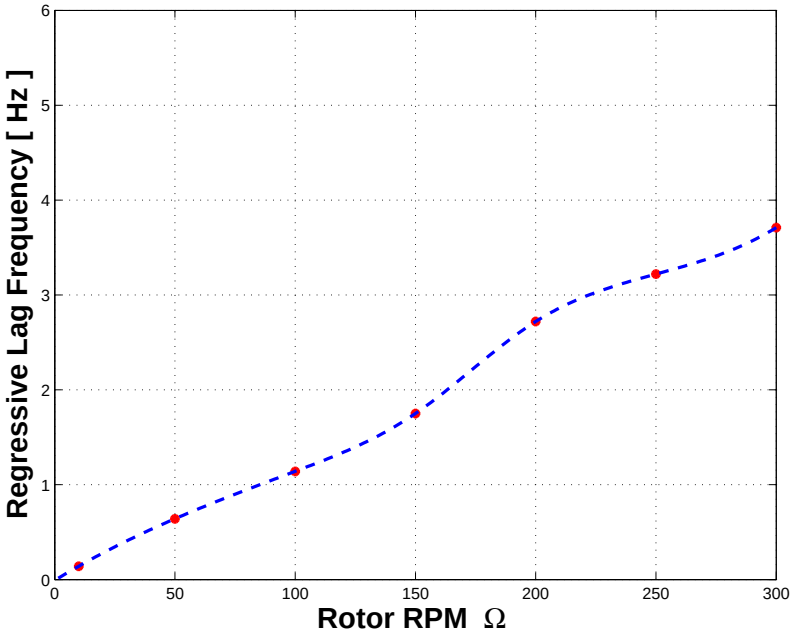

Figure 5.17: Lag regressive frequency as a function of rotor speed - Semi-active damping law

component, at which application of selective damping or semi-active damping makes little difference.

5.5.5 Selective Damping Law 2

The control law for selective damping law 2 is given by Equation 4.12 in previous chapter with the regressive lag velocity $\dot{\phi}_{\mathrm{r}}$ replaced by the damper regressive stroke rate $\dot{q}_{\mathrm{r}}$. Figures 5.32 and 5.33 show the damping rate and the lag frequency variation with respect to rotor speed. Results are extracted for rotor speed of 150 RPM. The damper stroke motion is shown in Figure 5.34. The damper stroke rate and its regressive component are shown in Figure 5.35. The normal load variation and the friction force variation in each damper attached to the blade are shown in Figures 5.36 and 5.37 respectively. Finally, work done by the damper is shown in Figure 5.38. On comparison with results for selective damping law 1, there is not much significant difference in the results due to the absence of phase difference between overall lag motion and lag regressive component, represented by damper stroke rate and its regressive component respectively, as visible from the damper stroke rate

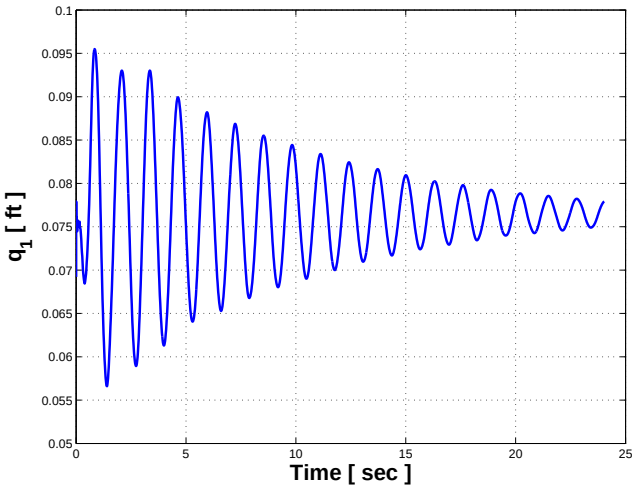

(a) Blade 1

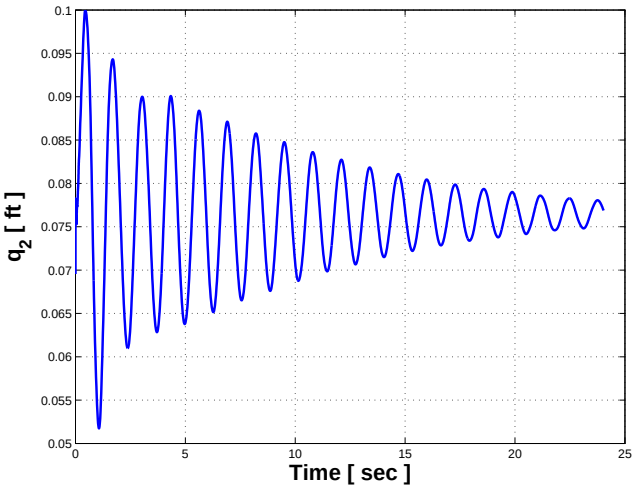

(b) Blade 2

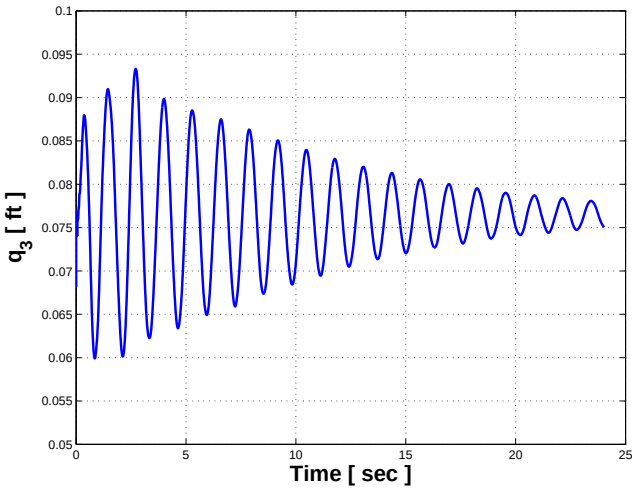

(c) Blade 3

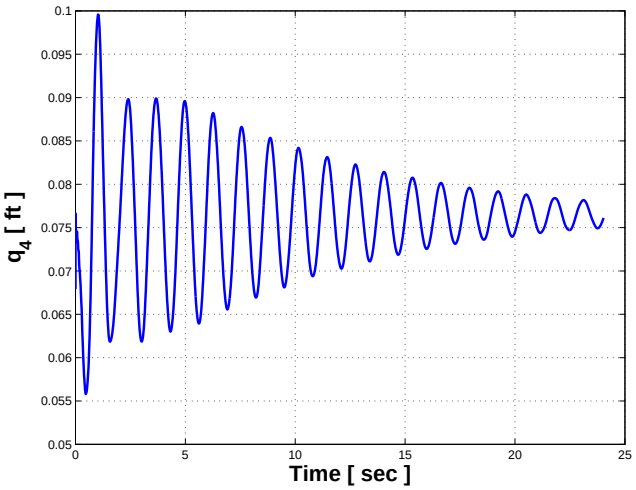

(d) Blade 4

Figure 5.18: Damper stroke - Semi-active damping law

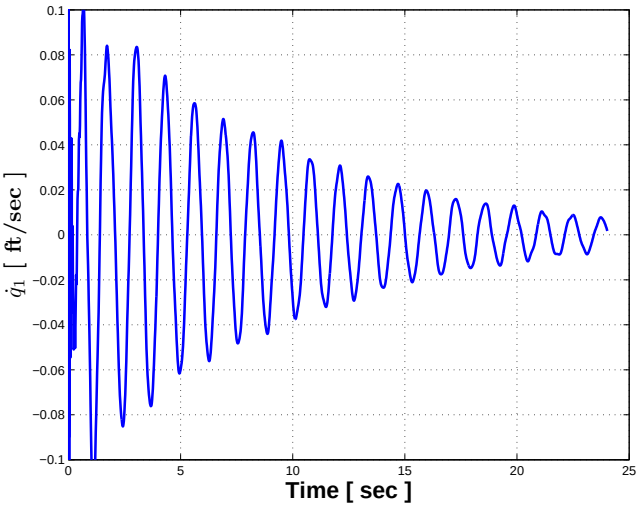

(a) Blade 1

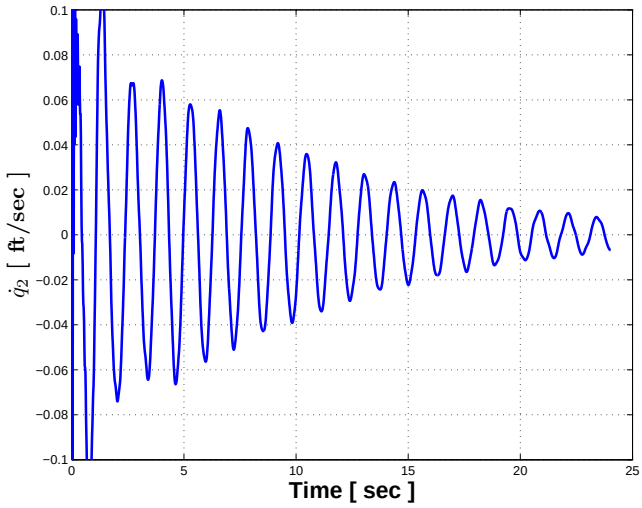

(b) Blade 2

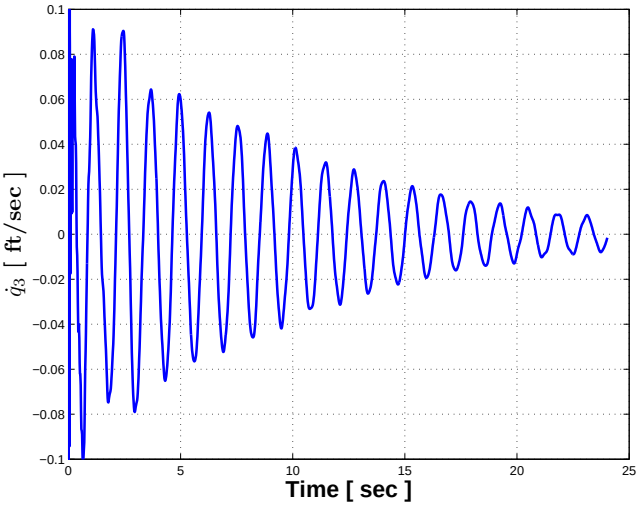

(c) Blade 3

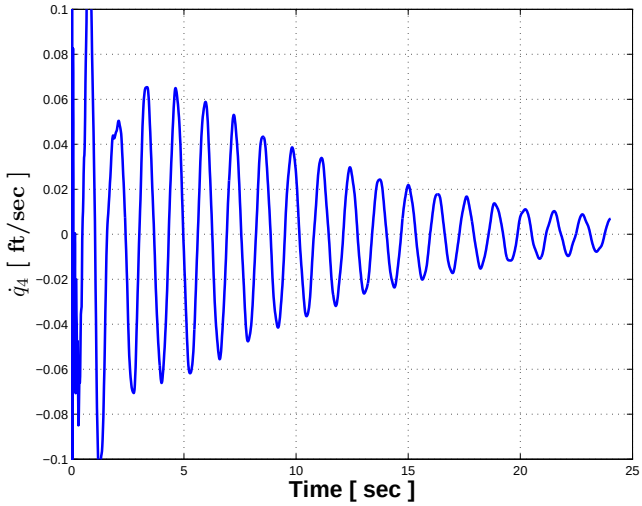

(d) Blade 4

Figure 5.19: Damper stroke rate - Semi-active damping law

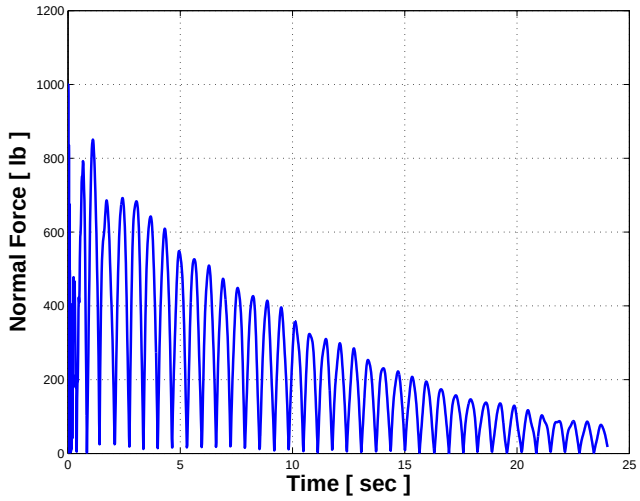

(a) Blade 1

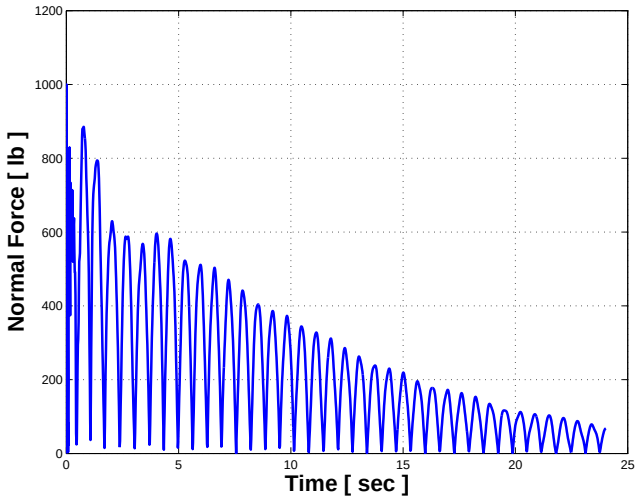

(b) Blade 2

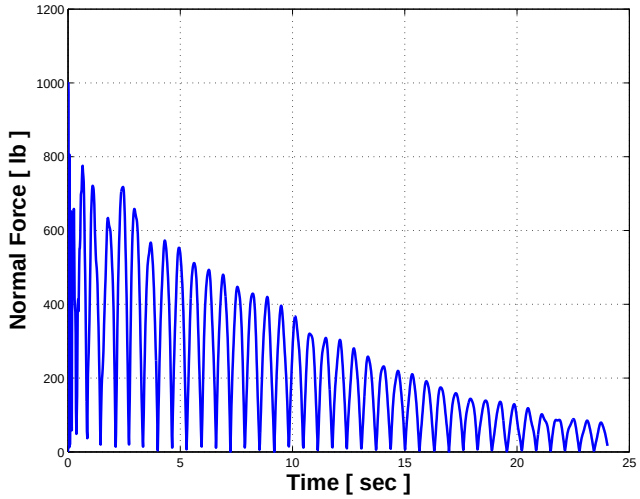

(c) Blade 3

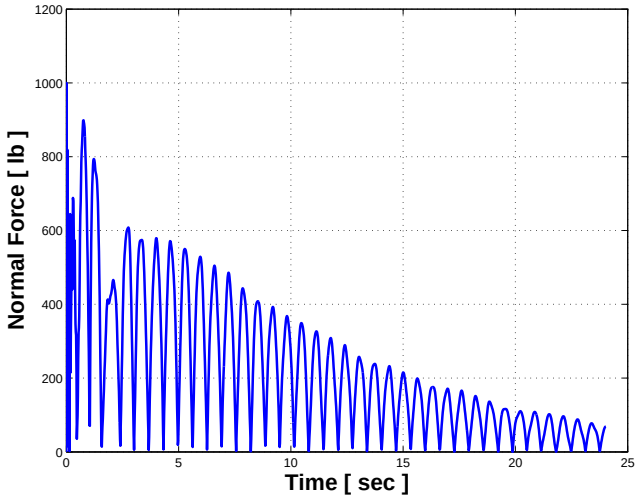

(d) Blade 4

Figure 5.20: Normal load variation - Semi-active damping law

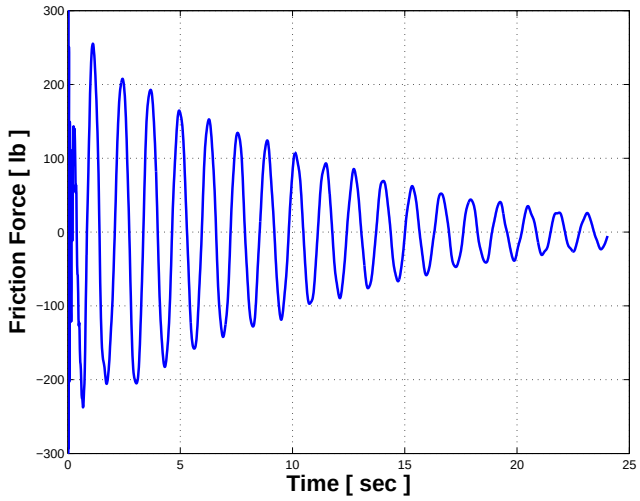

(a) Blade 1

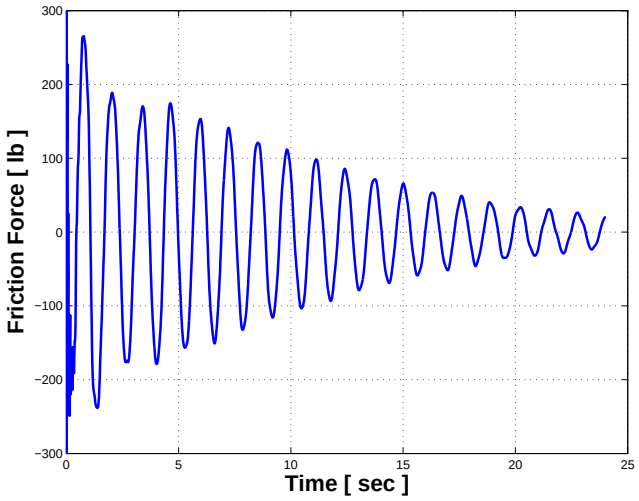

(b) Blade 2

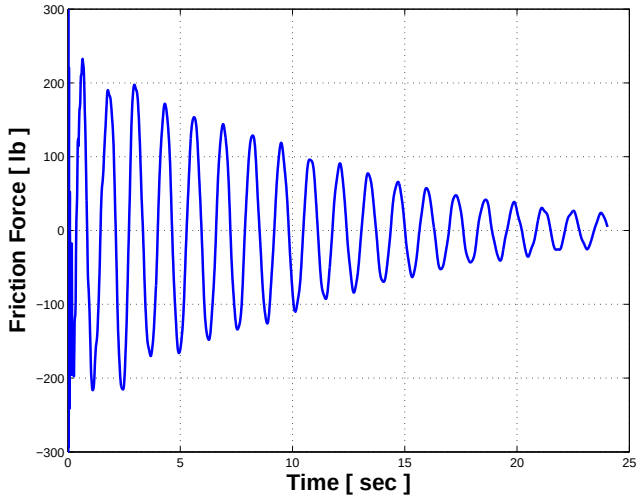

(c) Blade 3

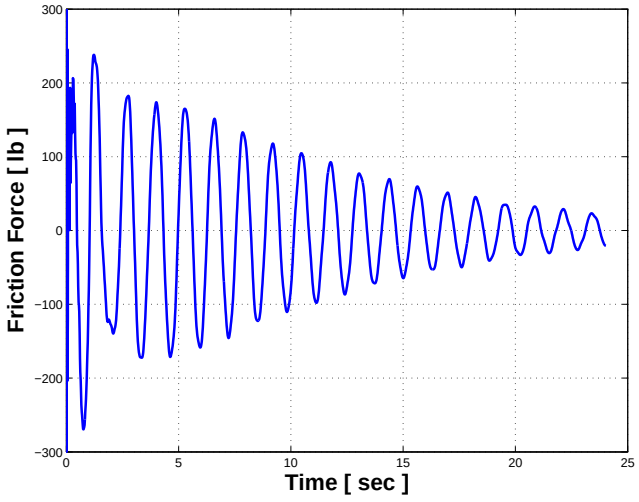

(d) Blade 4

Figure 5.21: Friction force variation - Semi-active damping law

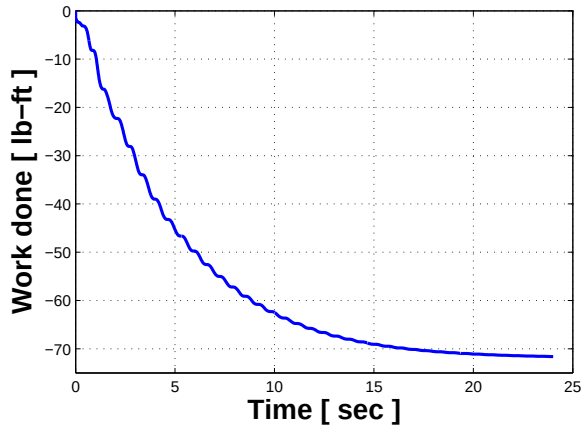

(a) Blade 1

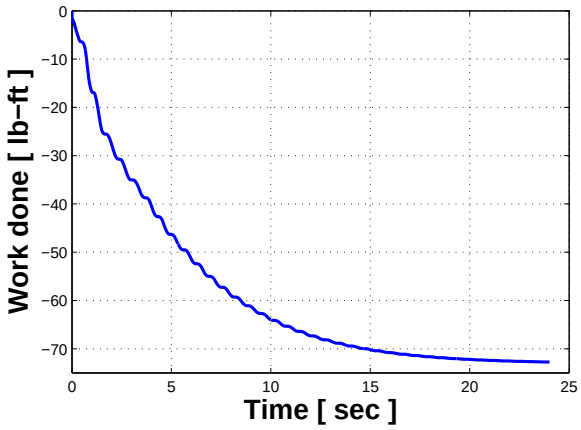

(b) Blade 2

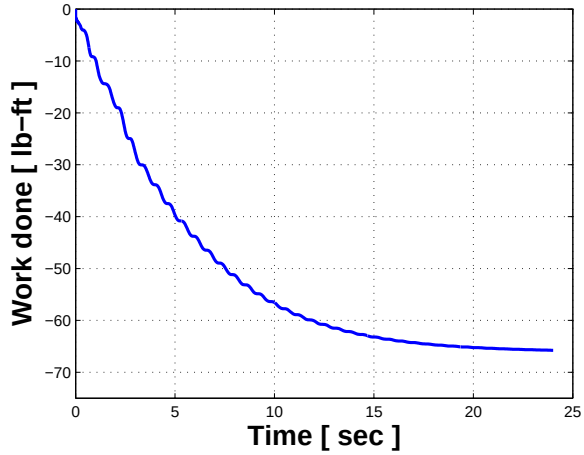

(c) Blade 3

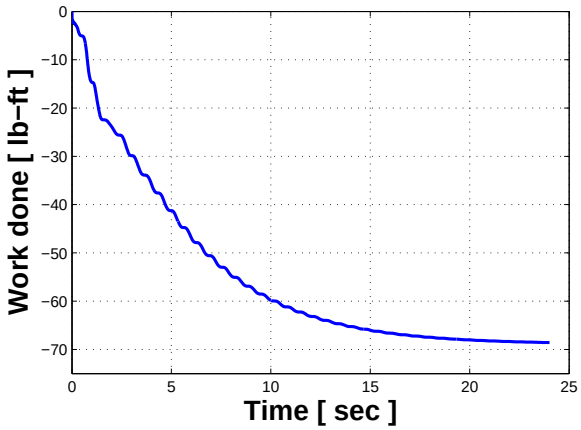

(d) Blade 4

Figure 5.22: Work done by the damper - Semi-active damping law

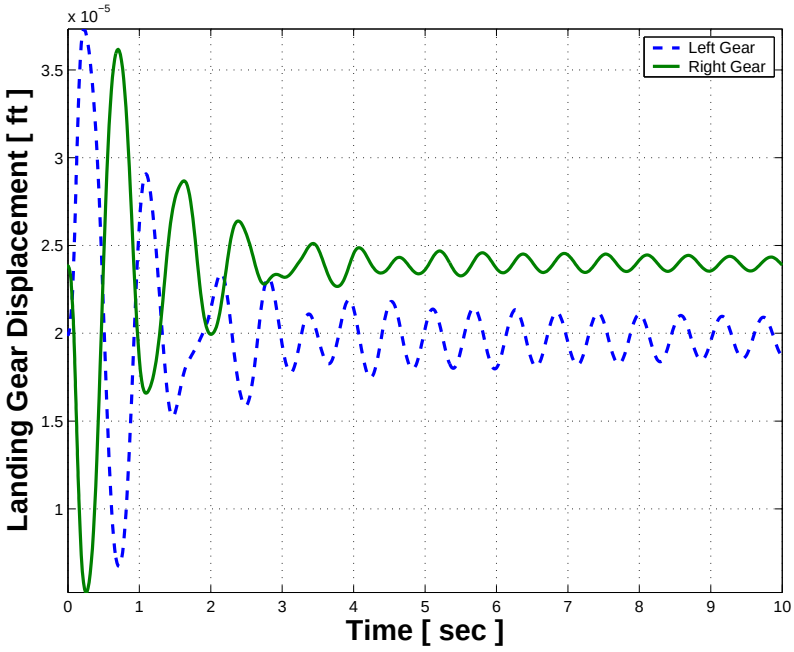

Figure 5.23: Landing gear motion - Semi-active damping law

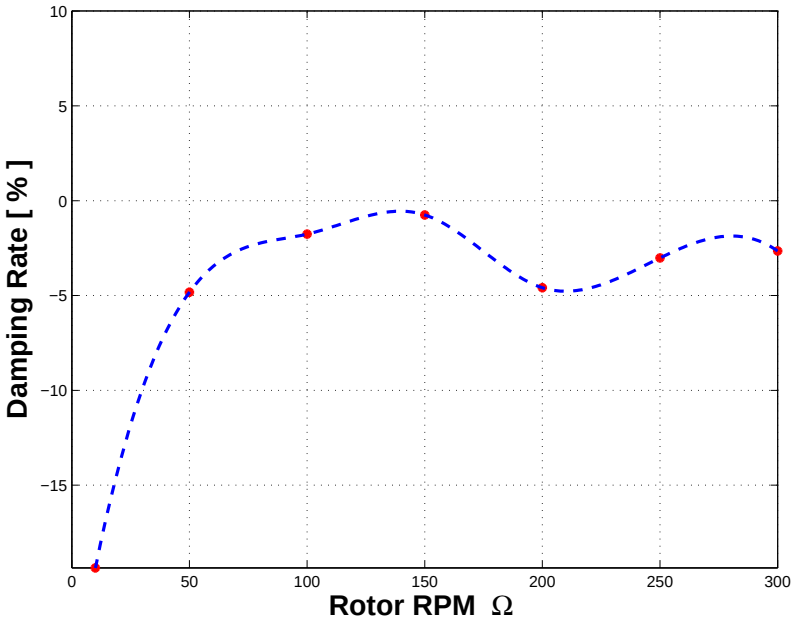

Figure 5.24: Damping as a function of rotor speed - Selective damping law 1

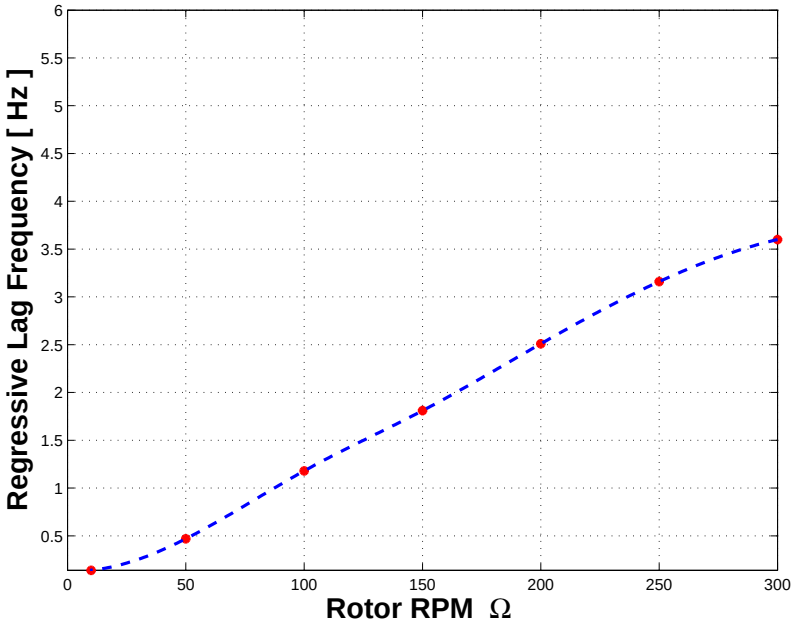

Figure 5.25: Lag regressive frequency as a function of rotor speed - Selective damping law 1

plot. Consequently, the two selective damping strategies yields similar results. A similar behavior is observed with the classical ground resonance model as well.

5.6 Higher normal load effect

Results obtained so far belong to a case of a constant saturation normal load N_{max} and the constant damping parameter $\dot{\phi}_0$. From above results, it is clear that stability can be achieved with the semi-active damper with the damper load almost 10 times lower than the hydraulic damper load. A careful look at the normal load developed by the actuator reveals that the applied normal load never exceeded the 1300 *lbs* magnitude although the saturation load level is set at 2000 *lbs*. This is due to the effect of the damping parameter $\dot{\phi}_0$ which establishes control over the normal load magnitude by controlling the slope of the load profile. A higher damping rate can, thus, be obtained by setting a lower magnitude of the parameter. Next, a study is conducted to understand the effect of higher friction load for achieving faster lag damping. Simulations are conducted for saturation load level of magnitude 5000 *lbs* and reduced magnitude of $\dot{\phi}_0$ to 0.1. Figure 5.39 shows the overall damper performance. It is seen that higher frictional load at low relative velocity results in

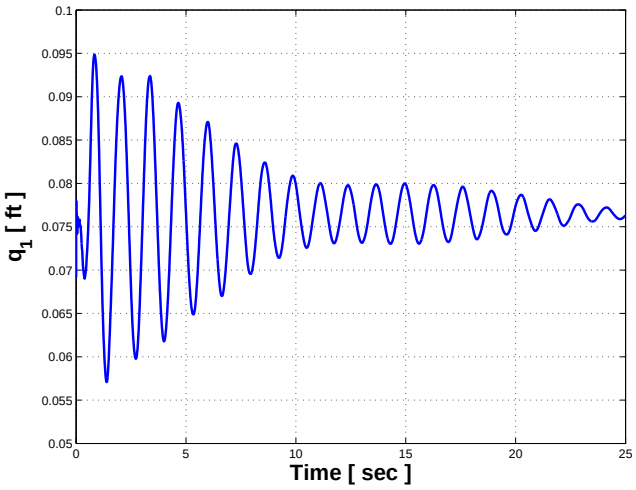

(a) Blade 1

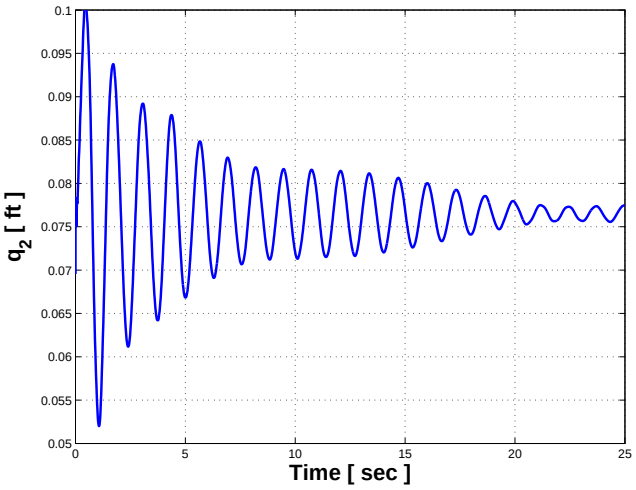

(b) Blade 2

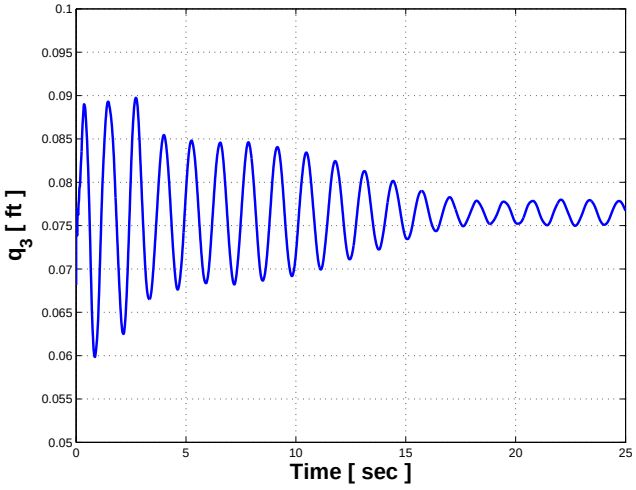

(c) Blade 3

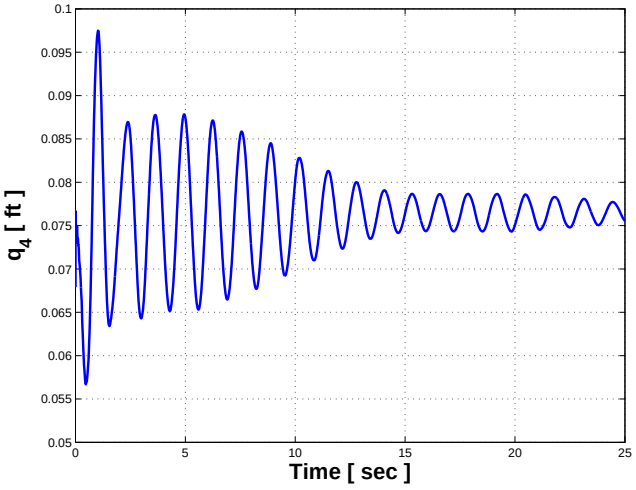

(d) Blade 4

Figure 5.26: Damper stroke - Selective damping law 1

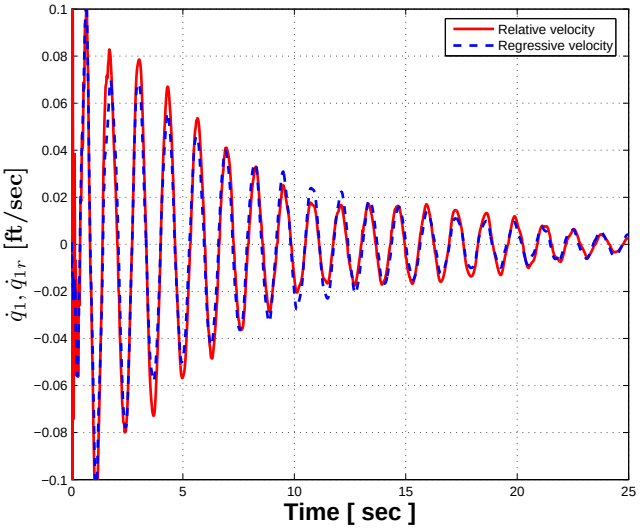

(a) Blade 1

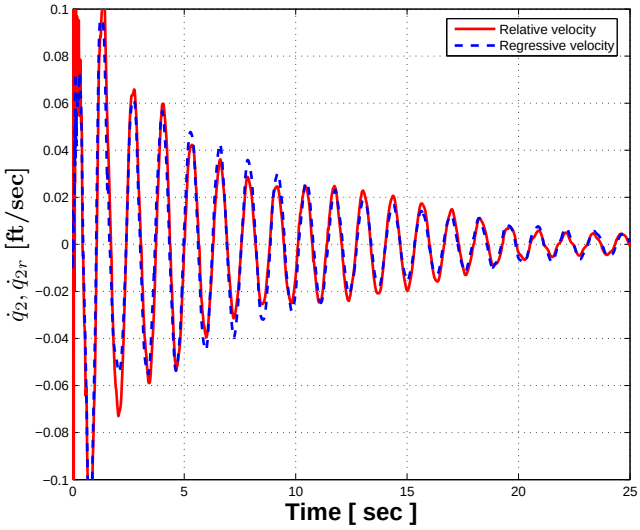

(b) Blade 2

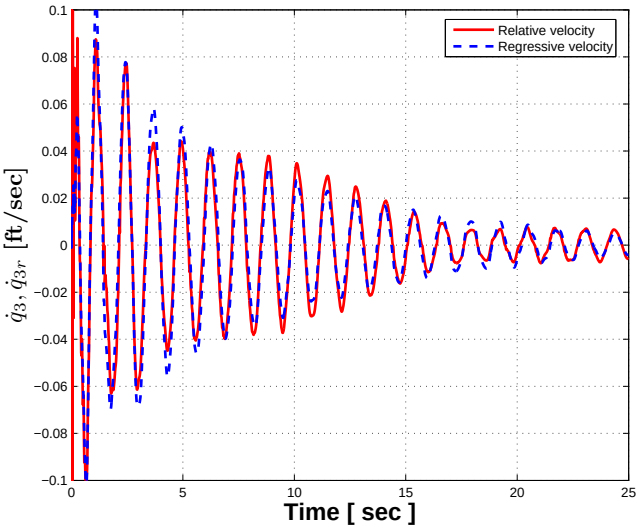

(c) Blade 3

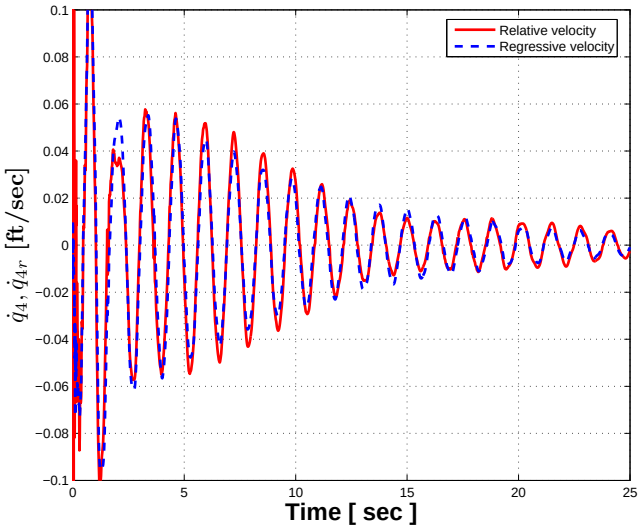

(d) Blade 4

Figure 5.27: Damper stroke rate, regressive stroke rate - Selective damping law 1

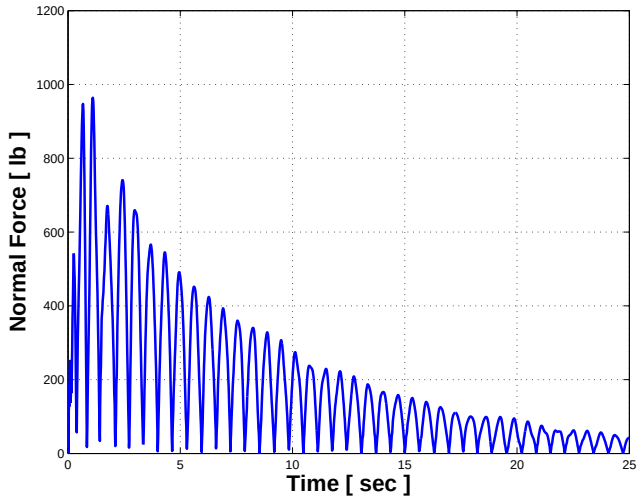

(a) Blade 1

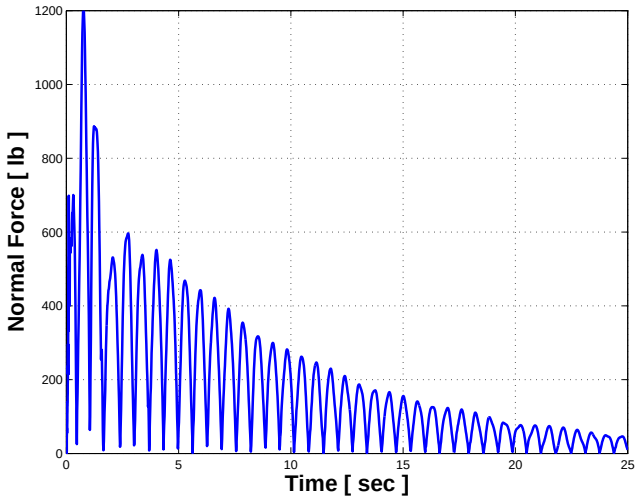

(b) Blade 2

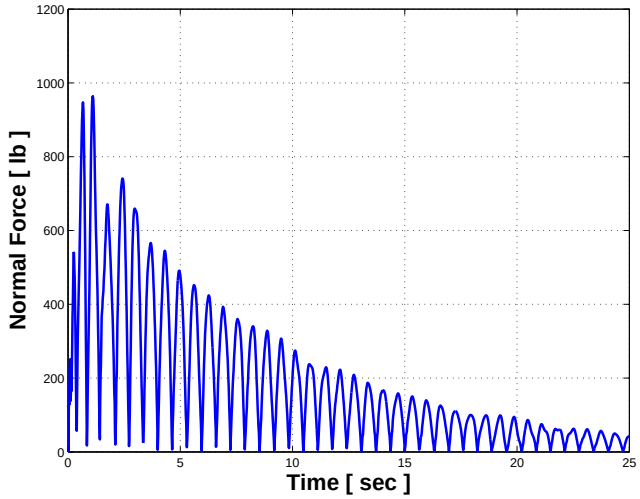

(c) Blade 3

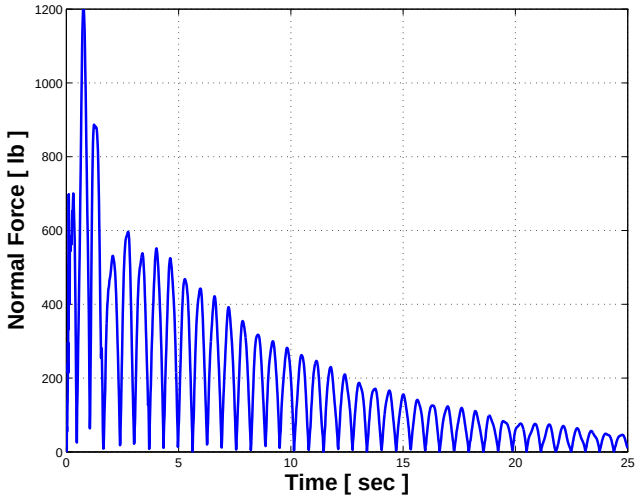

(d) Blade 4

Figure 5.28: Normal load variation - Selective damping law 1

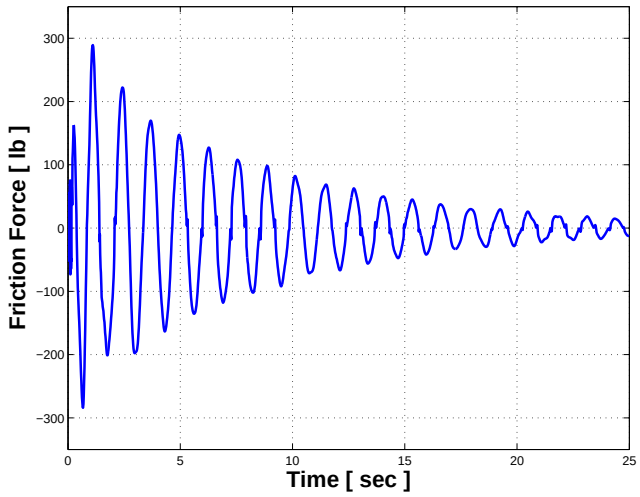

(a) Blade 1

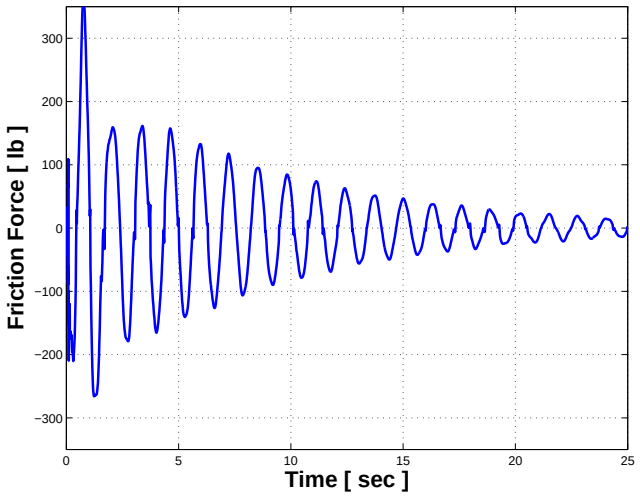

(b) Blade 2

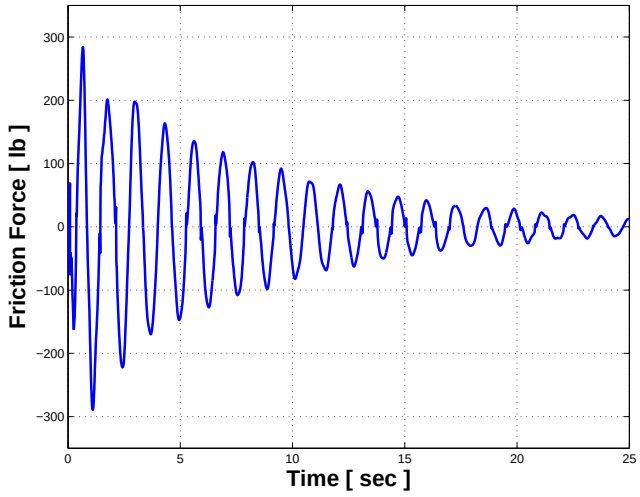

(c) Blade 3

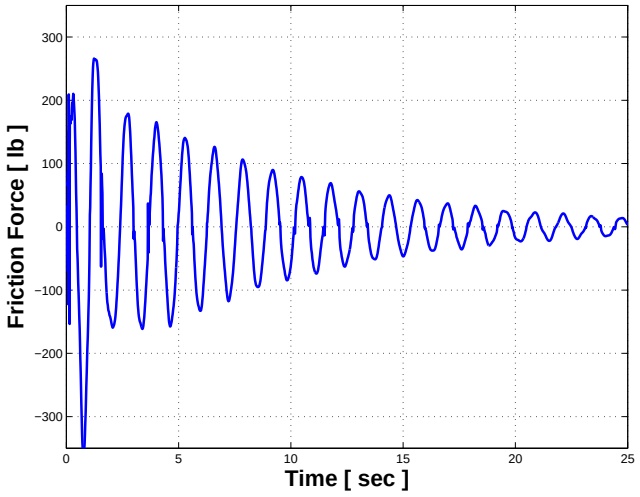

(d) Blade 4

Figure 5.29: Friction force variation - Selective damping law 1

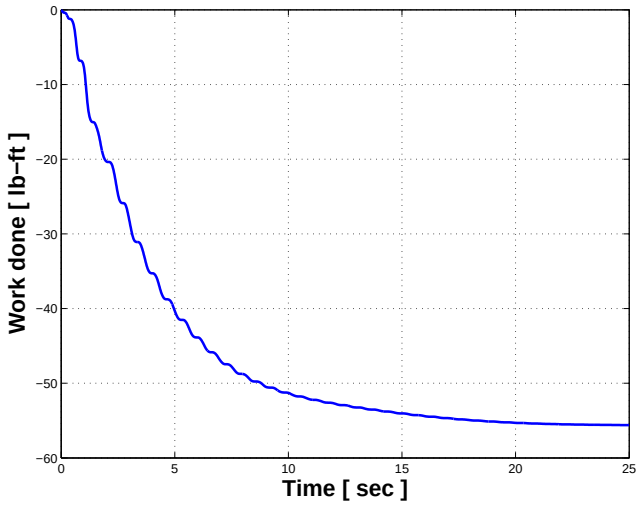

(a) Blade 1

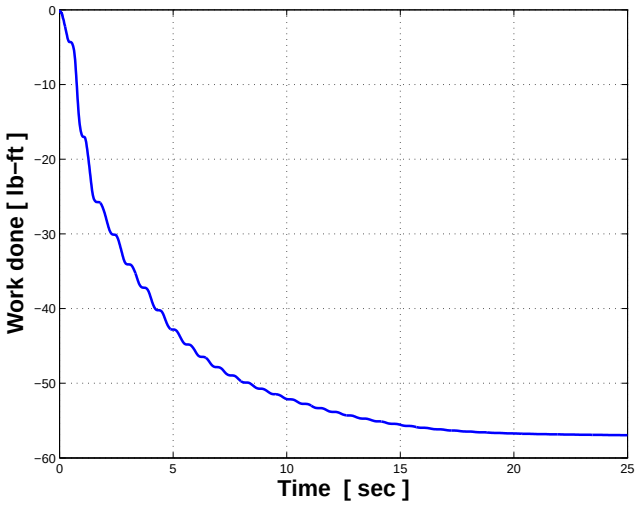

(b) Blade 2

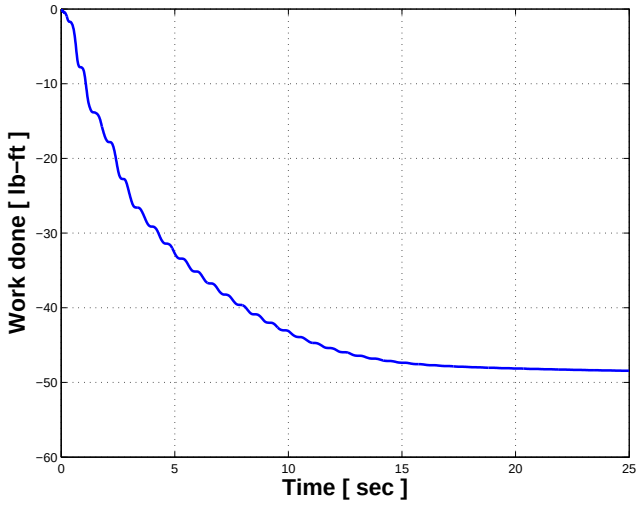

(c) Blade 3

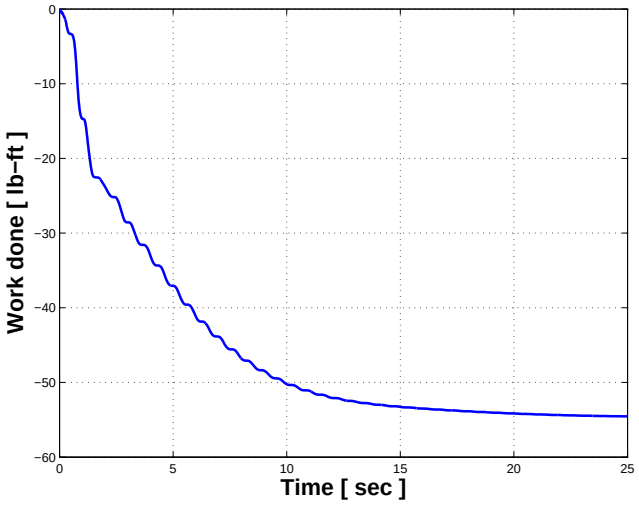

(d) Blade 4

Figure 5.30: Work done by the damper - Selective damping law 1

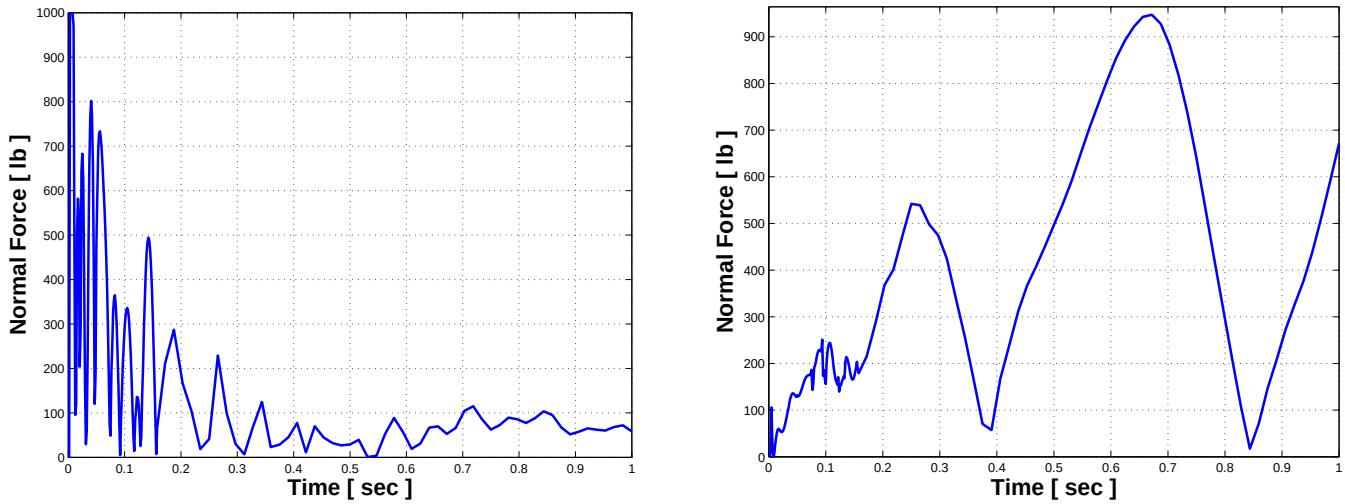

(a) Semi-active damper

(b) Selective damper 1

Figure 5.31: Normal load comparison - Semi active damping law vs. Selective damping law 1

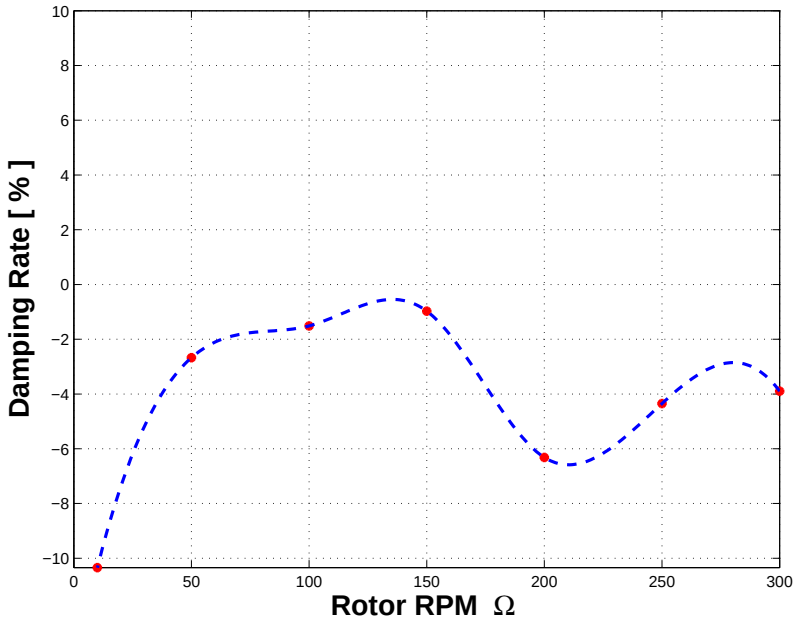

Figure 5.32: Damping as a function of rotor speed - Selective damping law 2

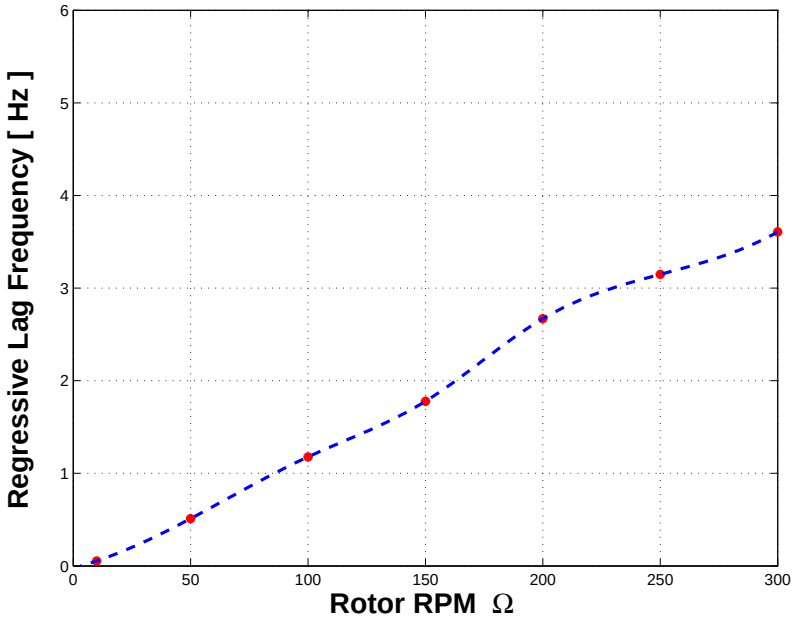

Figure 5.33: Lag regressive frequency as a function of rotor speed - Selective damping law 2

stick-slip phenomenon occurring at high frequencies. Consequently, lag motion, although rendered stable, never dies out completely. A few strategies are tried to alleviate this in this section with all simulations performed for the case of selective damping law 2.

5.6.1 Notch implementation

In order to reduce the amount of load applied at small relative velocity, which is the reason behind the stick-slip phenomenon, being observed in the previous case, the controller law is amended so that when the magnitude of the relative velocity is less than the specified notch velocity, $v_{no}(> 0)$, the damper applies no force. The modified law can be written as

$$N = \begin{cases} \tanh\left(\frac{\dot{q} - \mathrm{v_{no}} sign(\dot{q})}{\dot{\phi}_0}\right) N_{max} & \text{if } \frac{|\dot{q}|}{\mathrm{v_{no}}} > 1 \\ 0 & \text{otherwise} \end{cases} \tag{5.5}$$

The modified control law is compared with the control law without notch velocity implementation in Figure 5.40. The modified law simply represents a shift in application of the previous law until relative velocity reaches a definite magnitude represented by notch velocity.

Again, simulations are obtained at 150 RPM for two values of notch velocities, v_{no}

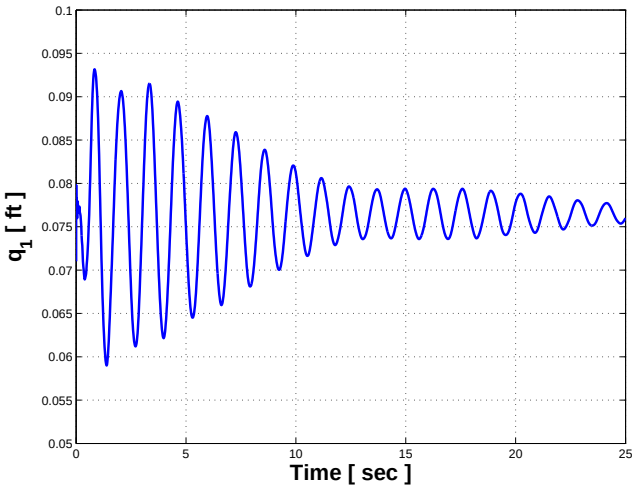

(a) Blade 1

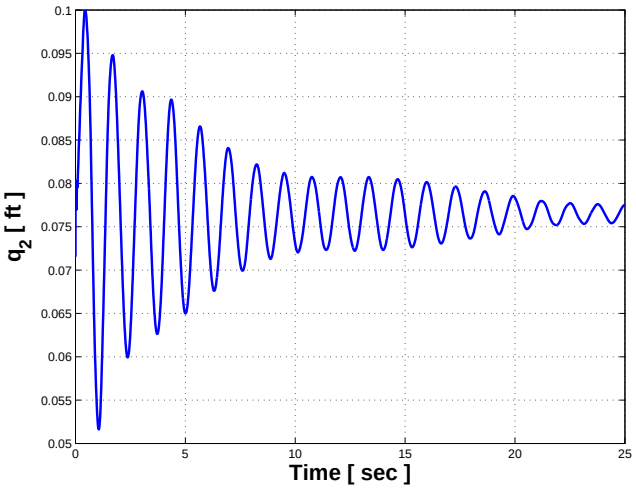

(b) Blade 2

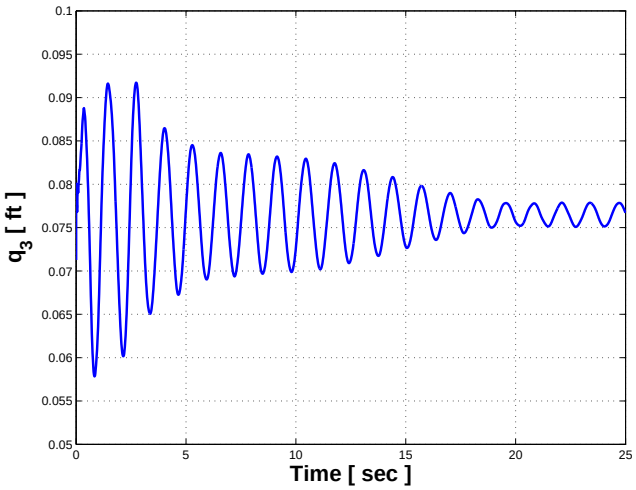

(c) Blade 3

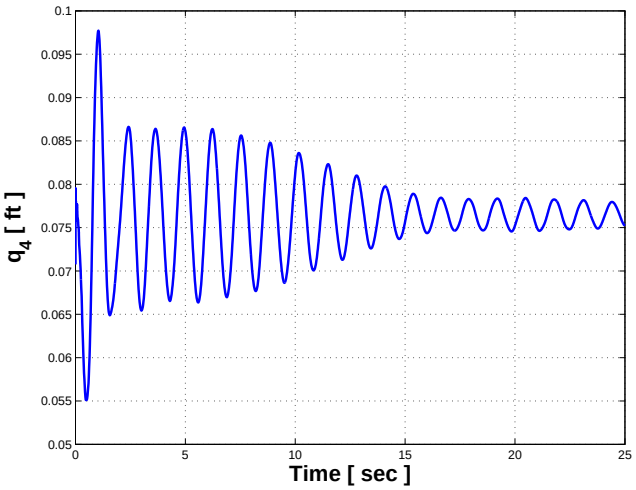

(d) Blade 4

Figure 5.34: Damper stroke - Selective damping law 2

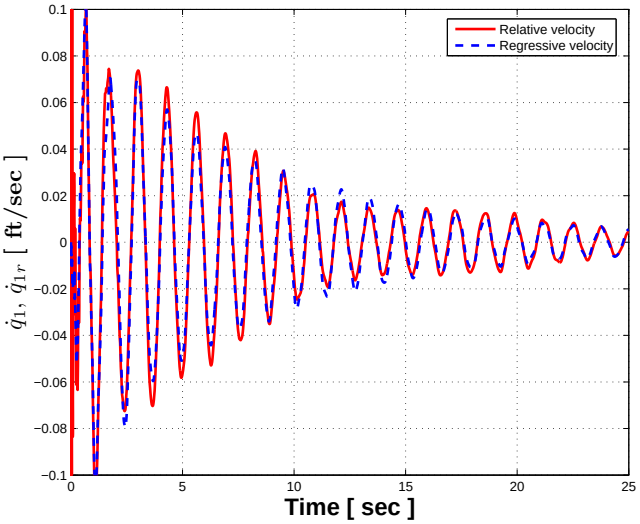

(a) Blade 1

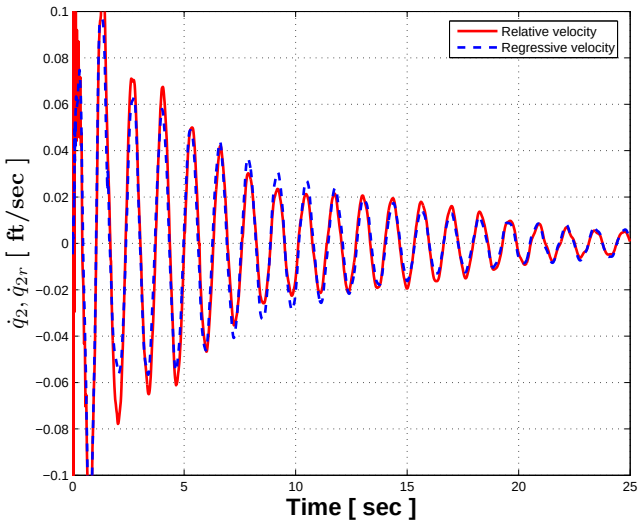

(b) Blade 2

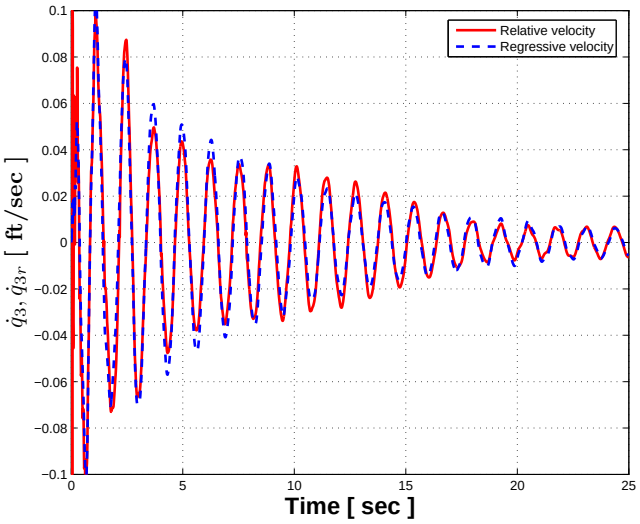

(c) Blade 3

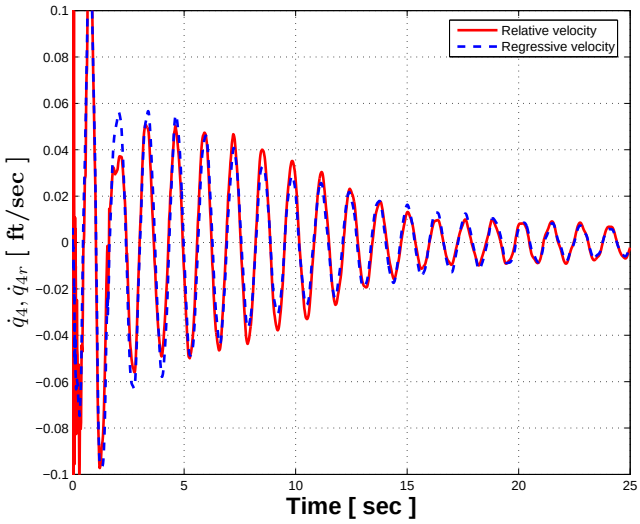

(d) Blade 4

Figure 5.35: Damper stroke rate, regressive stroke rate - Selective damping law 2

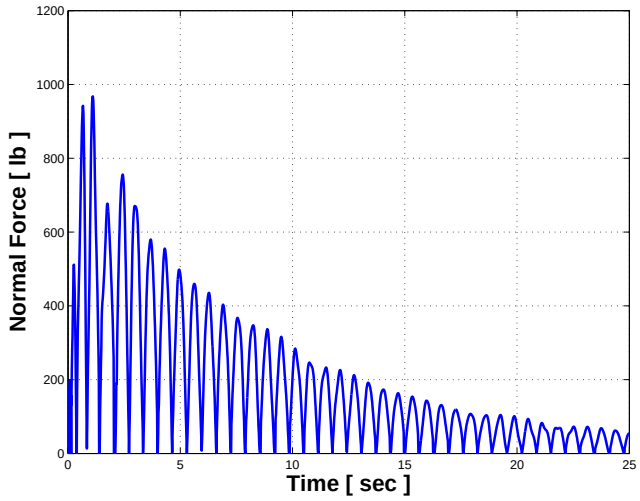

(a) Blade 1

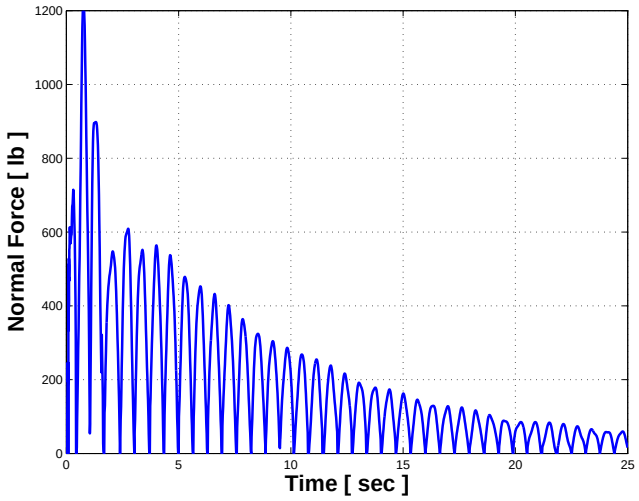

(b) Blade 2

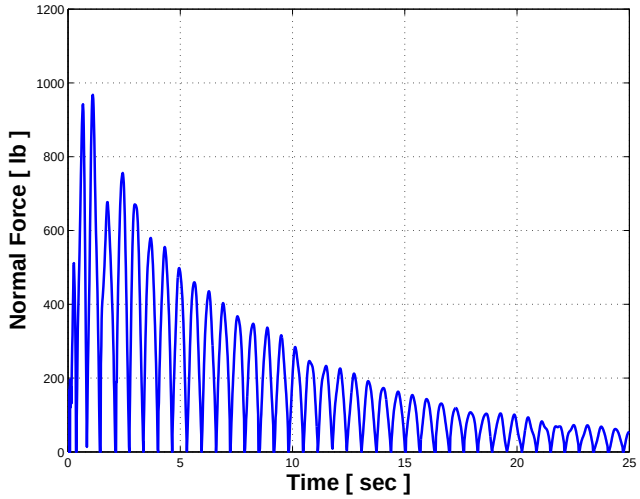

(c) Blade 3

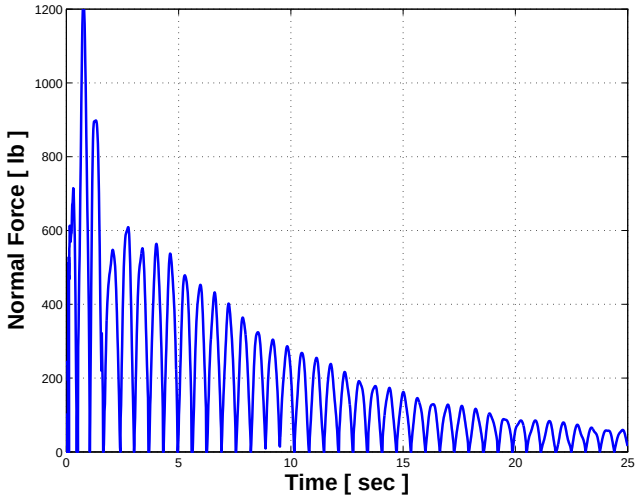

(d) Blade 4

Figure 5.36: Normal load variation - Selective damping law 2

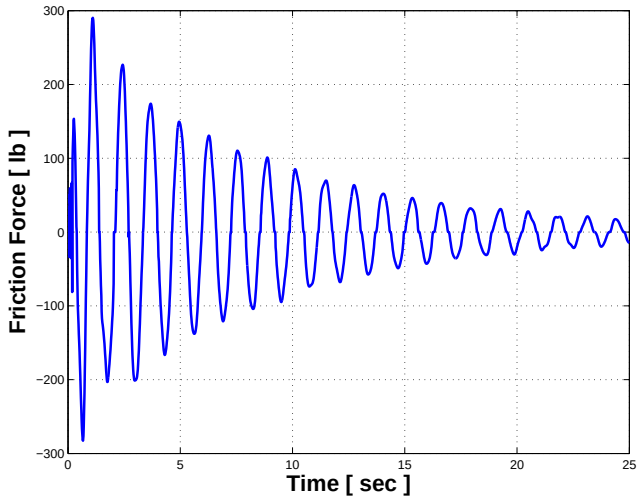

(a) Blade 1

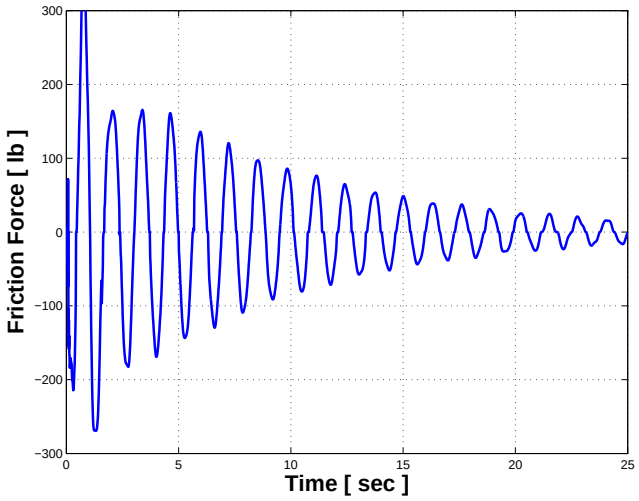

(b) Blade 2

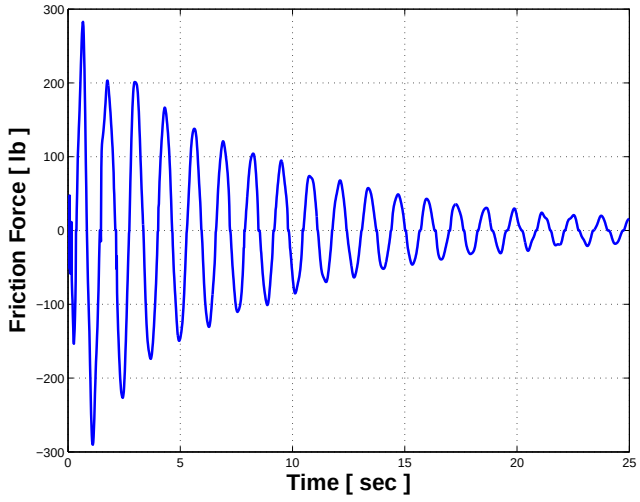

(c) Blade 3

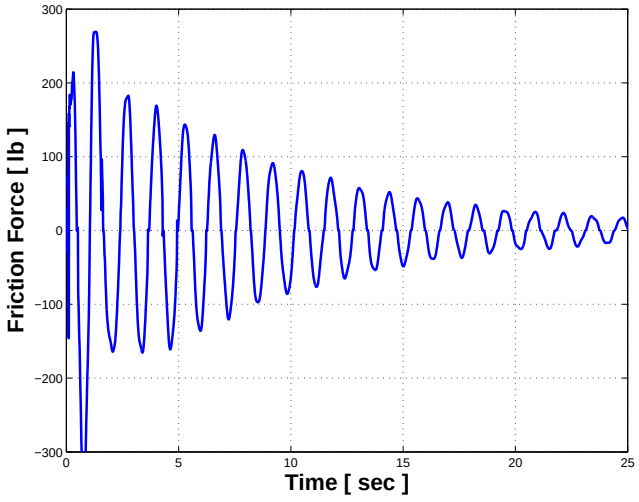

(d) Blade 4

Figure 5.37: Friction force variation - Selective damping law 2

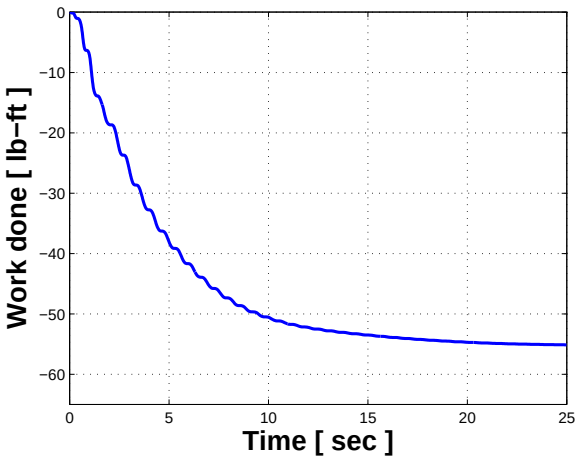

(a) Blade 1

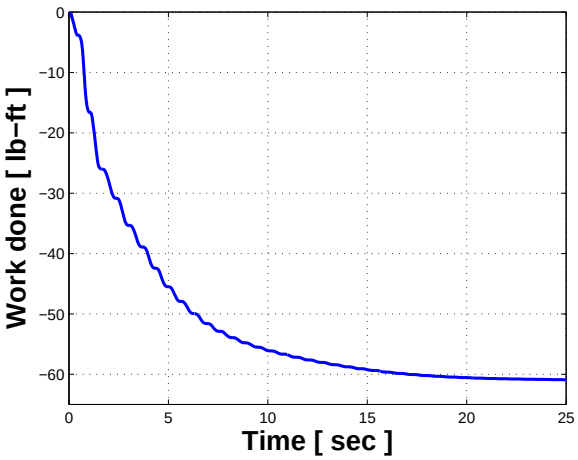

(b) Blade 2

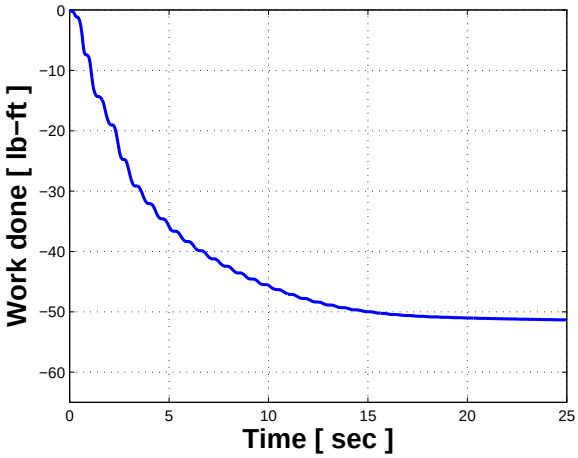

(c) Blade 3

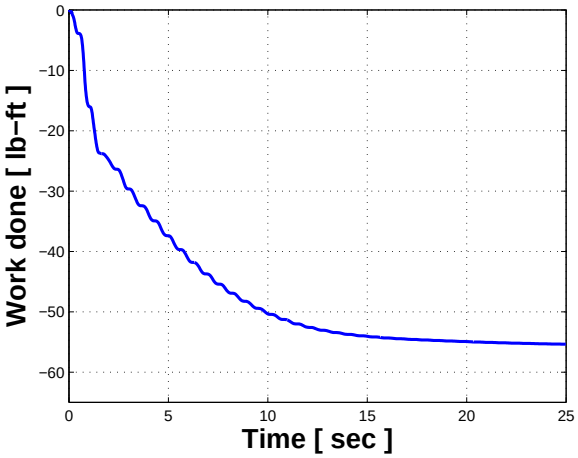

(d) Blade 4

Figure 5.38: Work done by the damper - Selective damping law 2

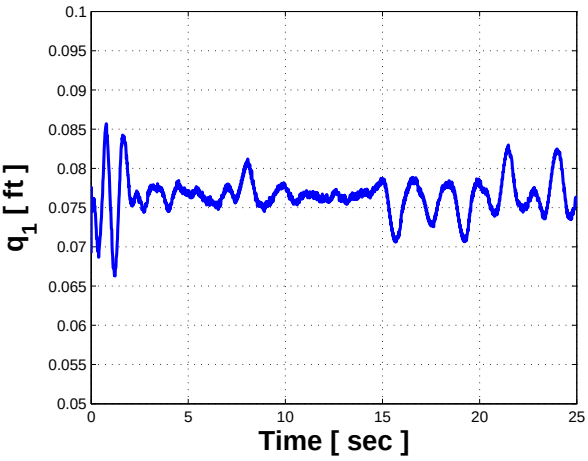

(a) Damper stroke

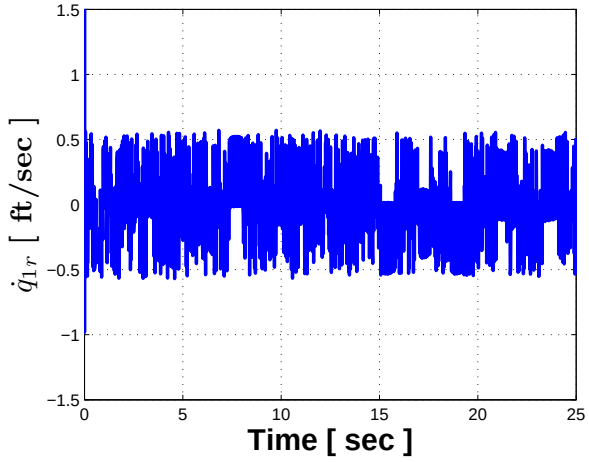

(b) Damper stroke rate

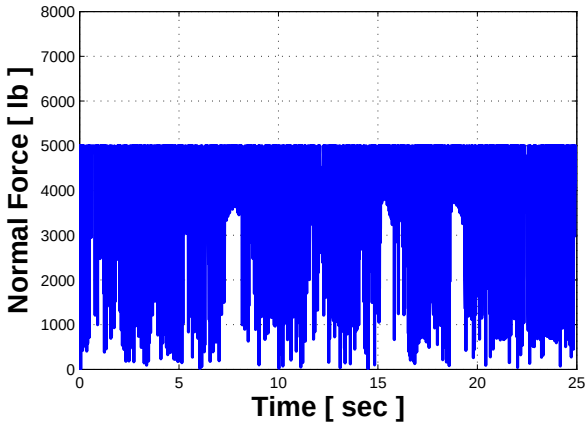

(c) Normal force

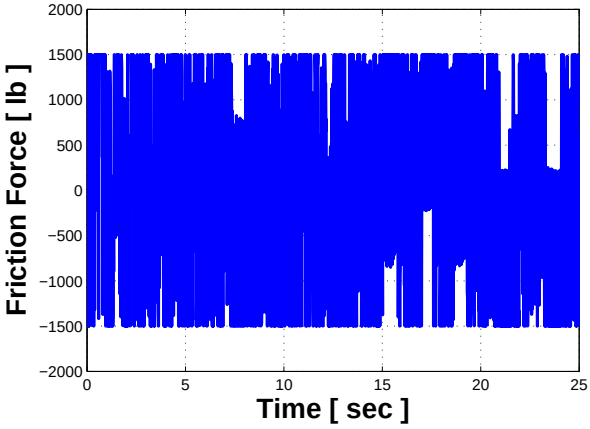

(d) Friction force

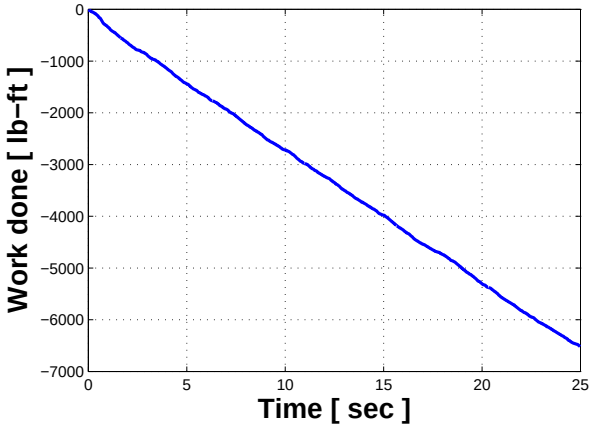

(e) Work done

Figure 5.39: Damper performance at $N_{max} = 5000$, $\dot{\phi}_0 = 0.1$

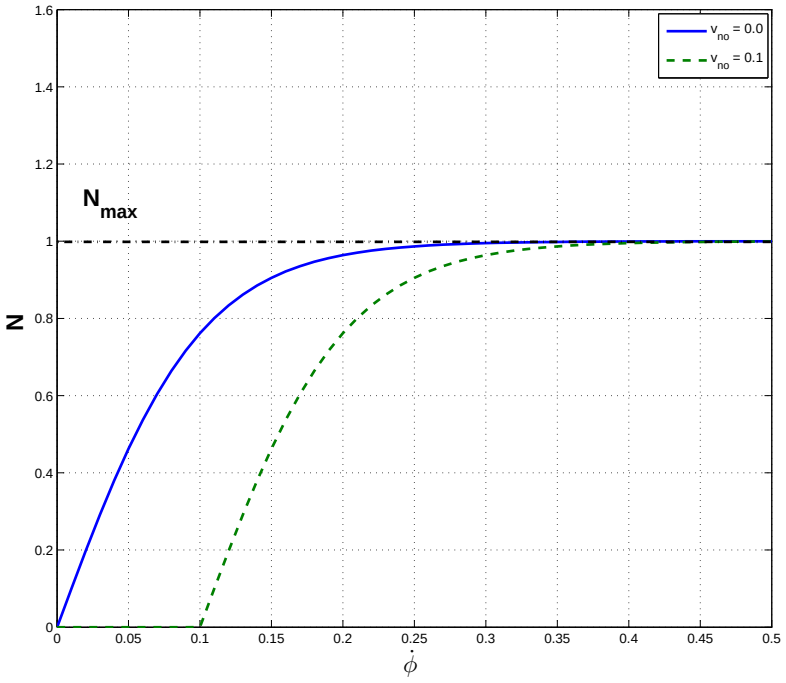

Figure 5.40: Controller law variation - with and without notch implementation

$= 0.01$ and $v_{no} = 0.005$ respectively. For higher notch velocity, a stable but undamped motion is obtained as expected, since the friction load applied is much less than the one required to obtain a stable damping rate. In contrast, lower notch velocity resulted in sticking-slipping at high frequency as in the previous case. Although notch implementation eliminated application of normal load at low relative velocity, it did not prevent a sharp rise of normal load level which is a feature of tanh function governing the controller response.

5.6.2 Modified control law

The control law based on trigonometric function tanh has a high slope at low argument value resulting in sharp rise of normal load whenever the relative velocity is in the process of changing direction. In order to enforce a slower normal load level growth at low relative velocity, controller law governing actuator response is modified as

$$N = \begin{cases} \frac{1}{2}\left(1 - \cos\left(\pi \frac{\dot{q}}{\dot{\phi}_0}\right)\right) N_{max} & \text{if } \left|\frac{\dot{q}}{\dot{\phi}_0}\right| \leq 1 \\ N_{max} & \text{otherwise} \end{cases} \tag{5.6}$$

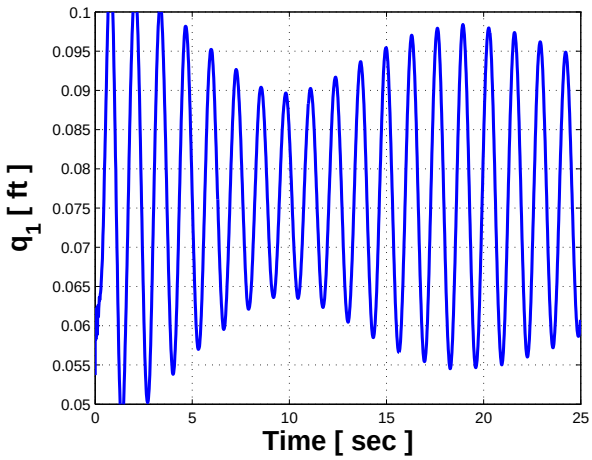

(a) Damper stroke

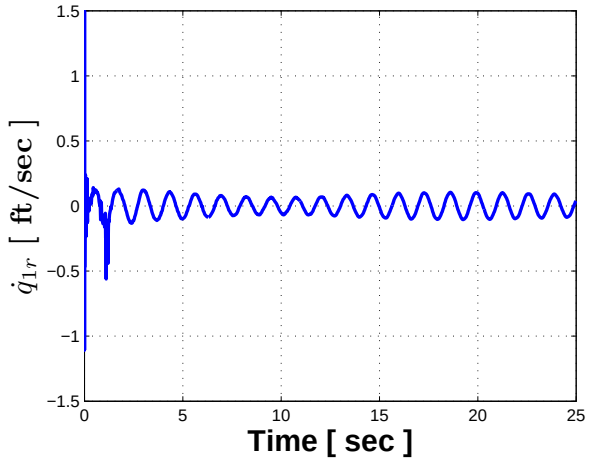

(b) Damper stroke rate

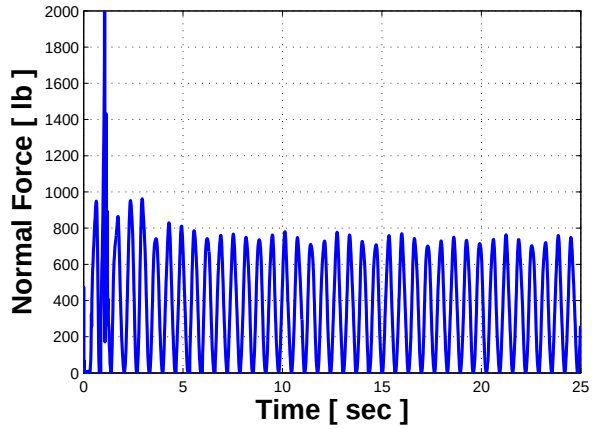

(c) Normal force

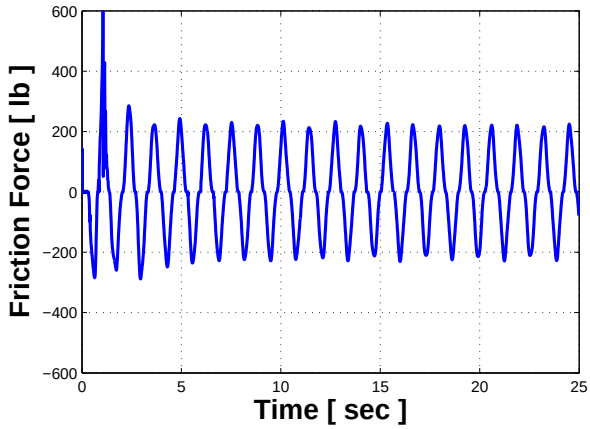

(d) Friction force

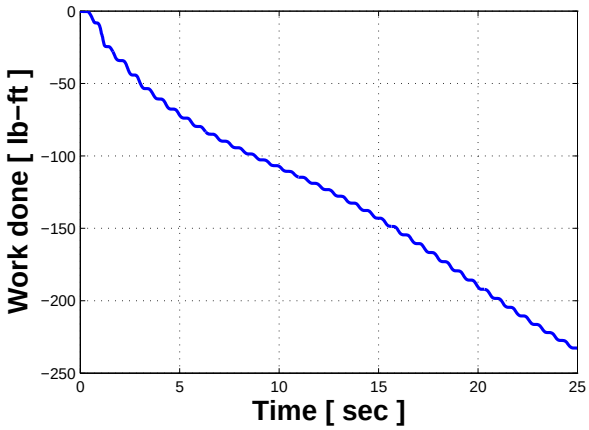

(e) Work done

Figure 5.41: Damper performance at $N_{max} = 5000$, $\dot{\phi}_0 = 0.1$, $v_{no} = 0.01$

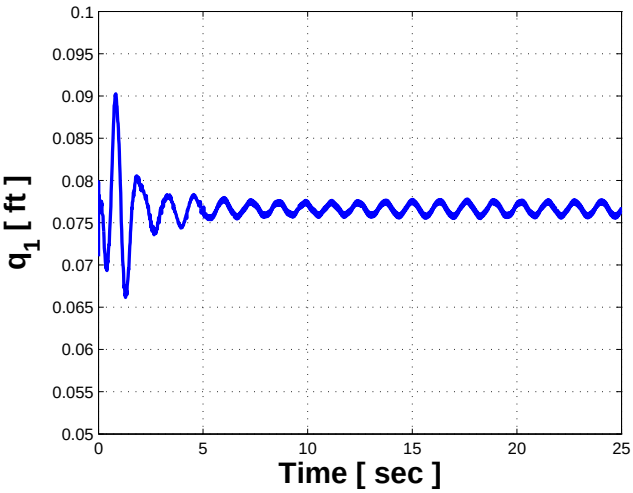

(a) Damper stroke

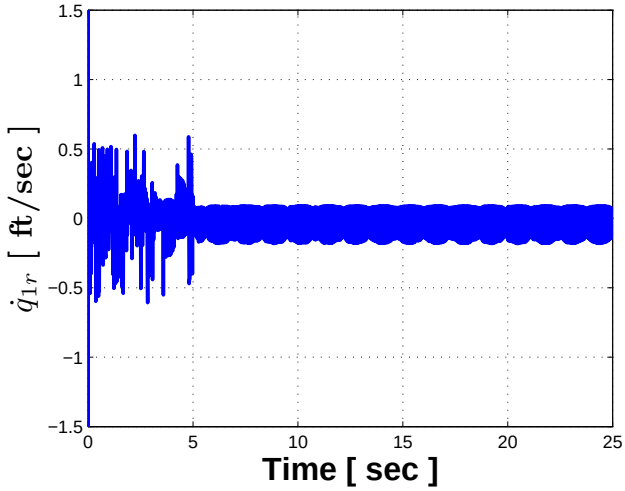

(b) Damper stroke rate

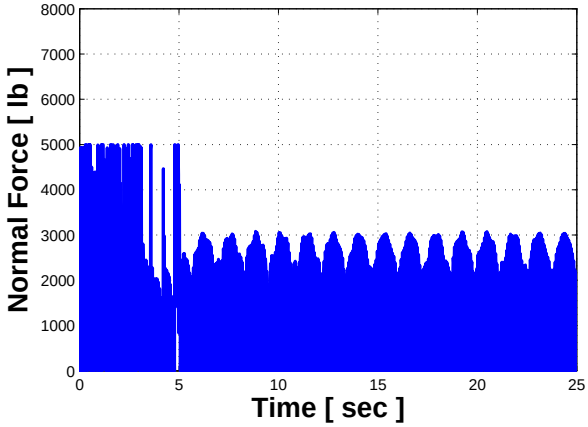

(c) Normal force

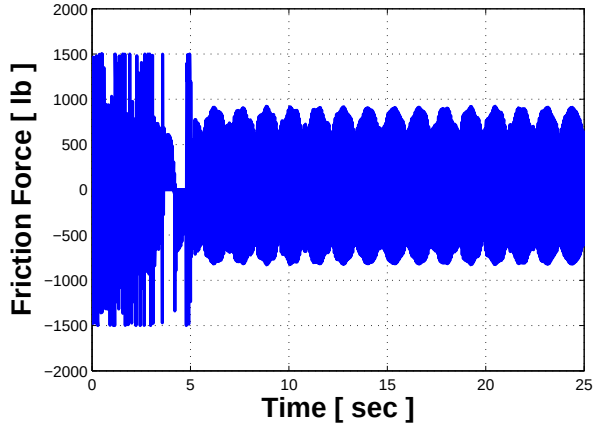

(d) Friction force

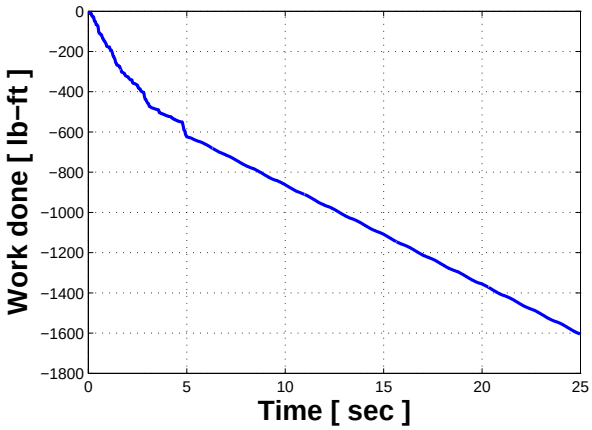

(e) Work done

Figure 5.42: Damper performance at $N_{max} = 5000$, $\dot{\phi}_0 = 0.1$, $v_{no} = 0.005$

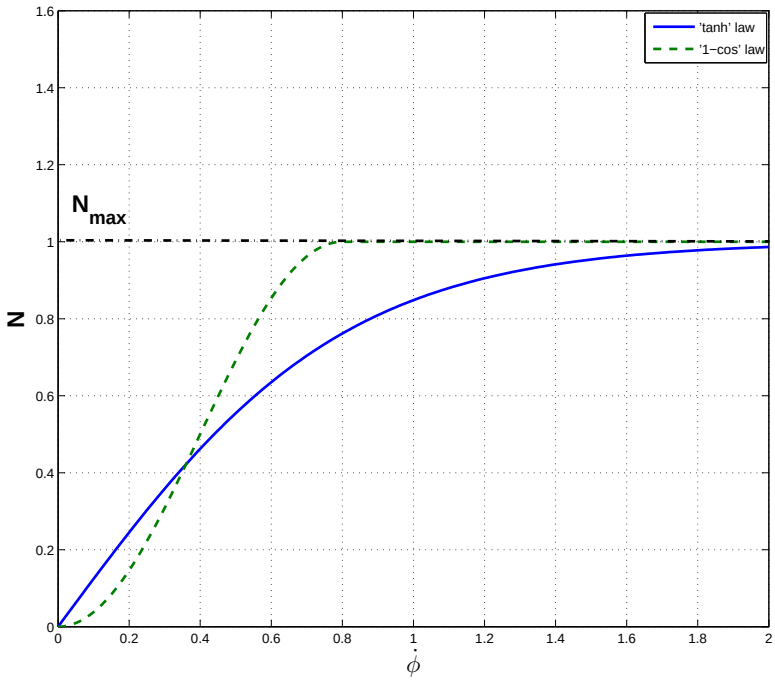

Figure 5.43: Controller laws comparison at $\dot{\phi}_0 = 0.8$

The modified control law based on the 'cos' function is compared to the previous control law in Figure 5.43.

The parameter $\dot{\phi}_0$, although performing the same function of defining the steepness of load profile, does not resemble in magnitude to its counterpart in the tanh law. The parameter is lowered to a value of 0.01 and simulations are conducted with the modified controller at 150 RPM. Results are plotted in Figure 5.44. It is observed that even with the modified control law, there is no improvement in the damper performance.

From above results, it is clear that neither the implementation of notch nor lowering the steepness of actuator load at low relative velocity are possible solution to alleviate the high frequency stick-slip phenomenon. This self-exciting phenomenon is a result of small perturbations in relative velocity, probably a result of numerical error, magnified at higher normal load levels. Several strategies tested to alleviate this, thus, failed to obtain a satisfactory solution. The sensitivity of the controller to minor perturbations reflects need for more precise controller that will avoid stick-slip response of the system. From the

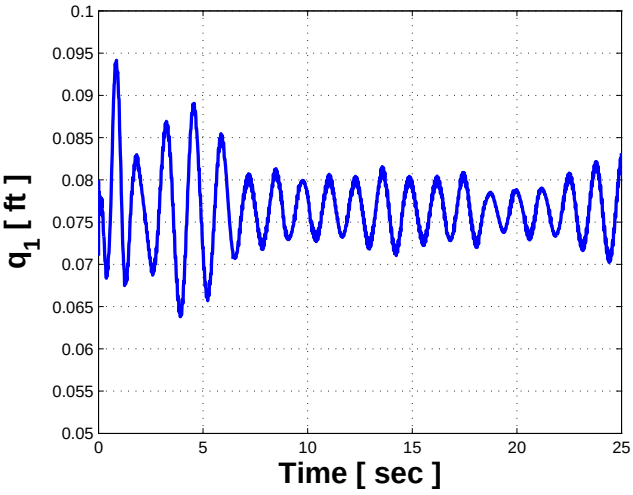

(a) Damper stroke

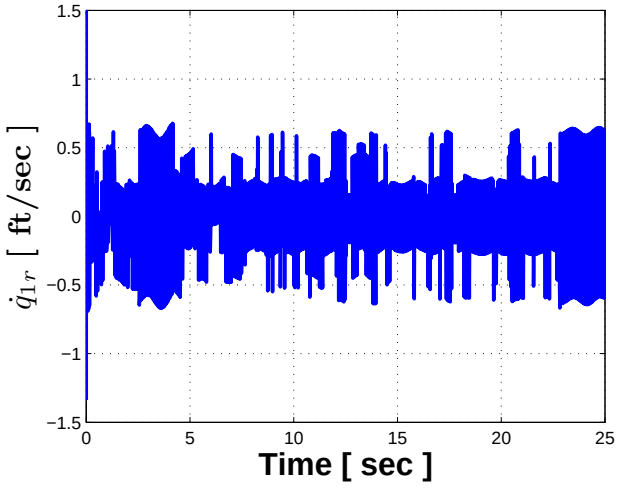

(b) Damper stroke rate

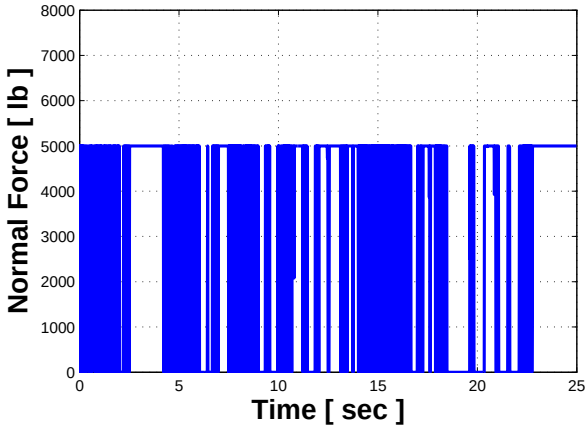

(c) Normal force

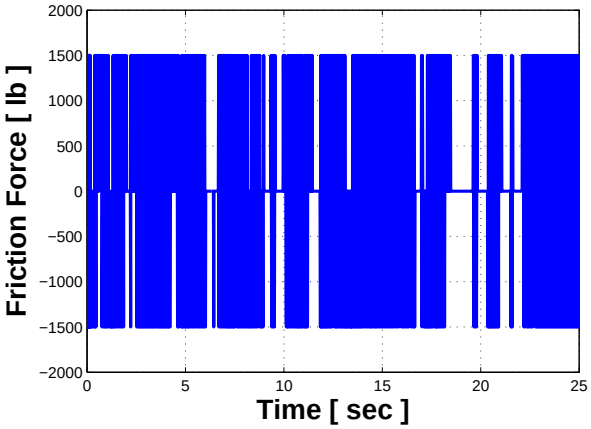

(d) Friction force

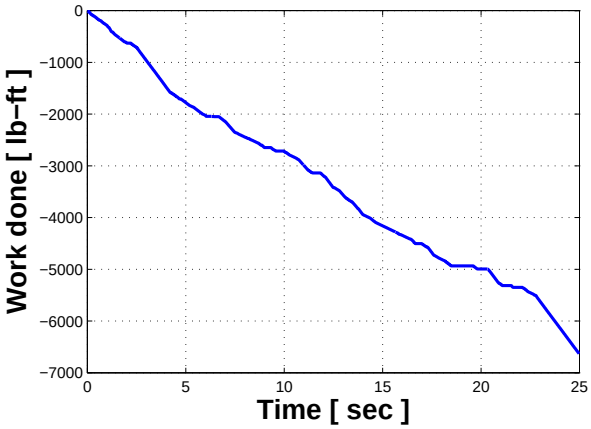

(e) Work done

Figure 5.44: Damper performance at $N_{max} = 5000$, $\dot{\phi}_0 = 0.01$ with modified controller

practical standpoint, feedback of relative velocity from sensor will include noise as well and the control law has to be robust enough to filter out the pure signal from unwanted noise. In short, better controller has to be designed that can properly identify the stick-slip region and avoid it.

CHAPTER VI

SEMI-ACTIVE LEAD-LAG DAMPER DESIGN

An innovative design of a semi-active lead lag damper is proposed and various aspects of its design in consideration to its practical application in commercial rotors are investigated in this chapter. The adaptive damping is achieved in the damper by actively controlling the passive frictional resistance at the joint interface in the lag damper. This type of semi-active joint is designed in such a way that the normal force in the frictional interface can be controlled. A mechanism comprising of piezoelectric stack actuator is used to actively modulate the normal force. The actuator response at a particular instant is determined by the centralized controller based on the feedback of sensed lag motion of all the blades.

6.1 Control Architecture

A centralized control system based on feedback law is envisioned for aeromechanical stability of rotors. A block diagram of control system is shown in Figure 6.1. The semi-active lag dampers are attached to each blade of the rotor system. The feedback of lag motion is provided to the controller by the velocity transducers attached to the blades. Based on the sensed state of the lag modes in conjunction with the control law programmed inside the system, commands are generated by the system for each individual dampers. Lead lag dampers then respond to the controller by generating the required amount of friction force.

6.2 Piezoelectric Stack Actuator

Piezoelectric stack actuators are chosen for controlling the frictional resistance in the damper. The number of actuators of given geometric specification and load generating capacity required in the damper design depends on the damping capacity desired for a particular rotor configuration. Each actuator is mounted such that it applies a normal force on the frictional interface. The friction force can be adjusted through applied voltage to meet the desired

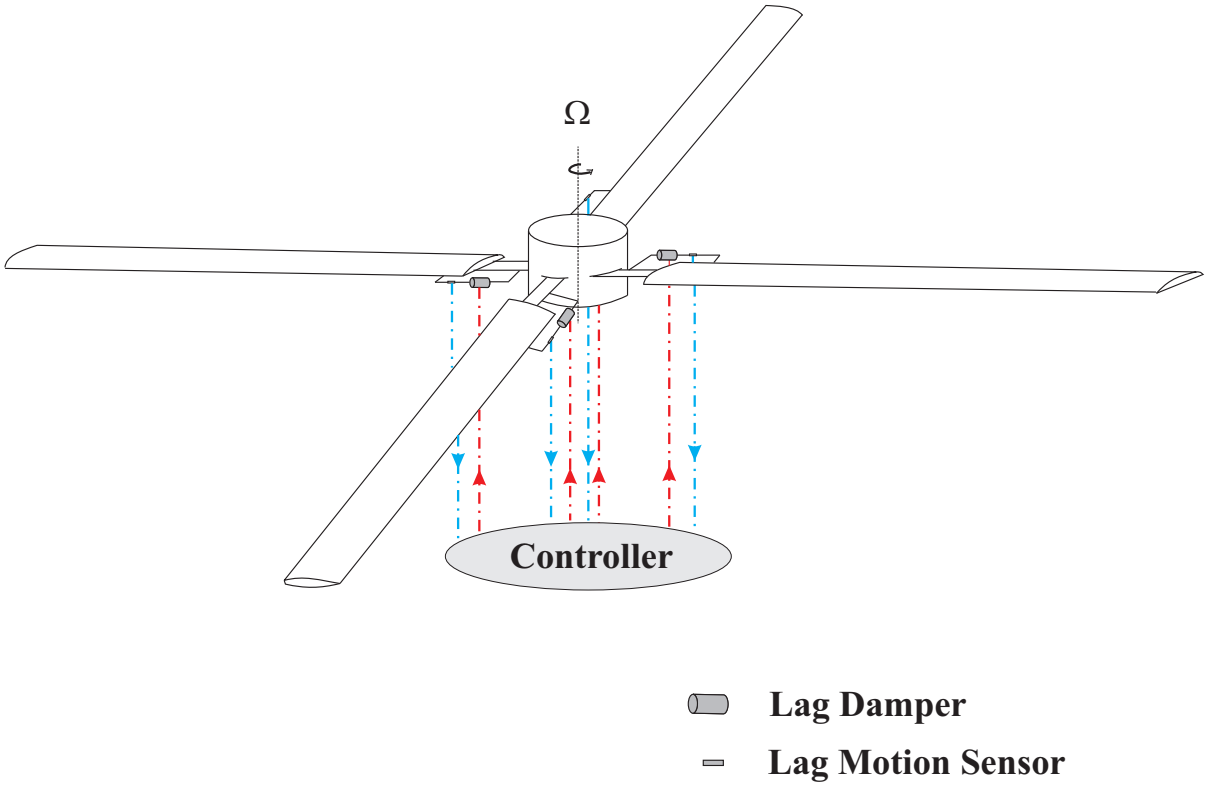

Figure 6.1: Centralized control scheme for semi-active lag damping

damping level. A single piezoelectric element is shown in Figure 6.2(a) and a piezoelectric stack is shown in Figure 6.2(b). Because the actuator only needs to change the normal force exerted onto the joint element, it requires little actuating displacement and mechanical power. The stack, which comprises of a number of piezo layers, is a very stiff structure with a high capacitance. It is suitable for handling high compressive force and collecting a large volume of charge. The stack actuator uses d_{33} actuation, where the coefficient represents the '3-direction' or the thickness direction piezoelectric strain coefficient due to the applied electric field in the same direction.

Referring to Figure 6.2(a), for a single piezo disc, the blocked force per unit voltage is given by

$$\frac{F_b}{V} = d_{33} K_a \tag{6.1}$$

where K_a is the longitudinal stiffness of the piezoelectric element in the '3-direction' and is given by

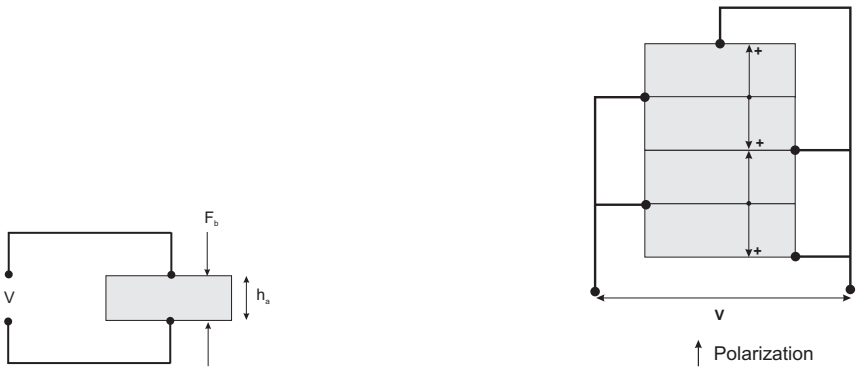

(a) Single disc actuator (b) Stack actuator

Figure 6.2: Piezoelectric actuator

$$K_a = \frac{E_{33} A_a}{h_a} \tag{6.2}$$

where E_{33} is the Young's modulus of the piezoelectric material in the '3-direction', A_a is the cross-sectional area of the piezoelectric element and h_a is its thickness. The free displacement per unit voltage applied is given by

$$\frac{\Delta L_{0_{single}}}{V} = d_{33} \tag{6.3}$$

For the piezoelectric stack with N_e elements shown in Figure 6.2(b), blocked force remains the same as for a single element and is given by Equation 6.1, but the stiffness is reduced by a factor of N_e and is given as

$$K_a = \frac{E_{33} A_a}{N_e h_a} \tag{6.4}$$

This means that the free displacement of the stack of elements is increased by a factor of N_e

$$\Delta L_0 = N_e d_{33} V \tag{6.5}$$

From Equation 6.1, the voltage required for desired damping level can be ascertained.

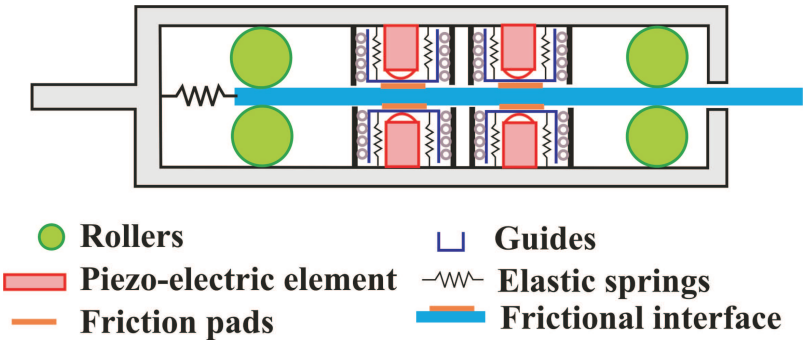

Figure 6.3: Proposed lag damper design

6.3 Semi-Active Lead Lag Damper Model

The proposed lag damper model is shown in Figure 6.3. The design consists of a rectangular chamber with a set of piezoelectric stack actuators attached to the top and bottom surface of the chamber, and a damper arm running in between the actuators that is connected to the chamber through a spring on one end and to the lag motion attachment of the blade on other end. The motion of the damper arm is kept unidirectional by constraining the motion with rollers. The frictional resistance in the damper is modulated by the actuators through application of controlled normal load over the frictional interface which is formed by the friction pads attached on the surface of damper arm and guides attached to the actuators. There is a small clearance between the friction pads and the guides under zero resistance condition. The clearance can be made as small as possible so that applied voltage goes in to generating normal force rather than in free displacement.

One of the major limitations in the use of piezoceramic materials is that they can only reliably withstand compressive loads, but are notoriously weak in tension and shear. The purpose of the guides is to provide shear relief to the piezoceramic actuators and thus avoid problems of shear failure. The shear forces are transmitted into the guides rather than into the piezoelectric actuator, thus avoiding shear failure. Acting purely on the control signals generated by the centralized controller, the lag damper is either in the 'off' or 'on' state at any instant in time. When it is switched from the 'off' to 'on' state or commanded to generate a higher normal load level than the one at a previous instant, stack actuators

thrust upon the guide surface until the desired magnitude of normal load is transferred to the interface. When it is signalled to reduce damping level, voltage supply to the actuators is reduced, thus leading to reduced strain in the actuators. When damper is turned 'off' by the controller, actuators have zero strain and the guides are retracted by springs attached to them.

The damper works in association with the sensor and controller. The sensors attached to the blades sense the lag motion and pass the signal onto the controller which in turn decides the frictional resistance to be generated at a particular instant for each blade and commands the power plant to supply appropriate voltage to the actuator to generate the desired normal force. The piezoelectric actuator has the ability to generate large forces at high speed but with very small strain. A piezoelectric actuator interacts with a coupled mechanism, where the piezo-mechanical performance is defined by the two interacting stiffnesses S_{piezo} and S_{mech}, the stiffness of actuator and the stiffness of the actuated mechanics respectively. The characteristics of a stack actuator are shown in Figure 6.4. When the stiffness of the restraining material acting against the actuator is infinite, maximum or the block force is developed. Under no restraint, the actuator displaces maximum and the displacement is termed as stroke.

A static analysis is needed to estimate the damping capacity of the proposed damper model. The damper configuration in Figure 6.3 shows two stack actuators present on either side of the frictional interface. Depending on the damping level requirements, multiple actuators can be accommodated in the damper. The equivalent spring-actuator model representation of the damper is shown in Figure 6.5. The damper model with multiple actuators would entail similar analysis although with the different equivalent spring stiffness of the chamber at actuator locations. The model includes every element of the damper represented by an equivalent spring. The naming convention used to refer to stiffness of various elements is given in Table 6.1.

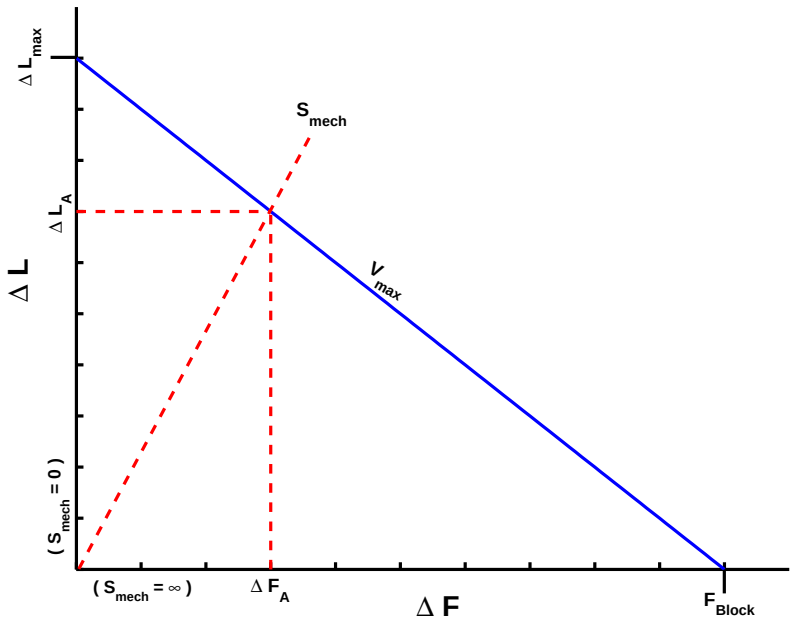

Figure 6.4: Quasi-static characteristics of piezoelectric actuator

Table 6.1: Nomenclature for stiffness of damper elements

Description	**Symbol**
Spring stiffness of the chamber	K_c
Stiffness of the stack actuator	K_a
Stiffness of the guide	K_g
Stiffness of the spring attached to the guide	K_s
Spring stiffness of the friction pad	K_{fp}
Spring stiffness of the frictional interface	K_{fi}

The stiffness of the actuator is available from the catalogue supplied by the manufacturer. The equivalent spring stiffness of guides, friction pads and that of the interface is obtained using formulation for a bar member undergoing axial deformation

$$K = \frac{EA}{t} \tag{6.6}$$

where E, A, and t refers to elastic coefficient, cross-sectional area and thickness of the element respectively.

The enclosed chamber undergoes bending and its stiffness is evaluated in the next section. Once that becomes known, stiffness of the entire structure is evaluated.

6.3.1 Spring Stiffness of Chamber

The chamber is analyzed as a frame structure comprised of four beams. The schematic diagram of the chamber is shown in Figure 6.6 and its deformed configuration is shown in Figure 6.7. The symmetry in the deformed mode of the chamber can be observed from the diagram which is further used as a basis for simplified analysis. The static analysis results in following equation for the spring stiffness of the chamber at the actuator location.

$$K_c = \frac{96EI\,(l+h)}{(l-d)^2\left[(l+d)^2 + 4h\,(l+d) + 4d\,(h-d)\right]} \tag{6.7}$$

The stiffness term contains several parameters such as material properties, dimensions of the damper and spacing between the actuator directly affecting the damper performance for a given design.

At any instant of time, damper is either in the 'off' or 'on' state. While in the 'off' state which is also the default configuration, the actuator is in relaxed state and the actuator-guide combination is isolated from the frictional interface. When damper is turned 'on', until the voltage applied to the actuator is below critical level, damper is still inactive i.e., does not generate any frictional resistance. At the critical voltage, the actuator-guide combination makes first contact with the frictional interface and any further voltage increment

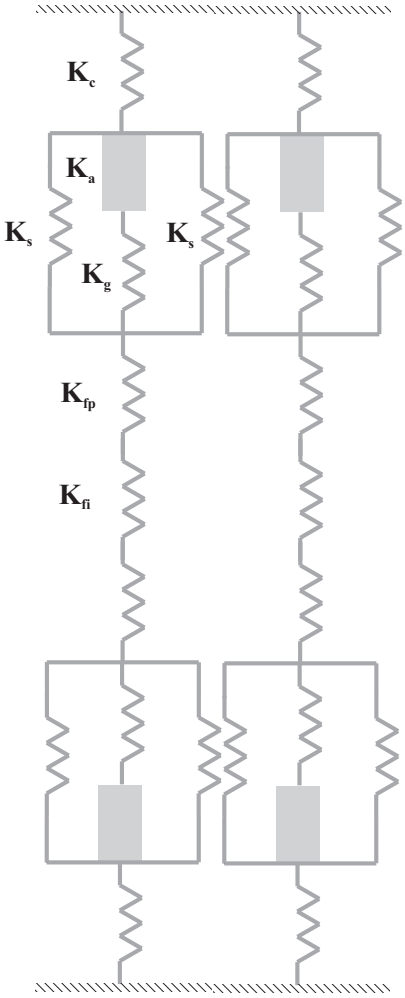

Figure 6.5: Spring model of the lag damper

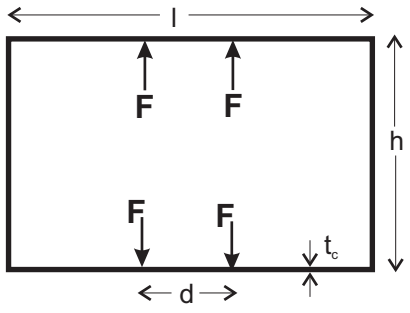

Figure 6.6: Schematic diagram of damper chamber

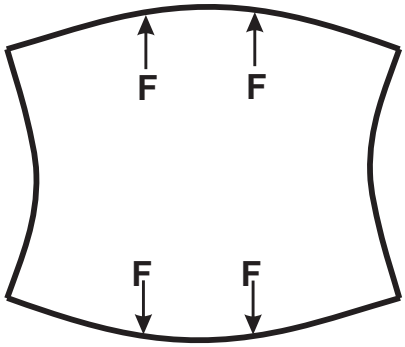

Figure 6.7: Damper deformed configuration

goes towards increasing normal load over the frictional interface with little contribution towards elastic deformation of damper elements. Thus, while in 'on' condition, the damper has two distinct configurations trailing each other when damper switches from 'on' to 'off' state or vice-versa. The two successive configurations are further referred as 'open' and 'closed' configurations. In the 'open' configuration, the actuator is still acting against the load due to the guide and its spring attachment. In the 'closed' configuration, the actuator is acted upon by spring load of additional elements such as the friction pad and the frictional interface.

In either of 'on' or 'off' configurations, the spring-actuator equivalent model of damper is symmetric. Taking advantage of symmetry, we need to model only a part of the actual structure about the line of symmetry and this simplifies the analysis.

6.3.2 Open configuration

In the open or 'non-reactive' configuration, the damper can be represented by an equivalent spring-actuator model as shown in Figure 6.8. The stiffness of the effective spring load acting on the actuator is obtained from a simplified configuration, different steps along the simplified design are shown as well in the figure.

$$K_{\mathit{eff}} = \frac{2K_g K_s}{2K_s + K_g} \tag{6.8}$$

The static model assumes that the application of electrical and mechanical loads to the

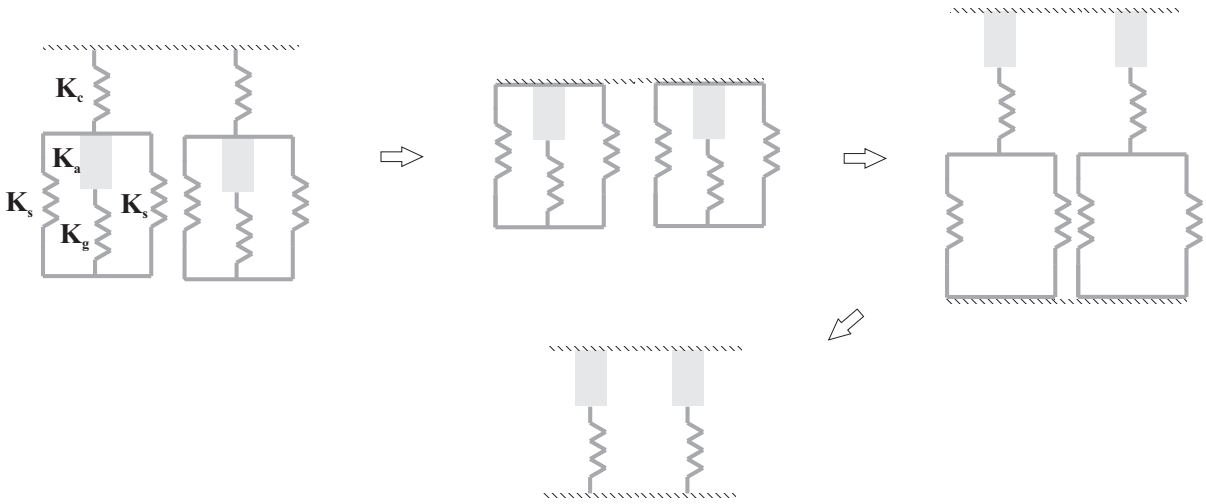

Figure 6.8: Spring model of the lag damper in 'open' configuration

actuator constitutes an equilibrium process. Further, piezoelectric and stiffness properties of the stack are assumed to remain constant throughout the process. The stack is assumed to be devoid of any prestressing by an internal spring inside the casing.

The maximum displacement of a piezo actuator acting against a spring load is given as

$$\Delta L \approx \Delta L_0 \left(\frac{K_a}{K_a + K_{eff}} \right) \tag{6.9}$$

Substituting for ΔL_0 from Equation 6.3, displacement of the piezoelectric actuator in terms of applied voltage is determined to be

$$\Delta L \approx N_e d_{33} \left(\frac{K_a}{K_a + K_{eff}} \right) V \tag{6.10}$$

The damper is in an open configuration until the actuator-guide arrangement displaces by an amount equal to the clearance between the friction pad and the guide which is equivalent to making the first contact. The following relation is satisfied by the stack expansion/contraction and guide deformation during the open configuration

$$\Delta L + \Delta L_g < c \tag{6.11}$$

where ΔL_g is axial deformation of guide and c is the clearance. The guide deformation can

be evaluated as

$$\Delta L_g = \frac{K_a}{K_g}\Delta L \tag{6.12}$$

From Equations 6.11 and 6.12, critical voltage V_c, required to displace actuator-guide combination by an amount c can be evaluated as

$$V_c = \frac{1}{N_e d_{33}} \left(\frac{K_a + K_{eff}}{K_a}\right) \left(\frac{K_g}{K_a + K_g}\right) c \tag{6.13}$$

Once the clearance gap is filled, the damper is in a closed configuration.

6.3.3 Closed configuration

The damper model in this case involves stiffness from the frictional pads and the frictional interface which can be simplified to an equivalent mirror-half actuator-spring configuration as shown in Figure 6.9. Following various stages of simplification as shown in the figure, the effective stiffness of the spring load acting against each piezo actuator is obtained as

$$K_{eff} = \frac{K_N}{K_D} \tag{6.14}$$

where $K_N = 4K_cK_{fp}K_gK_s + 2K_cK_{fi}K_gK_s + 2K_{fi}K_{fp}K_gK_s + K_cK_{fi}K_{fp}K_g$ and

$K_D = 4K_cK_{fp}K_s + 2K_cK_{fi}K_s + 2K_{fi}K_{fp}K_s + 2K_cK_{fp}K_g + K_cK_{fi}K_g + K_{fi}K_{fp}K_g + K_cK_{fi}K_{fp}$

The displacement of the actuator can be evaluated as in the previous case and is given by Equation 6.10 with K_{eff} replaced by the one obtained in Equation 6.14. The external force developed by the actuator can be obtained in terms of voltage as

$$F_b = K_{eff}\Delta L = N_e d_{33} \frac{K_a K_{eff}}{K_a + K_{eff}} (V - V_c) \tag{6.15}$$

6.4 Power Requirements

Electric power requirements are a major factor in designing active material actuation systems. Piezo actuators operate as capacitive loads. For static operation only the leakage current has to be supplied, which is in the micro-amp or sub-micro-amp range due to high internal resistance of the piezo material, resulting in negligible current leakage. Hence, piezo

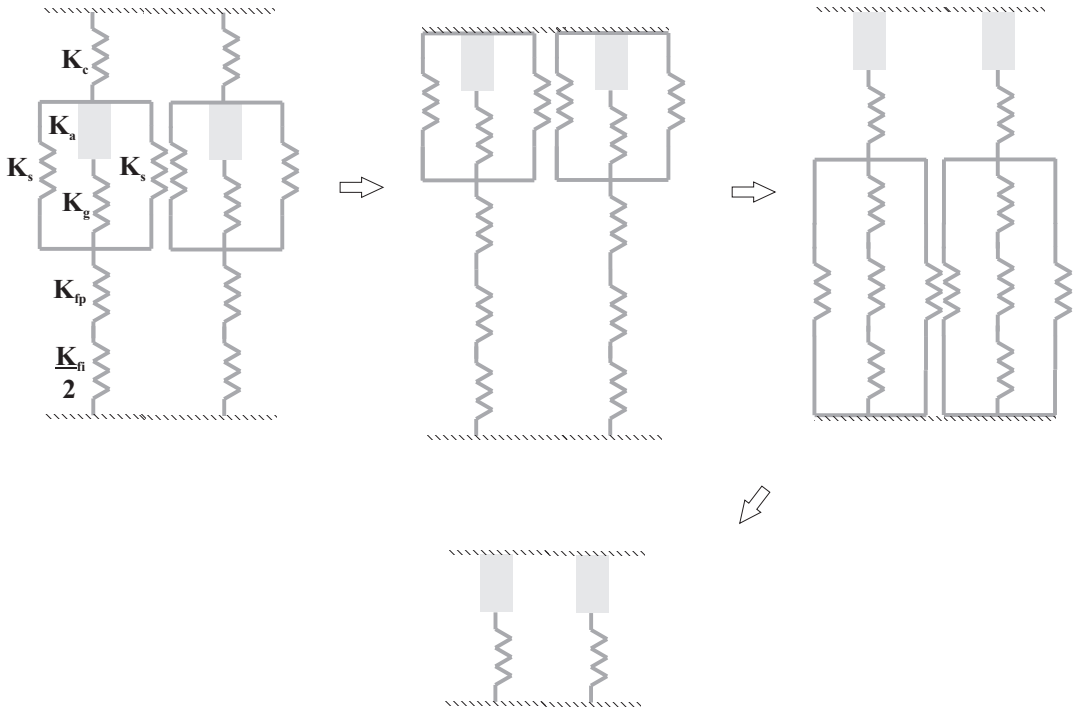

Figure 6.9: Spring model of the lag damper in 'closed' configuration

actuators consume almost no energy in a static application and therefore produce virtually no heat.

The semi-active lag damping concept presented in this work involves dynamic operation of the piezo actuator. Depending on the instantaneous direction and magnitude of regressive mode content in the lag mode in conjunction with control law, power input to the strain actuator is decided. The actuator of given electromechanical properties supplied by the manufacturer is calibrated beforehand to generate desired resistance for known voltage application. As seen from above equations, capacity to generate load of definite magnitude by an actuator not only depends on the stiffness of the actuator but that of other elements in the damper as well. In dynamic applications the power consumption increases linearly with frequency and actuator capacitance. High-load actuators with larger ceramic cross sections have higher capacitance than small actuators.

6.4.1 Electrical Power Input

For applied voltage of the form $v(t) = V_0 + V\sin(\omega t)$, peak power per cycle is obtained by the authors of the reference [49] for low-damping mechanical system, driven well below the mechanical resonance frequency and is given as

$$P_{in} = \omega\chi(v_0)\left(1 - (k_{33})^2 \frac{r}{1+r}\right)\left(\frac{1}{2}CV^2\right) \tag{6.16}$$

where C is the stress-free capacitance of the actuator, r is the stiffness ratio given as

$$r = \frac{K_{eff}}{K_a} \tag{6.17}$$

and $\chi(v_0)$ is an approximation for the reactive power coefficient in the range $-1.5 < v_0 = \frac{V_0}{V} < 1.5$, given by the formula

$$\chi(\nu_0) \approx 1 + 1.62\,|v_0| \tag{6.18}$$

The full stroke electromechanical coupling coefficient of the actuator referred by symbol k_{33} in the Equation 6.16 is given as

$$(k_{33})^2 = \frac{d_{33}^2}{s_{33}^E \varepsilon_{33}^T} \tag{6.19}$$

where s_{33} and ε_{33} are zero-field elastic compliance and zero-stress electrical permittivity respectively.

While the above expression for power input to an induced strain actuator is specific to the voltage input for which it is derived, nonetheless certain inferences can be made about dynamic power and energy capabilities for the proposed adaptive lag damper based on piezo actuation.

The reference electrical energy amplitude, $(1/2)\,CV^2$, the last factor in Equation 6.16 can be easily calculated for a given active material stack from manufacturers' specifications. It can be observed from the equation that input power increases linearly with frequency. The second and third factors in Equation 6.16 are modifiers that take into account the bias voltage effects and the external loading conditions, respectively. The peak input power per cycle is observed to vary strongly with the stiffness ratio, r. A plot of the normalized peak

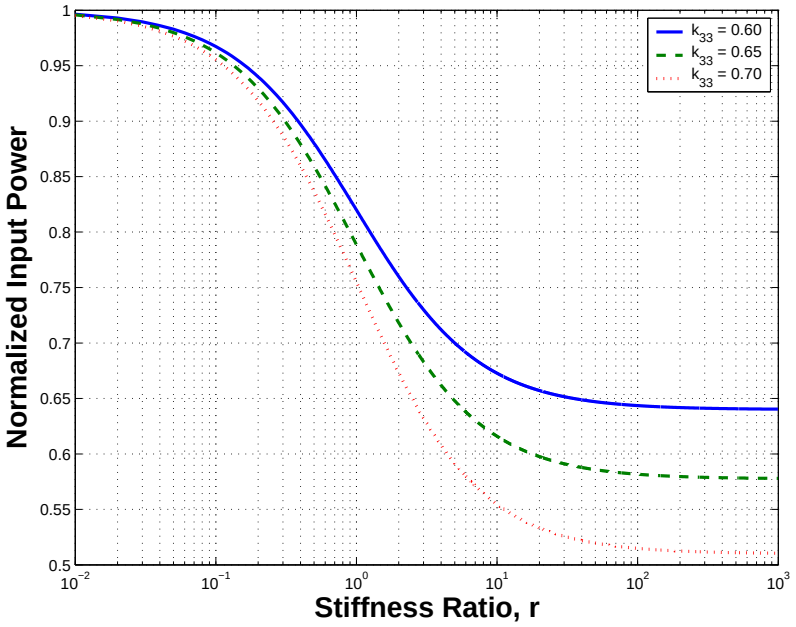

Figure 6.10: Variation of input power with stiffness ratio

input power vs. stiffness ratio r as shown in Figure 6.10 reveals that the peak input power per cycle decreases as the stiffness ratio increases. For a fully blocked actuator ($r \rightarrow \infty$), the relative reduction in peak input power is maximum, and equal to $(k_{33})^2$. The practical values of k_{33} varies between 0.6 and 0.7, with a potential power reduction of as much as 50% for a fully blocked actuator. This implies that in order to achieve power savings, damper elements contributing to K_{eff} has to be made as stiff as possible. A fully blocked actuator also has zero output displacement and hence does not deliver any power output.

6.4.2 Mechanical Power Output

The power output from an induced strain actuator varies strongly with frequency. For low damping mechanical systems, driven well below the mechanical resonance frequency, power output amplitude as obtained by authors of the reference [49] is given as

$$P_{out} = \omega \frac{r}{(1+r)^2} \left[\frac{1}{2} K_a u^2 \right] \tag{6.20}$$

where u is the dynamically induced strain displacement amplitude. From the relation, it can be observed that power output increases linearly with frequency. The effect of stiffness ratio on power output is visualized by plotting normalized power output with respect to

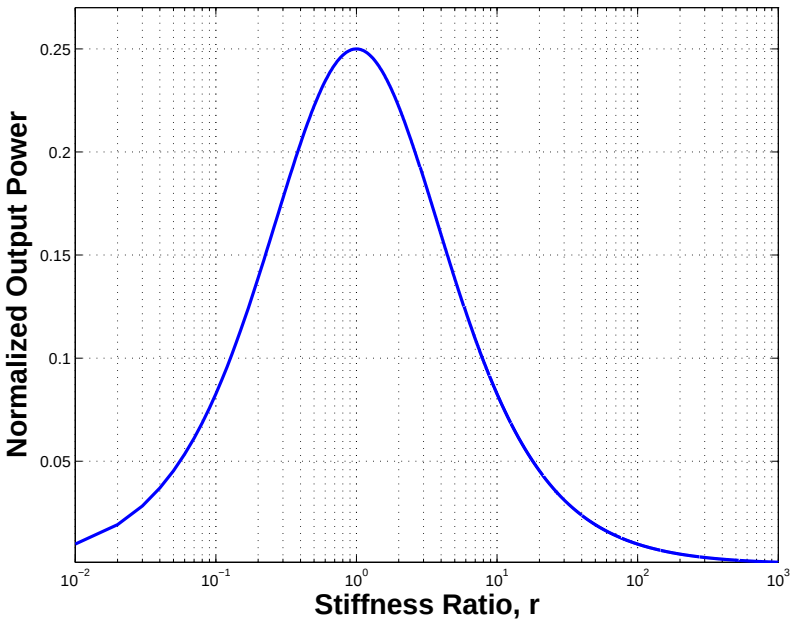

Figure 6.11: Variation of output power with stiffness ratio

stiffness ratio as in Figure 6.11. The output power increases with increase in stiffness ratio and then decreases.

6.5 Size and Damping Capacity

An analysis of the damping capacity provided by the proposed damper is needed for preliminary design. The damper dimensions are kept in line with those of the hydraulic dampers installed in rotors of commercial helicopters. As discussed in power requirements section, input power is minimum when effective stiffness of the equivalent spring load acting on the actuator is high compared to that of actuator itself. In order to achieve it, stiffness of all the damper components except the guide springs, is assumed to be reasonably high. Guide springs are needed just for retracting the guide when the damper is 'off' or when actuator load is reduced and springs with minimal stiffness to do the job is desired. Springs of high stiffness would adversely affect the purpose of achieving high K_{eff}. For other damper components, a high stiffness to weight material of adequate strength is the best choice for performance. The chamber component constituting the major portion of the damper weight is needed to be designed with a light weight material with high stiffness. A highly stiff carbon-composite material would be an ideal choice. The guides and beam for which

thickness affects their axial stiffness can be made out of thin aluminium or steel plate. The metal components can be made of desired thickness by flame cutting or by much advanced laser cutting techniques. Other important components to consider are the brake pads which are designed to be made of carbon-carbon composite material infiltrated with tough ceramic particles. A further discussion on the choice of brake pad material is given in the next section dealing with design and maintenance issues. A nominal thickness for all the damper components have been assumed for preliminary investigation. A clearance is designed between pads and guides for damper to be operational in two different states 'on' and 'off'. Since the total motion of the actuator is on the order of tens of micrometers, the actuation mechanism must have a high output impedance and small clearance in order to exert a significant force on the brake pads. The objectives can be achieved by precise machining and assembly of the damper components as well as precise positioning of the brake pad relative to the guide surface. It is not intended that these preliminary design analysis be precise, but rather they should be within an accepted tolerance. The assumed dimensions and properties of various damper components are given in Table 6.2. The mechanical tolerance or the clearance between the guides and the frictional interface has been assumed to be 4×10^{-4} inches. Two different actuators from different manufactures are considered for analysis. The manufactures' specified properties of stack actuators are given in Table 6.3. Using the equations obtained, damper performance is evaluated for the given actuators as shown in Table 6.4. It is seen that the proposed semi-active damper design integrated with commercially available actuators can generate load comparable to that generated by a UH-60 hydraulic lag damper.

6.6 Design and Maintenance

For any sophisticated design, manufacturing and operating costs, ease of maintenance, and efficiency are the most relevant factors in deciding the success of the design. The specific

Table 6.2: Dimensions and Properties of Damper and its Components

Chamber	Elastic stiffness, E_c (Ksi)	29,000
	Length, l (in)	6.0
	Actuator spacing, d (in)	2.0
	Thickness, t_c (in)	1.2
Guide	Elastic stiffness, E_g (Ksi)	10,000
	Thickness, t_g (in)	0.8
Friction pads	Elastic stiffness, E_{fp} (Ksi)	29,000
	Thickness, t_{fp} (in)	0.4
	Friction coefficient, μ	0.35
Friction interface	Elastic stiffness, E_{fi} (Ksi)	29,000
	Thickness, t_{fi} (in)	1.2
Guide springs	Elastic stiffness, K_s (lb/in)	0.0

Table 6.3: Actuator Dimensions and Properties

	P-045.40P	**P-247.70**
Manufacturer	PI Ceramic	Polytec PI
Diameter (in)	1.77	1.38
Length (in)	2.48	3.94
Blocking force (lb)	9200	6744
Free displacement (in)x10^{-6}	2.36	4.72
Stiffness (lb/ft)x10^6	46.59	25.35
Blocking voltage (V)	1000	1000

Table 6.4: Actuator Performance Comparison

	Actuator 1	**Actuator 2**
Critical voltage, V_c (V)	166	123
Single Actuator maximum output, F_b (lb)	2200	2300
Equivalent normal force (4 Actuators), N_{max} (lb)	8800	9200
Damper maximum resistance (lb)	3020	3220

components of the proposed lag damper design which contribute the most to identified goals are the piezoelectric actuator and friction pads. These components can be selected from the ones commercially available with a wide variety of performance index. The simplified damper design provides easy assembly of these parts. In comparison to a hydraulic damper, friction dampers have no hydraulic lines and thus have no leakage problems. The Fluidlastic damper and elastomeric dampers utilizing complex material and fluids are costly while our damper requires simple components in association with the control law to do adaptive selective damping.

A design like this would require fewer resources and the production of cost effective and sophisticated lag dampers can be achieved in little time. Damper maintenance will be due to wearing of friction pads and reduced performance of the stack actuator; other parts are less subjected to action and thus less wear and tear. The maintenance and design related issues of these two parts are considered separately in the following sections.

6.6.1 Actuator

The use of stack actuator for force generation in the lag damper has several advantages. Piezoelectric actuators can bear loads up to several tons and position within a range of more than 100 μm with sub-nanometer resolution. The smallest changes in the operating voltage are converted into smooth movements which are purely based on solid state technology and not influenced by stiction/friction or threshold voltages. Piezoelectric actuators offer the fastest response time available. A range of commercially available actuators have time constants in microseconds and acceleration rates of more than 10,000g's. A piezoelectric actuator has neither gears nor rotating shafts. Since its displacement is based on pure solid-state effects, it exhibits no wear and tear. The endurance tests conducted on actuators showed no change in performance after several billion cycles. Piezoelectric actuators employ ceramic elements that do not need any lubricants and exhibit no wear or abrasion.

This makes them clean-room compatible and ideally suited for ultra-high-vacuum applications. The piezoelectric effect is based on electric fields and functions down to almost zero kelvin, albeit at reduced specifications. However, the insulation materials used in standard piezo actuators are sensitive to humidity. These actuators are not recommended in environments with high relative humidity (more than 60%). Ceramic insulation is available for actuators operating under extreme conditions (high temperature, high humidity, vacuum, etc.). With this insulation, actuators can operate reliably at temperatures ranging up to 150° C, much higher than the 80° C limit found with conventional multilayer actuators. The ceramic insulation makes sure that actuators are significantly less susceptible to environmental influences than bare piezoelectric actuators and therefore have a much longer lifetime, especially when used under extreme conditions such as high humidity

There is no generic formula to determine the lifetime of a piezo actuator because of the many influencing parameters, such as temperature, humidity, voltage, acceleration, load, operating frequency, insulation materials, etc. The actuators are designed and built for maximum lifetime under actual operating conditions. The operating voltage range values in the technical data tables are based on years of experience with scientific and industrial applications. For maximum lifetime, operating voltage should not exceed the manufactures' specifications.

6.6.2 Friction Pads

The success of the friction damper design is also dependent on the material selection and design of the two contacting frictional surfaces. Due to limited output displacement of the actuating mechanism and machining and assembly tolerances, material wear should be minimized. Additionally, since the maximum brake torque is directly proportional to the friction coefficient (for a given maximum normal force), the frictional coefficient of the two contacting surface has to be maximized. The contacting surfaces are therefore, designed to minimize wear, while still retaining a large friction coefficient. The composition, thickness, and other properties of the friction layer formed when two surfaces interact with each other

mechanically and chemically, determine the brake's effectiveness and wear rate. Recently, much of the emphasis has been on carbon-carbon composites, used in brakes for airplanes, race cars, and high-end passenger cars. The carbon-carbon composite brake pads are infiltrated with tough ceramic particles to better resist wear. The idea is to never have to replace the pads. This combination provides extremely high wear resistance and a coefficient of friction of approximately 0.45. Carbon brakes addresses the need for higher temperature withstand capability and a brake that would not "fade" as the brake grew hotter.

By using damper selectively during parts of the speed range, number of applications of brake can be significantly reduced and hence brake life increased. In fact, damper operation is required for certain rotor speed range when helicopter is on ground to avoid ground resonance and for certain maneuvering flight cases. The damper can be made operational during onset of instability determined by stability margin and can be turned 'off' thereafter.

CHAPTER VII

CONCLUSIONS

The research efforts presented in this dissertation may be divided into five main parts. First, a fundamental study of selective damping strategy using semi-active friction damper is conducted. Second, ground resonance analysis is conducted on a classical two dimensional rotor-fuselage-landing gear model with embedded control laws for semi-active friction based lag damping. Third, ground resonance analysis is performed on a comprehensive computational model of UH-60 rotorcraft with an integrated lag damper model. Three semi-active control laws with varying levels of selectivity for regressive lag damping are analyzed to validate and confirm stability trends associated with adaptive friction based damper design. Fourth, studies are conducted on UH-60 model to study the effects of damper parameters such as saturation load level and damping coefficient on damper performance. Finally, a conceptual design of the semi-active friction based lag damper is presented. The major conclusions reached from five parts of the research are presented followed by the concluding remarks. In the end, some recommendations for further research on this topic, are presented in this chapter.

7.1 Study of Semi-Active Selective Damping Strategy

The objective of this research is to gain an understanding of the selective damping strategies when using a semi-active friction based damper. A system model is designed such that its response is similar to that of lag motion of rotor blades. The lag motion consists of the regressive lag mode and higher nP modes. While the regressive mode is unstable, the other modes do not affect the stability of the system with respect to ground resonance. System response is assumed to consist of two modes: one representing regressive lag mode and the other representing the 1P mode. The selective damping strategy dealt with modulating

the normal force applied at the frictional interface to enhance damping of one mode while reducing the energy dissipated for the other. Several control strategies are devised in a heuristic manner. In the first strategy, a normal force is applied when the relative velocity of the target mode is in a certain range around the maximum. The second control strategy is derived from the first one by adding a condition requiring the total relative velocity and the targeted mode velocity to have the same direction for the normal force to be applied. Making the friction force proportional to the velocity of the selected modal component is another way of achieving selective damping. The third strategy consists of making the normal force proportional to velocity of the target mode. In addition, normal force is applied only when total relative velocity and the targeted mode velocity have the same direction.

The second strategy results in the maximum level of selective damping which is determined by percentage of energy dissipated of the target mode. The first strategy results in the least amount of selective damping of the target mode. In terms of total amount of energy dissipated of the target mode in the same time interval, first strategy performs better than the others. The third strategy gives a compromise performance between the first and the second strategy.

7.2 Ground Resonance Analysis Using Classical Model

The classical ground resonance model by Coleman is used for preliminary analysis of semi-active damping strategies. The classic ground resonance analysis model is derived in the nonrotating frame for configurations with and without viscous lag damper. In the stable zone, the cyclic mode has two distinct frequencies, the regressive and the progressive frequency respectively, while in the unstable zone, the cyclic mode has a single dominant frequency, the regressive frequency, which is responsible for the initiation of instability. The coalescence of regressive lag mode with the fuselage mode results in the ground resonance instability and cannot be suppressed with dampers in the fuselage/landing gear system only. For the rotor with an integrated friction damper, equations are derived in rotating reference

frame. The rotor aerodynamic forces have little influence on ground resonance compared to the structural and inertial forces in the absence of pitch-lag coupling. Different control algorithms are applied to study the effectiveness of selective damping strategies. In the first selective damping strategy, normal load is made proportional to the hyperbolic tangent variation of the regressive lag mode while in the second strategy, an additional condition is imposed on control law of the first strategy requiring the damper to be active only when lag velocity and its regressive component have the same direction.

Both selective damping strategies showed promising blade lag damping augmentation and are equally effective in stabilizing ground resonance. Results showed that the second selective damping does not have any significant advantage over the first selective strategy for lag damping due to negligible difference between regressive mode and rest of the lag mode components. The second selective damping strategy utilizes the frequency or the phase difference between the modal components to damp a specific modal component while limiting damping of other modes. The frequency as well as phase between the regressive component and the rest of the components of lag motion are found to be negligible and hence of no significant benefit.

7.3 Ground Resonance Analysis on UH-60 Model

A comprehensive model of the rotorcraft is developed using multibody finite element based formulations. The semi-active lag damping concept is implemented as a feedback control law modulating the frictional resistance in the lag joint attached to the blade and hub. The rotor configuration with hydraulic damper is chosen as the baseline case for comparison. Three different control strategies governing the actuator behavior are considered. In the first approach, the normal force is a function of the damper stroke rate which is directly proportional to the lag velocity. This semi-active variation of friction level has zero selectivity level for any mode, which means that it does not discriminates amongst modal components. The second and third strategies are same as the first and second strategy

considered in the classical ground resonance analysis with the regressive velocity replaced by the regressive component of the damper stroke rate. Simulations are conducted for a range of rotor speeds from rest to nominal speed to obtain the regressive frequency and damping rate as a function of rotor speed. Damping rate for a particular lag frequency is obtained from the time history of the lag mode using the Prony's method. The stability of the system with reference to ground resonance motion and effectiveness of the concept is analyzed and compared for each damper configuration.

1. There is a significant potential for improving damper performance by replacing a passive lag dampers with semi-active dampers. Damping level comparable to those provided by hydraulic lag dampers can be achieved with semi-active dampers. Furthermore, damping levels provided by semi-active damper can be adaptively tuned to meet the required damping level for specific flight conditions. The adaptive nature of the damper allows it to be in service when desired. In flight configuration when high damping is not required (usually forward flight), the damping can be reduced using an active signal. The reduced damping would reduce the damper loads and thus increase the damper life. In addition, this type of damper could actively compensate for the loss of damping due to environmental changes by sensing the applied force and comparing it with the desired one.

2. On comparing the second damping strategy with the first semi-active damping strategy, no significant difference is found concerning the magnitude of load level applied and the amount of dissipated energy. This is primarily due to the fact that the regressive component is the dominant lag mode component in the zone of instability.

3. The second and the third damping strategies yield a similar response. This confirms the observation obtained with the classical ground resonance model that the frequency difference between regressive mode and rest of lag mode components is negligible. The presence of phase or frequency difference between the modal components is necessary for the third selective strategy to distinguish between the modal components and subsequently damp the desired modes.

7.4 Effect of Higher Normal Loads

The damper operation at higher normal load leads to occurrence of high frequency stick-slip events. Two strategies are tested. In one of the strategy, the control law is redesigned such that for relative velocity below a specific level, referred as notch velocity, the normal load vanishes. The idea is to have zero normal load whenever relative velocity transitions from one direction to the other. However, this strategy does not seem to alleviate the problem. The second strategy involves modifying the control law such that rate of normal load rise at lower velocity is low as well. This is done by modifying the control law based on 'tanh' law to that based on '$1 - \cos$' variation. No significant improvement is observed with the modified law. A detailed observation of the relative velocity and normal load variation plots for above results leads to the conclusion that possible reason behind this high frequency stick slip phenomenon is the small perturbations in relative velocity due to numerical error which are magnified at higher normal loads. This results in a self-exciting phenomenon where a large jump in relative velocity magnitude results into large frictional resistance as per the control law which further cause spikes in relative velocity and the process repeats itself. This is purely a controller driven numerical problem and not a physical limitation of the concept.

7.5 Conceptual Design of the Lag Damper

A conceptual design of a semi-active friction lead lag damper is proposed. The adaptive damping is achieved in the lag damper by actively controlling the passive frictional resistance in the joint using piezoelectric modulation of the normal force. The instantaneous response of the actuator is determined by the centralized controller based on feedback of sensed lag motion of all the blades. The various aspects of the damper design with regard to its practical application in commercial rotors are investigated. Some of the features of the proposed lag damper are:

1. The damper design is such that multiple stack actuators can be accommodated if

higher damping capacity is needed. This also provides a fail-safe feature to the damper design. The maximum friction force generated in the proposed damper configuration with four commercially available embedded actuators, is shown to be comparable to that of a UH-60 hydraulic damper. The geometric dimensions of the proposed damper are comparable to those of the hydraulic damper in UH-60 rotor.

2. The simplified spring-actuator model of the damper in the 'open' and 'closed' configuration are developed and are useful in preliminary investigation of the damping capacity of the damper.

3. The power consumption in the damper is proportional to the frequency of operation which is the same as the lag mode frequency or the regressive lag frequency depending on the semi-active or the selective damping strategy. The power requirement analysis is conducted for sinusoidal voltage operation. It is seen that minimum power input can be achieved by the choice of appropriate dimensions and material of the damper components such that equivalent stiffness of the spring load acting directly on the actuator is high compared to that of actuator stiffness.

7.6 Concluding Remarks

The semi-active damping strategy definitely has potential for lag damping augmentation. This concept is very appealing since it does not make use of complex mechanical components and eliminates the need for expensive materials as in hydraulic and elastomeric dampers. The damper design is simple and provides easy assembly and maintenance of its parts. The piezoelectric actuators with life cycle of the order of billion cycles will certainly minimize associated maintenance cost. Furthermore, damper design accommodates several piezoelectric actuators which other than providing the tunable maximum damping level provides a fail-safe feature as well.

The damping provided by the semi-active dampers is tunable by design and can be tuned to various flight conditions. This is in contrast with conventional designs that rely on a pre-determined damping level, which must be a compromise between the optimal damping levels that would be required for the various flight conditions. Furthermore, the centralized control system can operate the various dampers in a locally optimal manner.

The adaptive nature of the damper allows it to be turned 'off' ino the absence of instability that eliminates unwanted loading on parts of the system which is often a cause of fatigue. Furthermore, this eliminates degradation in damping characteristics due to continuous temperature and stress cycling.

The adaptive feature of the damper allows loads proportional to the instability level and thus results in reduced loads in the blade as well as less wear and fatigue of the damper and lead-lag link. In addition, it results in very modest amount of power required for operation.

7.7 Recommendations for Further Work

The present study has focused on the feasibility of blade lag damping using semi-active friction dampers. It should by no means "close the book" on this approach. On the contrary, it should open up research on the application of friction based adaptive lag damping in helicopter rotor design. Further research work is recommended on the following aspects.

The present research investigates the effectiveness of a semi-active damper for ground resonance only. The verification of the concept for air resonance phenomenon is necessary before any practical application is possible. The analysis can be done on the same model with just the inclusion of flight load cases governing the airload distribution and blade pitch variation. The two selective damping strategies can be tested and compared for maneuvering flights as well.

So far, the damper has been considered to remain active at all times during the operational interval of the rotor. The damper operation is unnecessary once a definite stability margin level is achieved. A control strategy governing switching 'on' and 'off' of the active damper is needed to prolong the life of the damper and prevent unnecessary loading on the associated mechanical components.

An experimental investigation of the strategy needs to be conducted to verify analytical findings. To begin with, a model damper can be manufactured and tested to observe its hysteretic characteristics within the laboratory settings by feeding the stroke motion taken from the time history of the lead-lag motion observed in a actual rotor. On successful validation of the damper effectiveness, world tower test can be conducted on a prototype lead-lag damper.

At higher loads, the damper results in stick-slip phenomenon due to inefficient handling of numerical errors by the controller. Making the actuator response proportional to the relative velocity results in high-frequency noise in actuator response due to excitation of numerical errors associated with computation of relative velocity. Hence, an analytical strategy that keeps the actuator response proportional to relative velocity over a broad range but still prevents controller responding to minor perturbations in velocity has to be devised.

APPENDIX A

GROUND RESONANCE MODEL

A.1 With No Damper

Referring to the Figure 4.1, coordinates of an arbitrary point p in the blade is

$$x = q_x + e\cos(\psi_i) + r\cos(\psi_i + \phi_i) \tag{A.1}$$

$$y = q_y + e\sin(\psi_i) + r\sin(\psi_i + \phi_i) \tag{A.2}$$

Time rate dependency of the position of the point is

$$\dot{x} = \dot{q}_x - e\Omega\sin(\psi_i) - r\left(\Omega + \dot{\phi}_i\right)\sin(\psi_i + \phi_i) \tag{A.3}$$

$$\dot{y} = \dot{q}_y + e\Omega\cos(\psi_i) + r\left(\Omega + \dot{\phi}_i\right)\cos(\psi_i + \phi_i) \tag{A.4}$$

where $\psi_i = \Omega t + \frac{2\pi}{N}(i-1)$ and $\phi_i = \phi_i(t)$

Kinetic Energy of the i^{th} blade is given by

$$T_b^i = \frac{1}{2}\int_0^L (\dot{x}^2 + \dot{y}^2)dm \tag{A.5}$$

$$T_b^i = \frac{1}{2}\dot{q}_x^2 \int_0^L dm + \frac{1}{2}\dot{q}_y^2 \int_0^L dm + \frac{1}{2}e^2\Omega^2 \int_0^L dm + \frac{1}{2}\left(\Omega + \dot{\phi}_i\right) \int_0^L r^2 dm - \dot{q}_x e\Omega \sin(\psi_i) \int_0^L dm +$$
$$\dot{q}_y e\Omega \cos(\psi_i) \int_0^L dm - \dot{q}_x \left(\Omega + \dot{\phi}_i\right) \sin(\psi_i + \phi_i) \int_0^L r dm + \dot{q}_y \left(\Omega + \dot{\phi}_i\right) \cos(\psi_i + \dot{\phi}_i) \int_0^L r dm +$$
$$e\Omega \left(\Omega + \dot{\phi}_i\right) \cos(\phi_i) \int_0^L r dm \tag{A.6}$$

Substituting $\int_0^L dm = m$, $\int_0^L r^2 dm = I$, $\int_0^L r dm = S$, where m is the mass of blade and I and S are the mass moment of Inertia and first mass moment about the axis of rotation respectively.

$$T_b^i = \frac{1}{2}m\dot{q}_x^2 + \frac{1}{2}m\dot{q}_y^2 + \frac{1}{2}me^2\Omega^2 + \frac{1}{2}I\left(\Omega + \dot{\phi}_i\right) - m\dot{q}_x e\Omega \sin(\psi_i) + m\dot{q}_y e\Omega \cos(\psi_i) -$$
$$S\dot{q}_x \left(\Omega + \dot{\phi}_i\right) \sin(\psi_i + \phi_i) + S\dot{q}_y \left(\Omega + \dot{\phi}_i\right) \cos(\psi_i + \dot{\phi}_i) + Se\Omega \left(\Omega + \dot{\phi}_i\right) \cos(\phi_i) \tag{A.7}$$

Total kinetic energy is obtained as summation of kinetic energy of hub and those of individual blades

$$T = T_{hub} + \sum_{i=1}^{N} T_b^i = \frac{1}{2}M_x\dot{q}_x^2 + \frac{1}{2}M_y\dot{q}_y^2 + \sum_{i=1}^{N} T_b^i \tag{A.8}$$

where N refers to the number of blades on the rotor.

Total potential energy is obtained from fuselage and lag attachment, represented by equivalent springs.

$$U = \frac{1}{2}k_x q_x^2 + \frac{1}{2}k_y q_y^2 + \frac{1}{2}\sum_{i=1}^{N} k_q \phi_i^2 \tag{A.9}$$

Variation of the work done by viscous dampers

$$\delta W = -c_x\dot{q}_x\delta q_x - c_y\dot{q}_y\delta q_y \tag{A.10}$$

which can be written as

$$\delta W = \begin{bmatrix} Q_x & Q_y \end{bmatrix} \begin{bmatrix} \delta q_x \\ \delta q_y \end{bmatrix} \tag{A.11}$$

where $Q_x = -c_x \dot{q}_x$ and $Q_y = -c_y \dot{q}_y$

From Euler-Lagrange Principle

$$\begin{aligned} \frac{\partial L}{\partial q_x} - \frac{d}{dt}\left(\frac{\partial L}{\partial \dot{q}_x}\right) &= -Q_x \\ \frac{\partial L}{\partial q_y} - \frac{d}{dt}\left(\frac{\partial L}{\partial \dot{q}_y}\right) &= -Q_y \\ \frac{\partial L}{\partial \phi_i} - \frac{d}{dt}\left(\frac{\partial L}{\partial \dot{\phi}_i}\right) &= 0 \end{aligned} \tag{A.12}$$

where $L = T - U$

Lag motion are assumed to remain small, and hence, terms containing products of ϕ and $\dot{\phi}$ are neglected yielding

$$\left(M_x + \sum_{i=1}^{N} m\right) \ddot{q}_x - S \sum_{i=1}^{N} \frac{d^2}{dt^2} \left(\phi_i \sin(\psi_i)\right) + k_x q_x + c_x \dot{q}_x = 0 \tag{A.13}$$

$$\left(M_y + \sum_{i=1}^{N} m\right) \ddot{q}_y + S \sum_{i=1}^{N} \frac{d^2}{dt^2} \left(\phi_i \sin(\psi_i)\right) + k_y q_y + c_y \dot{q}_y = 0 \tag{A.14}$$

$$I\ddot{\phi}_i - S\ddot{q}_x \sin(\psi_i) + S\ddot{q}_y \cos(\psi_i) + \left(k_q + Se\Omega^2\right) \phi_i = 0 \tag{A.15}$$

In nonrotating frame of reference, blade lag angle for a four bladed rotor ($N = 4$) can be written as

$$\phi_i = \zeta_0 + \zeta_s \sin(\psi_i) + \zeta_c \cos(\psi_i) + \zeta_E (-1)^i \tag{A.16}$$

where

$$\textit{Collective mode} \quad : \quad \phi_{coll} = \zeta_0 \tag{A.17}$$

$$\textit{Differential mode} \;:\; \phi_{diff} = (-1)^i \zeta_E \tag{A.18}$$

$$\textit{Cyclic mode} \;:\; \phi_{cyc} = \zeta_s \sin(\psi_i) + \zeta_c \cos(\psi_i) \tag{A.19}$$

Following mathematical relations can be obtained using Equation A.16

$$\begin{aligned}
\sum_{i=1}^{N} \left[\frac{d^2\phi_i}{dt^2}\right] &= \frac{N}{2}\ddot{\zeta}_0 \\
\sum_{i=1}^{N} \left[(-1)^i \frac{d^2\phi_i}{dt^2}\right] &= \frac{N}{2}\ddot{\zeta}_E \\
\sum_{i=1}^{N} \left[\frac{d^2\left(\phi_i \sin\left(\psi_i\right)\right)}{dt^2}\right] &= \frac{N}{2}\ddot{\zeta}_s \\
\sum_{i=1}^{N} \left[\frac{d^2\left(\phi_i \cos\left(\psi_i\right)\right)}{dt^2}\right] &= \frac{N}{2}\ddot{\zeta}_c \\
\sum_{i=1}^{N} \left[\sin\left(\psi_i\right) \frac{d^2\phi_i}{dt^2}\right] &= \frac{N}{2}\ddot{\zeta}_s - N\Omega\dot{\zeta}_c - \frac{N}{2}\Omega^2\zeta_s \\
\sum_{i=1}^{N} \left[\cos\left(\psi_i\right) \frac{d^2\phi_i}{dt^2}\right] &= \frac{N}{2}\ddot{\zeta}_c + N\Omega\dot{\zeta}_s - \frac{N}{2}\Omega^2\zeta_c
\end{aligned} \tag{A.20}$$

By multiplying Eq.A.15 by $(-1)^i$, $\cos(\psi_i)$, and $\sin(\psi_i)$ separately and summing the output for all the $N(N = 4)$ blades gives

$$(-1)^{i-1} I\ddot{\phi}_i + (-1)^i S\ddot{q}_x \sin(\psi_i) + (-1)^{i-1} S\ddot{q}_y \cos(\psi_i) + (-1)^{i-1} \left(k_q + Se\Omega^2\right) \phi_i = 0 \tag{A.21}$$

$$I\ddot{\phi}_i \sin(\psi_i) - S\ddot{q}_x \sin^2(\psi_i) + S\ddot{q}_y \sin(\psi_i)\cos(\psi_i) + \left(k_q + Se\Omega^2\right)\sin(\psi_i) = 0 \tag{A.22}$$

$$I\ddot{\phi}_i \cos(\psi_i) - S\ddot{q}_x \cos(\psi_i)\sin(\psi_i) + S\ddot{q}_y \cos^2(\psi_i) + \left(k_q + Se\Omega^2\right)\cos(\psi_i) = 0 \tag{A.23}$$

Substituting for terms in Equations A.13, A.14, A.15, A.21, A.22, and A.23 by corresponding terms in A.20

$$\frac{\ddot{q}_x}{R} - \frac{N}{2}\frac{S}{R\left(M_x + Nm\right)}\ddot{\zeta}_s + \frac{k_x}{\left(M_x + Nm\right)}\frac{q_x}{R} + \frac{c_x}{M_x + Nm}\frac{\dot{q}_x}{R} = 0 \tag{A.24}$$

$$\frac{\ddot{q}_y}{R} + \frac{N}{2}\frac{S}{R\left(M_y + Nm\right)}\ddot{\zeta}_c + \frac{k_y}{\left(M_y + Nm\right)}\frac{q_y}{R} + \frac{c_y}{M_y + Nm}\frac{\dot{q}_y}{R} = 0 \tag{A.25}$$

$$I\ddot{\zeta}_0 + \left(k_q + Se\Omega^2\right)\zeta_0 = 0 \tag{A.26}$$

$$I\ddot{\zeta}_E + \left(k_q + Se\Omega^2\right)\zeta_E = 0 \tag{A.27}$$

$$I\left(\ddot{\zeta}_s - 2\Omega\dot{\zeta}_c - \Omega^2\zeta_s\right) - Sq_x + \left(k_q + Se\Omega^2\right)\zeta_s = 0 \tag{A.28}$$

$$I\left(\ddot{\zeta}_c + 2\Omega\dot{\zeta}_s - \Omega^2\zeta_c\right) + Sq_y + \left(k_q + Se\Omega^2\right)\zeta_c = 0 \tag{A.29}$$

Writing in non-dimensionalized form using following terms

Nondimensional time, $\tau = \Omega t$

Fuselage motion x-direction, $\bar{q_x} = \frac{q_x}{R}$

Fuselage motion y-direction, $\bar{q_y} = \frac{q_y}{R}$

Blade first mass moment, $\bar{S_\zeta} = \frac{RS}{I}$

Blade Lag frequency, $v_\zeta = \sqrt{\frac{eS}{I} + \frac{k_q}{\Omega^2 I}}$

Fuselage Inertia in x-direction $\bar{M_x} = \frac{(M_x + Nm)R^2}{NI}$

Fuselage Inertia in y-direction, $\bar{M_y} = \frac{(M_y + Nm)R^2}{NI}$

Fuselage frequency in x-direction, $\frac{\omega_x}{\Omega} = \sqrt{\frac{k_x}{M_x + Nm}}$

Fuselage frequency in y-direction, $\frac{\omega_y}{\Omega} = \sqrt{\frac{k_y}{M_y + Nm}}$

Fuselage damper in x-direction, $\bar{c}_x = \frac{c_x}{M_x + Nm}$

Fuselage damper in y-direction, $\bar{c}_y = \frac{c_y}{M_y + Nm}$

On substituting, following equations result

$$\frac{d^2\bar{q}_x}{d\tau^2} - \frac{\bar{S}_\zeta}{2\bar{M}_x}\frac{d^2\zeta_s}{d\tau^2} + \frac{\omega_x^2}{\Omega^2}\bar{q}_x + \bar{c}_x\frac{d\bar{q}_x}{d\tau} = 0 \tag{A.30}$$

$$\frac{d^2\bar{q}_y}{d\tau^2} + \frac{\bar{S}_\zeta}{2\bar{M}_y}\frac{d^2\zeta_c}{d\tau^2} + \frac{\omega_y^2}{\Omega^2}\bar{q}_y + +\bar{c}_y\frac{d\bar{q}_y}{d\tau} = 0 \tag{A.31}$$

$$\frac{d^2\zeta_0}{d\tau^2} + v_\zeta^2\zeta_0 = 0 \tag{A.32}$$

$$\frac{d^2\zeta_E}{d\tau^2} + v_\zeta^2\zeta_E = 0 \tag{A.33}$$

$$\frac{d^2\zeta_s}{d\tau^2} - 2\frac{d\zeta_c}{d\tau} - \bar{S}_\zeta\frac{d^2\bar{q}_x}{d\tau^2} + \left(v_\zeta^2 - 1\right)\zeta_s = 0 \tag{A.34}$$

$$\frac{d^2\zeta_c}{d\tau^2} + 2\frac{d\zeta_s}{d\tau} + \bar{S}_\zeta\frac{d^2\bar{q}_y}{d\tau^2} + \left(v_\zeta^2 - 1\right)\zeta_c = 0 \tag{A.35}$$

The collective and differential rotor modes (in the nonrotating frame) given by Equations A.32 and A.33 respectively are decoupled from other modes for the isotropic rotor. The two modes can be eliminated from consideration and remaining equations can be written in first order form as

$$S\frac{d\dot{\underline{X}}}{d\tau} = B\underline{X} \tag{A.36}$$

where $\underline{X} = \begin{bmatrix} \bar{q}_x & \bar{q}_y & \zeta_s & \zeta_c & \frac{d\bar{q}_x}{d\tau} & \frac{d\bar{q}_y}{d\tau} & \frac{d\zeta_s}{d\tau} & \frac{d\zeta_c}{d\tau} \end{bmatrix}$ and S and B are given by

$$S = \begin{bmatrix} 1 & 0 & 0 & 0 & 0 & 0 & 0 & 0 \\ 0 & 1 & 0 & 0 & 0 & 0 & 0 & 0 \\ 0 & 0 & 1 & 0 & 0 & 0 & 0 & 0 \\ 0 & 0 & 0 & 1 & 0 & 0 & 0 & 0 \\ 0 & 0 & 0 & 0 & 1 & 0 & -\frac{\bar{S}_\zeta}{2\bar{M}_x} & 0 \\ 0 & 0 & 0 & 0 & 0 & 1 & 0 & \frac{\bar{S}_\zeta}{2\bar{M}_y} \\ 0 & 0 & 0 & 0 & -\bar{S}_\zeta & 0 & 1 & 0 \\ 0 & 0 & 0 & 0 & 0 & \bar{S}_\zeta & 0 & 1 \end{bmatrix}$$

$$B = \begin{bmatrix} 0 & 0 & 0 & 0 & 1 & 0 & 0 & 0 \\ 0 & 0 & 0 & 0 & 0 & 1 & 0 & 0 \\ 0 & 0 & 0 & 0 & 0 & 0 & 1 & 0 \\ 0 & 0 & 0 & 0 & 0 & 0 & 0 & 1 \\ -\frac{\omega_x^2}{\Omega^2} & 0 & 0 & 0 & -\bar{c}_x & 0 & 0 & 0 \\ 0 & -\frac{\omega_y^2}{\Omega^2} & 0 & 0 & 0 & -\bar{c}_y & 0 & 0 \\ 0 & 0 & 1-v_\zeta^2 & 0 & 0 & 0 & 0 & 2 \\ 0 & 0 & 0 & 1-v_\zeta^2 & 0 & 0 & -2 & 0 \end{bmatrix}$$

A.2 With Friction Damper for Lag motion

Variation of the work done by viscous and friction dampers

$$\delta W = -c_x \dot{q}_x \delta q_x - c_y \dot{q}_y \delta q_y - \sum_{i=1}^{N} \mu N_i d_i \mathrm{sgn}(\dot{\phi}_i) \delta \phi_i \tag{A.37}$$

which can be written as

$$\delta W = \begin{bmatrix} Q_x & Q_y & Q_1 & ... & Q_N \end{bmatrix} \begin{bmatrix} \delta q_x \\ \delta q_y \\ \delta \phi_1 \\ ... \\ \delta \phi_N \end{bmatrix} \tag{A.38}$$

where $Q_i = -\mu N_i d_i sgn(\dot{\phi}_i)$

Equations of motion in the rotating frame can then be obtained using Euler-Lagrange principle as

$$\frac{d^2\bar{q}_x}{d\tau^2} - \frac{1}{N}\frac{\bar{S}_\zeta}{\bar{M}_x}\sum_{i=1}^{N}\frac{d^2}{d\tau^2}\left(\phi_i \sin(\psi_i)\right) + \frac{\omega_x^2}{\Omega^2}\bar{q}_x + \bar{c}_x\frac{d\bar{q}_x}{d\tau} = 0 \tag{A.39}$$

$$\frac{d^2\bar{q}_y}{d\tau^2} + \frac{1}{N}\frac{\bar{S}_\zeta}{\bar{M}_y}\sum_{i=1}^{N}\frac{d^2}{d\tau^2}\left(\phi_i \cos(\psi_i)\right) + \frac{\omega_y^2}{\Omega^2}\bar{q}_y + \bar{c}_y\frac{d\bar{q}_y}{d\tau} = 0 \tag{A.40}$$

$$\frac{d^2\phi_i}{d\tau^2} - \bar{S}_\zeta\sum_{i=1}^{N}\frac{d^2\bar{q}_x}{d\tau^2}\sin(\psi_i) + \bar{S}_\zeta\sum_{i=1}^{N}\frac{d^2\bar{q}_y}{d\tau^2}\cos(\psi_i) + v_\zeta^2\phi_i + \bar{c}_{d_i}\mathrm{sgn}\left(\frac{d\phi_i}{d\tau}\right) = 0 \tag{A.41}$$

where $\bar{c}_x = \frac{c_x}{M_x+Nm}$, $\bar{c}_y = \frac{c_y}{M_y+Nm}$, and $\bar{c}_{d_i} = \frac{\mu N_i d_i}{I\Omega^2}$

Above equations can be written in the first order form as

$$S\dot{\underline{X}} = B\underline{X} + U \tag{A.42}$$

where $\underline{X} = \begin{bmatrix} \bar{q}_x & \bar{q}_y & \phi_1 & \phi_2 & \phi_3 & \phi_4 & \frac{d\bar{q}_x}{d\tau} & \frac{d\bar{q}_y}{d\tau} & \frac{d\phi_1}{d\tau} & \frac{d\phi_2}{d\tau} & \frac{d\phi_3}{d\tau} & \frac{d\phi_4}{d\tau} \end{bmatrix}$

and S and B are given by

$$S = \begin{bmatrix}
1 & 0 & 0 & 0 & 0 & 0 & 0 & 0 & 0 & 0 & 0 & 0 \\
0 & 1 & 0 & 0 & 0 & 0 & 0 & 0 & 0 & 0 & 0 & 0 \\
0 & 0 & 1 & 0 & 0 & 0 & 0 & 0 & 0 & 0 & 0 & 0 \\
0 & 0 & 0 & 1 & 0 & 0 & 0 & 0 & 0 & 0 & 0 & 0 \\
0 & 0 & 0 & 0 & 1 & 0 & 0 & 0 & 0 & 0 & 0 & 0 \\
0 & 0 & 0 & 0 & 0 & 1 & 0 & 0 & 0 & 0 & 0 & 0 \\
0 & 0 & 0 & 0 & 0 & 0 & 1 & 0 & -S_{x1} & -S_{x2} & -S_{x3} & -S_{x4} \\
0 & 0 & 0 & 0 & 0 & 0 & 0 & 1 & S_{y1} & S_{y2} & S_{y3} & S_{y4} \\
0 & 0 & 0 & 0 & 0 & 0 & -\bar{S}_\zeta\sin(\psi_1) & \bar{S}_\zeta\cos(\psi_1) & 1 & 0 & 0 & 0 \\
0 & 0 & 0 & 0 & 0 & 0 & -\bar{S}_\zeta\sin(\psi_2) & \bar{S}_\zeta\cos(\psi_2) & 0 & 1 & 0 & 0 \\
0 & 0 & 0 & 0 & 0 & 0 & -\bar{S}_\zeta\sin(\psi_3) & \bar{S}_\zeta\cos(\psi_3) & 0 & 0 & 1 & 0 \\
0 & 0 & 0 & 0 & 0 & 0 & -\bar{S}_\zeta\sin(\psi_4) & \bar{S}_\zeta\cos(\psi_4) & 0 & 0 & 0 & 1
\end{bmatrix}$$

$$B = \begin{bmatrix} 0 & 0 & 0 & 0 & 0 & 0 & 1 & 0 & 0 & 0 & 0 & 0 \\ 0 & 0 & 0 & 0 & 0 & 0 & 0 & 1 & 0 & 0 & 0 & 0 \\ 0 & 0 & 0 & 0 & 0 & 0 & 0 & 0 & 1 & 0 & 0 & 0 \\ 0 & 0 & 0 & 0 & 0 & 0 & 0 & 0 & 0 & 1 & 0 & 0 \\ 0 & 0 & 0 & 0 & 0 & 0 & 0 & 0 & 0 & 0 & 1 & 0 \\ 0 & 0 & 0 & 0 & 0 & 0 & 0 & 0 & 0 & 0 & 0 & 1 \\ -\frac{\omega_x^2}{\Omega^2} & 0 & -S_{x1} & -S_{x2} & -S_{x3} & -S_{x4} & -\bar{c}_x & 0 & 2C_{x1} & 2C_{x2} & 2C_{x3} & 2C_{x4} \\ 0 & -\frac{\omega_y^2}{\Omega^2} & C_{y1} & C_{y2} & C_{y3} & C_{y4} & 0 & -\bar{c}_y & 2S_{y1} & 2S_{y2} & 2S_{y3} & 2S_{y4} \\ 0 & 0 & -v_\zeta^2 & 0 & 0 & 0 & 0 & 0 & 0 & 1 & 0 & 0 \\ 0 & 0 & 0 & -v_\zeta^2 & 0 & 0 & 0 & 0 & 0 & 0 & 1 & 0 \\ 0 & 0 & 0 & 0 & -v_\zeta^2 & 0 & 0 & 0 & 0 & 0 & 0 & 1 \\ 0 & 0 & 0 & 0 & 0 & -v_\zeta^2 & 0 & 0 & 0 & 0 & 0 & 0 \end{bmatrix}$$

where $S_{xi} = \frac{1}{N}\frac{\bar{S}_\zeta}{\bar{M}_x}\sin(\psi_i)$, $S_{yi} = \frac{1}{N}\frac{\bar{S}_\zeta}{\bar{M}_y}\sin(\psi_i)$, $C_{xi} = \frac{1}{N}\frac{\bar{S}_\zeta}{\bar{M}_x}\cos(\psi_i)$, and $C_{yi} = \frac{1}{N}\frac{\bar{S}_\zeta}{\bar{M}_y}\cos(\psi_i)$

$$U = \begin{bmatrix} 0 & 0 & 0 & 0 & 0 & 0 & 0 & 0 & -\bar{c}_{d_1}\mathrm{sgn}\left(\frac{d\phi_1}{d\tau}\right) & -\bar{c}_{d_2}\mathrm{sgn}\left(\frac{d\phi_2}{d\tau}\right) & -\bar{c}_{d_3}\mathrm{sgn}\left(\frac{d\phi_3}{d\tau}\right) & -\bar{c}_{d_4}\mathrm{sgn}\left(\frac{d\phi_4}{d\tau}\right) \end{bmatrix}^T$$

A.3 Transformation

The information about system variables in nonrotating reference frame can be obtained from the response of the system in rotating frame as

$$\zeta_0 = \frac{1}{4}\left(\phi_1 + \phi_2 + \phi_3 + \phi_4\right) \tag{A.43}$$

$$\zeta_E = \frac{1}{4}\left(-\phi_1 + \phi_2 - \phi_3 + \phi_4\right) \tag{A.44}$$

$$\zeta_s = \frac{1}{2}\left(\phi_1\sin(\psi_1) + \phi_2\sin(\psi_2) + \phi_3\sin(\psi_3) + \phi_4\sin(\psi_4)\right) \tag{A.45}$$

$$\zeta_c = \frac{1}{2}\left(\phi_1\cos(\psi_1) + \phi_2\cos(\psi_2) + \phi_3\cos(\psi_3) + \phi_4\cos(\psi_4)\right) \tag{A.46}$$

APPENDIX B

MULTIBLADE COORDINATE TRANSFORMATION

From system response in rotating frame, lag velocities $\dot{\phi}_1$, $\dot{\phi}_2$, $\dot{\phi}_3$, $\dot{\phi}_4$ for each of the respective four blades are obtained.

Using multiblade coordinate transformation, lag velocity of i^{th} blade can be written as

$$\dot{\phi}_i = \dot{\zeta}_0 + \Omega\left(\zeta_s \cos(\psi_i) - \zeta_c \sin(\psi_i)\right) + \dot{\zeta}_s \sin(\psi_i) + \dot{\zeta}_c \cos(\psi_i) + \dot{a}_E(-1)^i \tag{B.1}$$

Regressive component of the lag mode is expressed as

$$\dot{\phi}_{ir} = \left(\dot{\zeta}_s - \zeta_c\Omega\right)\sin(\psi_i) + \left(\dot{\zeta}_c + \zeta_s\Omega\right)\cos(\psi_i) \tag{B.2}$$

Multiplying B.1 by $\sin(\psi_i)$ and summing the resulting term for all the blades

$$\sum_{i=1}^{4} \dot{\phi}_i \sin(\psi_i) = 2\left(\dot{\zeta}_s - \zeta_c\Omega\right) \tag{B.3}$$

Similarly, multiplying B.1 by $\cos(\psi_i)$ and summing the resulting term for all the blades

$$\sum_{i=1}^{4} \dot{\phi}_i \cos(\psi_i) = 2\left(\dot{\zeta}_c + \zeta_s\Omega\right) \tag{B.4}$$

Regressive lag velocity for i^{th} blade can now be obtained from lag velocities using Equations B.3 and B.4 as

$$\dot{\phi}_{ir} = \frac{1}{2}\sin(\psi_i)\sum_{j=1}^{4}\dot{\phi}_j \sin(\psi_j) + \frac{1}{2}\cos(\psi_i)\sum_{j=1}^{4}\dot{\phi}_j \cos(\psi_j) \tag{B.5}$$

REFERENCES

[1] Akbay, Z. and Aktan, H. M., "Abating earthquake effects on buildings by active slip brace devices," *Shock Vibrations*, vol. 2, pp. 133–142, 1995.

[2] Azvine, B., Tomlinson, G. R., and Wynne, R. J., "Use of active constrained layer damping for controlling resonant vibration," *Smart Materials and Structure*, vol. 4, no. 1, pp. 1–6, 1995.

[3] Bauchau, O. A., "Computational schemes for flexible, nonlinear multi-body system," *Multibody System Dynamics*, vol. 2, pp. 169–225, 1998.

[4] Bauchau, O. A. and Bottasso, C. L., "On the design of energy preserving and energy decaying schemes for flexible, nonlinear multi-body systems," *Computer Methods in Applied Mechanics and Engineering*, vol. 169, pp. 61–79, 1999.

[5] Bauchau, O. A., Bottasso, C. L., and Nikishkov, Y. G., "Modeling rotorcraft dynamics with finite element multibody procedures," *Mathematics and Computer Modeling*, vol. 33, pp. 1113–1137, 2001.

[6] Bauchau, O. A. and Guernsey, D., "On the choice of appropriate bases for nonlinear dynamic modal analysis," *Journal of the American Helicopter Society*, vol. 38, pp. 28–36, 1993.

[7] Bauchau, O. A. and Hodges, D. H., "Analysis of nonlinear multi-body systems with elastic couplings," *Multibody System Dynamics*, vol. 3, pp. 168–188, 1999.

[8] Bauchau, O. A. and Joo, T., "Computational schemes for nonlinear elastodynamics," *International Journal for Numerical Methods in Engineering*, vol. 45, pp. 693–719, 1999.

[9] Bauchau, O. A. and Liu, H., "On the modeling of hydraulic components in rotor systems," *http://pweb.ae.gatech.edu/people/obauchau/Publications.html*, 2005.

[10] Baz, A. and Ro, J., "Actively-controlled constrained layer damping," *Sound Vibration Magazine*, vol. 28, pp. 18–21, 1994.

[11] Bousman, W., "An investigation of helicopter roter blade flap vibratory loads," *48th Annual AHS Forum, Washington D.C.*, pp. 977–999, June 3-5 1992.

[12] Bousman, W. G., "An experimental investigation of the effects of aeroelastic couplings on aeromechanical stability of a hingeless rotor helicopter," *Journal of the American Helicopter Society*, vol. 26, no. 1, 1981.

[13] Bousman, W. G., "An experimental investigation of the effects of aeroelastic couplings on aeromechanical stability of a hingeless rotor helicopter," *Journal of the American Helicopter Society*, pp. 46–53, 1981.

[14] Bousman, W. G., "The effects of structural flap-lag and pitch-lag coupling on soft inplane hingeless rotor stability in hover," *NASA Technical Paper 3002*, May 1990.

[15] Bousman, W. G., Sharpe, D. L., and Ormiston, R. A., "An experimental study of techniques for increasing the lead-lag damping of soft inplane hingeless rotors," *Proceedings of the 32nd Annual V/STOL Forum of the American Helicopter Society, Washington, DC*, 1976.

[16] Cai, C., Zheng, H., and Liu, G. R., "Vibration analysis of a beam with pcld patch," *Applied Acoustics*, vol. 65, no. 11, pp. 1057–1076, 2004.

[17] Canudas de Wit, C., Olsson, H., Åstrm, K. J., and Lischinsky, P., "A new model for control of systems with friction," *IEEE Transactions on Automatic Control*, vol. 40, no. 3, pp. 419–425, 1995.

[18] Carlson, R. M., "Ground resonance characterization and control," *From da Vinci to Today and Beyond: The Top Technology Achievements in Vertical Flight History, M.E.R., The American Helicopter Society: Washington, DC.*, pp. 15–16, 1994.

[19] Chen, P. and Chopra, I., "Wind tunnel testing of a smart rotor with individual blade twist control," *Journal of Intelligent Material Systems and Structures*, vol. 8, pp. 414–425, 1997.

[20] Chopra, I., "Perspectives in aeromechanical stability of helicopter rotors," *Vertica*, vol. 14, no. 4, 1990.

[21] Coleman, R. P., "Theory of self excited mechanical oscillations of hingeless rotor blades," *NACA*, 1943.

[22] Coleman, R. P. and Feingold, A. M., "Theory of self-excited mechanical oscillations of helicopter rotors with hinged blades," *NACA*, 1958.

[23] Derham, R. and Hagood, N., "Rotor design using smart materials to actively twist the blades," *Proceedings of the 52nd American Helicopter Society Annual Forum, Washington, DC*, 1996.

[24] Donham, R. E., Cardinale, S. V., and Sachs, I. B., "Ground and air resonance characteristics of a soft in-plane rigid rotor system," *Journal of the American Helicopter Society*, vol. 14, no. 4, 1969.

[25] Dowell, D. J. and Cherry, S., "Semi-active friction dampers for seismic response control of structures," *Proceedings of 5th U.S National Conference on Earthquake Engineering*, vol. 1, pp. 819–828, 1994.

[26] Dupont, P., Kasturi, P., and Stokes, A., "Semi-active control of friction dampers," *Journal of Sound and Vibration*, vol. 202, no. 2, pp. 203–218, 1997.

[27] Dyke, S. J. and Spencer Jr., B. F., "Seismic response control using multiple MR dampers," *Proceedings of the 2nd International Workshop on Structural Control, Hong Kong*, pp. 163–173, 1996.

[28] Dyke, S. J., Spencer Jr., B. F., Sain, M. K., and Carlson, J. D., "An experimental study of MR dampers for seismic protection," *Smart Materials and Structures: Special Issue on Large Civil Structures*, vol. 7, pp. 693–703, 1998.

[29] Fasana, A., Garibaldi, L., Giorcelli, E., and Ruzzene, M., "Passive damping of beams with constrained viscoelastic material source," *Proceedings of SPIE - The International Society for Optical Engineering*, vol. 3045, pp. 184–189, 1997.

[30] Ferri, A., "Modeling and analysis of nonlinear sleeve joints of large space structures," *Journal of Spacecraft and Rockets*, vol. 25, pp. 354–360, 1988.

[31] Ferri, A. A., "Investigation of damping from nonlinear sleeve joints of large space structures," *Proceedings of the ASME 11th Biennial Conference on Mechanical Vibrations and Noise, Boston, MA*, September 27-30 1987.

[32] Ferri, A. A., "Modeling and analysis of nonlinear sleeve joints of large space structures," *AIAA Journal of Spacecrafts and Rockets*, vol. 25, no. 5, pp. 354–360, 1988.

[33] Ferri, A. A., "Damping and vibration of beams with various types of frictional support conditions," *Proceedings of the AIAA/ASME/ASCE/AHS/AHS 30th Structures, Structural Dynamics and Materials Conference, Mobile, AL*, April 3-5 1989.

[34] Ferri, A. A. and Heck, B. S., "Active and passive joints for damping augmentation of large space structures," *Proceedings of the American Control Conference*, pp. 2978–2983, 1990.

[35] Ferri, A. A. and Heck, B. S., "Analytical investigation of damping enhancement using active and passive structural joints," *Journal of Guidance, Control, and Dynamics*, vol. 15, no. 5, pp. 1258–1264, 1992.

[36] Ferri, A. A. and Heck, B. S., "Semi-active suspension using dry friction energy dissipation," *Proceedings of the American Control Conference*, vol. 1, pp. 31–35, 1992.

[37] Friedmann, P. P., "Rotary-wing aeroelasticity with application to vtol vehicles," *Proceedings of the 31st AIAA / AHS / ASME / ASCE / ASC Structures, Structural Dynamics and Materials Conference, Long Beach, CA*, 1990.

[38] Friedmann, P. P., "Rotary-wing aeroelasticity: Current status and future trends," *AIAA Journal*, vol. 42, no. 2, 2004.

[39] Friedmann, P. and Venkatesan, C., "Coupled helicopter rotor/ body aeromechanical stability comparison of theoretical and experimental results," *Journal of Aircraft*, vol. 22, no. 2, pp. 148–155, 1985.

[40] Gabel, R., "Exact mechanical instability boundaries as determined from the coleman equation," *of the American Helicopter Society*, vol. 7, no. 1, 1962.

[41] Gandhi, F., "Concepts for damperless aeromechanically stable rotors," *Proceedings of the Royal Aeronautical Society Innovations in Rotorcraft Technology Conference, London, UK*, 1997.

[42] Gandhi, F. and Hathaway, E., "Optimized aeroelastic couplings for alleviation of helicopter ground resonance," *Journal of Aircraft*, vol. 35, no. 4, pp. 582–590, 1998.

[43] Gandhi, F. and Malovrh, B., "Influence of balanced rotor anisotropy on helicopter aeromechanical stability," *AIAA Journal*, vol. 37, no. 10, pp. 1152–1160, 1999.

[44] Gandhi, F. and Weller, W., "Active aeromechanical stability augmentation using fuselage state feedback," *Proceedings of the 53rd Annual Forum of the American Helicopter Society, Virginia Beach*, 1997.

[45] Gaul, L., Albrecht, H., and Wirnitzer, J., "Semi-active of large space truss structures using friction joints," *Proceedings of the SPIE- The International Society for Optical Engineering*, vol. 4935, pp. 232–243, 2002.

[46] Gaul, L., Albrecht, H., and Wirnitzer, J., "Semi-active friction damping of flexible lightweight structures," *AMAS/ECCOMAS/STC Workshop on Smart Materials and Structures - SMART'03, Poland*, September 2-5 2003.

[47] Gaul, L. and Nitsche, R., "Friction control for vibration suppression," *Mechanical Systems and Signal Processing*, vol. 14, no. 2, pp. 139–150, 2000.

[48] Ginder, J. M., Davis, L. C., and Elie, L. D., "Rheology of magnetorheological fluids: Models and measurements," *International Journal of Modern Physics B*, vol. 10, no. 23-24, pp. 3293–3303, 1996.

[49] Giurgiutiu, V. and Rogers, C. A., "Dynamic power and energy capabilities of commercially-available electro-active induced-strain actuators," *Journal of Intelligent Material Systems and Structures*, vol. 7, pp. 656–667, November 1996.

[50] Gordaninejad, F., Saiidi, M., Hansen, B. C., and Chang, F. K., "Magnetorheological fluid dampers for control of bridges," *Proceedings of the Second World Conference on Structural Control, Kyoto, Japan*, pp. 991–1000, 1999.

[51] Ham, N. D., Behal, B. L., and McKillip, R. M., J., "Helicopter rotor lag damping augmentation through individual-blade control," *Vertica*, vol. 7, no. 4, pp. 361–371, 1983.

[52] Hathaway, E. and Gandhi, F., "Individual blade control for alleviation of helicopter ground resonance," *AIAA/ASME/ASCE/AHS/ASC Structures, Structural Dynamics & Materials Conference*, pp. 2507–2517, 1998.

[53] Hayen, J. C. and Iwan, W. D., "Response control of structural systems using active interface damping," *Proceedings of 1st World Conference on Structural Control, University of South California, Los Angeles*, vol. 1, pp. 23–32, 1994.

[54] Hertz, T. J. and Crawley, E. F., "Displacement dependent friction in space structural joints," *AIAA Journal*, vol. 23, pp. 1996–2000, 1985.

[55] Hohenemser, K. H., "Hingeless rotorcraft flight dynamics," *AGARDograph*, 1974.

[56] Hooper, W. E., "Helicopter ground resonance - the effect of rotor and fuselage damping," *NACA*, 1959.

[57] Howlett, J. J., "Uh-60a black hawk engineering simulation program: Vol. i - mathematical model," *Technical Report, NASA CR-166309*, December 1981.

[58] Huber, H., "Will rotor hubs lose their bearings? a survey of bearingless main rotor development," *Proceedings of the 18th Europen Rotorcraft Forum, Avignon, France*, 1992.

[59] Hurt, M. K. and Wereley, N. M., "Controllable fluid dampers for helicopter rotor stability augmentation," *Proceedings of the 37th AIAA/ASME/AHS Adaptive Structures Forum, Salt Lake City, Utah*, 1996.

[60] Johnson, W., "Influence of unsteady aerodynamics on hingeless rotor ground resonance," *Journal of Aircraft*, vol. 19, no. 8, pp. 668–673, 1982.

[61] Kamath, G. M. and Wereley, N. M., "Distributed damping of rotorcraft flexbeams using electrorheological fluids," *Proceedings of the 35th AIAA/ASME/ASCE/AHS/ASC Structures, Structural Dynamics, and Materials Conference, Salt Lake City, UT*, 1995.

[62] Kamath, G. M. and Wereley, N. M., "A nonlinear viscoelastic-plastic model for electrorheological fluids," *Smart Materials and Structures*, vol. 6, no. 3, pp. 351–359, 1997.

[63] Kamath, G. M., Wereley, N. M., and Jolly, M. R., "Analysis and testing of a model-scale magnetorheological fluid helicopter lag mode damper," *Proceedings of of the 53rd Annual Forum, American Helicopter Society, Alexandria*, 1997.

[64] Kamath, G. M. and Werely, N. M., "System identification of electrorheological fluid-based dampers using a nonlinear viscoelastic-plastic phenomenological model," *Proceedings of the AIAA Aerospace Sciences Conference, Reno, Neveda*, January 6-7 1997.

[65] Kessler, C. and Reichert, G., "Active control to augment rotor lead-lag damping," *The Aeronautical Journal*, pp. 245–258, 1998.

[66] King, S. P., "The effect of pitch-flap and pitch-lag coupling on air resonance," *Westland Helicopters Limited, Yeovil, Dynamics Department Report, No. GEN/DYN/RES/005R*, July 1971.

[67] Lane, J. S. and Ferri, A. A., "Optimal control of a semi-active, frictionally damped joint," *Proceedings of the American Control Conference*, vol. 4, pp. 2754–2759, 1992.

[68] Lesieutre, G. A. and Lee, U., "A finite element for beams having segmented active constrained layers with frequency-dependent viscoelastic," *Smart Materials and Structures*, vol. 5, pp. 615–627, 1996.

[69] Liao, W. H. Wang, K. W., "Characteristics of enhanced active constrained layer damping treatments with edge elements, Part II: System analysis," *ASME Journal of Vibration and Acoustics*, vol. 120, no. 4, pp. 894–900, 1998.

[70] Liao, W. H. and Wang, K. W., "On the active-passive hybrid control actions of active constrained layers," *ASME Journal of Vibration and Acoustics*, vol. 119, no. 4, pp. 563–572, 1997.

[71] Liao, W. H. and Wang, K. W., "Characteristics of enhanced active constrained layer damping treatments with edge elements, Part I: Finite element model development and validation," *ASME Journal of Vibration and Acoustics*, vol. 120, no. 4, pp. 886–893, 1998.

[72] Lytwyn, R. T., Miao, W., and Woitsch, W., "Airborne and ground resonance of hingeless rotors," *Journal of the American Helicopter Society*, vol. 16, no. 2, 1971.

[73] Maier, T. H., Sharpe, D. L., and Lim, J. W., "Fundamental investigation of hingeless rotor aeroelastic stability, test and correlation," *Proceedings of the 51st American Helicopter Society Annual Forum (Fort Worth, TX), Alexandria, VA*, pp. 1176–1190, 1995.

[74] Marathe, S., Gandhi, F., and Wang, K. W., "The effect of model uncertainty on magnetorheological fluid damper based systems under feedback linearization control," *ASME International Mechanical Engineering Congress and Exposition/Adaptive Structures and Materials Systems, Anaheim, CA*, vol. 83, pp. 129–140, Nov 15-20 1998.

[75] Marathe, S., Gandhi, F., and Wang, K. W., "Helicopter blade response and aeromechanical stability with a magneto-rheological fluid based lag dampers," *Journal of Intelligent Material Systems and Structures*, 1998.

[76] McGuire, D. P., "Fluidlastic^{TM} dampers and isolators for vibration control on helicopters," *Proceedings of the 50th Annual Forum, AHS*, vol. 1, pp. 295–303, May 11-13 1994.

[77] Menq, C. H., Griffin, J. H., , and Bielak, J., "The forced response of shrouded fan stages," *Journal of Vibration, Acoustics, Stress and Reliability in Design*, vol. 108, pp. 50–55, 1986.

[78] Menq, C. H., Griffin, J. H., and Bielak, J., "The influence of a variable normal load on the forced vibration of a frictionally damped structure," *Journal of Engineering for Gas Turbines and Power*, vol. 108, pp. 300–305, 1986.

[79] Miao, W., "Influence of pitch axis location and orientation on rotor aeroelastic stability," *Vertica*, vol. 11, no. 1, 1987.

[80] Nagabhushanam, J. and Gaonkar, G. H., "Rotorcraft air resonance in forward flight with various dynamic inflow models and aeroelastic couplings," *Vertica*, vol. 8, no. 4, 1984.

[81] Namba, H., Akoi, S., and Natori, M., "Passive and active systems of adaptive joints for truss structures in space," *Proceedings of the 32nd AIAA/ASME/ASCE/AHS/ASC Structures, Structural Dynamics and Materials Conference, Baltimore, MD*, 1991.

[82] Nitsche, R. and Gaul, L., "Semi-active control of friction driven systems," *Proceedings of the International Modal Analysis Conference- IMAC*, vol. 1, pp. 64–70, 2001.

[83] Ohta, M., Masaki, N., Sakamoto, T., and Fujita, S., "Development of semi-active mass damper using electro-rheological fluid for reduction of floor vibration," *Proceedings of the ASME Pressure Vessels and Piping Conference, Montreal, Canada*, pp. 99–104, 1996.

[84] Ormiston, R. A., "Techniques for improving the stability of soft inplane hingeless rotors," *NASA TN X-62390*, October 1974.

[85] Ormiston, R. A., "Investigations of hingeless rotor stability," *Vertica*, vol. 7, no. 2, 1983.

[86] Ormiston, R. A., "Rotor-fuselage dynamic coupling characteristics of helicopter air and ground resonance," *Proceedings of the AHS/NUAA Vertical Flight Technology Seminar, Nanjing, China*, 1985.

[87] Ormiston, R. A., "Rotor-fuselage dynamics of helicopter air and ground resonance," *Journal of the American Helicopter Society*, pp. 3–20, 1991.

[88] Ormiston, R. A., "The challenge of the damperless rotor," *Proceedings of the 22nd European Rotorcraft Forum, Brighton, England*, September 17-19 1996.

[89] Panda, B. and Mychalowycz, E., "Aeroelastic stability wind tunnel testing with analytical correlation of the comanche bearingless main rotor," *Journal of American Helicopter Society*, pp. 207–217, 1997.

[90] Panda, B., Mychalowycz, E., and Tarzanin, F. J., "Application of passive dampers to modern helicopters," *Smart Materials and Structures*, vol. 5, pp. 509–516, 1996.

[91] Pun, J. and Semercigil, S. E., "Semi-active vibration control of a flexible arm using joint stiffness control," *Proceedings of the International Modal Analysis Conference*, vol. 1, pp. 195–201, 1997.

[92] Rainbow, J., "The magnetic fluid clutch," *AIEE Transactions*, vol. 67, pp. 1308–1315, 1948.

[93] Sela, N. M. and Rosen, A., "Modeling the influence of inter-blade connections and variable rotor speed on the aeromechanical stability of helicopter," *Aerospace Science Technology*, no. 4, pp. 173–188, 2000.

[94] Sharpe, D. L., "An experimental investigation of the flap-lag torsion aeroelastic stability of the small-scaled hingless helicopter rotor in hover," *NASA TP2546, AVSCOM TR 85-A-9*, 1986.

[95] Shen, I. Y., "Bending-vibration control of composites and isotropic plates through intelligent constrained-layer treatments," *Journal of Smart Material and Structures*, vol. 3, pp. 59–70, 1994.

[96] Shen, I. Y., "Hybrid damping through intelligent constrained layer treatments," *ASME Journal of Vibration and Acoustics*, vol. 116, pp. 341–349, 1994.

[97] Shen, I. Y., "Stability and controllability of Euler-Bernoulli beams with intelligent constrained layer treatments," *ASME Journal of Vibration and Acoustics*, vol. 118, pp. 70–77, 1996.

[98] Sims, N. D., Stanway, R., and Johnson, A. R., "Vibration control using smart fluids: A state-of-the-art review," *The Shock and Vibration Digest*, vol. 31, no. 2, pp. 195–203, 1999.

[99] Smith, C. B. and Wereley, N. M., "Active passive constrained layer damping of composite rotating flexbeams," *AIAA/ASME Adaptive Structures Forum, Salt Lake City, UT*, pp. 207–216, April 18-19 1996.

[100] Smith, C. B. and Wereley, N. M., "Composite rotorcraft flexbeams with viscoelastic damping layers for aeromechanical stability augmentation," *International Symposium on M3D III: Mechanics and Mechanisms of Material Damping*, vol. 1304, pp. 62–77, November 15-17 1997.

[101] Smith, E. C., "Aeroelastic and aeromechanical aspects of elastically coupled composite rotor blades," *U.S. Army Research Office Beamology Workshop, Aeroflightdynamics Directorate, ATCOM, NASA Ames Research Center, Moffett Field, CA*, 1992.

[102] Spencer Jr., B. F., Carlson, J. D., Sain, M. K., , and Yang, G., "On the current status of magnetorheological dampers: Seismic protection of full-scale structures," *Proceedings of the American Control Conference*, pp. 458–462, 1997.

[103] Spencer Jr., B. F. and Sain, M. K., "Controlling buildings: A new frontier in feedback," *IEEE Control Systems Magazine: Special Issue on Emerging Technologies*, vol. 17, no. 6, pp. 19–35, 1997.

[104] Straub, F. K., "Optimal control of helicopter aeromechanical stability," *Vertica*, vol. 11, no. 3, pp. 425–435, 1987.

[105] Straub, F. K. and Warmbrodt, W., "The use of active controls to augment rotor/fuselage stability," *Journal of the American Helicopter Society*, vol. 39, January 1994.

[106] Takahashi, M. D. and Friedmann, P. P., "Helicopter air resonance modeling and suppression using active control," *Journal of Guidance and Control*, vol. 14, no. 6, pp. 1294–1300, 1991.

[107] Taniwangsa, W. and Kelly, J. M., "Experimental testing of a semi-active control scheme for vibration suppression," *Proceedings of SPIE- Smart Structures and Materials*, vol. 3045, pp. 130–139, 1997.

[108] Tarzanin, F. J. and Panda, B., "Development and application of nonlinear elastomeric and hydraulic lag damper models," *Proceedings of the 36th Structures, Dynamics, and Materials Conference, New Orleans, Louisiana*, pp. 2534–2543, 1995.

[109] Tracy, A. L. and Chopra, I., "Aeroelastic stability investigation of a composite hingless rotor in hover," *Journal of Aircraft*, vol. 35, no. 5, pp. 791–797, 1998.

[110] Veley, D. E. and Rao, S. S., "A comparison of active, passive and hybrid damping in structural design," *Smart Materials and Structures*, vol. 5, pp. 660–671, 1996.

[111] Venkatesan, C., "Influence of aeroelastic couplings on coupled rotor/body dynamics," *Presented at the 6th International Workshop on Dynamics and Aeroelastic Stability Modeling of Rotorcraft Systems, Los Angeles, CA*, Nov. 8-10 1995.

[112] Wang, J. and Chopra, I., "Dynamics of helicopters with dissimilar blades," *Proceedings of the 47th Annual Forum of the American Helicopter Society*, pp. 1399–1412, 1991.

[113] Wang, J. and Chopra, I., "Dynamics of helicopters with dissimilar blades in forward flight," *Proceedings of the 17th European Rotorcraft Forum, Berlin*, 1991.

[114] Wang, J. and Chopra, I., "Dynamics of helicopters in ground resonance with and without blade dissimilarities," *Proceedings of the AIAA/AHS Dynamics Specialists Conference, Washington, DC*, 1992.

[115] Weiss, K. D., Carlson, J. D., and Nixon, D. A., "Viscoelastic properties of magneto- and electro-rheological fluids," *Journal of Intelligent Material Systems and Structures*, vol. 5, pp. 772–775, 1994.

[116] Weller, W. H., "Fuselage state feedback for aeromechanical stability augmentation of a bearingless rotor," *Presented at the 6th International Workshop on Dynamics and Aeroelastic Stability Modeling of Rotorcraft Systems, Los Angeles, CA*, vol. 41, no. 2, pp. 85–93, 1996.

[117] Weller, W. H. and Peterson, R. L., "Measured and calculated inplane stability characteristics for an advanced bearingless main rotor," *Journal of American Helicopter Society*, vol. 29, no. 3, pp. 45–53, 1984.

[118] Wereley, N. M. and Kamath, G. M., "Bringing relevance to freshman aerospace engineering: Demonstration of model scale comanche helicopter lag mode damper," *The International Journal of Engineering Education*, vol. 13, no. 5, pp. 369–375, 1997.

[119] Wereley, N. M., Kamath, G. M., and Madhavan, V., "Hysteresis modeling of semi-active magnetorheological helicopter dampers," *Journal of Intelligent Material Systems and Structures*, vol. 10, no. 8, pp. 624–633, 2000.

[120] Whiteman, W. E. and Ferri, A. A., "Displacement-dependent dry friction damping of a beam-like structure," *Journal of Sound and Vibration*, vol. 198, no. 3, pp. 313–329, 1996.

[121] Winslow, W. M., "Method and means for translating electrical impulses into mechanical force," *US Patent No. 2,417, 850*, 1947.

[122] Winslow, W. M., "Induced vibration of suspensions," *Journal of Applied Physics*, vol. 20, pp. 1137–1140, 1949.

[123] Yeager, W. T., Hamouda, M. H., and Mantany, W. R., "An experimental investigation of the aeromechanical stability of a hingless rotor in hover and forward flight," *NASA TM 89107, AVSCOM TR 89-A-003*, 1989.

[124] Zheng, H., Cai, C., Pau, G. S. H., and Liu, G. R., "Minimizing vibration response of cylindrical shells through layout optimization of passive constrained layer damping treatments," *Journal of Sound and Vibration*, vol. 279, no. 3-5, pp. 739–756, 2005.

[125] Zotto, M. D. and Loewy, R. G., "Influence of pitch-lag coupling on damping requirements to stabilize ground/air resonance," *Journal of American Helicopter Society*, vol. 37, no. 4, pp. 68–71, 1992.

VITA

Sandeep Agarwal was born at Jaipur, a north-western city in India, on September 10, 1977. He finished his high school at Jaipur in 1996. He joined the prestigious Indian Institute of Technology, Kharagpur for his undergraduate studies. He acquired B. Tech. in Aerospace Engineering in 2000. In August of 2000, Sandeep joined the Aerospace Engineering Department of Georgia Institute of Technology for Graduate studies. In December 2001, he acquired MS degree in Aerospace Engineering. Upon finishing his Masters degree, he continued his graduate studies at the Georgia Institute of Technology. His areas of research interest include Vibration Control of Rotary-Wing Aircraft, Smart Structures and Materials and Structural Morphing Technology. He is a member of AIAA and AHS.